

# Synthesis and Reactivity of Transition Metal and Main Group Hydrogenation Catalysts

by

Eliar Mosaferi

A thesis submitted in conformity with the requirements  
for the degree of Doctor of Philosophy

Department of Chemistry  
University of Toronto

© Copyright by Eliar Mosaferi 2019

# Synthesis and Reactivity of Transition Metal and Main Group Hydrogenation Catalysts

Eliar Mosaferi

Doctor of Philosophy

Department of Chemistry  
University of Toronto

2019

## Abstract

Since its discovery by Paul Sabatier, catalytic hydrogenation of unsaturated substrates has become the single largest industrial process to date and encompasses the production of many products, such as foods, agrochemicals, pharmaceuticals, and materials. Over the last century research in the area has predominantly focused on the use of transition metals such as palladium, platinum, rhodium, and ruthenium to develop heterogeneous and homogeneous hydrogenation catalysts. The research presented herein focuses on the use of ruthenium complexes bearing electron-rich phosphorylated N-heterocyclic carbene ligands as well as the development of main-group compounds for frustrated Lewis pair catalysis.

Complexes  $[\text{Ru}(0)\text{LL}'_2(\text{CO})]$  and  $[\text{RuHL}_2(\text{CO})][\text{Cl}]$ , where L = N-phosphorylated N-heterocyclic carbene (NHCP), and L' = triphenylphosphine, were prepared as a mixture by treatment of  $\text{RuHCl}(\text{CO})(\text{PPh}_3)_3$  with excess NHCP carbene and separated by crystallization. The zero-valent complex  $[\text{Ru}(0)\text{LL}'_2(\text{CO})]$  was shown to undergo rapid oxidative addition to the corresponding Ru(II) species when treated with small molecules to afford complexes of the general type  $[\text{RuHXLL}'(\text{CO})]$ , where L = N-phosphorylated N-heterocyclic carbene, L = triphenylphosphine, and X = H, SiPh<sub>3</sub>, or Si(H)Ph<sub>2</sub>.

The reaction of NHCP carbene with  $[\text{RuCl}_2(p\text{-cymene})]_2$  resulted in the isolation of the piano-stool half-sandwich complex  $[\text{RuCl}_2(p\text{-cymene})(\text{NHCP})]$  as well as an unusual arene-activated species. The half-sandwich complex was treated with a halide-abstracting agent to afford the cationic compound  $[\text{RuCl}(p\text{-cymene})(\text{NHCP})]^+$ , which was shown to rapidly undergo dihydrogen activation *via* an outer-sphere mechanism involving the phosphine appended to the carbene ligand.

To demonstrate the utility of main-group catalysts, trityl cations of the form  $[(4\text{-MeO-C}_6\text{H}_4)_x\text{CPh}_{3-x}][\text{BR}_4]$  were synthesized, where  $x = 1$  and  $3$ , and  $\text{R} = \text{F}$ , or  $\text{C}_6\text{F}_5$ . Treatment of equimolar solutions of  $[(4\text{-MeO-C}_6\text{H}_4)\text{CPh}_2][\text{BF}_4]$  and sterically encumbered phosphines with dihydrogen resulted in activation of dihydrogen but no catalytic activity was observed. The air- and moisture-stable  $[(4\text{-MeO-C}_6\text{H}_4)\text{CPh}_2][\text{BF}_4]$  was shown to be a potent Lewis acid catalyst in the hydrothiolation of olefins.

## Acknowledgments

First and foremost, I would like to thank Professor Douglas Stephan for giving me the opportunity to complete my degree in his group. His vast knowledge, unwavering support, and infectious enthusiasm have been invaluable in aiding my journey through grad school and as a result my experience has been immensely positive. I am thankful for the opportunities to learn and grow and will always look back on my years in his group with fondness. As well, I'd like to thank the members of my advisory committee, Prof. Morris and Prof. Song, for the invaluable advice throughout my degree.

I would also like to thank all the members of the Stephan group, both past and present, for their support and help both in and outside the lab. The life of a graduate student is heavily influenced by the peers around them and I am truly grateful to have known these wonderful group of colleagues, friends, and mentors. In particular, I'd like to thank Dr. Adam McKinty, Dr. Michael Boone, Dr. Colin Douglas, Dr. Adelle Vandersteen, and all other past and present members of C.S.S.G. for keeping me humble and for always being ready with a helping hand. In particular, the meetings held over glasses of Red Leaf juice were particularly useful. I'd especially like to thank Dr. Tim Johnstone, Dr. Andrew Jupp, and Kevin Szkop for their technical and mental support and the pleasant chats over afternoon coffee. As well I'd like to thank Dr. Andrew Jupp, Dr. Tim Johnstone, Kevin Szkop, Karlee Bamford, James Lafortune, and Alex Waked for editing my thesis and providing valuable feedback. And to all of the friends I have made in Toronto, whether in the lab or outside, I am forever grateful for your kindness, hospitality, and support.

As always, my family has been incredibly supportive and without their sacrifices I would not be where I am today. My parents, Hassan and Maryam, have always pushed me to be my best in all aspects of my life. They have supported me through the different chapters of my life. My brother, Yashar, has also been instrumental in my life. Much like my parents, he has been there for me time and time again. It has been their encouragement, support, and unconditional love that has allowed me to persevere through challenges. I owe an immense debt of gratitude to them for their unconditional love and look forward to the opportunity to support and encourage them in the future.

Last but not least, I would like to thank my incredible partner, Setareh Nourani. More than anyone she has been patient and supportive throughout this journey. Despite not being a chemist, she has patiently and enthusiastically played the role of my sound board and provided guidance when I faced problems in the lab. Equally, outside the lab she has shown an incredible amount of love and care and for that I owe her a great debt. Her enthusiasm and willingness to bear through my chemistry problems have been an invaluable asset. This work could not be completed without her undying support.

# Table of Contents

Acknowledgments.....	iv
Table of Contents .....	vi
List of Tables .....	ix
List of Schemes.....	x
List of Figures .....	xv
List of Abbreviations .....	xviii
Chapter 1 Introduction .....	1
1.1 Chemistry and Impact on Society.....	1
1.2 Catalysis.....	2
1.3 Transition Metal Hydrogenation.....	3
1.3.1 Heterogeneous Catalysts.....	3
1.3.2 Well-Defined Homogeneous Catalysts.....	3
1.4 Metal-Free Hydrogenation.....	10
1.4.1 Main-Group Catalysis.....	10
1.4.2 Frustrated Lewis Pairs (FLP).....	12
1.4.3 FLP Hydrogenations .....	16
1.5 N-Heterocyclic Carbenes (NHC).....	18
1.5.1 History of NHC Carbenes.....	18
1.5.2 NHC Complexes in Hydrogenation .....	23
1.6 Nitrile Butadiene Rubber .....	25
1.7 Lanxess Project .....	26
1.8 Scope of this Thesis .....	27
1.9 Contributions to Knowledge.....	27
1.9.1 Relevant Publications.....	27

1.9.2	Conference Presentations.....	28
1.9.3	Undergraduate Mentoring.....	28
Chapter 1	References .....	30
Chapter 2	Coordination Chemistry of N-Heterocyclic Phosphanyl Carbenes.....	38
2.1	Introduction.....	38
2.1.1	Zero-Valent Ruthenium Complexes .....	38
2.1.2	N-Heterocyclic Carbenes with Pendant Phosphorus Donors.....	38
2.2	Results and Discussion .....	42
2.2.1	Synthesis of Ru-NHCP Complexes .....	42
2.2.2	Reactivity of Ru-NHCP Complexes.....	50
2.3	Conclusion .....	56
2.4	Experimental Section.....	56
2.4.1	General Considerations.....	56
2.4.2	General Procedure for Hydrogenation .....	57
2.4.3	Synthetic Procedures.....	58
2.4.4	X-ray Crystallography .....	70
Chapter 2	References .....	73
Chapter 3	Rearrangement and Decomposition of Ru-NHCP Complexes .....	77
3.1	Introduction.....	77
3.1.1	Catalyst Decomposition and Deactivation.....	77
3.1.2	Rearrangement Reactivity of NHC complexes.....	78
3.2	Results and Discussion .....	79
3.3	Conclusion .....	89
3.4	Experimental Section.....	90
3.4.1	General Considerations.....	90
3.4.2	General Procedure for Hydrogenation .....	90

3.4.3	Synthetic Procedures.....	91
3.4.4	X-ray Crystallography .....	97
Chapter 3	References .....	101
Chapter 4	Frustrated Lewis Pair and Lewis Acid Chemistry of Carbon-Based Lewis Acids .....	104
4.1	Introduction.....	104
4.1.1	Group 13 Lewis Acids .....	104
4.1.2	Lewis Acids Beyond Group 13.....	106
4.2	Results and Discussion .....	110
4.2.1	Synthesis of Air-Stable Trityl Cations .....	110
4.2.2	Catalysis and Reactivity of Trityl Cations .....	112
4.3	Conclusion .....	122
4.4	Experimental Section.....	123
4.4.1	General Considerations.....	123
4.4.2	Synthetic Procedures.....	123
4.4.3	X-ray Crystallography .....	129
Chapter 4	References .....	132
Chapter 5	Conclusion and Future Work .....	139
5.1	Thesis Summary.....	139
5.2	Future Work .....	140
Chapter 5	References .....	144

## List of Tables

Table 1.3.1: Rates <sup>a</sup> of hydrogenation of variously substituted olefins with different catalyst types. .....	6
Table 2.2.1. Catalytic Hydrogenation of Olefins Using 2-7 and 2-8.....	55
Table 2.4.1. Select crystallographic data for 2-5, and 2-6.....	71
Table 2.4.2. Select crystallographic data for 2-7, 2-9, and 2-10.....	72
Table 3.2.1: Catalytic hydrogenation of olefins, carbonyls, and NBR rubber using 3-1 and 3-2.	82
Table 3.4.1: Select crystallographic data for complexes 3-4 and 3-5.....	99
Table 3.4.2: Select crystallographic data for complexes 3-7 and 3-9.....	100
Table 4.2.1: Hydrothiolation of methyl stilbene using various known Lewis acid catalysts. ....	117
Table 4.2.2: Catalytic olefin hydrothiolation using trityl tetrakis(pentafluorophenyl)borate.....	118
Table 4.2.3: Catalytic hydrothiolation of unsaturated species using catalyst 4-2.....	119
Table 4.4.1. Select Crystallographic Data for 4-2. ....	131

## List of Schemes

Scheme 1.3.1: Catalytic hydrogenation of 1-hexene using Wilkinson's Catalyst. ....	4
Scheme 1.3.2: Formation of catalytically active cationic Rh(III)- and Ir(III)-dihydride species. ..	5
Scheme 1.3.3: Substrate-directed diastereoselective reduction of terpen-4-ol. ....	7
Scheme 1.3.4: BINAP-Ru catalyzed asymmetric hydrogenation of functionalized ketones. ....	9
Scheme 1.3.5: BINAP/diamine-Ru catalyzed asymmetric hydrogenation of simple ketones.....	10
Scheme 1.4.1: Early example of transition metal-free reduction of unsaturated substrates. ....	11
Scheme 1.4.2: Reduction of olefins using Ca(nacnac)-based catalysts. ....	12
Scheme 1.4.3: Nucleophilic attack of Lewis base at Lewis acid resulting from the preclusion of adduct formation. ....	13
Scheme 1.4.4: Intermolecular FLP activation of dihydrogen (top) and generalized description of FLPs with preclusion of adduct formation as a result of steric bulk. ....	13
Scheme 1.4.5: Depiction of the formation of the encounter complex with active "pocket" for dihydrogen activation.....	14
Scheme 1.4.6: Formation and trapping of radical FLPs. ....	16
Scheme 1.4.7: Mechanism of FLP-catalyzed hydrogenation of imines. ....	17
Scheme 1.4.8: Proposed catalytic cycle for the FLP reduction of ketones and aldehydes. ....	18
Scheme 1.5.1: Proposed Breslow intermediate in the hydrogen/deuterium exchange of a trimethylthiazolium salt. ....	19
Scheme 1.5.2: Synthesis and trapping of persistent bis(phenyl)imidazolylidenes. ....	19
Scheme 1.5.3: Bertrand's phosphinocarbene (a), its mesomerically-formed phosphinoacetylene (c), and an intermediate zwitterionic species (b). ....	20

Scheme 1.5.4: Arduengo's synthesis of the first isolable, crystalline and persistent carbene. ....	20
Scheme 1.5.5: Partial transfer hydrogenation of alkynes catalyzed by Pd-NHC complex.....	24
Scheme 1.5.6: Reduction of heteroarenes using cationic Ir(III) species bearing mesoionic carbene ligands. ....	24
Scheme 1.5.7: Synthesis of catalytically active cyclometalated Ru-triazolylidene complex for olefin hydrogenation. ....	25
Scheme 2.1.1: Synthesis of selected zero-valent ruthenium species. ....	38
Scheme 2.1.2: Different synthetic protocols for the generation of N-phosphorylated imidazolium salts. ....	40
Scheme 2.1.3: Deprotonation of NHCP salts to yield free carbenes. ....	40
Scheme 2.1.4: Various transition metal complexes employing the bifunctional chelate of NHC-P ligands. ....	41
Scheme 2.1.5: Synthesis of a phosphine-tethered NHC carbene complex. ....	42
Scheme 2.2.1: Synthesis of imidazolium salt 2-1.....	42
Scheme 2.2.2: Synthesis of imidazole precursor 2-2 and imidazolium salt 2-3.....	42
Scheme 2.2.3: Synthesis of 2-5 and 2-6 from free carbene 2-4.....	43
Scheme 2.2.4: Selective synthesis of complex 2-5.....	44
Scheme 2.2.5: Reduction of Ru(II) nitrosyl complex to form a zero-valent, four-coordinate species. ....	47
Scheme 2.2.6: Initial proposed synthesis of a Ru(II)-NHCP using a bulkier NHCP carbene.....	48
Scheme 2.2.7: Proposed solution-phase reversibility of pendant alkyl arm in 2-7 to form 2-7a..	49
Scheme 2.2.8: Reaction of 2-11 with dihydrogen to afford the dihydride species 2-7b.....	50

Scheme 2.2.9: <i>In-Situ</i> generation of 2-8 from complex 2-5 by treatment with dihydrogen. ....	51
Scheme 2.2.10: Synthesis of 2-9 and 2-10.....	52
Scheme 2.2.11: Synthesis of 2-11.....	54
Scheme 2.2.12. Catalytic Reduction of Olefins Using Ruthenium-Hydride Catalysts. ....	55
Scheme 3.1.1: Synthesis of “normal” carbene adducts and their migration to "abnormal" imidazolylidene carbenes.....	78
Scheme 3.1.2: Rearrangement of N-picolyl substituted NHC <i>via</i> cleavage of C-N bond.....	78
Scheme 3.2.1: Synthesis of half-sandwich complex 3-1. ....	79
Scheme 3.2.2: Synthesis of cationic Ru-arene complex 3-2.....	80
Scheme 3.2.3: Reversible activation of dihydrogen by 3-2 to form statistical mixtures of H <sub>2</sub> and D <sub>2</sub> . ....	80
Scheme 3.2.4: Base-promoted functionalization of coordinated phosphines. ....	81
Scheme 3.2.5: Synthesis of arene-activated product 3-4. ....	83
Scheme 3.2.6: Proposed mechanistic pathway for the formation of 3-4 from half-sandwich complex 3-1. ....	85
Scheme 3.2.7: Synthesis of the analogous arene-activated complex 3-6. ....	87
Scheme 3.2.8: Attempted synthesis of a ruthenium-hydride catalyst for olefin hydrogenation... ..	88
Scheme 4.1.1: Activation of Cp <sub>2</sub> ZrMe <sub>2</sub> by tris(pentafluorophenyl)borane via methyl abstraction. ....	104
Scheme 4.1.2: Borocation structure motifs with vacant p-orbitals explicitly shown. ....	104
Scheme 4.1.3: First FLP activation of dihydrogen. ....	105

Scheme 4.1.4: Small molecule activation by a geminal Al/P Frustrated Lewis Pair (R=CH <sub>2</sub> <sup>t</sup> Bu, R'=p-tolyl). .....	106
Scheme 4.1.5: Dihydrogen activation by an intermolecular Al/P frustrated Lewis pair (R= <sup>t</sup> Bu, Mes) (top). Carbon dioxide fixation by an intermolecular Al/P frustrated Lewis pair (X=Cl, Br) (bottom).....	106
Scheme 4.1.6: Dihydrogen activation at the same carbon center using (alkyl)(amino)carbenes. ....	109
Scheme 4.1.7: All-carbon FLP using allenes (top) and acridinium Lewis acid in cleavage of H <sub>2</sub> (bottom).....	110
Scheme 4.2.1: Synthesis of air-stable trityl cations. ....	110
Scheme 4.2.2: Mesomeric stabilization of trityl cations.....	111
Scheme 4.2.3: Reversible adduct formation between 4-2 and <sup>t</sup> Bu <sub>3</sub> P.....	112
Scheme 4.2.4: Attempted step-wise reduction of an iminium salt using triarylmethane. ....	114
Scheme 4.2.5: Rh-catalyzed hydrothiolation of alkynes to 1,1-disubstituted olefins.....	115
Scheme 4.2.6: Hydrothiolation of heteroatom-activated alkenes using Pd(OAc) <sub>2</sub> .....	115
Scheme 4.2.7: Generation of borenium cation <i>via</i> abstraction of hydride from borane. ....	116
Scheme 4.2.8: Initial proposed catalytic hydrothiolation of methylstilbene using an <i>in-situ</i> generated borenium catalyst. ....	116
Scheme 4.2.9: Proposed catalytic cycle for hydrothiolation of olefins using trityl catalysts. ....	122
Scheme 5.2.1: Synthesis of various isomers of ruthenium-dihydride species bearing NHC ligands. ....	141
Scheme 5.2.2: Ruthenium transfer hydrogenation catalyst bearing phosphino-NHC ligand. NHC can be modified to bear N-substituents post-synthesis. ....	142

Scheme 5.2.3: Reversible activation of dihydrogen using a highly-substituted trityl cation. ....	142
Scheme 5.2.4: Staudinger formation of phosphinimine (top), and arrested intermediate in Staudinger reaction trapped by trityl cation (bottom).....	143

## List of Figures

Figure 1.2.1: Reaction coordinate diagram depicting changes in activation energy between catalyzed (red) and uncatalyzed (black) reactions. ....	2
Figure 1.3.1: Noyori's asymmetric ketone hydrogenation catalysts.....	8
Figure 1.3.2: Transition states of the BINAP/diamine-Ru and BINAP-Ru catalysts. ....	9
Figure 1.4.1: Proposed six-member transition state involved in the reduction of ketones using <sup>t</sup> BuOK catalyst. ....	11
Figure 1.4.2: Close contact distances in intra- and intermolecular FLPs providing evidence of "pocket" in encounter complex. ....	15
Figure 1.5.1: The stable tetramethylimidazolydene carbene (top) and depiction of mesomeric and inductive stabilization of Arduengo's carbene (bottom). ....	21
Figure 1.5.2: General depiction of mesoionic carbenes: abnormal imidazolydene (left) and 1,2,3-triazolydene (right). ....	22
Figure 1.5.3: Depiction of sphere created by the carbene substituents. % $V_{bur}$ is the percentage of this sphere that is occupied by the ligand ( $d$ = the metal-carbene bond, $r$ = radius of the sphere). ....	22
Figure 1.5.4: Various binding motifs of N-heterocyclic carbene ligands. ....	23
Figure 1.5.5: Chiral hydrogenation catalyst for asymmetric reduction of alkenes. ....	25
Figure 1.6.1: Depiction of various functional groups in nitrile butadiene rubber. ....	26
Figure 2.1.1: Various motifs of phosphorus-based imidazole ligands.....	39
Figure 2.2.1: Thermal ellipsoid plot of 2-5. Solvent and hydrogen atoms omitted for clarity. Grey: Carbon, Blue: Nitrogen, Orange: Phosphorus, Red: Oxygen, Pink: Ruthenium. ....	45

Figure 2.2.2: Thermal ellipsoid plot of one molecule in the asymmetric unit of 2-6. Solvent and hydrogen atoms (except hydride) omitted for clarity. Grey: Carbon, Blue: Nitrogen, Orange: Phosphorus, Red: Oxygen, Green: Chlorine Pink: Ruthenium.....	45
Figure 2.2.3: Ru(II)Cl <sub>2</sub> (MesImP <sup>t</sup> Bu <sub>2</sub> ) <sub>2</sub> , synthesized by Hofmann <i>et al.</i> ....	46
Figure 2.2.4: Thermal ellipsoid plot of 2-7. Hydrogen atoms (except hydride) omitted for clarity. ....	48
Figure 2.2.5: Select region of stacked variable temperature NMR spectra of 2-7 in toluene-d <sub>8</sub> . .	49
Figure 2.2.6. Rapid conversion of 2-5 (left) to 2-8 (right). Photographs taken 10 minutes apart.	51
Figure 2.2.7: Stacked <sup>31</sup> P{ <sup>1</sup> H} NMR spectra of 2-5 (top), 2-8 under dihydrogen (middle), and 2-8 after repeated cycles of freeze-pump-thaw (bottom). ....	52
Figure 2.2.8: Thermal ellipsoid plots of complexes 2-9 (left) and 2-10 (right). Grey: Carbon, Blue: Nitrogen, Orange: Phosphorus, Red: Oxygen, Pink: Ruthenium, Cyan: Silicon.....	53
Figure 3.1.1: Various olefin metathesis catalysts studied for decomposition and deactivation. ..	77
Figure 3.2.1: Phosphorylated imidazolium (2-1) and imidazolylidene (2-4) compounds. ....	79
Figure 3.2.2: Thermal ellipsoid plot of 3-4. Solvent and hydrogen atoms (except C21 proton) omitted for clarity. Grey: Carbon, Blue: Nitrogen, Orange: Phosphorus, Green: Chlorine, Pink: Ruthenium. ....	84
Figure 3.2.3: Complexes 2-5 and 2-6, as discussed in Chapter 2. ....	85
Figure 3.2.4: Thermal ellipsoid plot of 3-5. Hydrogen atoms omitted for clarity. Grey: Carbon, Blue: Nitrogen, Orange: Phosphorus, Green: Chlorine, Pink: Ruthenium. ....	86
Figure 3.2.5: Thermal ellipsoid plot of one molecule in the asymmetric unit of 3-7. Hydrogen atoms omitted for clarity. Grey: Carbon, Blue: Nitrogen, Green: Chlorine, Pink: Ruthenium. ....	87

Figure 3.2.6: Thermal ellipsoid plot of 3-9. Solvent and hydrogen atoms (except hydride) omitted for clarity. P1' is symmetry generated by a mirror plane along N1-Ru-N3. Grey: Carbon, Blue: Nitrogen, Green: Chlorine, Orange: Phosphorus, Pink: Ruthenium.....	89
Figure 4.1.1: The first isolated phosphonium cations. ....	107
Figure 4.1.2: Mesomeric forms of the first tricationic carbene-stabilized phosphonium species. ....	107
Figure 4.1.3: Highly Lewis acidic fluorophosphonium cations.....	107
Figure 4.2.1: Thermal ellipsoid plot of solid-state structure of 4-2. Grey: Carbon, Red: Oxygen, Green: Fluorine, Purple: Boron, White: Hydrogen.....	111
Figure 4.2.2: $^1\text{H}$ NMR spectrum of 4-2 and $^t\text{Bu}_3\text{P}$ showing approximate ratio of adduct and free phosphine. ....	112
Figure 4.2.3: Activation of $\text{H}_2$ by 4-2/ $\text{Mes}_3\text{P}$ FLP. Free $\text{Mes}_3\text{P}$ before addition of dihydrogen (bottom), phosphonium product (middle), and depiction of P-H coupling in phosphonium (top). ....	114
Figure 4.2.4: $^1\text{H}$ NMR spectrum of equimolar solution of trityl 4-2 and benzyl mercaptan, depicting upfield shift in proton resonances. ....	121

## List of Abbreviations

Å	angstrom, $10^{-10}$ m
°	degrees
°C	degrees Celsius
δ	chemical shift
η	eta (bonding mode)
μ	bridging
π	pi
σ	sigma
ΔG	Gibbs free energy
ΔH	enthalpy
AAC	(alkyl)(amino)carbene
Abs	absorption
Anal	analytical
Atm	atmosphere
Ar	Aryl
BCF	tris(pentafluorophenyl)borane
BINAP	2,2'-bis(diphenylphosphino)-1,1'-binaphthyl
b.p.	boiling point
br	broad
CAAC	cyclic(alkyl)(amino)carbene
calcd.	calculated
cat.	catalyst

CCD	charge coupled device
C <sub>6</sub> D <sub>6</sub>	deuterated benzene
CDCl <sub>3</sub>	deuterated chloroform
CD <sub>2</sub> Cl <sub>2</sub>	deuterated dichloromethane
C <sub>6</sub> F <sub>5</sub>	pentafluorophenyl
C <sub>6</sub> H <sub>5</sub> Cl	chlorobenzene
cm	centimeter
cm <sup>-1</sup>	wavenumber
CO	carbonyl
cod	cyclooctadiene
coeff	coefficient
conv.	conversion
cot	cyclooctatriene
Cp	cyclopentadienyl
Cp*	pentamethylcyclopentadienyl
Cy	cyclohexyl
d	doublet
DART	direct analysis in real time
d <sub>calc</sub>	calculated density
DCE	1,2-dichloroethane
DCM	dichloromethane, methylene chloride
dd	doublet of doublet
ddd	doublet of doublet of doublets
deg	degree

Dipp	2,6-diisopropylphenyl
$D_{X-Y}$	Through-space scalar coupling between X and Y atoms
$E_a$	activation energy
equiv.	equivalent
Et	ethyl
Et <sub>2</sub> O	diethyl ether
$F_c$	calculated structure factors
$F_o$	observed structure factors
FLP	frustrated Lewis pair
FTIR	Fourier transform infrared
g	gram
GOF	goodness of fit
h	hours
H <sub>2</sub>	dihydrogen
HOMO	highest occupied molecular orbital
HNBR	hydrogenated nitrile butadiene rubber
Hz	Hertz
$I$	nuclear spin
IAd	1,3-bis(adamantyl)imidazol-2-ylidene
IR	infrared
<i>i</i> Pr	<i>iso</i> -propyl
${}^nJ_{X-Y}$	n-bond scalar coupling constant between X and Y atoms
K	Kelvin
LUMO	lowest unoccupied molecular orbital

<i>m</i>	<i>meta</i>
m	multiplet
Me	methyl
MeCN	acetonitrile
Mes	mesityl; 2,4,6-trimethylphenyl
mg	milligram
MHz	megahertz
min	minute
mL	milliliter
mm	millimeter
mmol	millimole
mol	mole
mol%	mole percent
MS	mass spectrometry
m/z	mass-to-charge ratio
N <sub>2</sub>	dinitrogen
NBR	nitrile butadiene rubber
NHC	N-heterocyclic carbene
NHCP	N-heterocyclic carbeno-phosphine
NMR	nuclear magnetic resonance
<i>o</i>	<i>ortho</i>
O <sub>2</sub>	dioxygen
o/n	overnight
OTf <sup>-</sup>	trifluoromethanesulfonate

<i>p</i>	<i>para</i>
Ph	phenyl
POV-Ray	Persistence of Vision Raytracer
ppm	parts per million
PR <sub>3</sub>	tertiary phosphine
py	pyridine
q	quartet
R	residual factor
r.t.	room temperature
Rw	weighted residual factor
s	singlet
SIMes	1,3-bis(2,4,6-trimethylphenyl)-4,5-dihydroimidazol-2-ylidene
t	triplet
<sup>t</sup> Bu	<i>tert</i> -butyl
THF	tetrahydrofuran
tht	tetrahydrothiophene
TMS	trimethylsilyl
tol	toluene
TOF	turnover frequency
TON	turnover number
V	volume
VT	variable temperature
wt%	weight percent
Z	number of “formula units” per unit cell

# Chapter 1

## Introduction

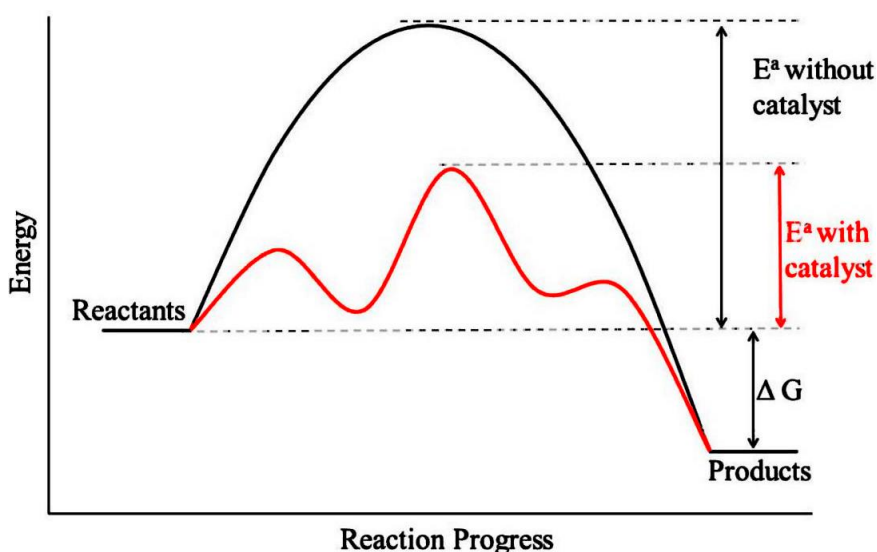
### 1.1 Chemistry and Impact on Society

The “Green Revolution”, also known as the Third Agricultural revolution, refers to a set of practices and technological advances in the 20<sup>th</sup> century that led to an unprecedented growth in human population.<sup>1</sup> The invention of high-yielding varieties of crops such as cereals and rice, in association with chemical pesticides and fertilizers, led to an exponential growth in human population. This boom in agricultural productivity was in large part spurred by the Haber-Bosch process, where ammonia could be produced on an industrial scale for the first time. However, the production of ammonia takes an enormous toll, as the process demands a whopping 2% of the annual global energy supply.<sup>2,3</sup> Despite the enormity of the effect of the Haber-Bosch process on humankind, it is by no means the only aspect of the chemical sciences that makes an impact around the world. Indeed, we cannot go any length of time without interacting with a product or offspring of chemical innovation. For example, advanced pharmaceuticals have dramatically improved the conditions and quality of life for many people around the globe and have had a large hand in the increase in average life expectancy since the early 20<sup>th</sup> century.

The exponential growth in human population described above has not been without its accompanying issues. As a result of this population boom the demand for natural resources, such as fossil fuels, has also expanded substantially. The result of this unsustainable increase in fossil fuel use has led to critical increases in greenhouse gas emissions, causing global climate changes that carry substantial consequences. Elsewhere, the negative effects of other chemical discoveries, such as tetraethyllead and thalidomide, have caused far-reaching issues throughout generations. While the role of chemistry in these issues cannot be understated, it is important to recognize that chemistry also plays a large part in alleviating many of the issues facing the world. Indeed, the development of cleaner energy sources has demanded a substantial and ever-growing segment of global efforts. As well, efforts have been directed towards the development and production of various “green” catalysts as a solution for the dwindling energy reserves. The work in this thesis will begin with the development of precious-metal catalysts for hydrogenation of various substrates, before shifting focus to more Earth-abundant elements in pursuit of metal-free catalytic systems based on the frustrated Lewis pair (FLP) chemistry of carbon Lewis acids.

## 1.2 Catalysis

A catalyst is a substance that increases the rates of forward and reverse reactions by lowering the activation energy (Figure 1.2.1).<sup>4</sup> Since the catalyst is not consumed in the overall reaction it can be used in small amounts. In biological systems, enzymes catalyze various reactions that are essential to the survival of all species.<sup>5</sup> Furthermore, catalysis is used extensively in industrial processes from the production of plastics,<sup>6,7</sup> to the synthesis of pharmaceuticals<sup>8</sup> and fine chemicals.<sup>9</sup>



**Figure 1.2.1: Reaction coordinate diagram depicting changes in activation energy between catalyzed (red) and uncatalyzed (black) reactions.**

Hydrogenation is described as any chemical transformation that results in the reduction of an unsaturated moiety, either directly by dihydrogen gas or *via* surrogates such 2-propanol, and is often carried out in the presence of a catalyst.<sup>10</sup> As one of the most ubiquitous industrial processes, hydrogenation is commonly employed in a variety of chemical transformations relevant to the food, agrochemical, pharmaceutical and polymer industries, as well as materials science.<sup>11</sup> In 1897, Paul Sabatier presented his findings on the catalytic hydrogenation of unsaturated substrates using transition metals.<sup>12</sup> Sabatier's seminal work was recognized, along with that of Victor Grignard, in 1912 with the awarding of the Nobel Prize in Chemistry. The evolution of organometallic chemistry in the early 20<sup>th</sup> century and the major advances of the 1960s and 1970s led to the discovery of various transition metal catalysts that exhibited high activity for this fundamental transformation.<sup>11</sup>

## 1.3 Transition Metal Hydrogenation

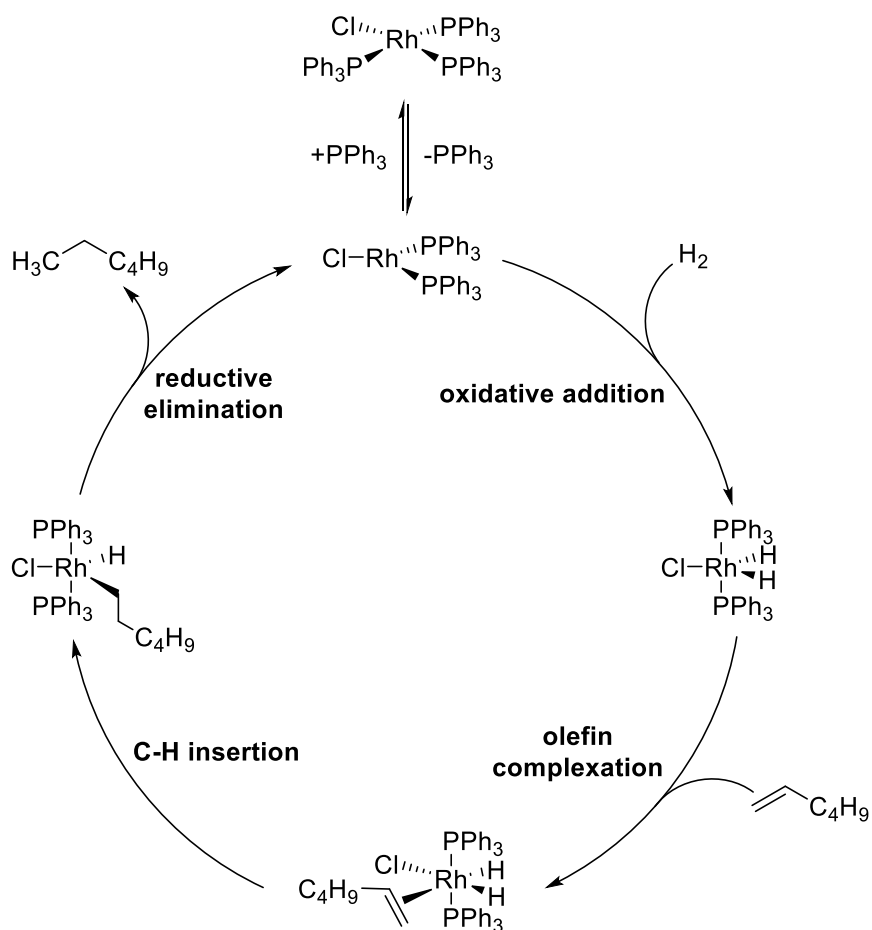
### 1.3.1 Heterogeneous Catalysts

Heterogeneous catalysts are more prevalent industrially due to their ease of use and the corresponding ease of post-reaction processing. However, heterogeneous catalysts are not as well-defined as their homogeneous analogues. Often, precious metal catalysts are supported on matrices such as activated charcoal, calcium carbonate, alumina, or barium sulfate. The most common of these are supported nickel catalysts, followed closely by noble metal systems such as Pt, Pd, Ru, and Rh.<sup>13</sup> In order to induce some degree of selectivity, catalyst “poisons” (such as coordinating functional groups) are employed to modify the solid surface of the catalyst. An early example of such a modification is Lindlar’s catalyst, whereby treatment of a barium sulfate-supported palladium species with quinoline results in a catalyst capable of reducing acetylenes selectively to the *cis*-alkenes.<sup>14</sup> Furthermore, developments in catalyst design and modifications have allowed the use of dihydrogen surrogates in transfer hydrogenation reactions, thus removing the need for gaseous H<sub>2</sub> in the reaction mixture.<sup>15</sup>

### 1.3.2 Well-Defined Homogeneous Catalysts

#### 1.3.2.1 Wilkinson’s Catalyst

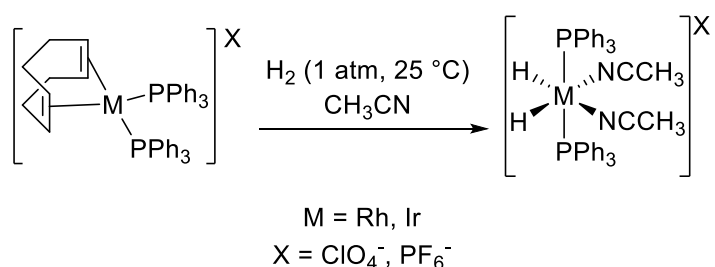
The first well-defined homogeneous hydrogenation catalyst was developed by Sir Geoffrey Wilkinson in the mid-1960s and bears his name.<sup>16</sup> Wilkinson’s catalyst is a coordination complex of rhodium that was shown to be an effective catalyst for the hydrogenation of olefins using molecular hydrogen.<sup>17</sup> The mechanism<sup>17,18</sup> of the reduction of olefins (Scheme 1.3.1) requires the initial dissociation of triphenylphosphine from the four-coordinate pre-catalyst to yield a 14-electron solvated species. Thus, the open coordination site allows oxidative addition of H<sub>2</sub> to form a Rh(III)-dihydride species that then undergoes complexation with an olefin. Subsequent insertion of the alkene substrate forms an alkyl-hydride complex, and reductive elimination furnishes the alkane product and regenerates the three-coordinate active catalyst.



**Scheme 1.3.1: Catalytic hydrogenation of 1-hexene using Wilkinson's Catalyst.**

Unfortunately, the reduction of acetylenes is difficult to control as they are fully reduced to the alkane *via* the production of *cis*-alkene intermediates. Furthermore, the reduction of alkenes is heavily controlled by the degree and type of substitution of the olefin. Indeed, the rate of hydrogenation of terminal olefins exceeds that of internal olefins, while *cis*-alkenes are more rapidly hydrogenated in comparison to *trans*-alkenes.<sup>16</sup> These findings are consistent with the mechanism described above and point to the complexation of the olefin as a key step in the reduction mechanism. Interestingly, while ethylene forms a stable adduct with the active catalytic species, no reduction to ethane gas is observed.<sup>16</sup> Thus, Wilkinson and coworkers conclude that ethylene acts as an effective poison that complexes with the three-coordinate Rh(I) species and prevents oxidative addition of  $\text{H}_2$ . Shortly after the original report of Wilkinson's catalyst, Osborn and coworkers showed that cationic species of the form  $[\text{M}(\text{cod})(\text{PPh}_3)_2]^+$  ( $\text{M} = \text{Rh}, \text{Ir}$ ;  $\text{cod} = 1,5\text{-cyclooctadiene}$ ) readily react with molecular hydrogen to form the corresponding metal-dihydrido salts, with concurrent release and reduction of the coordinated

diene to the alkane (Scheme 1.3.2).<sup>19-21</sup> Although not depicted here, other common solvents such as ethanol or acetone could also be used to furnish the dihydride salts. These trivalent monocationic species were shown to be effective catalysts for the hydrogenation of terminal olefins, with higher rates of reaction in comparison with Wilkinson's catalyst. However, the catalysts suffer from the same essential problems as Wilkinson's catalyst with respect to substitution of the olefinic group. Additionally, the use of coordinating solvents such as acetonitrile inhibits catalytic activity.<sup>19</sup>

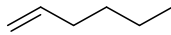
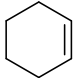
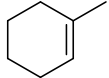
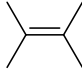


**Scheme 1.3.2: Formation of catalytically active cationic Rh(III)- and Ir(III)-dihydride species.**

### 1.3.2.2 Crabtree's Catalyst

As discussed above, the use of coordinating solvents in the Schrock-Osborn catalysts led to inhibition of reactivity and it was posited by Robert Crabtree and George Morris that the ligand dissociation step was limiting in these homogeneous systems.<sup>22</sup> In 1977, Crabtree and Morris reported on the synthesis of air-stable cationic iridium catalysts of the form [Ir(cod)(py)L][PF<sub>6</sub>] (py = pyridine; L = <sup>i</sup>Pr<sub>3</sub>P, PPh<sub>3</sub>, PCy<sub>3</sub>), whereby the active site of the catalyst is created by the irreversible loss of a ligand in a non-coordinating solvent such as CH<sub>2</sub>Cl<sub>2</sub>.<sup>23,24</sup> These cationic species have been demonstrated to outperform Wilkinson's catalyst as well as the Schrock-Osborn systems in the hydrogenation of terminal and internal disubstituted olefins, while also being the only catalyst of the three that can effectively and rapidly hydrogenate tri- and tetra-substituted olefins, thus giving birth to a new class of highly active hydrogenation catalysts (Table 1.3.1).<sup>22</sup>

**Table 1.3.1: Rates<sup>a</sup> of hydrogenation of variously substituted olefins with different catalyst types.**

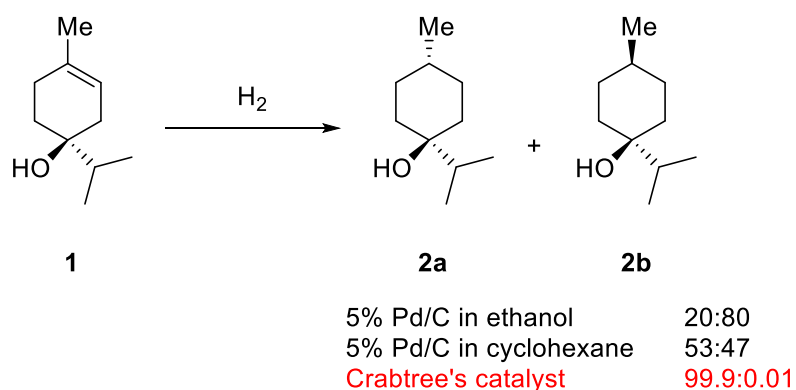
Catalyst precursor	Temp. (°C)	Solvent	Substrates			
						
[Ir(cod)PCy <sub>3</sub> (py)][PF <sub>6</sub> ]	0	CH <sub>2</sub> Cl <sub>2</sub>	6400	4500	3800	4000
[Ir(cod)(PMePh <sub>2</sub> ) <sub>2</sub> ][PF <sub>6</sub> ]	0	CH <sub>2</sub> Cl <sub>2</sub>	5100	5100	1900	50
	0	Me <sub>2</sub> CO	~10	0	0	0
[Rh(cod)(PPh <sub>3</sub> ) <sub>2</sub> ][PF <sub>6</sub> ]	25	CH <sub>2</sub> Cl <sub>2</sub>	4000	10	-	0
[RuHCl(PPh <sub>3</sub> ) <sub>3</sub> ]	25	C <sub>6</sub> H <sub>6</sub>	9000	7	-	0
[RhCl(PPh <sub>3</sub> ) <sub>3</sub> ]	25	C <sub>6</sub> H <sub>6</sub> /EtOH	650	700	13	0
	0		60	70	-	0

<sup>a</sup> In units of [(mol of substrate) (mol of catalyst)<sup>-1</sup> h<sup>-1</sup>]

The operative mechanism of the Crabtree catalyst is similar to that described for Wilkinson's catalyst. Activation of the catalyst proceeds *via* oxidative addition of dihydrogen to the air-stable [Ir(cod)PCy<sub>3</sub>(py)][PF<sub>6</sub>] to yield a dihydrido species similar to those described in Scheme 1.3.2.<sup>25</sup> This is followed by a rapid reduction and elimination of the coordinated diene ligand to furnish the catalytically active species. The reaction then proceeds through successive cycles of olefin ligation, dihydrogen activation, and reduction. Unfortunately, this mechanism does not account for the increased activity of Crabtree's catalyst with respect to tetra-substituted olefins. Recent studies have postulated different mechanisms for this challenging substrate.<sup>26</sup> The currently accepted model proposes an Ir(III)/Ir(V) cycle wherein coordination of the olefin to the Ir(III)-dihydride species is followed by the coordination and oxidative addition of a second molecule of dihydrogen.<sup>27</sup> This highly acidic Ir(V) species then protonates the olefin and furnishes a

trihydride-alkyl cation that finally releases the reduced alkane by reductive elimination, thus reforming the Ir(III) intermediate.

Crabtree's catalyst was also found to be influenced by various directing groups in the diastereoselective reduction of terpen-4-ols (Scheme 1.3.3). This is due to the haptophilicity of the hydroxyl group, or in other words, the ability of the hydroxyl group to direct the reaction through binding to a secondary agent, such as the surface of a heterogeneous catalyst.<sup>28</sup> In the reduction of **1**, the use of palladium on carbon in ethanol under relatively severe conditions (50 °C, 7 atm H<sub>2</sub>) leads to a product distribution of 20:80 in favour of the *cis*-isomer **2b** given that reduction occurs preferentially on the less-hindered face of the molecule. By contrast, using [Ir(cod)py(PCy<sub>3</sub>)]PF<sub>6</sub> leads to an almost quantitative formation of isomer **2a** under very mild conditions (0 °C, 1 atm H<sub>2</sub>).<sup>29</sup> This change in selectivity is attributed to the complexation of the hydroxyl oxygen atom to the iridium center, thus "locking" the olefin in place and presenting only one face of the substrate molecule to the catalyst.<sup>30</sup> Furthermore, it was found that carbonyl groups are also capable of directing hydrogenation in order to achieve diastereoselectivity.<sup>31</sup>

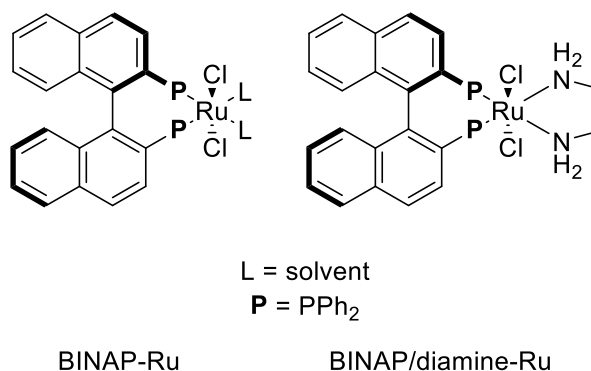


**Scheme 1.3.3: Substrate-directed diastereoselective reduction of terpen-4-ol.**

### 1.3.2.3 Noyori Catalyst

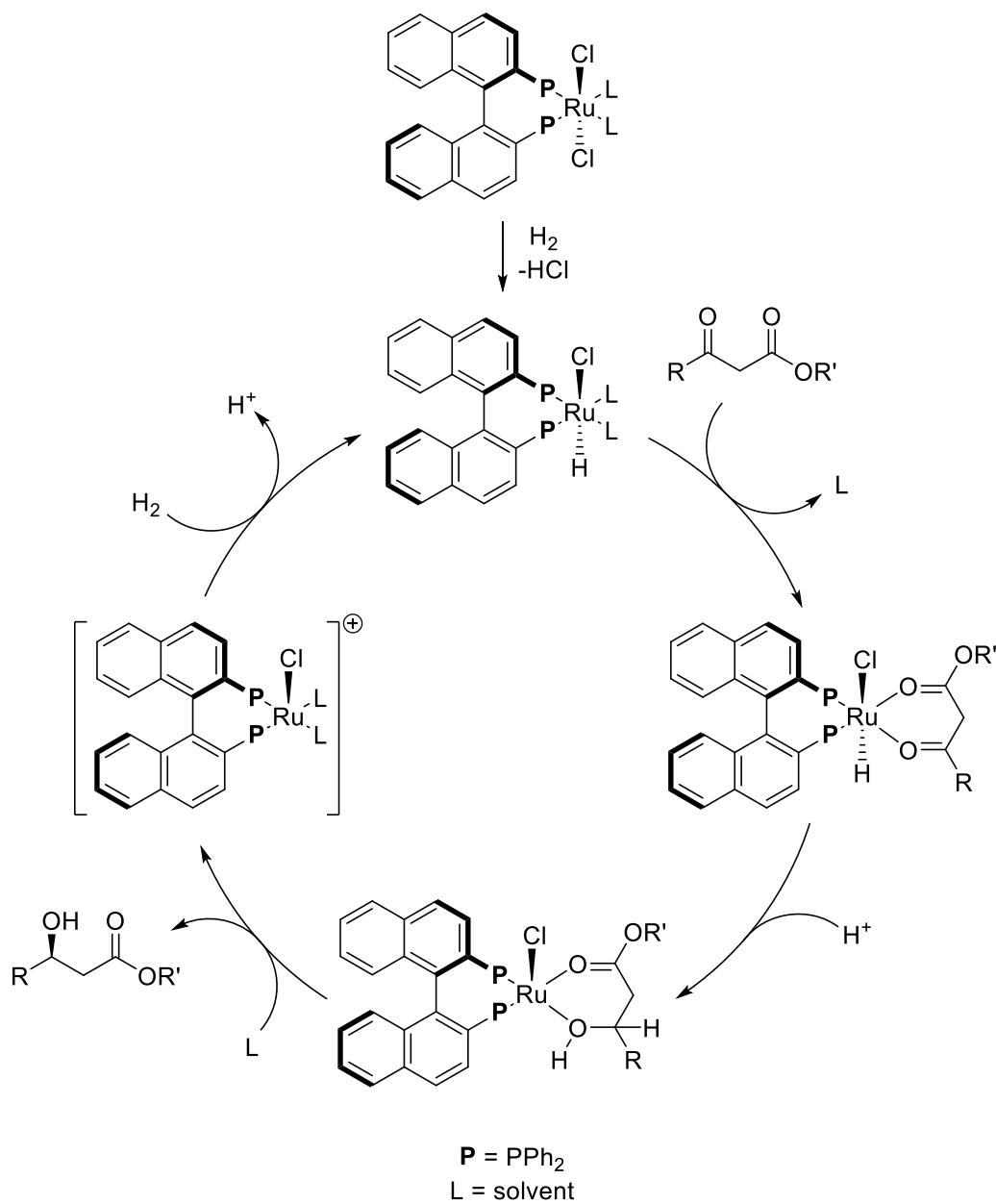
Concurrent with the work of Robert Crabtree, others have made significant contributions to the field of homogeneous hydrogenation. In particular, Noyori and Knowles were each awarded the Nobel Prize in Chemistry in 2001 for their ground-breaking efforts in asymmetric hydrogenation, along with Sharpless for work on chiral oxidation catalysis.<sup>32–34</sup> While the stoichiometric, asymmetric reduction of ketones was previously known<sup>35</sup>, Noyori *et al.* developed a practical

catalytic approach.<sup>36</sup> Two versions of the catalyst were developed with different selectivity (Figure 1.3.1).<sup>37,38</sup>

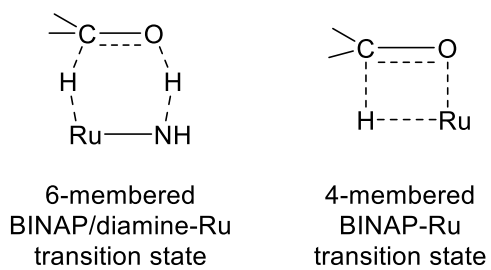


**Figure 1.3.1: Noyori's asymmetric ketone hydrogenation catalysts.**

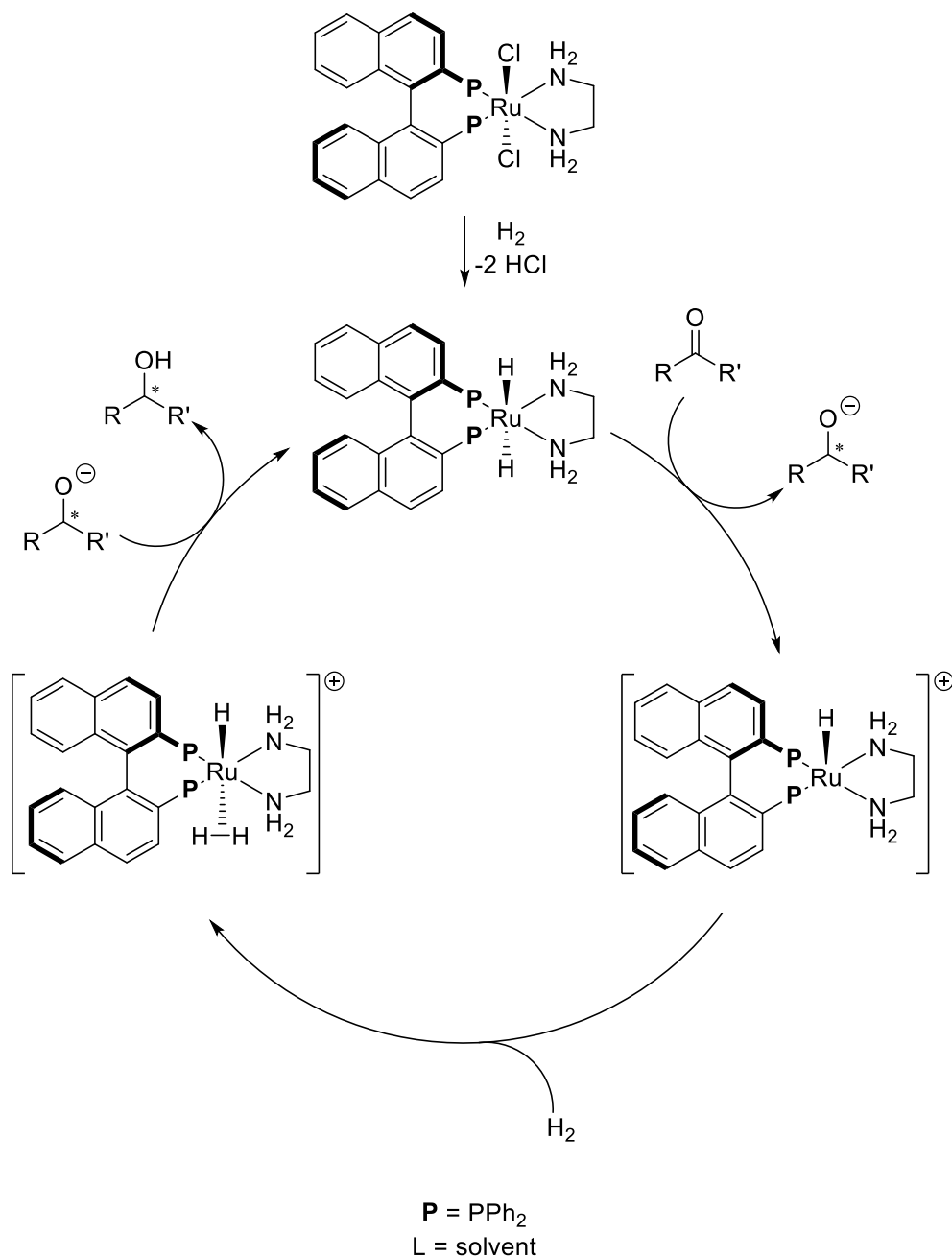
The BINAP-Ru catalyst effects the hydrogenation of  $\alpha,\beta$ -functionalized ketones and is limited to substrates with nearby heteroatoms. The mechanism (Scheme 1.3.4) of reduction involves the reaction of the precatalyst with dihydrogen to form the hydrido-chloride catalytic species with concurrent loss of HCl. Subsequent coordination of the  $\alpha,\beta$ -functionalized ketone is followed by concerted proton and hydride delivery to form the alcohol product, which is then released. Activation of dihydrogen by the resulting cationic species regenerates the active catalyst. The BINAP/diamine-Ru catalyst, on the other hand, is effective in the reduction of both simple ketones,<sup>39</sup> as well as olefinic, aromatic, and heteroaromatic ketones.<sup>40</sup> The reason for the difference in reactivity is due to the difference in the transition states of the two catalysts (Figure 1.3.2). The BINAP-Ru catalyst proceeds through a 4-membered transition state. Conversely, the BINAP/diamine-Ru system is stabilized *via* a 6-membered transition state that involves the diamine ligand. As a result, the mechanism (Scheme 1.3.5) involves the non-innocent diamine ligand in the activation of dihydrogen and reduction of the ketone substrate.



**Scheme 1.3.4: BINAP-Ru catalyzed asymmetric hydrogenation of functionalized ketones.**



**Figure 1.3.2: Transition states of the BINAP/diamine-Ru and BINAP-Ru catalysts.**



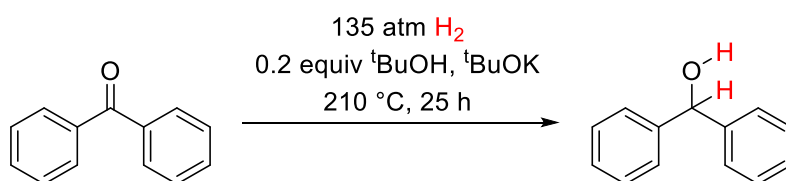
**Scheme 1.3.5: BINAP/diamine-Ru catalyzed asymmetric hydrogenation of simple ketones.**

## 1.4 Metal-Free Hydrogenation

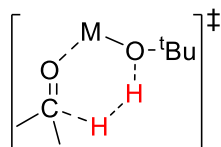
### 1.4.1 Main-Group Catalysis

Motivated by the cost, toxicity and rarity of precious metals, the field of hydrogenation chemistry continues to evolve. Given the history discussed above, chemical principles dictated the necessity of transition metals for hydrogenation catalysis. However, a very early and

breakthrough example of hydrogenation in the absence of transition metal species was reported by Bollyky and Walling in 1964.<sup>41</sup> They describe the use of bases such as potassium *tert*-butoxide in alcoholic solvents to effect the reduction of ketones (Scheme 1.4.1). A study of the kinetics of this reaction revealed that it is first-order in all three reactants, thus suggesting a six-membered transition state (Figure 1.4.1).<sup>42</sup> While the conditions for this transformation are significantly harsher in comparison to those used by Wilkinson and Crabtree at the time, it illustrates that transition metals don't necessarily hold a monopoly when it comes to hydrogenation.

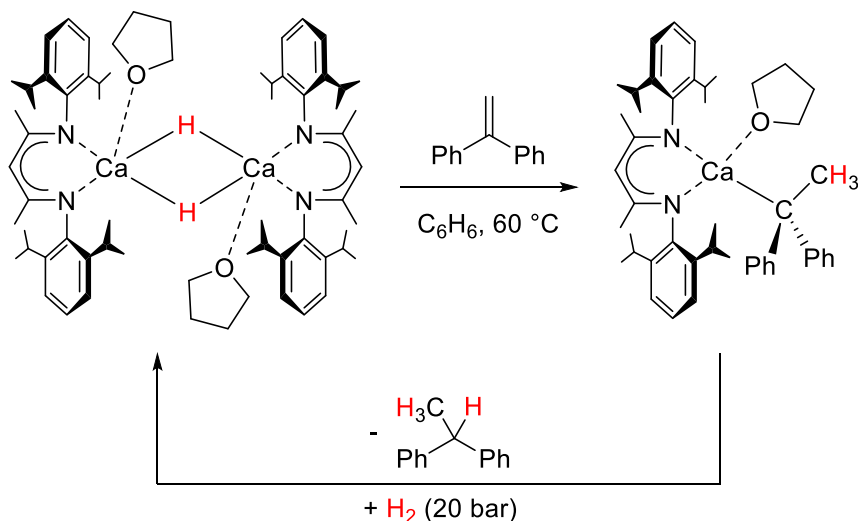


**Scheme 1.4.1: Early example of transition metal-free reduction of unsaturated substrates.**



**Figure 1.4.1: Proposed six-member transition state involved in the reduction of ketones using *t*BuOK catalyst.**

In the first decade of the 21<sup>st</sup> century, two crucial findings further elevated the role of main-group elements in hydrogenation reactions. In 2008, Harder and coworkers described an unprecedented process by which olefins can be reduced to alkanes using a calcium-based catalyst under relatively mild reaction conditions (Scheme 1.4.2).<sup>43</sup> This seminal work was followed by another strategy employing LiAlH<sub>4</sub> to reduce imines.<sup>44</sup>

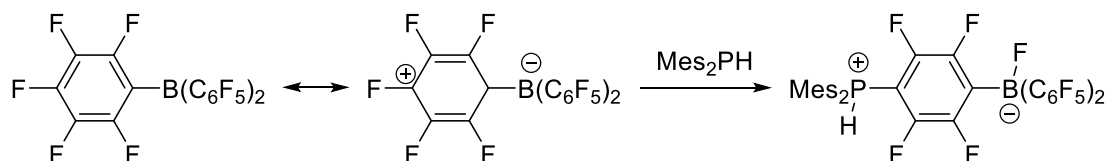


**Scheme 1.4.2: Reduction of olefins using Ca(nacnac)-based catalysts.**

### 1.4.2 Frustrated Lewis Pairs (FLP)

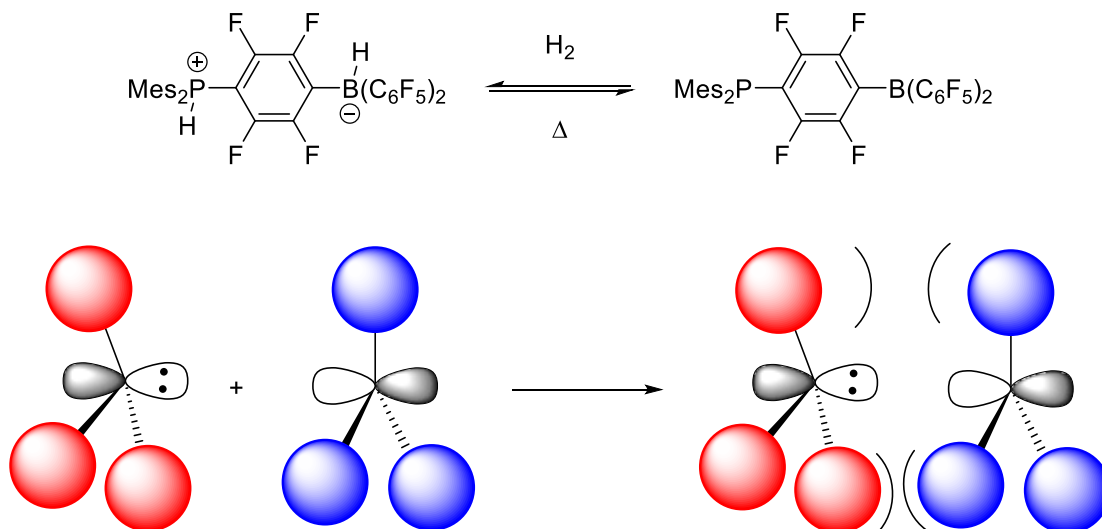
In 1923, Gilbert Lewis proposed a description of acids and bases that categorized molecules as electron acceptors and electron donors that has become vital to our understanding and interpretation of main group and transition metal chemistry.<sup>45</sup> One of the main consequences of such a description is the formation of Lewis acid-base adducts that arise from the combination of Lewis acids and bases; a simple demonstration is the adduct ammonia-borane,  $\text{NH}_3 \cdot \text{BH}_3$ , formed when the Lewis acid borane ( $\text{BH}_3$ ) is reacted with the Lewis base ammonia ( $\text{NH}_3$ ). This simple concept of Lewis pair adducts forms the basis of transition metal complexes and is an integral part of their role in a catalytic cycle, owing to the association and dissociation of various Lewis basic ligands, substrates, or products to and from the Lewis acidic metal center. Furthermore, Lewis' principles of acid-base reactions also extend to the realm of surface science and solid-state chemistry to account for the adsorption of materials onto surfaces or within cavities.

In 2006, Welch and Stephan discovered the inability of sterically hindered Lewis acids and bases to form classical Lewis adducts.<sup>46</sup> Instead, the Lewis base in question was shown to undergo nucleophilic attack at the *para*-positions of the chosen Lewis acid, affording an air- and moisture-stable zwitterionic salt (Scheme 1.4.3).



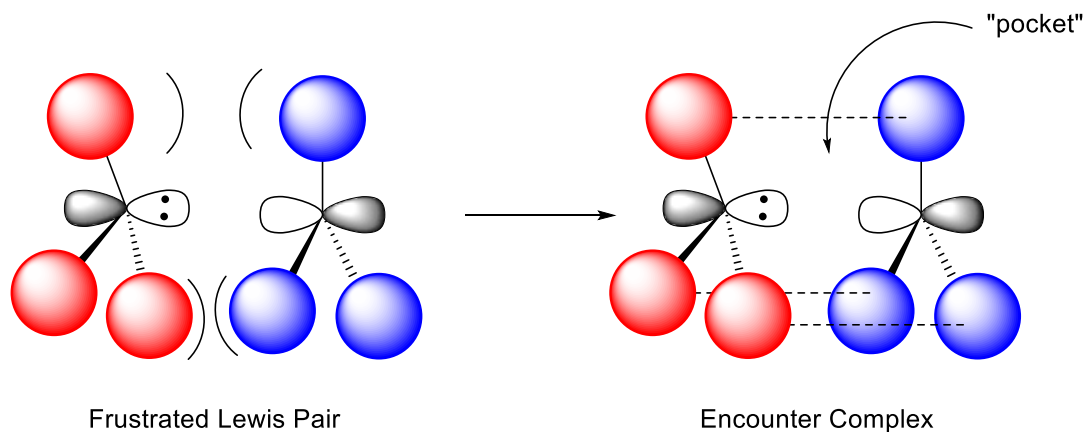
**Scheme 1.4.3: Nucleophilic attack of Lewis base at Lewis acid resulting from the preclusion of adduct formation.**

Further studies demonstrated that, upon exchange of the B-F fluoride with hydride using silanes, the resulting zwitterions can reversibly activate dihydrogen (Scheme 1.4.4, top).<sup>46</sup> While this discovery involved the use of intramolecular Lewis acids and bases, it was followed by a much less esoteric study in 2007 that reported the use of bulky donors such as tris(*tert*-butyl)phosphine ( $\text{tBu}_3\text{P}$ ) or trimesitylphosphine ( $\text{Mes}_3\text{P}$ ) as well as bulky acceptors such as tris(pentafluorophenyl)borane ( $\text{B}(\text{C}_6\text{F}_5)_3$  or BCF) in the activation of  $\text{H}_2$  at ambient temperatures.<sup>47</sup> In both cases, it is the inability to form classical Lewis acid-base adducts that provides unquenched reactivity (Scheme 1.4.4, bottom), allowing the acid and base to receive and donate electron density to the  $\text{H}_2$  molecule. These special combination of sterically “frustrated” Lewis acids and bases gave birth to the term, and field, of frustrated Lewis pair (FLP) chemistry.<sup>48</sup>



**Scheme 1.4.4: Intermolecular FLP activation of dihydrogen (top) and generalized description of FLPs with preclusion of adduct formation as a result of steric bulk.**

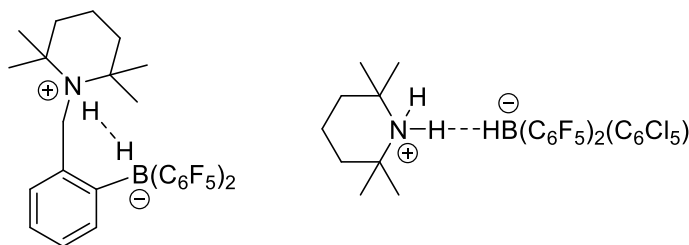
The mechanism of FLP activation of dihydrogen has been extensively studied computationally.<sup>49–54</sup> Two significant and currently accepted models were proposed by Stefan Grimme<sup>55,56</sup> and Imre Pápai.<sup>57,58</sup> In the former, an electric field model is proposed in which the sterically hindered Lewis pairs create a homogeneous electric field between them. Thus, the exposure of H<sub>2</sub> to this electric field causes heterolytic cleavage of the dihydrogen bond. Pápai, on the other hand, has proposed an electron-transfer model postulating that the electrons in the  $\sigma$ -bond of the H<sub>2</sub> molecule act as a Lewis base and forms an adduct with the Lewis acid, while the Lewis base simultaneously donates electrons into the  $\sigma^*$ -orbital of H<sub>2</sub>, thus resulting in heterolytic cleavage of the bond. Despite the differences between the two models, there is consensus regarding the existence of an “encounter complex”. The encounter complex is the result of a lack of dative bond formation between the Lewis acid and the Lewis base, creating a “pocket” for small molecules to enter, akin to the active site of enzymes. The formation and relative thermodynamic stability of this complex is attributed to the non-covalent interactions between the sterically congested substituents on the acid and base (Scheme 1.4.5).<sup>59</sup>



**Scheme 1.4.5: Depiction of the formation of the encounter complex with active "pocket" for dihydrogen activation.**

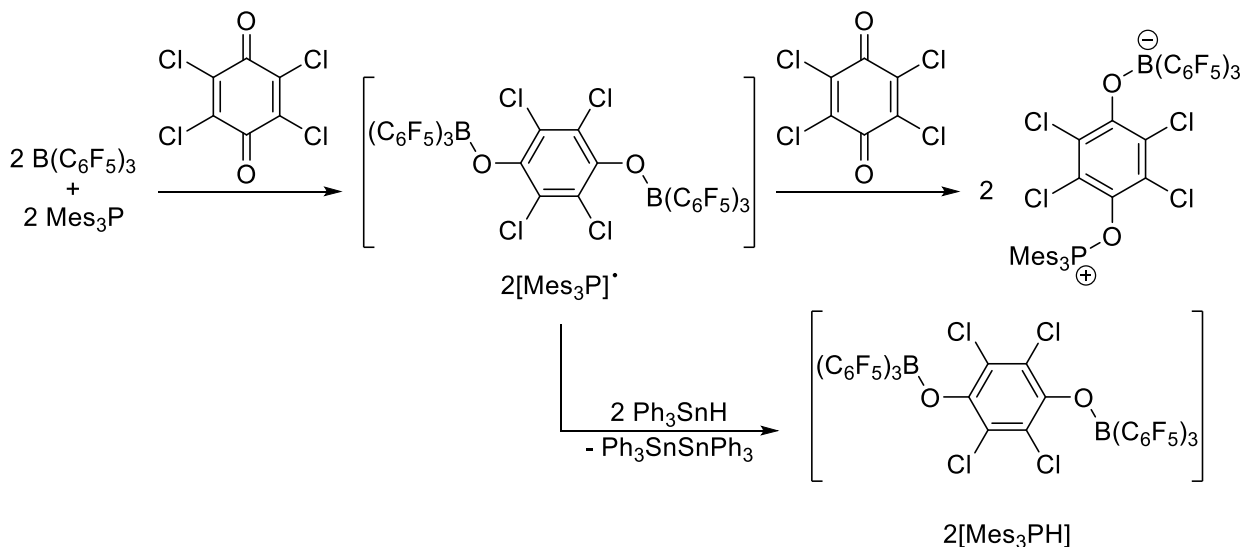
Experimental evidence for the existence of the encounter complex exists.<sup>60</sup> Using <sup>19</sup>F{<sup>1</sup>H} HOESY NMR experiments, a mixture of BCF and R<sub>3</sub>P (R = <sup>t</sup>Bu, Mes) shows through-space interactions between the proton nuclei of the phosphine substituent and fluorine nuclei of the C<sub>6</sub>F<sub>5</sub> rings. Additionally, Repo and Rieger have reported a close contact distance of 1.674(8) Å between the hydride and proton of an intramolecular FLP while Ashely *et al.* have made similar

observations in an intermolecular FLP system with a proton-hydride contact distance of 1.805(1) Å (Figure 1.4.2).<sup>61,62</sup>



**Figure 1.4.2: Close contact distances in intra- and intermolecular FLPs providing evidence of "pocket" in encounter complex.**

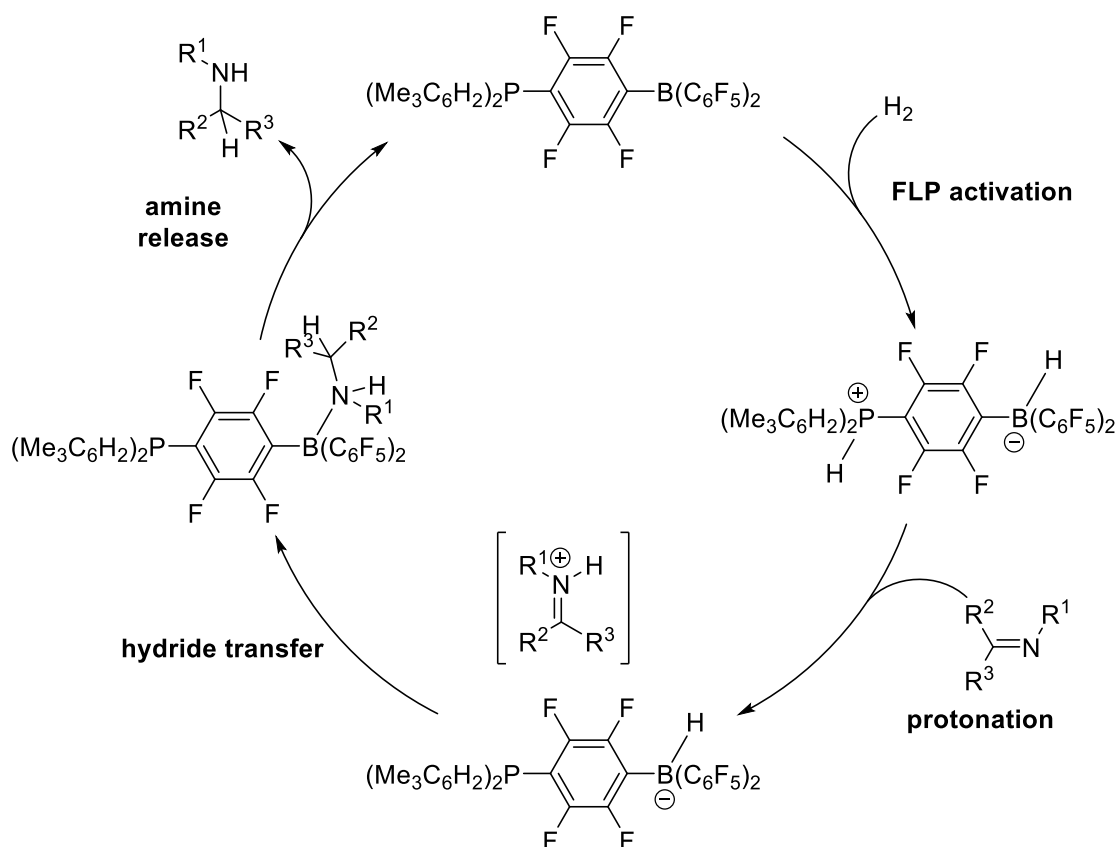
While the notion of heterolytic cleavage of dihydrogen has been accepted for some time, a recent report from Stephan and coworkers has proposed a new activation pathway involving single electron transfer (SET) mechanisms.<sup>63</sup> It has been shown that the reactions of  $\text{Mes}_3\text{P}$  and  $\text{E}(\text{C}_6\text{F}_5)_3$  ( $\text{E} = \text{B}, \text{Al}$ ) produce a radical phosphonium cation, indicating a SET pathway. In the case of  $\text{B}(\text{C}_6\text{F}_5)_3$ , the radical phosphonium species can be isolated *via* the use of a radical trap such as  $\text{Ph}_3\text{SnH}$ , yielding the dimer  $\text{Ph}_3\text{SnSnPh}_3$  and the phosphonium salt  $[\text{Mes}_3\text{PH}][\text{HB}(\text{C}_6\text{F}_5)_3]$ . Furthermore, the radical intermediate formed from the reaction of  $\text{Mes}_3\text{P}$  and  $\text{B}(\text{C}_6\text{F}_5)_3$  can be observed with the use of tetrachloro-1,4-benzoquinone and the radical phosphonium can once again be trapped with tin-hydrides (Scheme 1.4.6). On the other hand, the reaction of  $\text{Ph}_3\text{SnH}$  with  ${}^t\text{Bu}_3\text{P}$  and  $\text{B}(\text{C}_6\text{F}_5)_3$  only results in the heterolytic cleavage of the Sn-H bond and affords  $[\text{Ph}_3\text{SnP}^t\text{Bu}_3][\text{HB}(\text{C}_6\text{F}_5)_3]$ .



**Scheme 1.4.6: Formation and trapping of radical FLPs.**

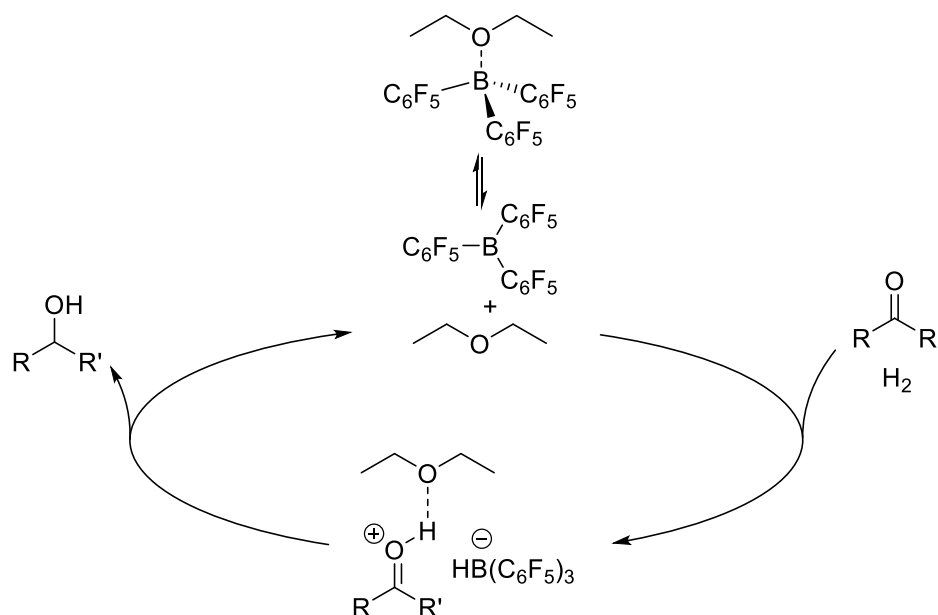
### 1.4.3 FLP Hydrogenations

The developments in FLP chemistry have paralleled the evolution of transition metal catalysis some 50-60 years ago and have accelerated dramatically in the last decade. Indeed, the FLP chemistry of a variety of acid-base combinations and applications towards capture and activation of a wide range of small molecules have been reviewed by multiple authors.<sup>59,64–69</sup> Shortly after the initial discovery of FLP activation of dihydrogen, Stephan *et al.* reported on the catalytic reduction of imines, aziridines, and protected nitriles.<sup>70</sup> In this case, the substrate acts as the Lewis base, eliminating the need for an external phosphine base. The mechanism of this hydrogenation reaction, using an imine substrate for illustration (Scheme 1.4.7), is proposed to proceed *via* heterolytic cleavage of dihydrogen by the FLP, yielding the protonated imine with concurrent generation of the hydride at the Lewis acid. Subsequently, transfer of the hydride to the iminium intermediate furnishes the reduced product and regenerates the Lewis acid.<sup>46,56,71</sup>



**Scheme 1.4.7: Mechanism of FLP-catalyzed hydrogenation of imines.**

Recently, the groups of Stephan and Ashley simultaneously reported on the use of  $\text{B}(\text{C}_6\text{F}_5)_3$  in the hydrogenation of ketones and aldehydes in ethereal solvents.<sup>72,73</sup> The mechanism first involves the dissociation of the borane-ether adduct, followed by  $\text{H}_2$  activation between the Lewis acidic borane and Lewis basic ethereal solvent. The highly acidic solvent-derived oxonium cation then protonates the carbonyl substrate and subsequent hydride transfer to the substrate-derived oxonium salt furnishes the alcohol product and relinquishes free  $\text{B}(\text{C}_6\text{F}_5)_3$  (Scheme 1.4.8).



**Scheme 1.4.8: Proposed catalytic cycle for the FLP reduction of ketones and aldehydes.**

To illustrate the wider utility of frustrated Lewis pairs in hydrogenation chemistry, various groups have demonstrated the reduction of olefins,<sup>74–76</sup> enamines and enones,<sup>77,78</sup> N-heterocycles,<sup>79</sup> and arenes,<sup>80</sup> among others.<sup>81</sup>

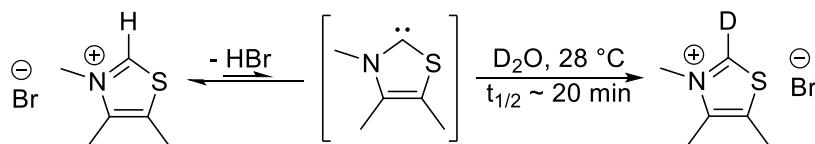
## 1.5 N-Heterocyclic Carbenes (NHC)

### 1.5.1 History of NHC Carbenes

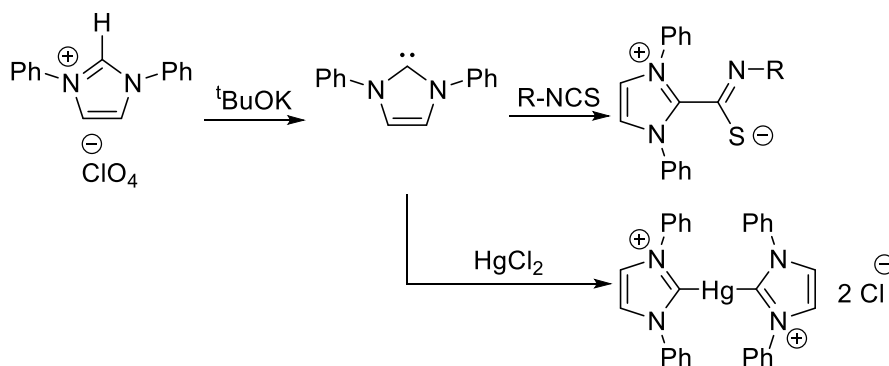
Carbenes have been reported in scientific literature as early as 1903, postulated by Eduard Buchner and Leon Feldmann in the cyclopropanation studies of ethyl diazoacetate with toluene.<sup>82</sup> In 1912, Hermann Staudinger reported on the  $\text{:CH}_2$  intermediate in the cyclopropanation reaction of alkenes using diazomethane.<sup>83</sup> Little would Buchner and Staudinger know of the efforts that were to follow and the impact such molecules were to have on the field of chemistry, both academically and industrially. Today, carbenes are commonplace in many chemical transformations as stabilizing ligands.

Carbenes had generally been described as highly reactive species, however, in 1957 Breslow proposed a free carbene intermediate in the exchange of a proton for a furfural residue in the catalytic cycle of benzoin condensation involving vitamin B<sub>1</sub>.<sup>84</sup> The thiazolium moiety involved is observed to exchange a hydrogen atom for deuterium in D<sub>2</sub>O (Scheme 1.5.1). The isolation of

this so-called Breslow intermediate was finally achieved in 2012.<sup>85</sup> Furthermore, in 1970, Wanzlick provided a simple route to the formation of what were to become known as persistent carbenes, although Wanzlick did not isolate the free carbenes but rather obtained them as coordination complexes of mercury and isothiocyanates (Scheme 1.5.2).<sup>86</sup> The reason for the relative stability of these carbenes was attributed, by Wanzlick and Hoffmann, to the aromaticity of the N-heterocyclic ring.<sup>87,88</sup>

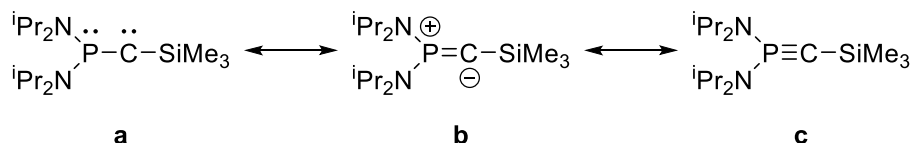


**Scheme 1.5.1: Proposed Breslow intermediate in the hydrogen/deuterium exchange of a trimethylthiazolium salt.**



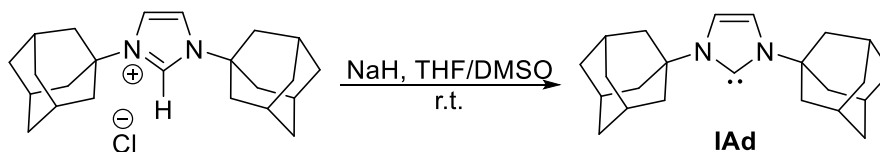
**Scheme 1.5.2: Synthesis and trapping of persistent bis(phenyl)imidazolyidenes.**

Another breakthrough came in 1988 when Bertrand and coworkers isolated a phosphinocarbene compound that was proposed to exist as a mesomeric distribution between the phosphinoacetylene species and phosphino carbene (Scheme 1.5.3).<sup>89,90</sup> At the time, the lack of a solid-state structure of the carbene in question presented doubt as to the true nature of the phosphinocarbene. Indeed, the  $^{13}\text{C}\{^1\text{H}\}$  NMR resonance of the carbenic carbon atom at ~140 ppm indicates a strong degree of multiple bond character between the carbon and phosphorus atoms.



**Scheme 1.5.3: Bertrand's phosphinocarbene (a), its mesomerically-formed phosphinoacetylene (c), and an intermediate zwitterionic species (b).**

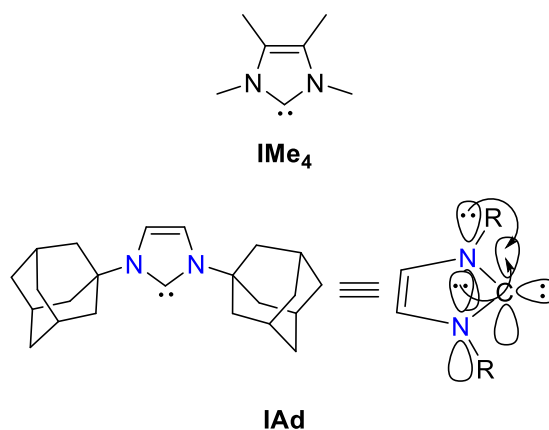
The biggest innovation finally came in 1991 when Arduengo *et al.* reported the synthesis of a stable, isolable, and crystalline free carbene by the deprotonation of an imidazolium chloride with a strong base (Scheme 1.5.4).<sup>91</sup> This carbene became the forerunner for a large class of compounds that would be known as Arduengo-type carbenes or, more generally, N-heterocyclic carbenes (NHC). The bis(adamantyl)imidazolyliene (IAd) was found to be indefinitely stable at room temperature in the absence of water and oxygen and the carbenic carbon presents a characteristic <sup>13</sup>C NMR signal at 211 ppm.<sup>92</sup> The X-ray structure of the compound shows C-N bond lengths that are longer than those in the parent imidazolium salt, indicating some loss of multiple bond character.



**Scheme 1.5.4: Arduengo's synthesis of the first isolable, crystalline and persistent carbene.**

Within the class of compounds known as N-heterocyclic carbenes lie a wide range of substitution patterns, ring sizes, and degrees of heteroatom stabilization. However, a general depiction of the IAd described above is shown below. While it was initially proposed that the steric properties of the adamantyl groups are responsible for the remarkable stability of the carbene, it is now understood to provide a relatively minor contribution. As a follow-up, Arduengo and coworkers have shown that the tetramethylimidazolyliene (IME<sub>4</sub>) compound is also stable, despite lacking the steric congestion of the bis(adamantyl) analogue (Figure 1.5.1).<sup>93</sup> NHC carbenes were generally found to be thermodynamically stable. The relative electronegativity of the nitrogen atoms results in inductive  $\sigma$ -withdrawing of the electrons in the  $\sigma$ -type orbital on the carbenic carbon while the  $\pi$ -electrons of the nitrogen centers mesomerically donate into the empty  $\pi$ -type orbital of the central carbon (Figure 1.5.1). These findings show that the carbene is best

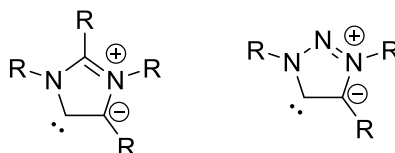
described with a singlet ground state structure and that the carbenic atom features a lone-pair in a formally  $sp^2$ -hybridized orbital as well as an empty, unhybridized  $p$ -orbital. Additionally, the constraint of the carbene as a result of the 5-membered ring framework helps force the central carbon into a more  $sp^2$ -like arrangement.



**Figure 1.5.1: The stable tetramethylimidazolyliidene carbene (top) and depiction of mesomeric and inductive stabilization of Arduengo's carbene (bottom).**

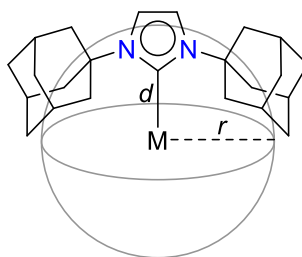
The above general principles apply to all NHC carbenes, but the relative importance of each individual factor will differ greatly between subclasses of these compounds. NHCs derived from heteroaromatic compounds such as imidazoles and oxazoles benefit from a significant degree of stabilization as a result of their partial aromaticity; this stabilization effect has been calculated to be on the order of  $25 \text{ kcal mol}^{-1}$  for imidazolyliidenes, thus enabling the use of less sterically demanding substituents on the central 5-membered ring.<sup>94</sup> On the other hand, many persistent carbenes exhibit the same stability without the need for aromaticity. The first example of such a compound, 1,3-di(mesityl)imidazolin-2-ylidene (SIMes), was presented by Arduengo in 1995.<sup>95</sup> Furthermore, there is no need for both heteroatoms to be nitrogen, as many examples of stable carbenes exist that substitute one of the nitrogen atoms with sulfur or oxygen atoms.<sup>96</sup> Incredibly, Bertrand and coworkers have shown that stable carbenes can be made without the need for two heteroatoms.<sup>97</sup> These carbenes, formally based on pyrrolidines, are referred to as cyclic(alkyl)(amino)carbenes (CAAC) and display comparatively unusual reactivity. The absence of the second heteroatom provides the carbenic carbon with reduced  $\pi$ -donation into the empty  $p$ -orbital while at the same time reducing the  $\sigma$ -withdrawing effect of the heteroatoms.<sup>98</sup> Thus, CAACs are slightly more nucleophilic while being significantly more electrophilic than

NHCs. Additionally, other carbenes bearing only one adjacent heteroatom can be synthesized. Mesoionic, or “abnormal”, carbenes are a class of compounds for which a non-zwitterionic resonance form cannot be drawn (Figure 1.5.2). Consequently, these carbenes are generally more nucleophilic than their “normal” analogues but can present vastly different reactivity.<sup>99,100</sup>



**Figure 1.5.2: General depiction of mesoionic carbenes: abnormal imidazolylidene (left) and 1,2,3-triazolylidene (right).**

Two of the most common descriptive parameters associated with carbenes are their buried volume ( $\%V_{\text{bur}}$ ) for steric effects and Tolman electronic parameter (TEP) for electronic effects.<sup>101,102</sup> Buried volume is analogous to the cone angle metric of phosphine ligands: the sphere occupied by the substituents on the carbene provide an estimated measure of the steric congestion around the metal center to which the carbene is coordinated (Figure 1.5.3). TEP, on the other hand, provides a measure of the nucleophilicity of the carbene ligand. Originally developed for phosphines, the carbene or phosphine ligand in question is coordinated to a metal carbonyl complex such as  $\text{Ni}(\text{CO})_4$  and the infrared stretching frequency of the carbonyl ligands in the resulting complex is measured. The degree to which the C-O bond is weakened relative to free  $\text{Ni}(\text{CO})_4$  gives an estimate of the electron-donating capability of the ligand.

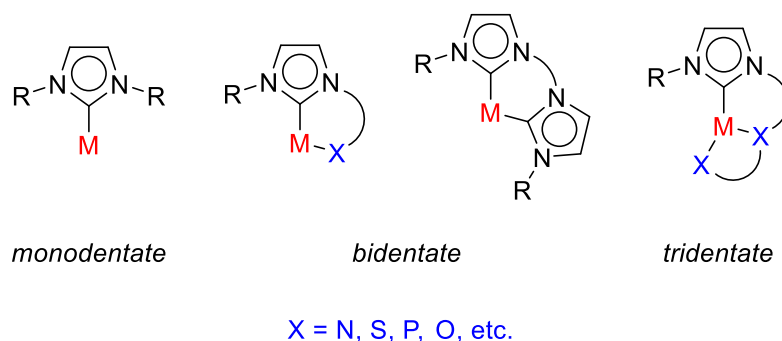


**Figure 1.5.3: Depiction of sphere created by the carbene substituents.  $\%V_{\text{bur}}$  is the percentage of this sphere that is occupied by the ligand ( $d$  = the metal-carbene bond,  $r$  = radius of the sphere).**

Since their first isolation in 1991, NHCs have become an integral part of the chemistry of many transition metals, as well as organocatalysts in their own right and many research groups have made formative contributions to the understanding of structure, coordination, and reactivity of these compounds and to applications in many varied fields.<sup>103–105</sup>

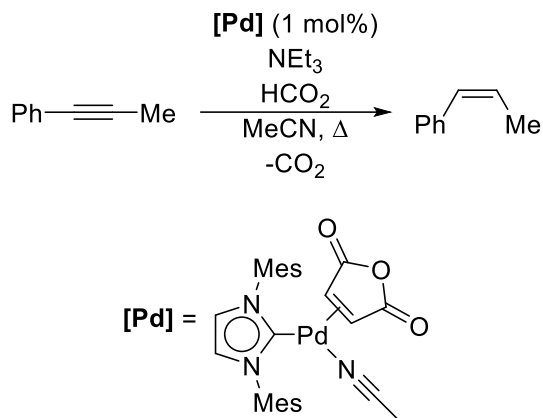
## 1.5.2 NHC Complexes in Hydrogenation

N-heterocyclic carbene ligands are generally defined with respect to their denticity, termed as monodentate, bidentate, and tridentate (Figure 1.5.4). Regarding the latter two, the pendant arm can consist of a variety of electron-donating heteroatoms or even another NHC fragment. As discussed above, these ligands are strong  $\sigma$ -donors and exhibit good  $\pi$ -acidity. Thus, they serve as excellent candidates for the stabilization of transition metal species for a variety of catalytic reactions.<sup>106,107</sup>



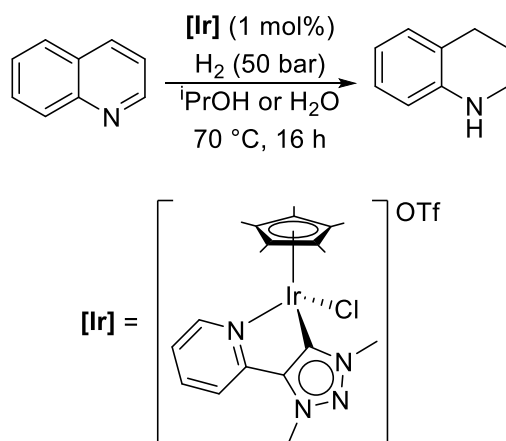
**Figure 1.5.4: Various binding motifs of N-heterocyclic carbene ligands.**

Indeed, since the pioneering work of Herrmann metal-NHC complexes have come to be used in a wide range of catalytic reactions.<sup>108</sup> Herein, the utility of these complexes in hydrogenation chemistry will be discussed. For instance, the partial hydrogenation of alkynes to olefins is a valuable reaction in organic chemistry as it finds extensive use in the synthesis of biologically relevant compounds found in natural products, pharmaceuticals, or fragrance chemicals.<sup>109</sup> Elsevier and coworkers have reported on the selective transfer hydrogenation of alkynes to *cis*-olefins using a Pd(NHC) catalyst and acetic acid as the hydrogen surrogate (Scheme 1.5.5).<sup>110,111</sup> Meanwhile, the same catalyst furnishes complete reduction of the alkyne to the corresponding alkane when treated with dihydrogen gas instead of a surrogate.<sup>112</sup>

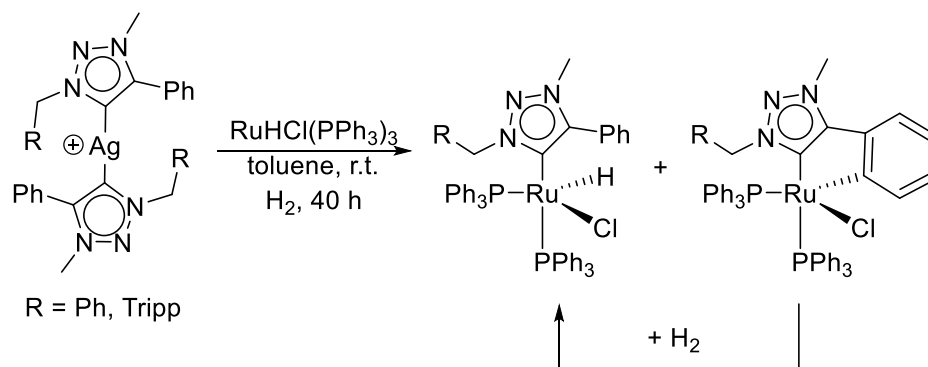


**Scheme 1.5.5: Partial transfer hydrogenation of alkynes catalyzed by Pd-NHC complex.**

As well, Albrecht and Beller have reported the hydrogenation of heteroarenes using iridium(III) catalysts bearing mesoionic, or “abnormal”, carbenes (Scheme 1.5.6).<sup>113</sup> Remarkably, these iridium catalysts with triazolylidene carbene ligands display impressive stability as these reductions are carried out in protic or aqueous solvents. Further examples of hydrogenation take advantage of cyclometalated ligands that, upon addition of an H<sub>2</sub> source, furnish the active metal catalyst. Our group has demonstrated the use of 1,2,3-triazolylidene ligands (Scheme 1.5.7) to hydrogenate a variety of olefinic residues using dihydrogen gas.<sup>114</sup> Similarly, others have shown the ability of cyclometalated transition metal-NHC complexes to activate H<sub>2</sub> or other surrogates and effect the hydrogenation of ketone substrates.<sup>115–117</sup>

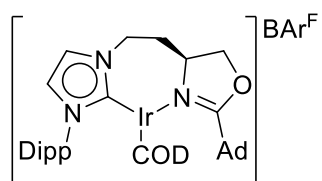


**Scheme 1.5.6: Reduction of heteroarenes using cationic Ir(III) species bearing mesoionic carbene ligands.**



**Scheme 1.5.7: Synthesis of catalytically active cyclometalated Ru-triazolylidene complex for olefin hydrogenation.**

Finally, as is the trend in many other aspects of synthetic chemistry, there has been a concerted effort in the field of asymmetric hydrogenation. This valuable process provides a viable route to stereoselective products that find use in pharmaceutical, agrochemical, and food industries. Herrmann and coworkers also pioneered the use of chiral NHC carbenes for use in asymmetric catalysis<sup>118</sup> and since then many other groups have contributed to the field.<sup>119–121</sup> The first efficient asymmetric hydrogenation catalyst was reported by Burgess and coworkers in 2001, consisting of an Ir(I) species bearing a bidentate NHC carbene (Figure 1.5.5).<sup>122</sup> Since then, many groups have reported catalysts of varying degrees of efficiency, synthetic utility, and substrate selectivity in the asymmetric reduction of alkenes, carbonyls, and imines.<sup>123</sup>

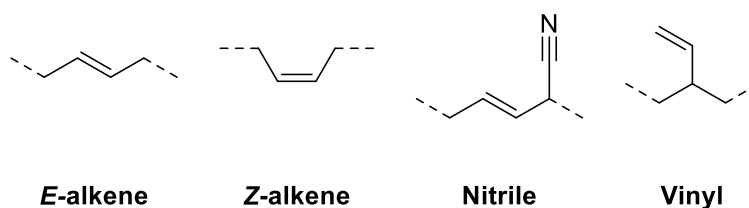


**Figure 1.5.5: Chiral hydrogenation catalyst for asymmetric reduction of alkenes.**

## 1.6 Nitrile Butadiene Rubber

A specific industrial use of catalytic olefin hydrogenation is in the modification of nitrile butadiene rubber (NBR). NBR is a co-polymer of butadiene and acrylonitrile that is synthesized on an industrial scale using anionic emulsion polymerization.<sup>124</sup> The resulting product contains a mixture of *E*- and *Z*-alkene functional groups, as well as vinyl and nitrile groups (Figure 1.6.1). The latter two functional groups confer NBR with many useful properties, such as stability in

oils, fats, and fuels, as well as low permeability and high temperature resistance.<sup>125</sup> Due to these highly desirable properties, NBR is used heavily as a synthetic plastic for machine belts, automotive tubing, and shoe soles. Post-processing of NBR may be achieved *via* selective hydrogenation of the olefinic residues to create hydrogenated NBR (HNBR).<sup>125,126</sup> This polymer has even higher thermal stability compared to NBR as well as improved resistance to ozone and other potent oxidizing agents. As a result, HNBR is also used in automotive applications where thermal stability is desired.



**Figure 1.6.1: Depiction of various functional groups in nitrile butadiene rubber.**

## 1.7 Lanxess Project

Lanxess is a multinational polymers company and a large global manufacturer of NBR and HNBR rubber. In order to facilitate the modifications to NBR described above, Lanxess employs Wilkinson's catalyst for olefin hydrogenation. However, since Wilkinson's catalyst is based on the precious metal rhodium, there are considerable costs associated with this process. Thus, a catalytic system that uses cheaper and more readily obtainable technology would be advantageous and economically beneficial to Lanxess. In an ideal setting, Lanxess would like to produce their own technology to perform the olefin hydrogenation of NBR.

The work presented in this thesis is in part sponsored by Lanxess. As a result, the goals of portions of this thesis are twofold: first, the development of new hydrogenation catalysts that are derived from less expensive materials; second, the development of new hydrogenation catalysts that are distinct from any current patented technology. The majority of this thesis will focus on the development of novel olefin hydrogenation catalysts. While a large library of metal-carbene complexes exists for olefin hydrogenation, there is a gap in the literature with respect to N-phosphorylated N-heterocyclic carbene (NHCP) ligands and their utility as electron-rich and/or bifunctional ligands in olefin hydrogenation. Furthermore, metal-free alternatives to dihydrogen

activation and delivery to unsaturated substrates will also be explored, as they present less expensive and more environmentally-friendly alternatives to metal complexes.

## 1.8 Scope of this Thesis

The goal of this thesis is to develop proprietary olefin hydrogenation catalysts that could affect the hydrogenation of NBR to HNBR. Realizing a gap in the use of NHCP as transition-metal ligands, an effort was made to explore their use in the synthesis and application of novel olefin hydrogenation catalysis. In Chapter 2, the coordination chemistry of NHCP ligands is explored. The reactivity of these complexes towards small molecules such as dihydrogen and silanes are explored. Additionally, the catalytic activity of the prepared compounds will be probed.

Chapter 3 describes cationic ruthenium-NHCP complexes and the utility of the pendant phosphine moiety as a bifunctional catalytic system is explored. The motivation was to easily prepare new active species from readily available starting materials. It was discovered that NHCP ligands used in this context undergo rare rearrangement reactions to furnish new products. Due to the unique nature of their rearrangement, this portion was further studied as it was believed it could provide insights into the degradation pathways of catalysts and shed light on new synthetic approaches in the development of more robust catalysts.

Finally, Chapter 4 describes the exploration of metal-free systems in hydrogenation catalysis by utilizing frustrated Lewis pairs (FLP) derived from trityl Lewis acids and phosphorus- and nitrogen-based Lewis bases. Additionally, these FLP systems were also used in the activation of other element-hydrogen bonds.

The work described herein was completed solely by the author with the exception of collaborative efforts listed below, as well as elemental analyses which were completed in-house by departmental staff.

## 1.9 Contributions to Knowledge

### 1.9.1 Relevant Publications

Portions of this thesis are published or in preparation at time of writing.

#### **Chapter 2:**

Mosaferi, E., Pan, L., Wang, T., Sun, Y., Pranckevicius, C., Stephan, D. W. "Preparation and Reactivity of a Ru(0)-Phosphino-Carbene Complex." *Dalton Trans.*, **2016**, 46, 1354-1358.

### Chapter 3:

Mosaferi, E., Stephan, D. W. "Unusual Rearrangement and Reactivity of Ru-NHCP Half-Sandwich Complexes." *Manuscript in preparation*.

### Chapter 4:

Mosaferi, E., Ripsman, D., Stephan, D. W. "The air-stable carbocation salt [(MeOC<sub>6</sub>H<sub>4</sub>)CPh<sub>2</sub>][BF<sub>4</sub>] in Lewis acid catalyzed hydrothiolation of alkenes." *Chem. Commun.*, **2016**, 52, 8291-8293.

## 1.9.2 Conference Presentations

"Synthesis, Characterization, and Reactivity of a Ru(0)-Phosphino-Carbene Complex". Oral presentation at ACS National Conference in Boston, MA, August 2015

"Carbocations as Efficient Metal-Free Lewis Acids for the Hydrothiolation of Alkenes". Poster presentation at IRTG Symposium in Toronto, CA, April 2015; and in Pacificchem Conference in Honolulu, HI, December 2015.

"Synthesis and Reactivity of Novel Ru-NHCP Complexes". Oral presentation at CSC Conference in Toronto, CA, May 2017.

## 1.9.3 Undergraduate Mentoring

During my time in the Stephan group I had the good fortune of being mentored and guided by intelligent and caring graduate student peers as well as post-doctoral fellows in the group. Thus, I wished to pass on the same level of care and knowledge to younger students who were eager to start their careers in chemistry. First, Denise Peda joined the group as a second-year undergraduate student looking to acquire the basic and necessary technical and critical thinking skills required to succeed in a laboratory setting. Her project consisted of the FLP reduction of disulfide bonds to thiols using dihydrogen. While we were unable to effect such a transformation, I gained valuable information regarding my skills as a mentor. I strived to adapt my teaching to suit her learning needs. These were necessary skills for me, since shortly after

Denise left the group, I had the pleasure of mentoring another student during the summer and subsequent fall term. David Ripsman joined the Stephan lab, also as a second-year student, in the summer of 2015 and we quickly began work on the hydrothiolation of olefins. The initial goal of the project was to catalyze enantioselective addition of thiols to olefins using chiral borenium cations. David quickly discovered the reaction is catalytic in the trityl activating reagent and we proposed to synthesize air-stable trityl cations to carry out the reaction. I used the lessons learned from working with Denise to guide David more efficiently and he very quickly became independent in the lab, making use of Schlenk glassware and techniques as well as the inert gloveboxes. Furthermore, he became versed in analytical and characterization techniques and was able to independently acquire and assign NMR, IR, and MS spectra. Much of David's work is discussed in this thesis and published, as described above.

## Chapter 1 References

- (1) Farmer, B. H. *Mod. Asian Stud.* **1986**, *20*, 175–199.
- (2) Smil, V. *Enriching the Earth: Fritz Haber, Carl Bosch, and the Transformation of the World Food Production*, First Edit.; MIT Press, 2004.
- (3) Smith, B. E. *Science* **2002**, *297*, 1654–1655.
- (4) Crabtree, R. H. *Organometallic Chemistry of the Transition Metals*; Wiley-VCH: Hoboken, New Jersey, 2009.
- (5) Cox, D. L. N. a. M. M. *Principles of Biochemistry*, 3rd Ed.; Worth Publishing: New York, 2000.
- (6) Alt, H. G.; Köppl, A. *Chem. Rev.* **2000**, *100*, 1205–1221.
- (7) Malpass, D. B. *Introduction to Industrial Polyethylene: Properties, Catalysis, and Processes*; Wiley: Massachusetts, 2010.
- (8) Busacca, C. A.; Fandrick, D. R.; Song, J. J.; Senanayake, C. H. *Adv. Synth. Catal.* **2011**, *353*, 1825–1864.
- (9) *Catalysts for Fine Chemical Synthesis, Volume 1: Hydrolysis, Oxidation and Reduction*; Roberts, S. M., Poignant, G., Eds.; John Wiley & Sons: Chichester, England, 2002.
- (10) Hudlicky, M. *Reductions in Organic Chemistry*; American Chemical Society: Washington, DC, 1996.
- (11) Blaser, H.-U. *Top. Catal.* **2010**, *53*, 997–1001.
- (12) Sabatier, P. *Ind. Eng. Chem.* **1926**, *18*, 1005–1008.
- (13) Navalikhina, M. D.; Krylov, O. V. *Russ. Chem. Rev.* **1998**, *67*, 587–616.
- (14) Lindlar, H.; Dubuis, R. *Org. Syn.* **1973**, *5*, 880–882.
- (15) Johnstone, R. A. W.; Wilby, A. H.; Entwistle, I. D. *Chem. Rev.* **1985**, *85*, 129–170.

- (16) Osborn, J. A.; Jardine, F. H.; Young, J. F.; Wilkinson, G. *J. Chem. Soc. A*. **1966**, *0*, 1711–1732.
- (17) Young, J. F.; Osborn, J. A.; Jardine, F. H.; Wilkinson, G. *Chem. Commun.* **1965**, *0*, 131–132.
- (18) James, B. R. *Homogeneous Hydrogenation*; John Wiley & Sons: New York, 1973.
- (19) Shapley, J. R.; Schrock, R. R.; Osborn, J. A. *J. Am. Chem. Soc.* **1969**, *91*, 2816–2817.
- (20) Schrock, R. R.; Osborn, J. A. *J. Am. Chem. Soc.* **1976**, *98*, 2134–2143.
- (21) Schrock, R. R.; Osborn, J. A. *J. Am. Chem. Soc.* **1976**, *98*, 2143–2147.
- (22) Crabtree, R. H. *Acc. Chem. Res.* **1979**, *12*, 331–337.
- (23) Crabtree, R. H.; Morris, G. E. *J. Organomet. Chem.* **1977**, *135*, 395–403.
- (24) Crabtree, R. H.; Felkin, H.; Morris, G. E. *J. Organomet. Chem.* **1977**, *141*, 205–215.
- (25) Crabtree, R. H.; Demou, P. C.; Eden, D.; Mihelcic, J. M.; Parnell, C. A.; Quirk, J. M.; Morris, G. E. *J. Am. Chem. Soc.* **1982**, *104*, 6994–7001.
- (26) Källström, K.; Munslow, I.; Andersson, P. G. *Chem. Eur. J.* **2006**, *12*, 3194–3200.
- (27) Brandt, P.; Hedberg, C.; Andersson, P. G. *Chem. Eur. J.* **2003**, *9*, 339–347.
- (28) Thompson, H. W.; Naipawer, R. E. *J. Am. Chem. Soc.* **1973**, *95*, 6379–6386.
- (29) Crabtree, R. H.; Davis, M. W. *Organometallics* **1983**, *2*, 681–682.
- (30) Crabtree, R. H.; Davis, M. W. *J. Org. Chem.* **1986**, *51*, 2655–2661.
- (31) Schultz, A. G.; McCloskey, P. J. *J. Org. Chem.* **1985**, *50*, 5905–5907.
- (32) Noyori, R. *Angew. Chem. Int. Ed.* **2002**, *41*, 2008–2022.
- (33) Knowles, W. S. *Angew. Chem. Int. Ed.* **2002**, *41*, 1998–2007.
- (34) Sharpless, K. B. *Angew. Chem. Int. Ed.* **2002**, *41*, 2024–2032.

- (35) Ramachandran, P. V.; Brown, H. C. In *Reductions in Organic Synthesis*; American Chemical Society, 1996; pp 84–97.
- (36) Mashima, K.; Kusano, K.-H.; Sato, N.; Matsumura, Y.-I.; Nozaki, K.; Kumobayashi, H.; Sayo, N.; Hori, Y.; Ishizaki, T.; Akutagawa, S.; Takaya, H. *J. Org. Chem.* **1994**, *59*, 3064–3076.
- (37) Noyori, R.; Ohkuma, T.; Kitamura, M.; Takaya, H.; Sayo, N.; Kumobayashi, H.; Akutagawa, S. *J. Am. Chem. Soc.* **1987**, *109*, 5856.
- (38) Ohkuma, T.; Ooka, H.; Ikariya, T.; Noyori, R. *J. Am. Chem. Soc.* **1995**, *117*, 10417–10418.
- (39) Ohkuma, T.; Ooka, H.; Yamakawa, M.; Ikariya, T.; Noyori, R. *J. Org. Chem.* **1996**, *61*, 4872–4873.
- (40) Noyori, R.; Ohkuma, T. *Angew. Chem. Int. Ed.* **2001**, *40*, 40–73.
- (41) Walling, C.; Bollyky, L. *J. Am. Chem. Soc.* **1964**, *88*, 3750–3752.
- (42) Berkessel, A.; Schubert, T. J. S.; Mü, T. N. *J. Am. Chem. Soc.* **2002**, *124*, 8693–8698.
- (43) Spielmann, J.; Buch, F.; Harder, S. *Angew. Chem. Int. Ed.* **2008**, *47*, 9434–9438.
- (44) Elsen, H.; Färber, C.; Ballmann, G.; Harder, S. *Angew. Chem. Int. Ed.* **2018**, *57*, 7156–7160.
- (45) Lewis, G. N. *Valence and the Structure of Atoms and Molecules*; Chemical Catalogue Company, Inc.: New York, 1923.
- (46) Welch, G. C.; San Juan, R. R.; Masuda, J. D.; Stephan, D. W. *Science* **2006**, *314*, 1124–1126.
- (47) Welch, G. C.; Stephan, D. W. *J. Am. Chem. Soc.* **2007**, *129*, 1880–1881.
- (48) McCahill, J. S. J.; Welch, G. C.; Stephan, D. W. *Angew. Chem. Int. Ed.* **2007**, *46*, 4968–4971.

- (49) Pu, M.; Privalov, T. *J. Chem. Phys.* **2013**, *138*, 154305–154316.
- (50) Rajeev, R.; Sunoj, R. B. *Chem. Eur. J.* **2009**, *15*, 12846–12855.
- (51) Pu, M.; Privalov, T. *ChemPhysChem* **2014**, *15*, 2936–2944.
- (52) Grimme, S.; Liu, L.; Gerit Brandenburg, J. *Phil. Trans. R. Soc. A.* **2017**, 375.
- (53) Marwitz, A. J. V.; Dutton, J. L.; Mercier, L. G.; Piers, W. E. *J. Am. Chem. Soc.* **2011**, *133*, 10026–10029.
- (54) Rokob, T. A.; Bako, I.; Stirling, A.; Hamza, A.; Pápai, I. *J. Am. Chem. Soc.* **2013**, *135*, 4425–4437.
- (55) Mück-Lichtenfeld, C.; Grimme, S. *Dalton Trans.* **2012**, *41*, 9111–9118.
- (56) Grimme, S.; Kruse, H.; Goerigk, L.; Erker, G. *Angew. Chem. Int. Ed.* **2010**, *49*, 1402–1405.
- (57) Rokob, T. A.; Pápai, I. In *Frustrated Lewis Pairs I: Uncovering and Understanding*; Erker, G., Stephan, D. W., Eds.; Springer Berlin Heidelberg: Berlin, Heidelberg, 2013; pp 157–211.
- (58) Rokob, T. A.; Hamza, A.; Stirling, A.; Soós, T.; Pápai, I. *Angew. Chem. Int. Ed.* **2008**, *47*, 2435–2438.
- (59) Stephan, D. W. *J. Am. Chem. Soc.* **2015**, *137*, 10018–10032.
- (60) Rocchigiani, L.; Ciancaleoni, G.; Zuccaccia, C.; Macchioni, A. *J. Am. Chem. Soc.* **2014**, *136*, 112–115.
- (61) Zaher, H.; Ashley, A. E.; Irwin, M.; Thompson, A. L.; Gutmann, M. J.; Krämer, T.; O'hare, D. *Chem. Commun.* **2013**, *49*, 9755–9757.
- (62) Schulz, F.; Sumerin, V.; Heikkinen, S.; Pedersen, B.; Wang, C.; Atsumi, M.; Leskelä, M.; Repo, T.; Pyykkö, P.; Petry, W.; Rieger, B. *J. Am. Chem. Soc.* **2011**, *133*, 20245–20257.
- (63) Liu, L.; Cao, L. L.; Shao, Y.; Ménard, G.; Stephan, D. W. *Chem.* **2017**, *3*, 259–267.

- (64) Stephan, D. W.; Erker, G. *Angew. Chem. Int. Ed.* **2010**, *49*, 46–76.
- (65) Stephan, D. W. *Acc. Chem. Res.* **2015**, *48*, 306–316.
- (66) Stephan, D. W.; Erker, G. *Angew. Chem. Int. Ed.* **2015**, *54*, 6400–6441.
- (67) Stephan, D. W. *Science* **2016**, *354*, 1248–1256.
- (68) Stephan, D. W. *Org. Biomol. Chem.* **2012**, *10*, 5740–5746.
- (69) Paradies, J. *Synlett* **2013**, *24*, 777–780.
- (70) Chase, P. A.; Welch, G. C.; Jurca, T.; Stephan, D. W. *Angew. Chem. Int. Ed.* **2007**, *46*, 8050–8053.
- (71) Andra, T. R.; Hamza, A.; Stirling, A.; Papai, I. *J. Am. Chem. Soc.* **2009**, *131*, 2029–2036.
- (72) Mahdi, T.; Stephan, D. W. *J. Am. Chem. Soc.* **2014**, *136*, 15809–15812.
- (73) Scott, D. J.; Fuchter, M. J.; Ashley, A. E. *J. Am. Chem. Soc.* **2014**, *136*, 15813–15816.
- (74) Greb, L.; Ona-Burgos, P.; Schirmer, B.; Grimme, S.; Stephan, D. W.; Paradies, J. *Angew. Chem. Int. Ed.* **2012**, *51*, 10164–10168.
- (75) Hounjet, L. J.; Bannwarth, C.; Garon, C. N.; Caputo, C. B.; Grimme, S.; Stephan, D. W. *Angew. Chem. Int. Ed.* **2013**, *52* (29), 7492–7495.
- (76) Greb, L.; Daniliuc, C. G.; Bergander, K.; Paradies, J. *Angew. Chem. Int. Ed.* **2013**, *52*, 5876–5879.
- (77) Spies, P.; Schwendemann, S.; Lange, S.; Kehr, G.; Frohlich, R.; Erker, G. *Angew. Chem. Int. Ed.* **2008**, *47*, 7543–7546.
- (78) Reddy, J. S.; Xu, B. H.; Mahdi, T.; Frohlich, R.; Kehr, G.; Stephan, D. W.; Erker, G. *Organometallics* **2012**, *31*, 5638–5649.
- (79) Geier, S. J.; Chase, P. A.; Stephan, D. W. *Chem. Commun.* **2010**, *46*, 4884–4886.
- (80) Mahdi, T.; Heiden, Z. M.; Grimme, S.; Stephan, D. W. *J. Am. Chem. Soc.* **2012**, *134*,

4088–4091.

- (81) Lam, J.; Szkop, K. M.; Mosaferi, E.; Stephan, D. W. *Chem. Soc. Rev.* **2018**.
- (82) Buchner, E.; Feldmann, L. *Ber. Dtsch. Chem. Ges.* **1903**, *36*, 3509–3517.
- (83) Staudinger, H. *Ber. Dtsch. Chem. Ges.* **1912**, *45*, 501–509.
- (84) Breslow, R. *J. Am. Chem. Soc.* **1958**, *80*, 3719–3726.
- (85) Berkessel, A.; Elfert, S.; Yatham, V. R.; Neudörfl, J. M.; Schlörer, N. E.; Teles, J. H. *Angew. Chem. Int. Ed.* **2012**, *51*, 12370–12374.
- (86) Schönherr, H.; Wanzlick, H. *Liebigs Ann. Chem.* **1970**, *731*, 176–179.
- (87) Wanzlick, H. W. *Angew. Chem. Int. Ed.* **1962**, *1*, 75–80.
- (88) Gleiter, R.; Hoffmann, R. *J. Am. Chem. Soc.* **1968**, *90*, 5457–5460.
- (89) Igau, A.; Grützmacher, H.; Baceiredo, A.; Bertrand, G. *J. Am. Chem. Soc.* **1988**, *110*, 6463–6466.
- (90) Bertrand, G.; Reed, R. *Coord. Chem. Rev.* **1994**, *137*, 323–355.
- (91) Arduengo, A. J.; Kline, R. L. H. M. *J. Am. Chem. Soc.* **1991**, *11*, 361–363.
- (92) Tapu, D.; Dixon, D. A.; Roe, C. *Chem. Rev.* **2009**, *109*, 3385–3407.
- (93) Arduengo, A. J.; Rasika Dias, V.; Harlow, R. L.; Kline, M. *J. Am. Chem. Soc.* **1992**, *114*, 5530–5534.
- (94) Heinemann, C.; Müller, T.; Apeloig, Y.; Schwarz, H. *J. Am. Chem. Soc.* **1996**, *118*, 2023–2038.
- (95) Arduengo, A. J.; Goerlich, J. R.; Marshall, W. J. *J. Am. Chem. Soc.* **1995**, *117*, 11027–11028.
- (96) Melaimi, M.; Soleilhavoup, M.; Bertrand, G. *Angew. Chem. Int. Ed.* **2010**, *49*, 8810–8849.

- (97) Lavallo, V.; Canac, Y.; Präsang, C.; Donnadieu, B.; Bertrand, G. *Angew. Chem. Int. Ed.* **2005**, *44*, 5705–5709.
- (98) Frey, G. D.; Lavallo, V.; Donnadieu, B.; Schoeller, W. W.; Bertrand, G. *Science* **2007**, *316*, 439–441.
- (99) Schuster, O.; Yang, L.; Raubenheimer, H. G.; Albrecht, M. *Chem. Rev.* **2009**, *109*, 3445–3478.
- (100) Benhamou, L.; Chardon, E.; Lavigne, G.; Stéphane Bellemin-Laponnaz; Vincent, C. *Chem. Rev.* **2011**, *111*, 2705–2733.
- (101) Hillier, A. C.; Sommer, W. J.; Yong, B. S.; Petersen, J. L.; Cavallo, L.; Nolan, S. P. *Organometallics* **2003**, *22*, 4322–4326.
- (102) Tolman, C. A. *Chem. Rev.* **1977**, *77*, 313–348.
- (103) Hopkinson, M. N.; Richter, C.; Schedler, M.; Glorius, F. *Nature* **2014**, *510*, 485–496.
- (104) Díez-González, S.; Marion, N.; Nolan, S. P. *Chem. Rev.* **2009**, *109*, 3612–3676.
- (105) Enders, D.; Niemeier, O.; Henseler, A. *Chem. Rev.* **2007**, *107*, 5606–5655.
- (106) *N-Heterocyclic Carbenes in Transition Metal Catalysis*; Glorius, F., Ed.; Springer-Verlag Berlin Heidelberg, 2007.
- (107) Peris, E. *Chem. Rev.* **2018**, *118*, 9988–10031.
- (108) Herrmann, Wolfgang, A.; Elison, M.; Fischer, J.; Köcher, C.; Artus, G. R. J. *Angew. Chem. Int. Ed.* **1995**, *34*, 2371–2374.
- (109) Vries, J. G. d.; Elsevier, C. J. *The Handbook of Homogenous Hydrogenation*; Wiley-VCH: Weinheim, Germany, 2007.
- (110) Hauwert, P.; Maestri, G.; Sprengers, J. W.; Catellani, M.; Elsevier, C. J. *Angew. Chem. Int. Ed.* **2008**, *47*, 3223–3226.
- (111) Warsink, S.; Hauwert, P.; Siegler, M. A.; Spek, A. L.; Elsevier, C. J. *Appl. Organomet.*

*Chem.* **2009**, *23*, 225–228.

- (112) Hauwert, P.; Boerleider, R.; Warsink, S.; Weigand, J. J.; Elsevier, C. J. *J. Am. Chem. Soc.* **2010**, *132*, 16900–16910.
- (113) Vivancos, Á.; Beller, M.; Albrecht, M. *ACS Catal.* **2018**, *8*, 17–21.
- (114) Bagh, B.; McKinty, A. M.; Lough, A. J.; Stephan, D. W. *Dalton Trans.* **2015**, *44*, 2712–2723.
- (115) Balamurugan, G.; Ramesh, R.; Grzegorz, J. G. *ChemistrySelect* **2017**, *2*, 10603–10608.
- (116) Yaşar, S.; Çekirdek, S.; Özdemir, İ. *J. Coord. Chem.* **2014**, *67*, 1236–1248.
- (117) Semwal, S.; Ghorai, D.; Choudhury, J. *Organometallics* **2014**, *33*, 7118–7124.
- (118) Herrmann, W. A.; Goossen, L. J.; Köcher, C.; Artus, G. R. J. *Angew. Chem. Int. Ed.* **1996**, *35*, 2805–2807.
- (119) Perry, M. C.; Burgess, K. *Tetrahedron: Asymmetry* **2003**, *14*, 951–961.
- (120) Gade, L. H.; Bellemin-Lapponnaz, S. *Coord. Chem. Rev.* **2007**, *251*, 718–725.
- (121) Wang, F.; Liu, L.-J.; Wang, W.; Li, S.; Shi, M. *Coord. Chem. Rev.* **2012**, *256*, 804–853.
- (122) Powell, M. T.; Hou, D.-R.; Perry, M. C.; Cui, X.; Burgess, K. *J. Am. Chem. Soc.* **2001**, *123*, 8878–8879.
- (123) Zhao, D.; Candish, L.; Paul, D.; Glorius, F. *ACS Catal.* **2016**, *6*, 5978–5988.
- (124) Kaiser, A.; Brandau, S.; Klimpel, M.; Barner-Kowollik, C. *Macromo. Rapid Commun.* **2010**, *31*, 1616–1621.
- (125) Schulz, D. N.; Turner, S. R.; Golub, M. A. *Rubber Chem. Technol.* **1982**, *55*, 809–859.
- (126) Xie, H. Q.; Li, X. D.; Guo, J. S. *J. Appl. Polym. Sci.* **2003**, *90*, 1026–1031.

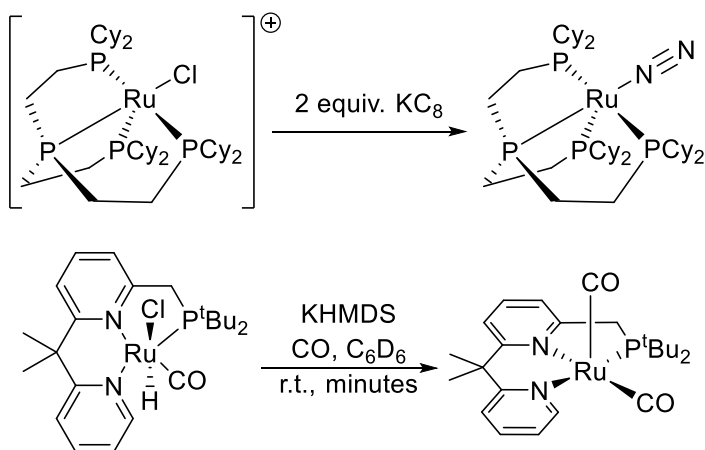
## Chapter 2

### Coordination Chemistry of N-Heterocyclic Phosphanyl Carbenes

#### 2.1 Introduction

##### 2.1.1 Zero-Valent Ruthenium Complexes

Ru(0) compounds have been used as valuable synthons in the synthesis Ru(II) complexes, which have been widely applied in various important chemical transformations including hydrogenations, hydrosilylations, and metathesis.<sup>1-3</sup> The synthesis of catalytically active species for such processes usually begins with Ru(II) synthons, although in some cases zero-valent ruthenium precursors are also used. For example, one route to Grubbs first-generation metathesis catalysts has employed Ru(cod)(cot) (cod = cyclooctadiene; cot = cyclooctatriene).<sup>4</sup> Similarly, Stephan *et al.* have employed the same precursor in the synthesis of Ru-dithiolate-alkylidene complexes.<sup>5</sup> Other Ru(0) complexes are also accessible from the reactions of carbene donors with Ru<sub>3</sub>(CO)<sub>12</sub>,<sup>6-8</sup> while reduction of Ru(II) has also been reported in the synthesis of N<sub>2</sub>-adducts of Ru(0) (Scheme 2.1.1).<sup>9</sup> Similarly, pyrazolylphosphaalkene complexes of Ru(0) are known, while Milstein and coworkers have recently developed related PNN-Ru(0) pincer complexes (Scheme 2.1.1).<sup>10,11</sup>

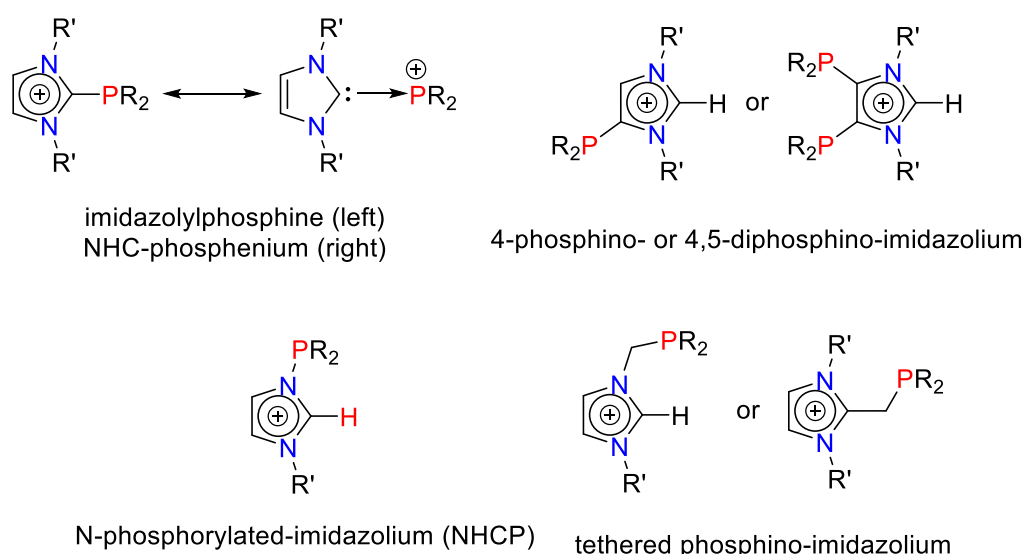


**Scheme 2.1.1: Synthesis of selected zero-valent ruthenium species.**

##### 2.1.2 N-Heterocyclic Carbenes with Pendant Phosphorus Donors

In recent years, electron-rich hybrid ligands incorporating both N-heterocyclic carbene (NHC) and pendant phosphorus donors have garnered considerable attention.<sup>12</sup> As mentioned in

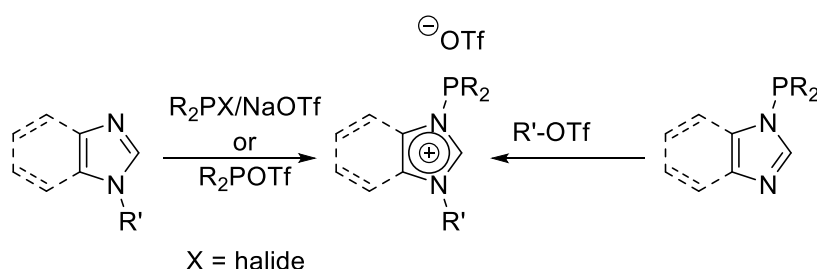
Chapter 1, NHCs have attracted considerable notice for their versatility and range of use amongst organometallic chemists. Some of the main reasons for the attraction of NHCs lie in the differences in their  $\sigma$ -donating and  $\pi$ -accepting properties compared to phosphine ligands, providing significant stabilization for the metal center. Furthermore, the increased air- and moisture-stability of NHCs has become an important factor in their use. Nonetheless, the ability to tune the electronic and steric properties of ligands is an immensely important feature and to that end, the combination of NHCs and pendant phosphorus donors can provide new avenues of reactivity and stability (Figure 2.1.1).



**Figure 2.1.1: Various motifs of phosphorus-based imidazole ligands.**

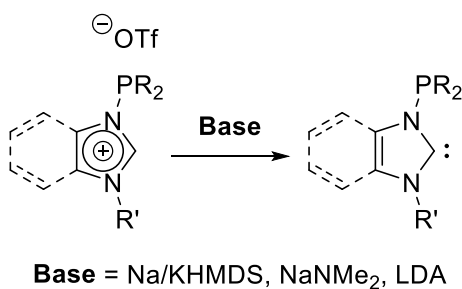
Both NHCs and ancillary phosphine ligands have been used to better stabilize and increase the efficiency of ruthenium-alkylidene complexes for olefin metathesis.<sup>13,14</sup> The first class of these ligands are the adducts of phosphines and the carbenic carbon in NHCs, often described as NHC-phosphenium salts, and have been studied for some time both chemically and computationally.<sup>15–17</sup> An alternative representation of this species can be drawn such that a positive charge resides on the phosphorus center (Figure 2.1.1). As a result of this charge, such adducts have been used as electron-deficient ligands in transition metal chemistry; by contrast NHCs are generally used to increase the electron density around a metal center.<sup>18,19</sup> The first reported synthesis of an NHC-phosphenium was in 1988 by Zoller *et al.*<sup>20</sup> Since then, numerous synthetic routes have been developed to efficiently afford the desired NHC-phosphenium salts or functionalize them as needed.<sup>21–23</sup>

The second class of NHC-phosphorus derivatives are phosphorylated at the nitrogen of the imidazolium ring, and these have been less extensively studied than their NHC-phosphenium counterparts.<sup>24–27</sup> The stabilities of these compounds are heavily influenced by the choice of counterion, and it appears that triflate anions are most effective at stabilizing these species. However, we have found that the tetrafluoroborate anion works reasonably well to furnish the desired product.<sup>28</sup> Synthetic approaches to these compounds differ only in whether the alkylation at the other nitrogen is carried out before or after phosphorylation of the imidazole ring (Scheme 2.1.2).



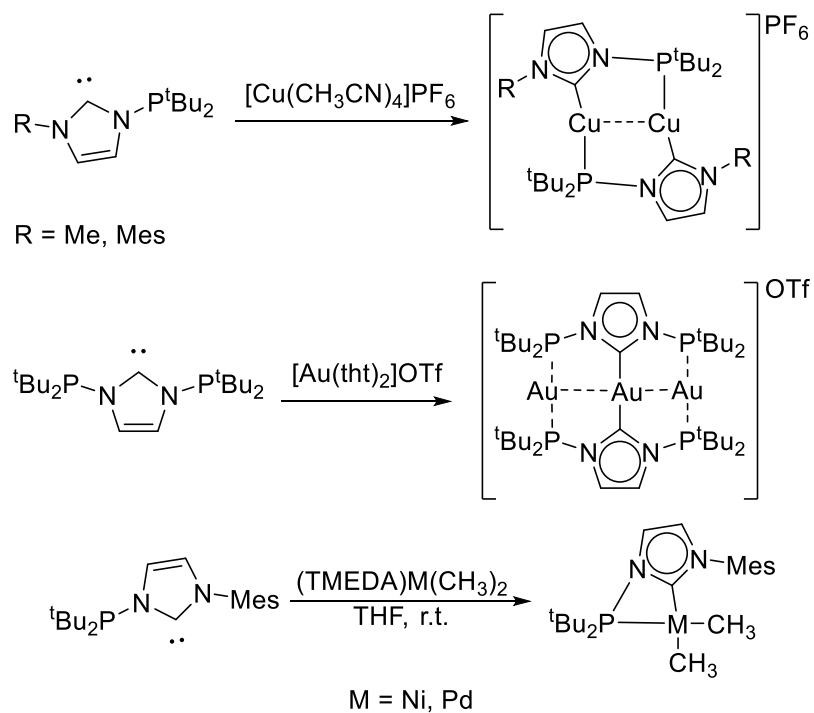
**Scheme 2.1.2: Different synthetic protocols for the generation of N-phosphorylated imidazolium salts.**

Furthermore, generation of the free carbenes from N-phosphorylated imidazolium salts is significantly controlled by the choice of base. Indeed, non-bulky oxygen bases such as NaOH and NaOMe result in ring-opened products or alkoxy adducts, respectively.<sup>24</sup> Only strong bases such as Na/KHMDS, NaNMe<sub>2</sub>, or lithium diisopropylamide (LDA) allow the successful formation and isolation of the free carbene (Scheme 2.1.3), which has been characterized crystallographically.

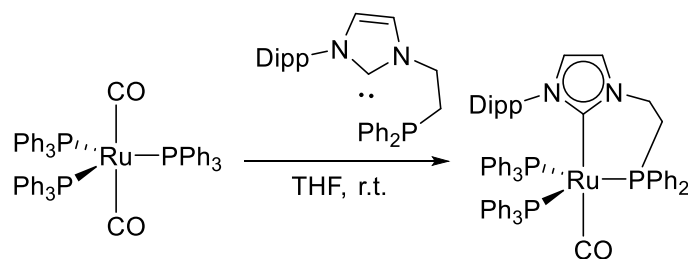


**Scheme 2.1.3: Deprotonation of NHCP salts to yield free carbenes.**

One synthetic difficulty associated with these compounds is their tendency to isomerize *via* migration of the phosphine fragment to the carbenic carbon, sometimes only with mild heating.<sup>27</sup> Increase of the steric bulk about the imidazolium and phosphorus centers can slow down or stop this isomerization. Several groups have focused on such ligands and their reactivity towards transition metals, and have synthesized a series of coinage metal phosphino-carbene complexes<sup>25,29,30</sup> as well as  $d^8$  metal derivatives (Scheme 2.1.4).<sup>31–33</sup> Similarly, the Lavigne group has reported the synthesis of NHCP ruthenium carbonyl species from Roper's Ru(0) complex (Scheme 2.1.5).<sup>34</sup> The Hofmann group has also applied these bulky, electron-rich ligands to the synthesis of olefin metathesis catalysts.<sup>35</sup> Building on this work, we sought to synthesize a range of Ru(0) and Ru(II) complexes bearing N-heterocyclic carbene-phosphine (NHCP) ligands. Furthermore, the reactivity of these compounds towards small molecules and catalysis will be explored.



**Scheme 2.1.4: Various transition metal complexes employing the bifunctional chelate of NHC-P ligands.**

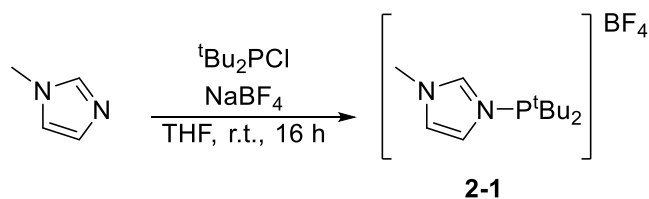


**Scheme 2.1.5: Synthesis of a phosphine-tethered NHC carbene complex.**

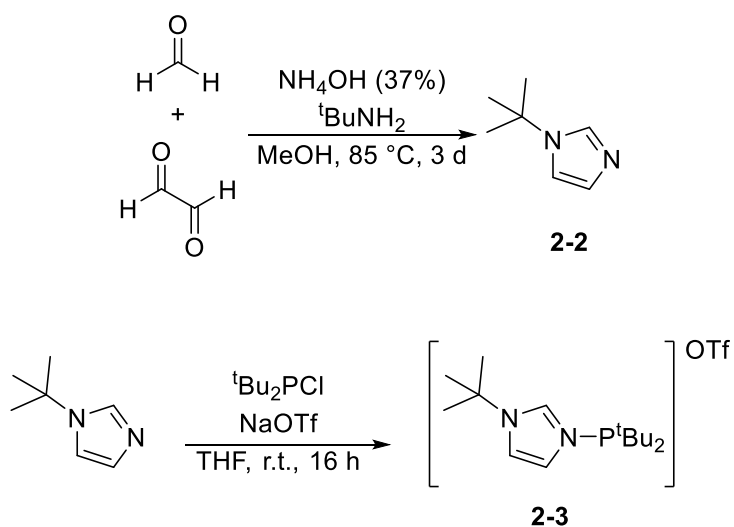
## 2.2 Results and Discussion

### 2.2.1 Synthesis of Ru-NHCP Complexes

The imidazolium salt **2-1** was synthesized according to literature procedures with some modifications, using commercially available reagents (Scheme 2.2.1).<sup>27,35</sup> Compounds **2-2** and **2-3** were also synthesized according to previously reported literature (Scheme 2.2.2).<sup>36</sup>

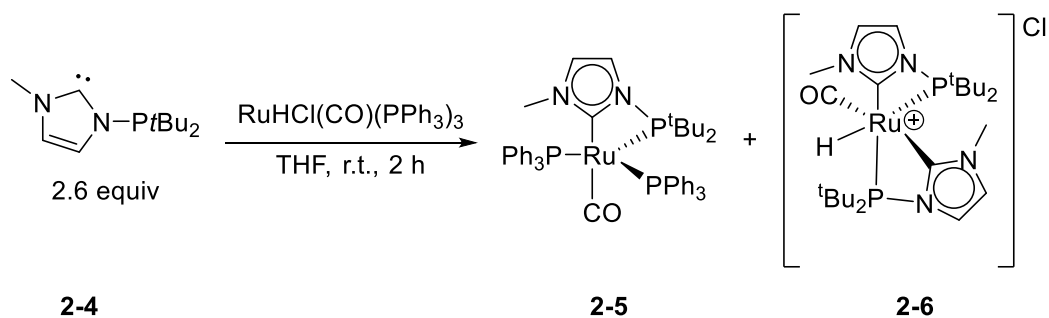


**Scheme 2.2.1: Synthesis of imidazolium salt 2-1.**



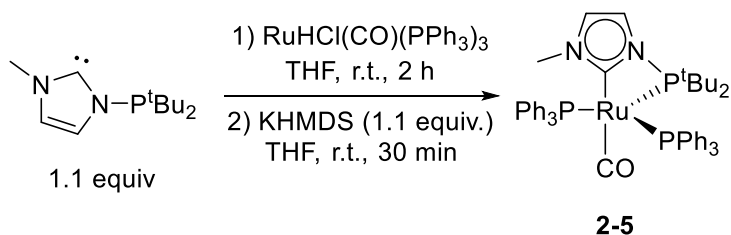
**Scheme 2.2.2: Synthesis of imidazole precursor 2-2 and imidazolium salt 2-3.**

The reaction of the phosphino-carbene **2-4** (2.6 equiv.) and  $\text{RuHCl}(\text{CO})(\text{PPh}_3)_3$  in THF at room temperature for 2 h results in a bright orange suspension. Removal of the solvent and extraction of the residue with hexanes affords complex **2-5** in 11% yield. Recrystallization of the remaining residue from  $\text{CH}_2\text{Cl}_2$ /pentane affords complex **2-6** as colourless crystals in 55% yield (Scheme 2.2.3).



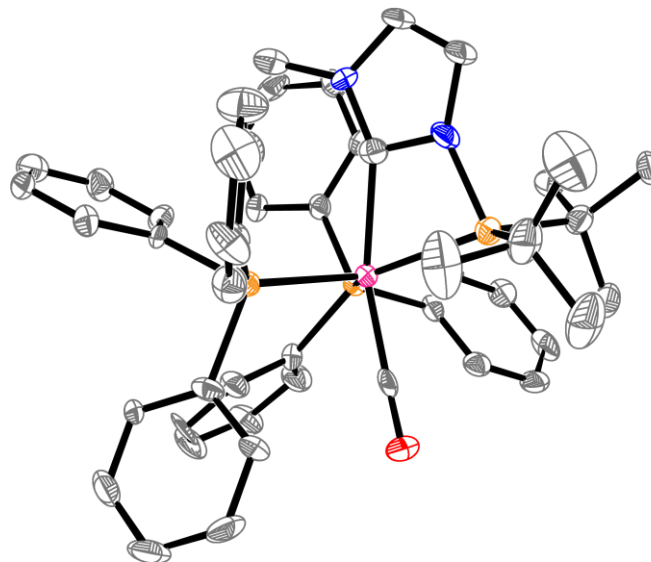
**Scheme 2.2.3: Synthesis of 2-5 and 2-6 from free carbene 2-4.**

Repeating the reaction with a 1.1:1 ratio of **2-4**: $\text{RuHCl}(\text{CO})(\text{PPh}_3)_3$  followed by addition of one equivalent of KHMDS results in a dark red solution. After stirring for 1 h, workup of the reaction afforded **2-5** cleanly, although it was isolated in a modest yield of 33% (Scheme 2.2.4). Both complexes were characterized spectroscopically; in the case of **2-5**,  $^{31}\text{P}\{^1\text{H}\}$  NMR data showed resonances at 48.8 ppm and 119.8 ppm with a  $^2J_{\text{P-P}}$  of 99 Hz.  $^1\text{H}$  and  $^{13}\text{C}\{^1\text{H}\}$  NMR spectra were consistent with the formulation, although the CO and carbene fragments could not be resolved despite collecting many transient scans. An infrared band for this Ru(0) carbonyl complex was observed at  $1909\text{ cm}^{-1}$ ; the small stretching frequency (relative to  $2143\text{ cm}^{-1}$  for CO, and  $2123\text{ cm}^{-1}$  for  $\text{Ni}(\text{CO})_4$ )<sup>37</sup> is indicative of a lengthened CO bond as a result of strong back-bonding from the electron-rich Ru(0) center. Similarly, the  $^{31}\text{P}\{^1\text{H}\}$  NMR data for **2-6** showed resonances at 101.1 and 129.8 ppm. The hydride resonance was observed at  $-12.42\text{ ppm}$  in the  $^1\text{H}$  NMR spectrum as a doublet of doublets with  $^2J_{\text{P-H}}$  coupling constants of 103 and 17 Hz, consistent with *trans* and *cis* configurations relative to the two phosphorus centers, respectively.  $^{13}\text{C}\{^1\text{H}\}$  NMR resonances at 182.4 and 214.0 ppm were attributed to the metal-bound CO and one of the carbene carbon atoms, respectively.

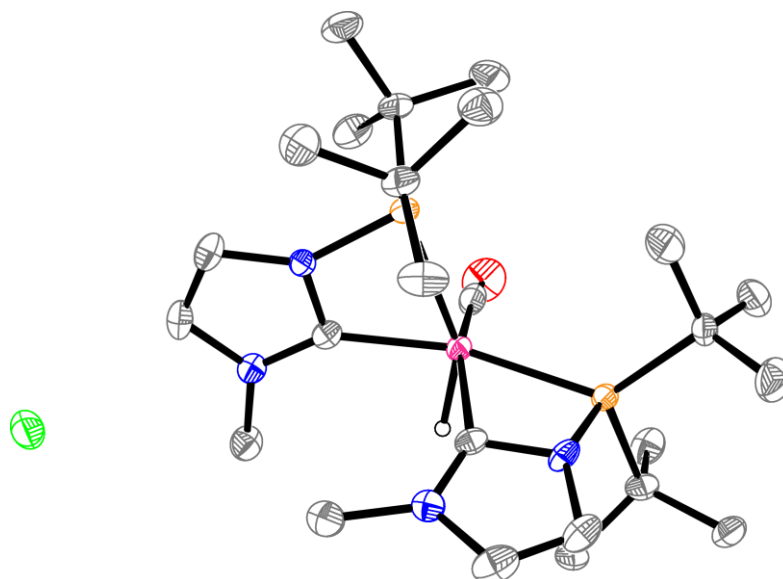


**Scheme 2.2.4: Selective synthesis of complex 2-5.**

An X-ray crystallographic study of **2-5** confirmed the formulation as a Ru(0)-carbonyl complex in space group  $R3$ , in which two PPh<sub>3</sub> ligands were coordinated to the Ru center (Figure 2.2.1). In addition, the phosphino-carbene ligand is bound in a bidentate,  $\kappa$ -C,  $\kappa$ -P manner, giving rise to Ru-C<sub>carbene</sub> and Ru-P<sub>tBu</sub> distances of 2.147(7) Å and 2.369(2) Å, respectively, with a C<sub>carbene</sub>-Ru-P<sub>tBu</sub> angle of 65.6(2)°, which are in good agreement with values reported by Hofmann *et al.* for similar  $\kappa$ -C,  $\kappa$ -P bidentate ligands.<sup>31,35</sup> The latter bond distance compares to the Ru-P<sub>Ph</sub> distances of 2.308(2) Å and 2.318(2) Å seen for the PPh<sub>3</sub> ligands, while the P<sub>Ph</sub>-Ru-P<sub>Ph</sub> angle was found to be 116.22(7)°. The Ru-C<sub>CO</sub> distance for the carbonyl fragment is 1.860(8) Å. The C-O bond length is 1.163(8) Å, which is slightly larger than the mean ruthenium-bound carbonyl CO bond length of 1.140(16) Å (CCDC Conquest, accessed August 14, 2018). The carbonyl ligand is oriented in a position almost *trans* to the carbene donor, with a C<sub>CO</sub>-Ru-C<sub>carbene</sub> angle of 161.9(3)°. Collectively, these data suggest that the best description of the geometry about Ru is a distorted trigonal bipyramid (geometry index is approximately 0.663) with the P donors occupying the trigonal plane and axial positions occupied by the carbene and carbonyl donors.



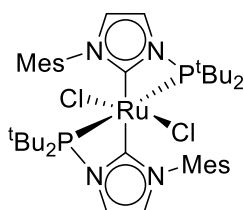
**Figure 2.2.1: Thermal ellipsoid plot of 2-5. Solvent and hydrogen atoms omitted for clarity. Grey: Carbon, Blue: Nitrogen, Orange: Phosphorus, Red: Oxygen, Pink: Ruthenium.**



**Figure 2.2.2: Thermal ellipsoid plot of one molecule in the asymmetric unit of 2-6. Solvent and hydrogen atoms (except hydride) omitted for clarity. Grey: Carbon, Blue: Nitrogen, Orange: Phosphorus, Red: Oxygen, Green: Chlorine Pink: Ruthenium.**

Complex **2-6** was also characterized crystallographically (Figure 2.2.2) and crystallizes in space group  $P2_1/n$  with two independent molecules in the asymmetric unit with similar bond metric data. These data confirmed **2-6** to be a 6-coordinate complex salt containing an outer-sphere

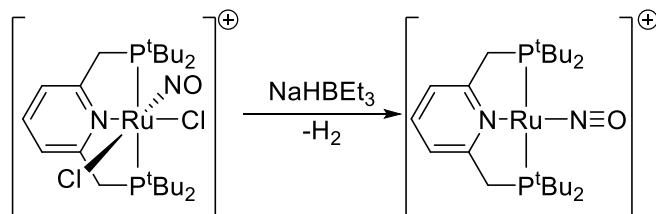
chloride anion. The geometry of the cation is that of a distorted octahedron in which two phosphino-carbene ligands are chelated to Ru, such that the two ligands adopt *cis* orientations relative to each other. One of the carbene donors is *trans* to one of the pendant phosphine arms, while the other carbene ligand is *trans* to the carbonyl fragment. The sixth coordination site is presumably occupied by the hydride, as evidenced by the  $^1\text{H}$  NMR data (*vide supra*), however this hydrogen atom was not located in the difference Fourier map. The Ru-C<sub>carbene</sub> distances in the two molecules in the asymmetric unit ranged from 2.043(6) Å to 2.112(5) Å, while the Ru-P distances ranged from 2.360(2) Å to 2.575(2) Å. In the case of the latter, the combination of the strong *trans* influence of the hydride, together with the strain of the four-membered chelate, and the steric congestion, account for this unusually long bond. The corresponding C-Ru-P angles range from 63.2(2)° to 65.9(2)°. This compares to the angle of chelation of 65.25(6)° observed in Ru(II)Cl<sub>2</sub>(MesImP<sup>t</sup>Bu<sub>2</sub>)<sub>2</sub> (Figure 2.2.3), as previously reported by Hofmann *et al.*<sup>31</sup> The Ru-C<sub>CO</sub> distances were 1.870(6) Å and 1.891(6) Å in the two molecules in the asymmetric unit. The infrared CO stretching frequency of this cationic species is 1937 cm<sup>-1</sup>, consistent with the oxidation of the zero-valent species to Ru(II), which decreases the extent of back-bonding and strengthens the CO bond.



**Figure 2.2.3: Ru(II)Cl<sub>2</sub>(MesImP<sup>t</sup>Bu<sub>2</sub>)<sub>2</sub>, synthesized by Hofmann *et al.***

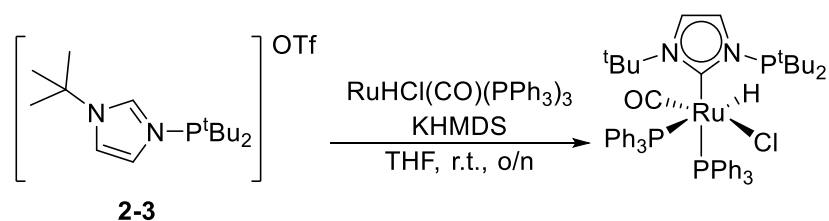
The formation of the Ru(0) species **2-5** presumably begins with chelation of the phosphino-carbene to Ru with displacement of triphenylphosphine. It is also interesting to note that chelation of phosphino-carbene to Ru was also proposed as the initial step in the previously reported reactions of this ligand with RuCl<sub>2</sub>(CHPh)(PCy<sub>3</sub>)<sub>2</sub>, although in that case the phosphine and carbene fragments add to the benzylidene fragment.<sup>32</sup> In the present case, the electron-rich and sterically crowded environment facilitates deprotonation and with formal loss of HCl affording **2-5**, or further substitution to generate **2-6**. Related loss of HCl from Ru(II) species are rare but the decomposition of Grubbs' second-generation catalyst has been studied computationally and shown to involve reductive elimination of HCl.<sup>38</sup> Similarly, the Milstein group have reported the synthesis of a (PNP)Ru(0) nitrosyl pincer complex *via* the reduction of

$\text{Ru(II)Cl}_2(\text{PNP})(\text{NO})$  with  $\text{NaHBEt}_3$  (Scheme 2.2.5).<sup>39</sup> Furthermore, the Whittlesey group reported that treatment of  $\text{RuHCl}(\text{PPh}_3)_3$  with excess of an electron-rich carbene in the presence of  $\text{H}_2$  gas also prompted loss of  $\text{HCl}$ , generating  $\text{RuH}_2(\text{NHC})_2(\text{PPh}_3)_2$ .<sup>40</sup>

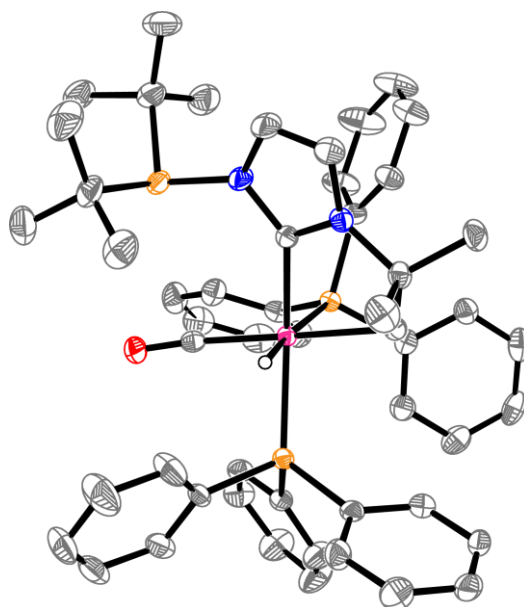


**Scheme 2.2.5: Reduction of Ru(II) nitrosyl complex to form a zero-valent, four-coordinate species.**

The analogous reaction of the *in-situ* generated carbene derived from **2-3** with  $\text{RuHCl}(\text{CO})(\text{PPh}_3)_3$  led to colour changes and NMR data were believed to be consistent with the generation of the product in Scheme 2.2.6, although this complex was not isolated. The  $^1\text{H}$  NMR spectrum shows a hydride resonance at -7.90 ppm as a doublet of doublets ( $^2J_{\text{P-H}} = 102$  Hz, 30 Hz), thus indicating that one phosphine moiety is *trans* to the hydride while the other phosphine is oriented in a *cis* fashion to the hydride. Additionally, the  $^{31}\text{P}\{^1\text{H}\}$  NMR spectrum shows resonances at 86.4, 56.9, and 33.6 ppm. These data suggest the pendant phosphine arm (86.4 ppm) is not coordinated to the Ru center. In this case, the steric interactions of the ligands presumably further crowds the geometry at Ru, precluding chelation of the phosphino-carbene. However, X-ray crystallographic analysis of the product confirmed the formulation as complex **2-7** (Figure 2.2.4). The bidentate chelation of the carbene gives rise to a  $\text{Ru-C}_{\text{carbene}}$  and  $\text{Ru-C}_{\text{alkyl}}$  bond lengths of 2.053(3) Å and 2.202(2) Å, respectively. Furthermore, the C-O bond length refined to 1.155(3) Å, slightly longer than that described for **2-5**, indicative of reduced back-bonding. The metal-bound hydrogen atom, found in the difference Fourier map, refined to a bond length of 1.58(3) Å. As expected, the  $\text{C}_{\text{carbene}}\text{-Ru-C}_{\text{alkyl}}$  bond angle is 76.69(11)°. Collectively, these data suggest that **2-7** is best described as a pseudo-octahedron.

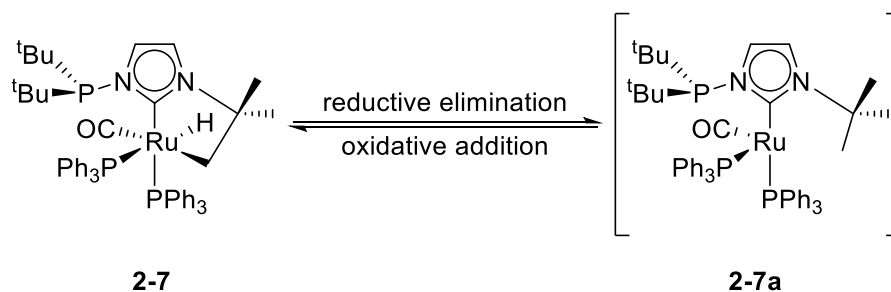


**Scheme 2.2.6: Initial proposed synthesis of a Ru(II)-NHCP using a bulkier NHCP carbene.**

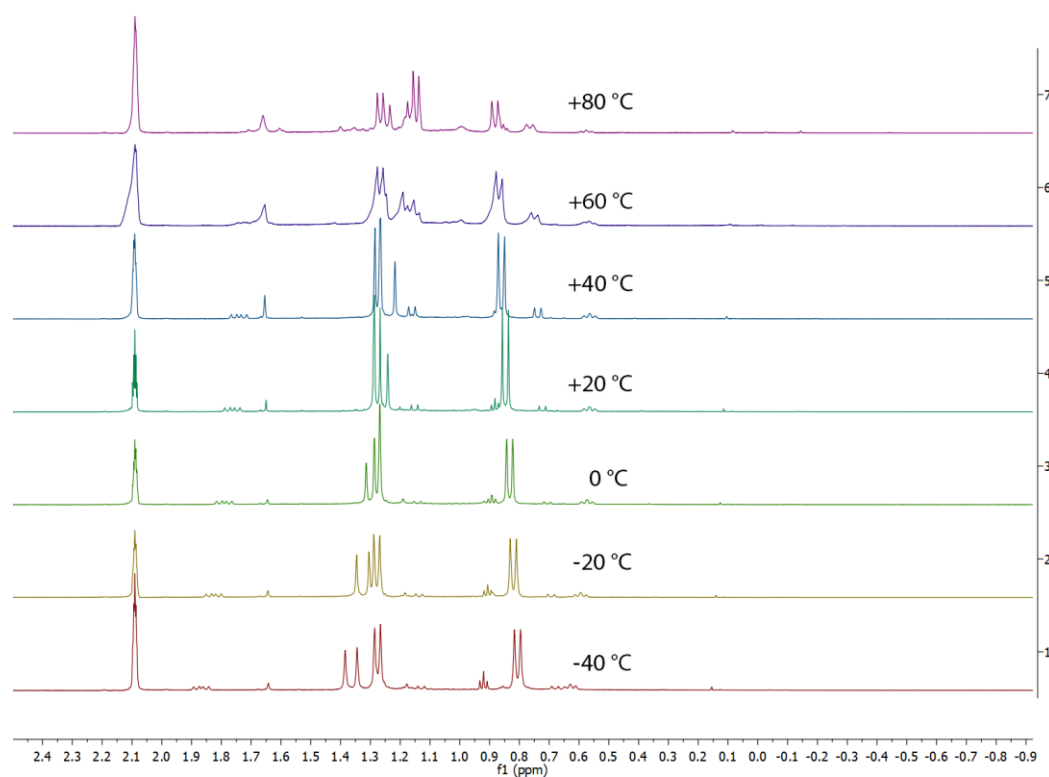


**Figure 2.2.4: Thermal ellipsoid plot of 2-7. Hydrogen atoms (except hydride) omitted for clarity.**

It was initially believed that the solid-state structure of **2-7** is in equilibrium with a Ru(0) synthon similar to **2-5** (Scheme 2.2.7). In order to further probe this idea, a toluene- $d_8$  solution of **2-7** was monitored by variable temperature (VT)  $^1\text{H}$  and  $^{31}\text{P}\{^1\text{H}\}$  NMR spectroscopy, ranging from  $-40$   $^\circ\text{C}$  to  $+80$   $^\circ\text{C}$  (Figure 2.2.5). The  $^1\text{H}$  NMR spectrum of the solution at elevated temperatures does not result in equivalent methyl resonances; instead, a decomposition to unidentifiable products is observed. Furthermore, while the room temperature  $^1\text{H}$  NMR spectrum shows overlap between the inequivalent *N-tert*-butyl methyl groups and the *P-tert*-butyl methyl resonances, cooling of the solution to  $-40$   $^\circ\text{C}$  helps resolve both methyl resonances.



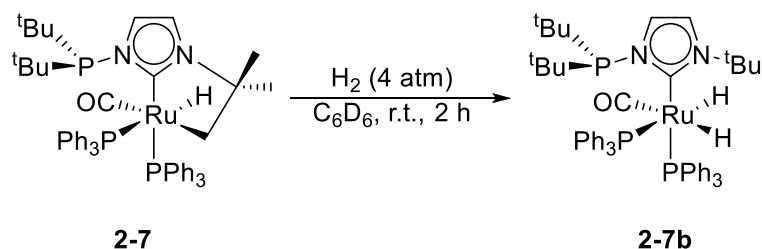
**Scheme 2.2.7: Proposed solution-phase reversibility of pendant alkyl arm in 2-7 to form 2-7a.**



**Figure 2.2.5: Select region of stacked variable temperature NMR spectra of 2-7 in toluene- $d_8$ .**

Additionally, **2-7** is seen to readily react with  $\text{H}_2$  (4 atm) at room temperature to form **2-7b** (Scheme 2.2.8). The  $^1\text{H}$  NMR spectrum of this product exhibits two distinct Ru-H resonances at -4.57 and -9.97 ppm with coupling to the two  $\text{PPh}_3$  moieties as well as to the other hydride. The resonance at -9.97 ppm displays a P-H coupling constant of 108.0 Hz, indicative of a *trans* orientation to one of the phosphine centers. The H-H coupling observed for both signals is 4.38 Hz which is typical of ruthenium dihydride species. Upon reaction with  $\text{H}_2$  the inequivalent N-

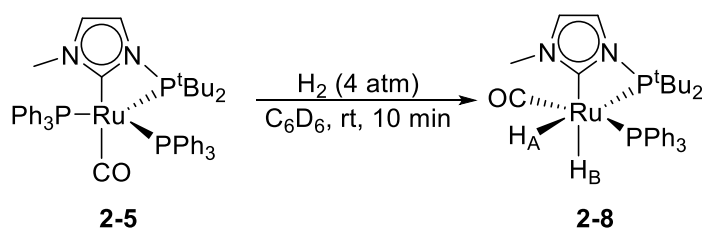
*tert*-butyl methyl groups, which previously resonated at different frequencies, transform into a sharp singlet at 1.63 ppm with a relative integration of 9:1 with respect to each hydride, further confirming that the addition of hydrogen takes place between the Ru center and the alkyl arm. Two mechanisms can be envisioned for the formation of the product. The first involves reductive elimination of the alkyl-hydride fragments to afford a R(0) complex followed by oxidative addition of dihydrogen to afford the corresponding dihydride species. The second mechanism involves displacement of PPh<sub>3</sub> with dihydrogen, followed by dihydride formation *via* hydrogenolysis of **2-7**, with subsequent reaction of hydride with a proton on the alkyl arm and evolution of hydrogen gas. However, VT experiments provide no evidence of a reductive elimination step to afford a Ru(0) complex. Interestingly, treatment of **2-7** with D<sub>2</sub> under the same conditions is shown to rapidly produce a statistical mixture of H<sub>2</sub> and HD. This must be accompanied by incorporation of deuterium into the alkyl arm of the ligand and is seen in the <sup>1</sup>H NMR spectrum of the reaction, where small complex resonances are observed close to the N-<sup>t</sup>Bu resonance as a result of splitting by deuterium atoms. Thus, we can posit that the second mechanism described above is more likely.



**Scheme 2.2.8: Reaction of 2-11 with dihydrogen to afford the dihydride species 2-7b.**

## 2.2.2 Reactivity of Ru-NHCP Complexes

In order to investigate the reactivity of the Ru(0)-NHCP complex, **2-5** was treated with various small molecules. When a bright orange/red solution of **2-5** was placed under H<sub>2</sub> (4 atm), a rapid colour change to pale yellow was observed (Scheme 2.2.9 and Figure 2.2.6), affording **2-8**. Monitoring the reaction by <sup>31</sup>P{<sup>1</sup>H} NMR spectroscopy, liberation of free PPh<sub>3</sub> was observed along with the formation of a new species with doublets at 65.4 and 125.2 ppm with a P-P coupling constant of 13 Hz. <sup>1</sup>H NMR spectra showed two hydride signals at -10.38 and -5.12 ppm, each with P-H and H-H coupling constants indicating presence of two distinct Ru-hydride units.

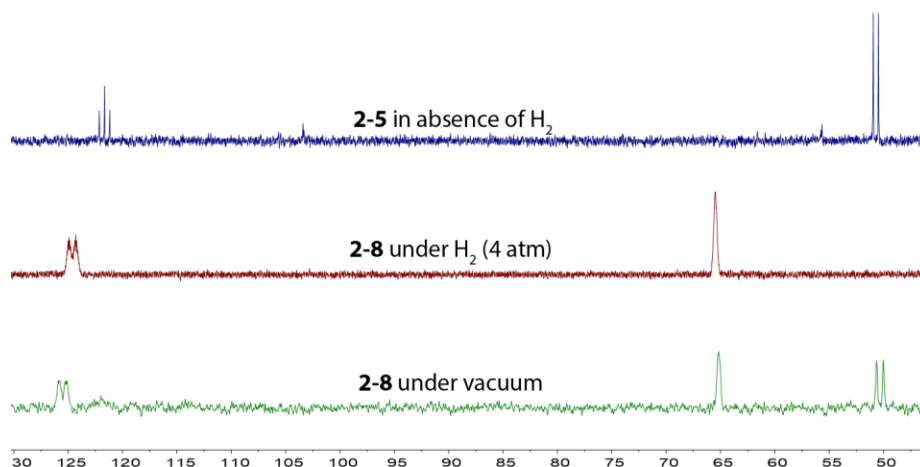


**Scheme 2.2.9: *In-Situ* generation of 2-8 from complex 2-5 by treatment with dihydrogen.**

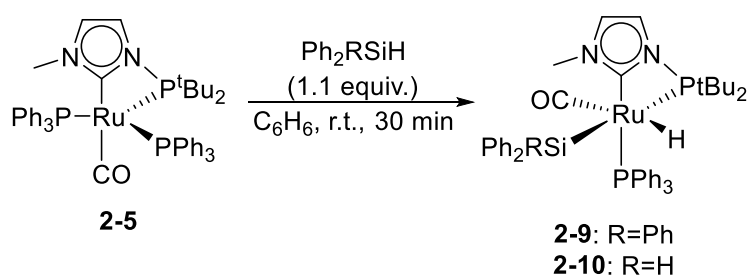
Although **2-8** could not be isolated, the NMR spectra indicate that one hydride unit is *trans* to a phosphine center, while the other hydride is oriented in a *cis* fashion to both phosphines. In an attempt to isolate **2-8**, it was found that the product decomposes to another species. NMR data indicate the partial recreation of **2-5** (Figure 2.2.7). This suggests some degree of reversibility in the oxidative addition of H<sub>2</sub> to **2-5**.



**Figure 2.2.6. Rapid conversion of 2-5 (left) to 2-8 (right). Photographs taken 10 minutes apart.**



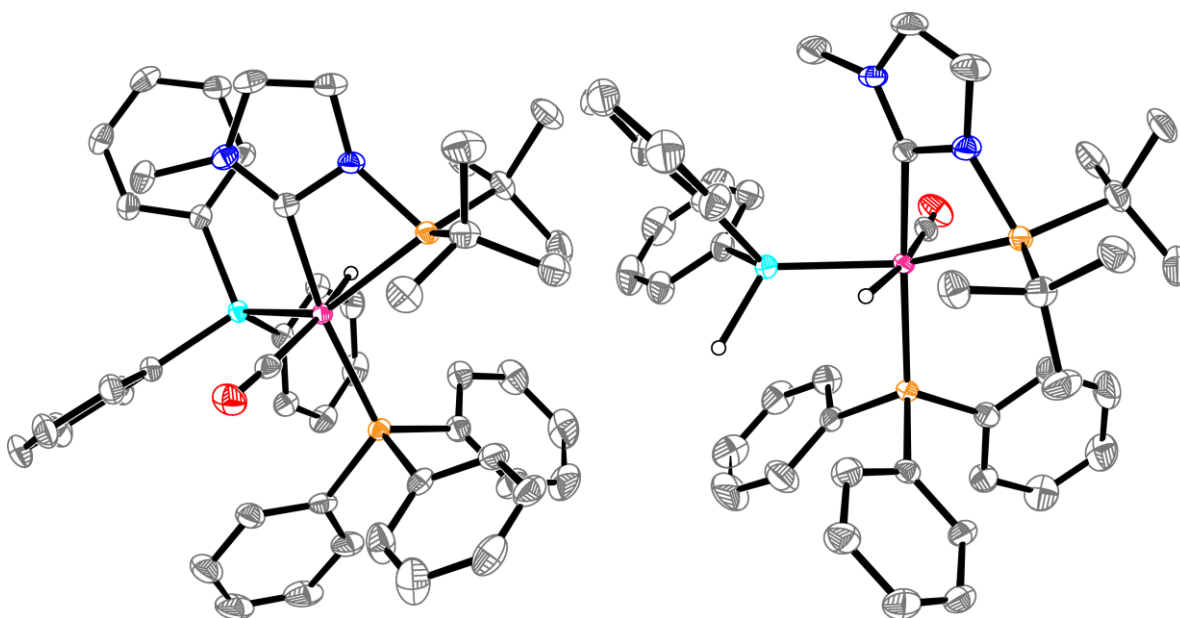
**Figure 2.2.7: Stacked  $^{31}\text{P}\{^1\text{H}\}$  NMR spectra of 2-5 (top), 2-8 under dihydrogen (middle), and 2-8 after repeated cycles of freeze-pump-thaw (bottom).**



**Scheme 2.2.10: Synthesis of 2-9 and 2-10.**

Complex **2-5** was also found to undergo oxidative addition of Si-H bonds (Scheme 2.2.10). Thus, addition of  $\text{Ph}_3\text{SiH}$  to **2-5** also quickly resulted in a colour change to pale yellow. However, in this case the solution could be dried, and the product extracted into pentane and recrystallized from benzene to give **2-9** as a pale-yellow solid in 80% yield. The  $^{31}\text{P}\{^1\text{H}\}$  NMR spectrum showed resonances at 55.7 and 103.4 ppm with a P-P coupling constant of 18 Hz, while the  $^1\text{H}$  NMR data revealed a Ru-H resonance at -4.20 ppm, with two P-H coupling constants of 19 and 15 Hz. The  $^{13}\text{C}\{^1\text{H}\}$  NMR spectrum showed the carbene resonance at 182.9 ppm with the CO resonance at 211.7 ppm. The infrared stretching frequency of the CO fragment is seen at  $1918\text{ cm}^{-1}$ . Despite prolonged acquisition times, efforts to observe a  $^{29}\text{Si}$  NMR signal were unsuccessful, owing to the extremely low sensitivity of the  $^{29}\text{Si}$  nucleus. Nonetheless, collectively these data confirm the formulation of **2-9**. The analogous reaction of **2-5** with  $\text{Ph}_2\text{SiH}_2$  afforded the analogous complex **2-10** in 71% yield (Scheme 2.2.10). The  $^1\text{H}$  NMR spectrum of **2-10** showed the Ru-H resonance at -4.61 ppm while the  $^{31}\text{P}\{^1\text{H}\}$  NMR data showed

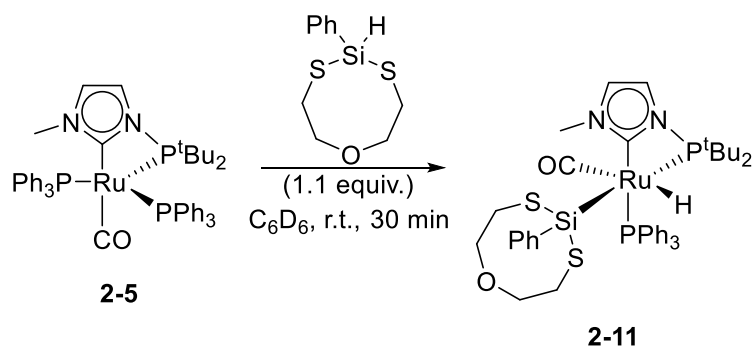
resonances at 58.5 and 104.5 ppm. The coupling constants in both spectra are similar to those found for **2-9**. The IR stretching frequency of the CO was observed at  $1931\text{ cm}^{-1}$ . In the case of **2-10**,  $^{29}\text{Si}\{^1\text{H}\}$  DEPT-135 experiments revealed a resonance at 19.6 ppm, with Si-P coupling constants of 96 and 19 Hz, indicative of *trans* and *cis* orientations relative to the phosphines, respectively.



**Figure 2.2.8: Thermal ellipsoid plots of complexes 2-9 (left) and 2-10 (right). Grey: Carbon, Blue: Nitrogen, Orange: Phosphorus, Red: Oxygen, Pink: Ruthenium, Cyan: Silicon.**

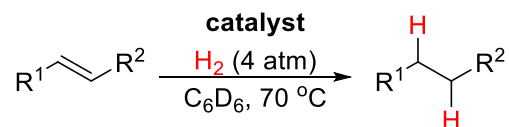
X-ray crystallography studies confirmed the solid-state structures of **2-9** and **2-10** (Figure 2.2.8), showing pseudo-octahedral geometries about Ru. In both cases, a *cis*-orientation of the silane fragment and hydride substituent is observed. In both structures, Si is *trans* to the pendant phosphine arm while the carbene is *trans* to  $\text{PPh}_3$ . In **2-9**, the  $\text{Ru-C}_{\text{carbene}}$  and  $\text{Ru-P}_{\text{Bu}}$  distances for the phosphino-carbene were  $2.075(2)\text{ \AA}$  and  $2.4838(5)\text{ \AA}$ , respectively, with a corresponding bite angle of  $64.94(6)^\circ$ . The corresponding bond lengths in **2-10** are  $2.090(3)\text{ \AA}$  and  $2.4712(8)\text{ \AA}$ , respectively, while the bite angle is  $64.67(7)^\circ$ . The  $\text{Ru-Si}$  bond lengths in **2-9** and **2-10** ( $2.3515(5)\text{ \AA}$  and  $2.4096(5)\text{ \AA}$ , respectively), are slightly longer than those found in other silyl derivatives.<sup>41–44</sup> These values are consistent with strong electron donation from the phosphino-carbene chelate.

Similarly, the cyclic dithiolate-silane derivative  $\text{PhHSi}(\text{SCH}_2\text{CH}_2)_2\text{O}$ , used previously in our lab for silylene synthesis, reacts with **2-5** in 5 minutes to afford complex **2-11** in 86% isolated yield (Scheme 2.2.11). The  $^1\text{H}$  NMR spectrum of **2-11** shows a Ru-H resonance at -4.50 ppm which exhibits coupling to two P atoms with coupling constants of 22 and 17 Hz. Like **2-9**, the  $^{31}\text{P}\{^1\text{H}\}$  NMR spectrum shows peaks at 54.9 and 102.2 ppm. The metal-bound CO gives rise to an infrared stretching frequency of  $1918\text{ cm}^{-1}$ . As with **2-9**, the NMR signal for the quaternary Si atom was not observed. The spectral data together with the steric demands of the silyl fragment suggest a geometry analogous to **2-9** and **2-10**; however, this could not be unambiguously confirmed as crystals suitable for X-ray diffraction could not be obtained. Efforts to use complexes **2-9** and **2-10** as hydrosilylation catalysts were explored using several unsaturated substrates. To our dismay, no hydrosilylated products were observed, despite various permutations of substrates, solvents, temperatures, or reaction times.



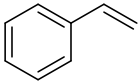
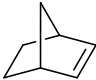
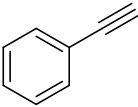

**Scheme 2.2.11: Synthesis of 2-11.**

Additionally, in an attempt to utilize the seemingly reversible oxidative addition of  $\text{H}_2$  to **2-5**, catalytic hydrogenations of olefins were investigated (Scheme 2.2.12). Although complex **2-8** was found to be catalytically active (Table 2.2.1), it can be seen that it is a poor hydrogenation catalyst, owing to the relatively large catalytic loading as well as long reaction times and increased reaction temperatures. Given that the oxidative addition of substrates to **2-5** is very rapid, due to the high electron density of the complex, one could surmise that the subsequent reductive elimination required for catalytic turnover is very slow, thus requiring long reaction times and increased temperatures.



**Scheme 2.2.12. Catalytic Reduction of Olefins Using Ruthenium-Hydride Catalysts.**

**Table 2.2.1. Catalytic Hydrogenation of Olefins Using 2-7 and 2-8.**

Substrate	Catalyst	Loading (% mol)	Time (h)	Conversion (%)	
	2-7	1.0	3	47	
	2-7	1.0	12	>99	
	2-7	1.0	16	>99	
	2-8	10	16	>99	
	2-8	10	72	>99	
	2-8	10	16	>99	
	nitrile butadiene rubber latex <sup>a,c,d</sup>	2-7	1.0	6	N.R.
		2-7	1.0	16	N.R.
		2-7	5.0	6	decomp.
		2-7	5.0	16	decomp.
		2-7	0.1	16	N.R.
		2-7	1.0	16	N.R.
nitrile butadiene rubber <sup>b,c,d</sup>	2-8	5.0	16	cross-link	
	2-8	0.1	16	decomp.	
	2-8	1.0	16	decomp.	
		5.0	16	decomp.	

<sup>a</sup> Used as emulsion in degassed water, C<sub>6</sub>H<sub>6</sub> solvent  
<sup>b</sup> Used as solution in degassed C<sub>6</sub>H<sub>5</sub>Cl  
<sup>c</sup> In Parr reactor, 50 bar H<sub>2</sub>, 60 °C  
<sup>d</sup> Catalytic loading in wt%

Complex **2-7** appears to be a much more competent catalyst, with smaller loadings and reaction times required. As discussed in Chapter 1, the hydrogenation of NBR is one of the inspirations for this work and thus, we attempted to test the catalytic activity of **2-7** with respect to NBR

rubber. The substrate was obtained as an emulsion in degassed water and the catalytic runs were carried out in benzene solvent in a high-pressure Parr reactor (50 bar H<sub>2</sub>). The product solution was analyzed by infrared spectroscopy and monitored for consumption of olefinic IR bands. Using 1.0 mol% **2-7**, no hydrogenation of the olefinic moieties was observed. Increasing the catalytic loading to 5.0 mol% did not lead to any desired product, and analysis of the solution by <sup>31</sup>P{<sup>1</sup>H} NMR spectroscopy indicated decomposition of the catalyst. As well, NBR was dissolved in degassed chlorobenzene and subjected to the catalytic conditions. However, it was found that the polymer was cross-linked at the nitrile functional groups with no hydrogenation of the olefinic groups observed.

## 2.3 Conclusion

A series of ruthenium complexes bearing N-phosphorylated N-heterocyclic carbene ligands were prepared using readily-synthesized precursors from inexpensive and commercially available starting materials. Ligand variants differ in the steric bulk of the N-alkyl substituents. Deprotonation of Ru(II)-hydrido-chloride species yields a zero-valent Ru-NHCP, whose solid-state structure was unambiguously assigned using X-ray diffraction studies. The Ru(0) complex was shown to readily undergo oxidative addition of dihydrogen and silanes to afford the corresponding divalent species. Changing of the steric bulk of the N-alkyl substituent to *tert*-butyl leads to C-H activation of the ligand. This species is observed to undergo reversible scrambling of D<sub>2</sub> to afford H<sub>2</sub> and D<sub>2</sub>. The viability of these species as olefin hydrogenation catalysts was tested. While compound **2-8** can hydrogenate simple alkenes, it is a poor catalyst and requires high loadings and long reaction times. Complex **2-7** is by comparison more active and able to hydrogenate olefins with lower loadings and shorter reaction periods. However, the application of compound **2-7** to hydrogenation of NBR latex proved unsuccessful as it led to either no reactivity, or decomposition of the catalyst and/or NBR rubber.

## 2.4 Experimental Section

### 2.4.1 General Considerations

All manipulations were carried out under an atmosphere of dry, O<sub>2</sub>-free N<sub>2</sub> employing a VAC Atmospheres glove box and a Schlenk vacuum-line. Solvents were purified with a Grubbs-type column system manufactured by Innovative Technology and dispensed into thick-walled Strauss glass flasks equipped with Teflon-valve stopcocks (pentanes, hexanes, toluene, tetrahydrofuran,

and dichloromethane). Anhydrous benzene was purchased from Sigma-Aldrich and used without further purification. Deuterated solvents were dried over the appropriate agents, vacuum-transferred into storage flasks with Young-type Teflon stopcocks and degassed accordingly ( $C_6D_6$ ,  $CD_2Cl_2$ , THF- $d_8$ , and  $CDCl_3$ ).  $^{31}P\{^1H\}$  NMR spectra were recorded at 25 °C on a Bruker 400 MHz spectrometer.  $^1H$  and  $^{13}C\{^1H\}$  NMR spectra were recorded at 25 °C on a Bruker 500 MHz spectrometer equipped with a cold probe.  $^{29}Si\{^1H\}$  NMR data were obtained via  $^{29}Si$  DEPT-135 experiments recorded at 25 °C on a Varian 500 MHz spectrometer. Chemical shifts are given relative to  $SiMe_4$  and referenced to the residual solvent signal ( $^1H$ ,  $^{13}C$ ,  $^{29}Si$ ) or relative to a standard ( $^{29}Si$ :  $SiMe_4$ ;  $^{31}P$ : 85%  $H_3PO_4$ ). Chemical shifts are reported in ppm and coupling constants are scalar values in Hz. Potassium bis(trimethylsilyl)amide (KHMDs), bis(mercaptoethyl)ether, ((HSC $_2$ H $_5$ ) $_2$ O), HPhSiCl $_2$ , triphenylsilane, diphenylsilane, di-*t*-butylchlorophosphine, and sodium tetrafluoroborate were purchased from Sigma-Aldrich and used without further purification.  $RuHCl(CO)(PPh_3)_3$  was acquired from Strem and used without further purification. Despite long acquisition times on a 500 MHz cryoprobe instrument, some quaternary carbons in the  $^{13}C$  NMR spectra were not observed. Furthermore, for quaternary Si atoms,  $^{29}Si$  DEPT-135 proved unsuccessful in obtaining  $^{29}Si$  NMR spectra, again despite prolonged acquisition times. Such instances are specifically mentioned for each occurrence.

## 2.4.2 General Procedure for Hydrogenation

### 2.4.2.1 Hydrogenation of Discrete Olefin Substrates

In the glovebox, 1 mmol of the olefin substrate was weighed out in a vial and dissolved in 0.5 mL of  $C_6D_6$ . The solution was added to a weighed amount of the appropriate catalysts (amounts listed in Table 2.2.1). The solution was syringed into an oven-dried J-Young type NMR tube. The reaction vessel was sealed and degassed three times using successive cycles of freeze-pump-thaw and backfilled with  $H_2$  (4 atm). The reaction vessel was heated as indicated and monitored by NMR spectroscopy.

### 2.4.2.2 Hydrogenation of Nitrile Butadiene Rubber

In the glovebox, the appropriate catalyst amount is weighed into a vial and dissolved in  $C_6H_5Cl$ . The solution was added to a vial containing a solution of 1.00 mL of 5 wt% NBR in chlorobenzene. The reaction vials were charged with stir bars and loaded into a Parr reactor pressure and sealed. The reactor was removed from the glovebox and purged five times with 20

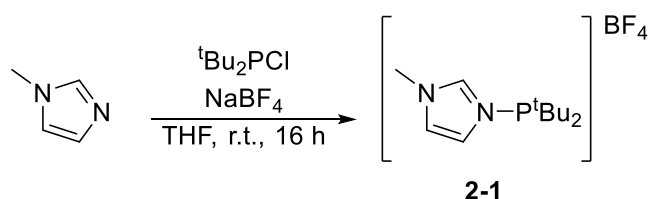
bar H<sub>2</sub> before being pressurized with 45 bar H<sub>2</sub>. The reactor was placed in the oil bath and allowed to equilibrate with the temperature, after which the pressure was increased to 50 bar overall. The reaction was allowed to stir for 6 to 16 hours as indicated. After completion of reaction the reactor was cooled to room temperature and carefully depressurized. The polymer was coagulated with the addition of methanol and vigorously shaken/sonicated. The solvent was decanted and the polymer was dried under vacuum before being dissolved in THF. An aliquot of the solution was placed in between KBr plates and then dried thoroughly in air. IR spectroscopy was used to determine yield of hydrogenated NBR (HNBR).

### 2.4.2.3 Hydrogenation of Nitrile Butadiene Rubber Latex

In the glovebox, the appropriate catalyst amount is weighed into a vial and dissolved C<sub>6</sub>H<sub>6</sub>. The reaction vessels were charged with stir bars and loaded into a Parr reactor pressure and sealed. The reactor was taken into an N<sub>2</sub> glovebag which had previously been purged 25-30 times with inert gas. The reactor was opened and 1 mL of NBR latex (emulsion in water) was added to each vial. The reactor was again sealed and purged five times with 20 bar H<sub>2</sub>. Procedure is then identical to NBR hydrogenation described above.

## 2.4.3 Synthetic Procedures

### 2.4.3.1 Synthesis of 1-(di(*tert*-butyl)phosphinoyl)-3-methyl-imidazolium tetrafluoroborate **2-1**



1-(di(*tert*-butyl)phosphanyl)-3-methyl imidazolium tetrafluoroborate was prepared according to literature procedures, with some modifications.<sup>27,31</sup> In a 20-mL scintillation vial, 1-methylimidazole (1.091 g, 13.29 mmol) and sodium tetrafluoroborate (1.595 g, 14.53 mmol) were combined in THF (5 mL) and cooled to -45 °C. While stirring, a solution of di-*t*-butylchlorophosphine (2.664 g, 14.75 mmol) in THF (3 mL) was added dropwise to the cold suspension. The mixture immediately became cloudy as a white precipitate formed. The reaction was stirred at -45 °C for 30 min and then allowed to warm to room temperature. Stirring

continued at room temperature overnight. The crude mixture was monitored by  $^{31}\text{P}\{^1\text{H}\}$  NMR spectroscopy and upon complete consumption of starting phosphine, the suspension was concentrated to dryness and the resulting white solid extracted with dichloromethane (2 x 5 mL). The extracts were filtered over a Celite plug and concentrated under vacuum to afford a white solid, which was washed with pentane (3 x 15 mL) and diethyl ether (3 x 15 mL). The resulting residue was dried under vacuum to afford the product as a microcrystalline white solid (2.8749 g, 69%).

$^1\text{H}$  NMR ( $\text{CD}_2\text{Cl}_2$ ):  $\delta$  3.15 (d,  $^3J_{\text{P-H}} = 14$  Hz, 18 H,  $\text{C}(\text{CH}_3)_3$ ), 5.94 (s, 3H, N- $\text{CH}_3$ ), 9.35 (s, 1H, CH on backbone), 9.36 (s, 1H, CH on backbone), 10.68 (s, 1H, N-CH-N).

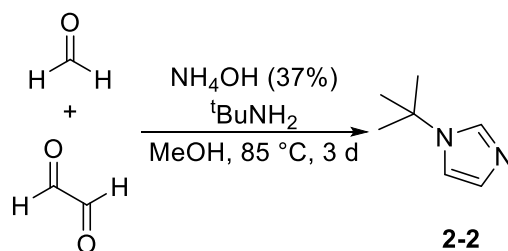
$^{13}\text{C}\{^1\text{H}\}$  NMR ( $\text{CD}_2\text{Cl}_2$ ):  $\delta$  28.1 (d,  $^2J_{\text{C-P}} = 16$  Hz,  $\text{C}(\text{CH}_3)_3$ ), 35.0 (d,  $^1J_{\text{C-P}} = 30$  Hz,  $\text{C}(\text{CH}_3)_3$ ), 36.7 (s, N- $\text{CH}_3$ ), 124.5 (s, CH on backbone), 126.6 (s, CH on backbone), 141.8 (s, N-CH-N).

$^{31}\text{P}\{^1\text{H}\}$  NMR ( $\text{CD}_2\text{Cl}_2$ ):  $\delta$  123.3 (s,  $\text{P}^t\text{Bu}_2$ ).

$^{19}\text{F}\{^1\text{H}\}$  NMR ( $\text{CD}_2\text{Cl}_2$ ):  $\delta$  -149.8 (s,  $\text{BF}_4^-$ ).

$^{11}\text{B}\{^1\text{H}\}$  NMR ( $\text{CD}_2\text{Cl}_2$ ):  $\delta$  -1.0 (s,  $\text{BF}_4^-$ ).

#### 2.4.3.2 Synthesis of N-*tert*-butyl-imidazole **2-2**



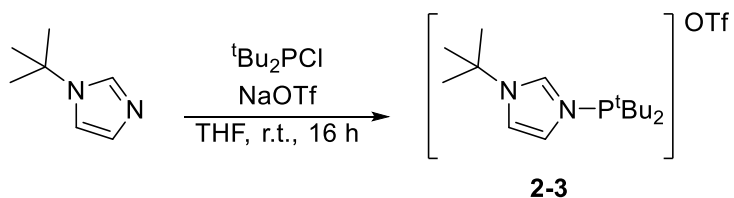
Glyoxal (40% w/w in  $\text{H}_2\text{O}$ , 16 mL, 140 mmol) and  $^t\text{BuNH}_2$  (15 mL, 143 mmol) were combined in MeOH (100 mL) in 2-neck flask equipped with condenser and dropping funnel. The orange-yellow solution was heated to 75  $^\circ\text{C}$  for 20 min while stirring. Formaldehyde (37% w/w in  $\text{H}_2\text{O}$ , 13 mL, 174 mmol) was added dropwise to the hot red/brown solution and the mixture was allowed to equilibrate to 75  $^\circ\text{C}$ . A dropping funnel was charged with  $\text{NH}_4\text{OH}$  (37%, 20 mL, 144 mmol) in MeOH (20 mL) and the solution was added dropwise (1 drop/s) to the hot mixture with vigorous stirring. The solution was heated at 85  $^\circ\text{C}$  for 3 d, after which the mixture was cooled to room temperature and all volatiles were removed under reduced pressure. The residue was

extracted with dichloromethane (3 x 20 mL) and washed with brine (3 x 50 mL). The organic layers were combined and dried over Na<sub>2</sub>SO<sub>4</sub>. The suspension was then filtered and concentrated under vacuum to afford a dark red oil. The product was obtained as a colourless liquid after distillation under static vacuum (b.p. 28 °C, 9.070 g, 52 %). Characterization is consistent with literature values.<sup>36</sup>

<sup>1</sup>H NMR (CDCl<sub>3</sub>): δ 1.54 (s, 9H, CH<sub>3</sub>), 6.97 (t, <sup>3</sup>J<sub>H-H</sub> = 1.2 Hz, 1H, CH on backbone), 7.05 (t, <sup>3</sup>J<sub>H-H</sub> = 1.4 Hz, 1H, CH on backbone), 7.57 (t, <sup>3</sup>J<sub>H-H</sub> = 1.2 Hz, N-CH-N).

<sup>13</sup>C{<sup>1</sup>H} NMR (CDCl<sub>3</sub>): δ 30.6 (s, CH<sub>3</sub>), 54.7 (s, C(CH<sub>3</sub>)<sub>3</sub>), 116.3 (s, CH on backbone), 129.1 (s, CH on backbone), 134.3 (s, N-CH-N).

### 2.4.3.3 Synthesis of 1-(di(*tert*-butyl)phosphinoyl)-3-*tert*-butyl-imidazolium triflate **2-3**



NaOTf (0.7590 g, 4.410 mmol) was added to a solution of **2-2** (0.514 g, 4.137 mmol) in THF (5 mL). The suspension was cooled to -45 °C while stirring and solution of <sup>t</sup>Bu<sub>2</sub>PCl (0.833 g, 4.613 mmol) in THF (5 mL) was added dropwise to cold suspension with vigorous stirring. The mixture was sealed and stirred at -45 °C for 30 minutes before being warmed to room temperature and stirred overnight. The suspension was then filtered over Celite and residue washed with THF (1 mL). The filtrate was evacuated to dryness and residue extracted with DCM (4 x 2 mL) and filtered over a Celite plug. The residue was washed with DCM (2 x 1 mL) and filtrate concentrated to 2 mL and triturated with pentanes (10 mL) until white solid precipitated. The product was collected on a glass frit and washed with pentanes (3 x 5 mL) and diethyl ether (3 x 5 mL) and subsequently dried under vacuum to afford **2-3** as a white solid (1.523 g, 88%).

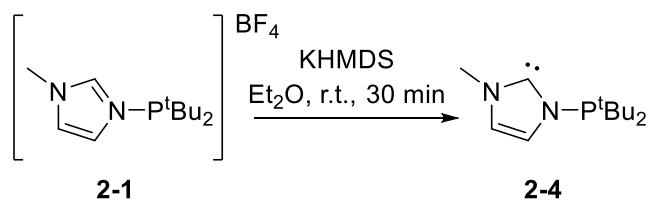
<sup>1</sup>H NMR (CDCl<sub>3</sub>): δ 1.23 (d, <sup>3</sup>J<sub>P-H</sub> = 13 Hz, 18H, P(C(CH<sub>3</sub>)<sub>3</sub>)<sub>2</sub>), 1.71 (s, 9H, NC(CH<sub>3</sub>)<sub>3</sub>), 7.65 (s, 1H, CH on backbone), 7.95 (s, 1H, CH on backbone), 8.78 (m, 1H, N-CH-N).

$^{13}\text{C}\{^1\text{H}\}$  NMR ( $\text{CDCl}_3$ ):  $\delta$  28.4 (d,  $^2J_{\text{P-C}} = 16$  Hz,  $\text{PC}(\text{CH}_3)_3$ ), 29.8 (s,  $\text{N-C}(\text{CH}_3)_3$ ), 35.3 (d,  $^1J_{\text{P-C}} = 30$  Hz,  $\text{PC}(\text{CH}_3)_3$ ), 61.2 (s,  $\text{N-C}(\text{CH}_3)_3$ ), 122.5 (s, br, CH on backbone), 123.3 (q,  $^1J_{\text{F-C}} = 321$  Hz, OTf, quartet only partly observable), 126.6 (s, br, CH on backbone) 139.0 (d,  $^2J_{\text{P-C}} = 32$  Hz, N-CH-N).

$^{31}\text{P}\{^1\text{H}\}$  NMR ( $\text{CDCl}_3$ ):  $\delta$  119.3 (s,  $\text{P}(\text{tBu})_2$ )

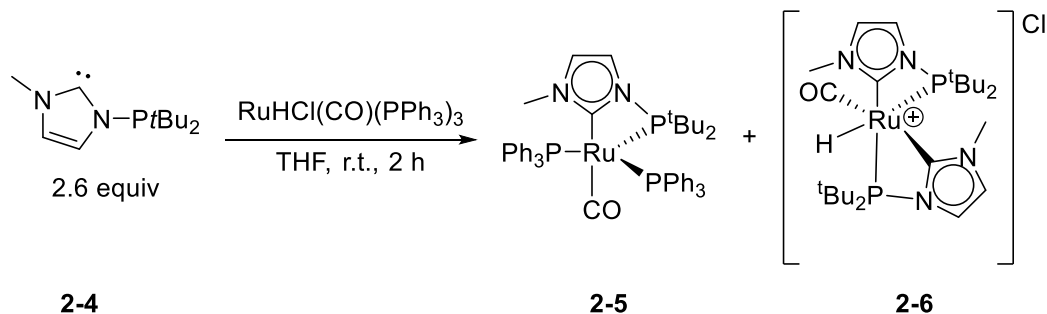
$^{19}\text{F}\{^1\text{H}\}$  NMR ( $\text{CDCl}_3$ ):  $\delta$  -78.2 (s, OTf).

#### 2.4.3.4 Synthesis of 1-(di(*tert*-butyl)phosphanyl)-3-methylimidazolylidene **2-4**



A 20 ml vial was charged with **2-1** (0.597 g, 1.909 mmol), suspended in diethyl ether (8 mL), and cooled to  $-45$  °C. KHMDS (0.403 g, 2.018 mmol) in diethyl ether (4 mL) was added dropwise to the stirring suspension to immediately afford a cloudy, pale yellow solution. The mixture was warmed to room temperature and stirred for a further 30 minutes. Concentration of mixture under vacuum afforded an off-white residue that was extracted with pentanes (2 x 4 mL) and filtered through a Celite plug. The yellow filtrate was concentrated under vacuum to 1 mL and a pale-yellow precipitate was observed. The vial was placed in the freezer overnight to complete crystallization of product. The yellow supernatant was then removed and discarded, and the residue was dried under vacuum to afford the desired product as off-white crystals (0.303 g, 70%). Characterization of product is consistent with literature values.<sup>31</sup>

### 2.4.3.5 Synthesis of complexes **2-5** and **2-6**



**2-4** (0.086 g, 0.380 mmol) and  $\text{RuHCl(CO)(PPh}_3)_3$  (0.137 g, 0.144 mmol) were combined in a vial equipped with a stir bar and THF (5 mL) to afford a beige suspension. After stirring for 15 minutes at room temperature the mixture became a bright orange suspension and stirring was continued at room temperature for 2 hours. The vial was then evacuated to dryness and the residue extracted with benzene (2 x 5 mL). Complex **2-5** (0.014 g, 11%) was obtained as orange-red crystals from the concentrated benzene solution overnight. The remaining residue was dissolved in minimal dichloromethane (2 mL). Layering of  $\text{CH}_2\text{Cl}_2$  solution with pentanes (10 mL) for one week afforded colourless x-ray quality crystals of complex **2-6** (0.049 g, 55%).

#### Characterization of Ru(0) complex **2-5**:

$^1\text{H NMR (C}_6\text{D}_6)$ :  $\delta$  1.13 (d,  $^3J_{\text{P-H}} = 13$  Hz, 18H,  $\text{C(CH}_3)_3$ ), 1.57 (s, 3H, N- $\text{CH}_3$ ), 5.67 (s, 1H, CH on backbone of carbene), 6.20 (dd,  $^3J_{\text{H-P}} = 3$  Hz,  $^3J_{\text{H-H}} = 2$  Hz, 1H, CH on carbene), 6.96–7.07 (m, 18H,  $\text{PPh}_3$ ), 7.66–7.70 (m, 12H,  $\text{PPh}_3$ ).

$^{13}\text{C}\{^1\text{H}\}$  NMR ( $\text{C}_6\text{D}_6$ ):  $\delta$  30.0 (d,  $^2J_{\text{C-P}} = 10$  Hz,  $\text{C(CH}_3)_3$ ), 35.1 (s, N- $\text{CH}_3$ ), 38.3 (d,  $^1J_{\text{C-P}} = 11$  Hz,  $\text{C(CH}_3)_3$ ), 122.0 (s, CH on carbene), 122.5 (d,  $^2J_{\text{C-P}} = 7$  Hz, CH on backbone of carbene), 127.6 (s, *m*- $\text{PPh}_3$ ), 129.0 (s, *p*- $\text{PPh}_3$ ), 134.2 (s, *o*- $\text{PPh}_3$ ).

$^{31}\text{P}\{^1\text{H}\}$  NMR ( $\text{C}_6\text{D}_6$ ):  $\delta$  48.8 (d,  $^2J_{\text{P-P}} = 99$  Hz,  $\text{PPh}_3$ ), 119.8 (t,  $^2J_{\text{P-P}} = 99$  Hz,  $\text{P}^t\text{Bu}_2$ ).

#### Elemental Analysis:

Calculated C: 66.88, H: 6.07, N: 3.18. Found C: 66.01, H: 5.98, N: 3.79.

$\nu_{\text{CO}} = 1909 \text{ cm}^{-1}$ .

\*Peaks corresponding to the CO, carbene, and *ipso* carbon atoms were not found despite long acquisition times.

### Characterization of Ru(II) complex 2-6:

**$^1\text{H}$  NMR ( $\text{CD}_2\text{Cl}_2$ ):**  $\delta$  -12.42 (dd,  $^2J_{\text{P-H}} = 103$  Hz,  $^2J_{\text{P-H}} = 17$  Hz, 1H, Ru-H), 1.28 (dd,  $^3J_{\text{P-H}} = 54$  Hz,  $^3J_{\text{P-H}} = 14$  Hz, 9H, C(CH<sub>3</sub>)<sub>3</sub>), 1.45 (dd,  $^3J_{\text{P-H}} = 38$  Hz,  $^3J_{\text{P-H}} = 15$  Hz, 9H, C(CH<sub>3</sub>)<sub>3</sub>), 3.19 (s, 3H, N-CH<sub>3</sub>), 3.78 (s, 3H, N-CH<sub>3</sub>), 7.07 (dt,  $^3J_{\text{P-H}} = 21$  Hz,  $^3J_{\text{P-H}} = 2$  Hz, 2H, CH on backbone of carbene), 7.21 (s, 1H, CH on backbone of carbene), 7.36 (s, 1H, CH on backbone of carbene).

**$^{13}\text{C}\{^1\text{H}\}$  NMR ( $\text{CD}_2\text{Cl}_2$ ):**  $\delta$  28.9 (d,  $^2J_{\text{P-C}} = 8$  Hz, C(CH<sub>3</sub>)<sub>3</sub>), 29.6 (d,  $^2J_{\text{P-C}} = 5$  Hz, C(CH<sub>3</sub>)<sub>3</sub>), 37.8 (d,  $^1J_{\text{P-C}} = 14$  Hz, C(CH<sub>3</sub>)<sub>3</sub>), 38.8 (d,  $^1J_{\text{P-C}} = 10$  Hz, C(CH<sub>3</sub>)<sub>3</sub>), 39.0 (d,  $^1J_{\text{P-C}} = 7$  Hz, C(CH<sub>3</sub>)<sub>3</sub>), 36.2 (s, N-CH<sub>3</sub>), 36.9 (s, N-CH<sub>3</sub>), 123.2 (d,  $^2J_{\text{P-C}} = 7$  Hz, CH on backbone of carbene), 123.4 (d,  $^2J_{\text{C-P}} = 7$  Hz, CH on backbone of carbene), 125.1 (s, CH on backbone of carbene), 125.3 (s, CH on backbone of carbene), 182.4 (m, CO), 214.0 (m, N-C-N).

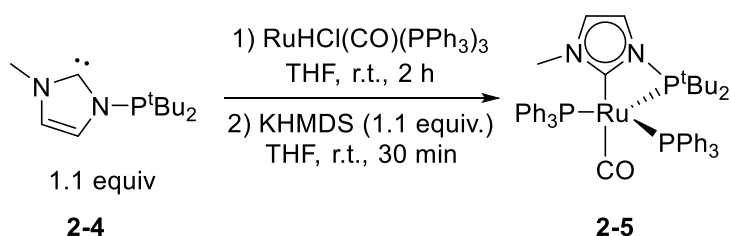
**$^{31}\text{P}\{^1\text{H}\}$  NMR ( $\text{CD}_2\text{Cl}_2$ ):**  $\delta$  101.1 (d,  $^2J_{\text{P-P}} = 187$  Hz, P<sup>t</sup>Bu<sub>2</sub>), 129.8 (d,  $^2J_{\text{P-P}} = 190$  Hz, P<sup>t</sup>Bu<sub>2</sub>).

### Elemental Analysis:

Calculated C: 48.58, H: 7.66, N: 9.06. Found C: 47.95, H: 6.95, N: 9.25.

\*Peak corresponding to the second carbene carbon was not found despite long acquisition times.

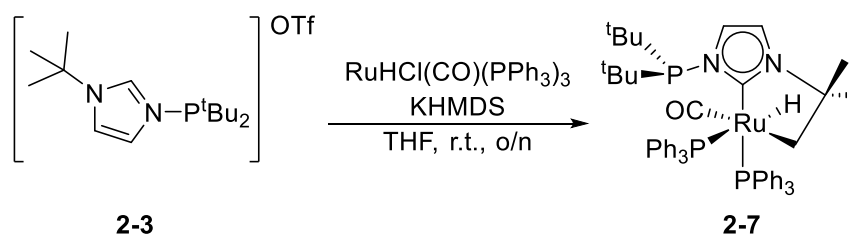
### 2.4.3.6 Selective Synthesis of complex 2-5



A 20 ml scintillation vial was equipped with a stir bar and RuHCl(CO)(PPh<sub>3</sub>)<sub>3</sub> (0.673 g, 0.709 mmol). A solution of **2-4** (0.174 g, 0.768 mmol) in THF (10 mL) was added to the vial to afford a beige suspension and the mixture was stirred at room temperature for 2 hours. Within 15 minutes a colour change from beige to bright orange/red was observed. After 2 hours KHMDS (0.234 g, 1.174 mmol) in THF (2 mL) was added dropwise to the orange suspension. The

mixture immediately became a dark red solution. The reaction mixture was allowed to carry on at room temperature for 1 hour; during which time the colour of the reaction became a very dark crimson red. The solution was then concentrated under vacuum to dryness and dark red residue washed with benzene (3 x 4 mL) to extract product. The extracts were filtered through a Celite plug and filtrate was concentrated to 2 mL. The vial was left standing overnight at room temperature to precipitate product and then the dark red supernatant was removed, and the residue was washed with pentanes (5 x 5 mL). Complex **2-5** was then dried under vacuum and obtained as a bright orange solid (0.202 g, 33%). Characterization of product consistent with data reported above.

#### 2.4.3.7 Synthesis of complex **2-7**



Solution of imidazolium triflate **2-3** (0.155 g, 0.369 mmol) in THF (3 mL) added to a suspension of RuHCl(CO)(PPh<sub>3</sub>)<sub>3</sub> (0.323 g, 0.340 mmol) in THF (2 mL). The beige suspension was stirred at -45 °C for 10 minutes and KHMDS (0.177 g, 0.885 mmol) in THF (3 mL) was added dropwise to the stirring suspension. The mixture warmed to room temperature and stirred overnight; colour was observed to change from beige to dark orange/red. The solution was evacuated to dryness and residue dissolved in benzene, whereby a precipitate was seen to form. Crimson red suspension passed through Celite plug and washed with benzene (1 mL). The filtrate was concentrated to 1 mL and added dropwise to stirring cold pentanes (10 mL) to afford a beige suspension, which was placed in freezer for two days. The solid was then collected on a glass frit, washed with pentanes (3 x 5 mL) and dried under vacuum to afford the product as a beige powder (0.182 g, 58%). X-ray quality crystals were grown from a concentrated benzene solution layered with pentane for several days. Several peaks in <sup>1</sup>H NMR spectrum overlap and thus both room temperature and low temperature data are provided below. However, some aryl proton resonances became too broad to be seen in the low-temperature spectrum. Unfortunately, <sup>13</sup>C{<sup>1</sup>H} variable temperature NMR spectra did not provide any information as all signals were too broad.

**$^1\text{H}$  NMR ( $\text{C}_6\text{D}_6$ ,  $25\text{ }^\circ\text{C}$ ):**  $\delta$  -7.90 (dd,  $^2J_{\text{P-H}} = 102\text{ Hz}$ ,  $^2J_{\text{P-H}} = 30\text{ Hz}$ , 1H, Ru-*H*), 0.86 (d,  $^3J_{\text{P-H}} = 12\text{ Hz}$ , 9H,  $\text{PC}(\text{CH}_3)_3$ ), 1.27-1.32 (m, 15H,  $\text{PC}(\text{CH}_3)_3$  and  $\text{C}(\text{CH}_3)_2$ ), 6.51 (d,  $^3J_{\text{P-H}} = 2\text{ Hz}$ , 1H, *CH* on carbene backbone), 6.90 (d,  $^4J_{\text{P-H}} = 2\text{ Hz}$ , 1H, *CH* on carbene backbone), 6.99-7.02 (m, 16H, Ar-*H*), 7.37-7.41 (m, 2H, Ar-*H*), 7.45-7.49 (m, 6H, Ar-*H*), 7.61-7.65 (m, 6H, Ar-*H*).

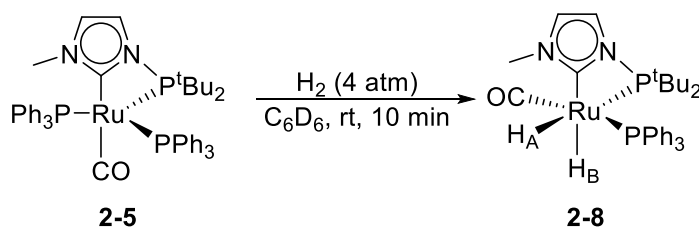
**$^1\text{H}$  NMR (toluene-*ds*,  $-40\text{ }^\circ\text{C}$ ):**  $\delta$  -7.85 (dd,  $^2J_{\text{P-H}} = 101\text{ Hz}$ ,  $^2J_{\text{P-H}} = 28\text{ Hz}$ , 1H, Ru-*H*), 0.79 (d,  $^3J_{\text{P-H}} = 12\text{ Hz}$ , 9H,  $\text{PC}(\text{CH}_3)_3$ ), 0.91 (t,  $^2J_{\text{H-H}} = 7\text{ Hz}$ , 2H, virtual triplet as a result of overlapping diastereotopic  $\text{CH}_2$  protons), 1.26 (d,  $^3J_{\text{P-H}} = 12\text{ Hz}$ , 9H,  $\text{PC}(\text{CH}_3)_3$ ), 1.33 (s, 3H, diastereotopic  $\text{CH}_3$ ), 1.37 (s, 3H, diastereotopic  $\text{CH}_3$ ), 6.42 (s, 1H, *CH* on carbene backbone), 6.80 (s, 1H, *CH* on carbene backbone), 6.96 (m, 12H, Ar-*H*), 7.00 (m, 4H, Ar-*H*), 7.54 (s, br, 6H, Ar-*H*).

**$^{31}\text{P}\{^1\text{H}\}$  NMR (toluene-*ds*,  $-40\text{ }^\circ\text{C}$ ):**  $\delta$  -6.6 (s, free  $\text{PPh}_3$ ), 32.3 (d,  $^2J_{\text{P-P}} = 16\text{ Hz}$ ,  $\text{PPh}_3$ ), 57.6 (d,  $^2J_{\text{P-P}} = 15\text{ Hz}$ ,  $\text{PPh}_3$ ), 84.4 (s,  $\text{P}^t\text{Bu}_2$ ).

### Elemental Analysis:

Calculated C: 67.74 H: 6.45 N: 3.04. Found C: 67.53 H: 6.38 N: 2.95.

### 2.4.3.8 Generation of complex **2-8**



A J-Young NMR tube was charged with complex **2-5** (0.053 g, 0.060 mmol) in  $\text{C}_6\text{D}_6$  (1 mL). The bright orange solution was degassed using three consecutive cycles of freeze-pump-thaw and backfilled with  $\text{H}_2$  (4 atm). The colour of the mixture rapidly changed from orange to pale yellow.  $^{31}\text{P}\{^1\text{H}\}$  NMR data indicated the dissociation of one triphenylphosphine moiety from the complex in solution. Isolation of the product for the purposes of IR and crystallographic analyses proved difficult as the product could not be crystallized.

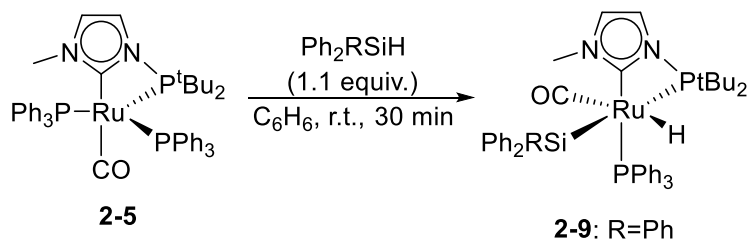
**$^1\text{H}$  NMR ( $\text{C}_6\text{D}_6$ ):**  $\delta$  : -10.38 (ddd,  $^2J_{\text{P-H}} = 103\text{ Hz}$ ,  $^2J_{\text{P-H}} = 23\text{ Hz}$ ,  $^2J_{\text{H-H}} = 5\text{ Hz}$ , 1H, Ru- $\text{H}_A$ ), -5.12 (ddd,  $^2J_{\text{P-H}} = 24\text{ Hz}$ ,  $^2J_{\text{P-H}} = 17\text{ Hz}$ ,  $^2J_{\text{H-H}} = 5\text{ Hz}$ , 1H, Ru- $\text{H}_B$ ), 1.01 (d,  $^3J_{\text{P-H}} = 13\text{ Hz}$ , 9H,  $\text{C}(\text{CH}_3)_3$ ), 1.17 (d,  $^3J_{\text{P-H}} = 13\text{ Hz}$ , 9H,  $\text{C}(\text{CH}_3)_3$ ), 3.17 (s, 3H, N- $\text{CH}_3$ ), 5.84 (br s, 1H, *CH* on

backbone of carbene), 6.12-6.13 (m, 1H, CH backbone of carbene), 7.00 – 7.14 (m, 18H, PPh<sub>3</sub>), 7.37 – 8.17 (m, 12H, PPh<sub>3</sub>).

<sup>13</sup>C{<sup>1</sup>H} NMR (C<sub>6</sub>D<sub>6</sub>): δ 27.5 (d, <sup>2</sup>J<sub>P-C</sub> = 2 Hz, C(CH<sub>3</sub>)<sub>3</sub>), 27.6 (d, <sup>2</sup>J<sub>P-C</sub> = 2 Hz, C(CH<sub>3</sub>)<sub>3</sub>), 34.0 (s, N-CH<sub>3</sub>), 34.1 (d, <sup>1</sup>J<sub>P-C</sub> = 9 Hz, C(CH<sub>3</sub>)<sub>3</sub>), 35.0 (d, <sup>1</sup>J<sub>P-C</sub> = 11 Hz, C(CH<sub>3</sub>)<sub>3</sub>) 118.2 (d, <sup>2</sup>J<sub>P-C</sub> = 4 Hz, CH on backbone of carbene), 119.5 (d, <sup>2</sup>J<sub>P-C</sub> = 2 Hz, CH on backbone of carbene), 132.1 (s, *p*-PPh<sub>3</sub>), 132.6 (s, *m*-PPh<sub>3</sub>), 136.0 (s, *o*-PPh<sub>3</sub>), 140.8 (dd, <sup>1</sup>J<sub>P-C</sub> = 35 Hz, <sup>3</sup>J<sub>P-C</sub> = 3 Hz, *ipso*-PPh<sub>3</sub>), 189.8 (dd, <sup>2</sup>J<sub>P-C</sub> = 77 Hz, <sup>2</sup>J<sub>P-C</sub> = 8 Hz, CO), 209.6 (dd, <sup>2</sup>J<sub>P-C</sub> = 9 Hz, <sup>2</sup>J<sub>P-C</sub> = 4 Hz, N-C-N).

<sup>31</sup>P{<sup>1</sup>H} NMR (C<sub>6</sub>D<sub>6</sub>): δ -5.4 (s, free PPh<sub>3</sub>), 65.4 (d, <sup>2</sup>J<sub>P-P</sub> = 13 Hz, PPh<sub>3</sub>), 125.2 (d, <sup>2</sup>J<sub>P-P</sub> = 13 Hz, N-P(<sup>t</sup>Bu<sub>2</sub>)).

### 2.4.3.9 Synthesis of complex **2-9**



To a bright orange benzene (8 mL) solution of complex **2-5** (0.044 g, 0.050 mmol) was added Ph<sub>3</sub>SiH (0.015 g, 0.056 mmol) in benzene (1 mL). The orange colour rapidly changed to pale yellow. The reaction was allowed to proceed at room temperature for 30 minutes before being evacuated to dryness. Pentane (8 mL) was added to the residue and stirred vigorously for 10 minutes. The suspension was filtered over Celite and washed with pentanes (2 mL). The yellow residue was dissolved in benzene (5 mL) and the filtrate was concentrated to dryness to afford complex **2-9** as a pale-yellow solid (0.035 g, 80%). X-ray quality crystals were grown by layering a saturated benzene solution of the product with pentane.

<sup>1</sup>H NMR (C<sub>6</sub>D<sub>6</sub>): δ : -4.20 (dd, <sup>2</sup>J<sub>P-H</sub> = 19 Hz, <sup>2</sup>J<sub>P-H</sub> = 15 Hz, 1H, Ru-H), 0.78 (d, <sup>3</sup>J<sub>P-H</sub> = 13 Hz, 9H, C(CH<sub>3</sub>)<sub>3</sub>), 1.38 (d, <sup>3</sup>J<sub>P-H</sub> = 13 Hz, 9H, C(CH<sub>3</sub>)<sub>3</sub>), 2.56 (s, 3H, N-CH<sub>3</sub>), 5.43 (bs, 1H, CH on carbene backbone), 6.06 (m, 1H, CH on carbene backbone), 7.37 – 7.73 (m, 30H, PPh<sub>3</sub>).

<sup>13</sup>C{<sup>1</sup>H} NMR (C<sub>6</sub>D<sub>6</sub>): δ 29.1 (d, <sup>2</sup>J<sub>P-C</sub> = 10 Hz, C(CH<sub>3</sub>)<sub>3</sub>), 29.2 (d, <sup>2</sup>J<sub>P-C</sub> = 8 Hz, C(CH<sub>3</sub>)<sub>3</sub>), 36.0 (s, N-CH<sub>3</sub>), 37.0 (d, <sup>1</sup>J<sub>P-C</sub> = 10 Hz, C(CH<sub>3</sub>)<sub>3</sub>), 37.5 (d, <sup>1</sup>J<sub>P-C</sub> = 15 Hz, C(CH<sub>3</sub>)<sub>3</sub>), 120.6 (s, CH on

carbene), 122.5 (d,  $^2J_{P-C} = 2$  Hz, CH on carbene), 128.0 (s, *m*-SiPh<sub>3</sub>), 128.3 (s, *m*-PPh<sub>3</sub>), 129.7 (s, *p*-SiPh<sub>3</sub>), 133.7 (s, *p*-PPh<sub>3</sub>), 133.9 (s, *ipso*-SiPh<sub>3</sub>), 135.3 (s, *o*-SiPh<sub>3</sub>), 135.9 (s, *o*-PPh<sub>3</sub>), 137.7 (d,  $^1J_{P-C} = 12$  Hz, *ipso*-PPh<sub>3</sub>), 182.9 (dd,  $^2J_{P-C} = 81$  Hz, 6 Hz, N-C-N), 211.7 (dd,  $^2J_{P-C} = 13$  Hz, 2 Hz, CO).

$^{31}\text{P}\{^1\text{H}\}$  NMR (C<sub>6</sub>D<sub>6</sub>):  $\delta$  55.7 (d,  $^2J_{P-P} = 18$  Hz, PPh<sub>3</sub>), 103.4 (d,  $^2J_{P-P} = 18$  Hz, N-P<sup>t</sup>Bu<sub>2</sub>).

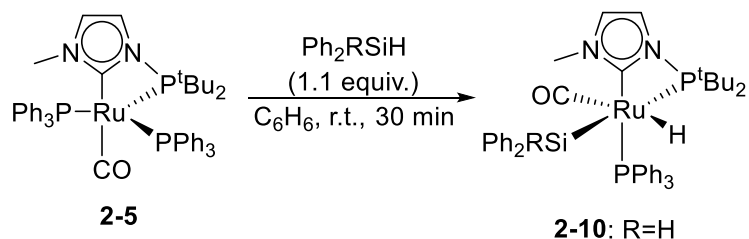
### Elemental Analysis:

Calculated C: 67.03, H: 6.20, N: 3.19. Found C: 66.87, H: 5.94, N: 2.89.

$\nu_{\text{CO}} = 1918$  cm<sup>-1</sup>.

\*Despite long acquisition times, no resonances were observed in the  $^{29}\text{Si}$  NMR spectra.

### 2.4.3.10 Synthesis of complex **2-10**



Complex **2-10** was obtained in a similar fashion to complex **2-9** (0.028 g, 71%). X-ray quality crystals were grown by layering a saturated benzene solution of the product with pentane.

$^1\text{H}$  NMR (C<sub>6</sub>D<sub>6</sub>):  $\delta$  -4.61 (td,  $^2J_{P-H} = 18$  Hz,  $^3J_{H-H} = 4$  Hz, 1H, Ru-H), 0.99 (d,  $^3J_{P-H} = 13$  Hz, 9H, C(CH<sub>3</sub>)<sub>3</sub>), 1.17 (d,  $^3J_{P-H} = 13$  Hz, 9H, C(CH<sub>3</sub>)<sub>3</sub>), 2.70 (s, 3H, N-CH<sub>3</sub>), 5.51 (s, 1H, CH on carbene backbone), 5.80 (m, 1H, Si-H), 6.05 (dd,  $^3J_{P-H} = 2$  Hz, 1H, CH on carbene backbone), 6.99 – 8.19 (m, 25H, Ar-H).

$^{13}\text{C}\{^1\text{H}\}$  NMR (C<sub>6</sub>D<sub>6</sub>):  $\delta$  29.1 (d,  $^2J_{P-C} = 6$  Hz, C(CH<sub>3</sub>)<sub>3</sub>), 29.2 (d,  $^2J_{P-C} = 4$  Hz, C(CH<sub>3</sub>)<sub>3</sub>), 36.3 (d,  $^1J_{P-C} = 9$  Hz, C(CH<sub>3</sub>)<sub>3</sub>), 36.4 (s, N-CH<sub>3</sub>), 37.0 (d,  $^1J_{P-C} = 14$  Hz, C(CH<sub>3</sub>)<sub>3</sub>), 188.2 (s, CH on carbene), 123.5 (d,  $^2J_{P-C} = 3$  Hz, CH on carbene), 127.9 (s, *m*-SiPh<sub>2</sub>), 128.2 (s, *m*-PPh<sub>3</sub>), 128.8 (s, *p*-SiPh<sub>2</sub>), 133.7 (s, *p*-PPh<sub>3</sub>), 134.3 (s, *o*-SiPh<sub>2</sub>), 135.8 (s, *o*-PPh<sub>3</sub>), 136.2 (s, *ipso*-SiPh<sub>2</sub>), 137.7 (d,  $^1J_{P-C} = 12$  Hz, *ipso*-PPh<sub>3</sub>).

$^{31}\text{P}\{^1\text{H}\}$  NMR ( $\text{C}_6\text{D}_6$ ):  $\delta$  58.5 (d,  $^2J_{\text{P-P}} = 17$  Hz,  $\text{PPh}_3$ ), 104.5 (d,  $^2J_{\text{P-P}} = 18$  Hz,  $\text{N-P}^t\text{Bu}_2$ ).

$^{29}\text{Si}\{^1\text{H}\}$  DEPT-135 NMR ( $\text{C}_6\text{D}_6$ ):  $\delta$  19.6 (dd,  $^2J_{\text{Si-Ptrans}} = 96$  Hz,  $^2J_{\text{Si-Pcis}} = 19$  Hz).

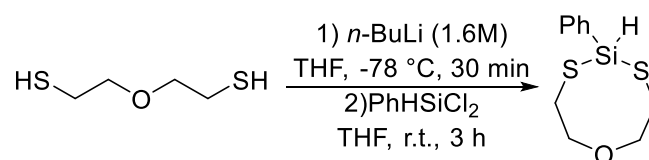
### Elemental Analysis:

Calculated C: 64.40, H: 6.28, N: 3.49. Found C: 64.00, H: 5.88, N: 3.11.

$\nu_{\text{CO}} = 1931 \text{ cm}^{-1}$ .

\*Peaks corresponding to the carbene and CO carbons were not found despite long acquisition times.

### 2.4.3.11 Synthesis of $\text{PhHSi}(\text{SCH}_2\text{CH}_2)\text{O}$



The cyclic silane was prepared according to a literature procedure with modifications.<sup>5</sup> To a solution of bis(mercaptoethyl)ether (0.095 g, 0.687 mmol) in THF (15 mL) in a 50 mL flask, *n*-BuLi (0.5 mL, 1.6M in hexane) was added dropwise at  $-78$  °C. The solution was stirred for 30 minutes before  $\text{PhHSiCl}_2$  (0.132 g, 0.743 mmol) was slowly added to the reaction mixture. The reaction was stirred at  $-78$  °C for 30 minutes and then allowed to continue for 3 hours at room temperature. Then, hexanes (30 mL) were added to the mixture to precipitate LiCl. The suspension was filtered, and the filtrate was evaporated under vacuum. The product was washed with pentane (5 x 30 mL) and dried under vacuum to afford the title compound as colourless crystals (0.145 g, 87%).

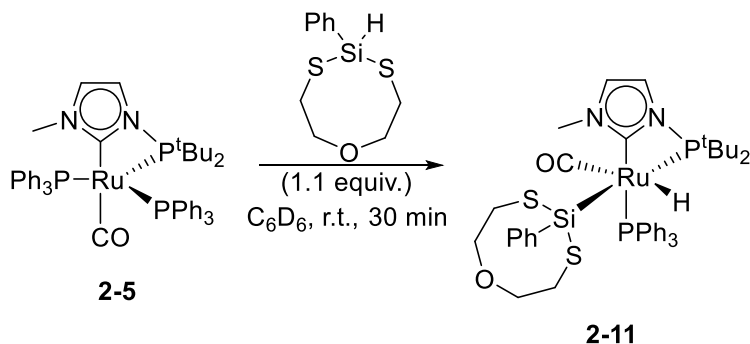
$^1\text{H}$  NMR ( $\text{CD}_2\text{Cl}_2$ ):  $\delta$  2.90-2.93 (m, 4H,  $\text{SCH}_2$ ), 3.63-3.68 (m, 2H,  $\text{CH}_2$ ), 3.85-3.90 (m, 2H,  $\text{CH}_2$ ), 5.80 (s, 1H, Si-H), 7.35-7.41 (m, 3H, Ph), 7.69-7.72 (m, 2H, Ph).

$^{13}\text{C}\{^1\text{H}\}$  NMR ( $\text{CD}_2\text{Cl}_2$ ):  $\delta$  29.1 (s,  $\text{SCH}_2$ ), 71.0 (s,  $\text{OCH}_2$ ), 127.9 (s, *m*-Ph), 130.0 (s, *p*-Ph), 133.9 (s, *o*-Ph), 136.2 (s, *ipso*-Ph).

$^{29}\text{Si}\{^1\text{H}\}$  DEPT-135 NMR ( $\text{CD}_2\text{Cl}_2$ ):  $\delta$  -2.8 (s, Si-H).

**Elemental Analysis:**

Calculated C:49.55, H: 5.82. Found C: 49.46, H: 5.80.

**2.4.3.12 Synthesis of complex 2-11**

Complex **2-11** was obtained in a similar fashion to complexes **2-9** and **2-10** (0.037 g, 86%).

**$^1\text{H}$  NMR ( $\text{C}_6\text{D}_6$ ):**  $\delta$  : -4.50 (dd,  $^2J_{\text{P-H}} = 22$  Hz,  $^2J_{\text{P-H}} = 17$  Hz, 1H, Ru-H), 0.77 (d,  $^3J_{\text{P-H}} = 14$  Hz, 9H, C(CH<sub>3</sub>)<sub>3</sub>), 1.23 (d,  $^3J_{\text{P-H}} = 13$  Hz, 9H, C(CH<sub>3</sub>)<sub>3</sub>), 2.11-2.18 (m, 1H, CH<sub>2</sub>), 2.42-2.53 (m, 2H, CH<sub>2</sub>), 2.77 (td,  $^2J_{\text{H-H}} = 14$  Hz,  $^3J_{\text{H-H}} = 4$  Hz, 1H, CH<sub>2</sub>), 3.19 (ddd,  $^2J_{\text{H-H}} = 16$  Hz,  $^3J_{\text{H-H}} = 13$  Hz,  $^3J_{\text{H-H}} = 4$  Hz, 2H, CH<sub>2</sub>), 3.78 (td,  $^2J_{\text{H-H}} = 13$  Hz,  $^3J_{\text{H-H}} = 4$  Hz, 1H, CH<sub>2</sub>), 3.94 (td,  $^2J_{\text{H-H}} = 12$  Hz,  $^3J_{\text{H-H}} = 4$  Hz, 1H, CH<sub>2</sub>), 4.54 (s, 3H, N-CH<sub>3</sub>), 5.96 (s, 1H, CH backbone of carbene), 6.08 (s, 1H, CH backbone of carbene), 6.88 – 8.20 (m, 20H, Ph).

**$^{13}\text{C}\{^1\text{H}\}$  NMR ( $\text{C}_6\text{D}_6$ ):**  $\delta$  28.7 (d,  $^2J_{\text{P-C}} = 5$  Hz, C(CH<sub>3</sub>)<sub>3</sub>), 28.8 (d,  $^2J_{\text{P-C}} = 5$  Hz, C(CH<sub>3</sub>)<sub>3</sub>), 29.1 (s, SCH<sub>2</sub>), 36.0 (d,  $^1J_{\text{P-C}} = 15$  Hz, C(CH<sub>3</sub>)<sub>3</sub>), 36.3 (d,  $^1J_{\text{P-C}} = 8$  Hz, C(CH<sub>3</sub>)<sub>3</sub>), 70.6 (s, OCH<sub>2</sub>), 120.1 (s, CH on carbene backbone), 123.9 (d,  $^2J_{\text{P-C}} = 2$  Hz, CH on carbene backbone), 127.9 (s, *m*-SiPh), 128.4 (s, *m*-PPh<sub>3</sub>), 129.9 (s, *p*-SiPh), 133.7 (s, *p*-PPh<sub>3</sub>), 134.3 (s, *o*-SiPh), 136.1 (s, *o*-PPh<sub>3</sub>), 136.2 (s, *ipso*-SiPh), 137.7 (d,  $^1J_{\text{P-C}} = 12$  Hz, *ipso*-PPh<sub>3</sub>).

**$^{31}\text{P}\{^1\text{H}\}$  NMR ( $\text{C}_6\text{D}_6$ ):**  $\delta$  54.9 (d,  $^2J_{\text{P-P}} = 20$  Hz, PPh<sub>3</sub>), 102.2 (d,  $^2J_{\text{P-P}} = 20$  Hz, N-PtBu<sub>2</sub>).

**Elemental Analysis:**

Calculated C: 57.25, H: 6.09, N: 3.26. Found C: 55.26, H: 5.26, N: 2.54.

$\nu_{\text{CO}} = 1918 \text{ cm}^{-1}$ .

\*Despite long acquisition times, no resonances were observed in the  $^{29}\text{Si}$  NMR spectra. Peaks corresponding to the carbene and CO carbons were not identified despite long acquisition times.

## 2.4.4 X-ray Crystallography

### 2.4.4.1 X-ray Data Collection and Reduction

Each crystal was coated in Paratone-N oil in the glove-box, mounted on a MiTeGen Micromount and placed under an  $\text{N}_2$  stream, thus maintaining a dry,  $\text{O}_2$ -free environment. The data were collected on a Bruker Apex II diffractometer employing Mo  $K\alpha$  radiation ( $\lambda = 0.71073 \text{ \AA}$ ). Data collection strategies were determined using Bruker Apex software and optimized to provide >99.5% data completion to a  $2\theta$  value of at least  $55^\circ$ . The data were collected at  $150(\pm 2) \text{ K}$  for all crystals. The frames were integrated with the Bruker SAINT software package using a narrow-frame algorithm. Data were corrected for absorption effects using the empirical multi-scan method (SADABS).<sup>45</sup>

### 2.4.4.2 X-ray Data Solution and Refinement

Non-hydrogen atomic scattering factors were taken from the literature tabulations.<sup>46</sup> The heavy atom positions were determined using direct methods employing the SHELXTL direct methods routine. The remaining non-hydrogen atoms were located from successive difference Fourier map calculations. The refinements were carried out by using full-matrix least squares techniques on  $F^2$ . In the final steps of each refinement, all non-hydrogen atoms were assigned anisotropic temperature factors in the absence of disorder or insufficient data. In the latter cases atoms were treated isotropically. C-H atom positions were calculated and allowed to ride on the carbon to which they are bonded. H-atom temperature factors were fixed at 1.20 times the isotropic temperature factor of the C-atom to which they are bonded. The H-atom contributions were calculated, but not refined. The locations of the largest peaks in the final difference Fourier map calculation as well as the magnitude of the residual electron densities in each case were of no chemical significance.

**Table 2.4.1. Select crystallographic data for 2-5, and 2-6.**

	(2-5)	(2-6)
Formula	C <sub>49</sub> H <sub>53</sub> N <sub>2</sub> OP <sub>3</sub> Ru	C <sub>62</sub> H <sub>114</sub> Cl <sub>4</sub> N <sub>8</sub> O <sub>2</sub> P <sub>4</sub> Ru <sub>2</sub>
Formula weight	879.91	1471.43
Crystal system	Trigonal	Monoclinic
Space group	<i>R</i> 3	<i>P</i> 2 <sub>1</sub> / <i>n</i>
a (Å)	35.628(4)	11.5609(8)
b (Å)	35.928(4)	28.1621(19)
c (Å)	10.4061	23.5527(15)
α (deg)	90	90
β (deg)	90	90.842(3)
γ (deg)	120	90
Volume (Å <sup>3</sup> )	11440(3)	7667.4(9)
Z	9	4
d (calc) gcm <sup>-3</sup>	1.150	1.275
R(int.)	0.1081	0.0992
Abs coeff, μ, mm <sup>-1</sup>	0.436	0.659
Data collected	9849	17544
Variables	513	750
>2σ(F <sub>o</sub> <sup>2</sup> )	6150	10694
R(>2σ)	0.0789	0.0605
R <sub>w</sub> (>2σ)	0.1771	0.1408
GOF	1.106	1.020

**Table 2.4.2. Select crystallographic data for 2-7, 2-9, and 2-10.**

	(2-7)	(2-9)	(2-10)
Formula	C <sub>52</sub> H <sub>59</sub> N <sub>2</sub> OP <sub>3</sub> Ru	C <sub>50</sub> H <sub>56</sub> Cl <sub>2</sub> N <sub>2</sub> OP <sub>2</sub> RuSi	C <sub>44</sub> H <sub>48</sub> N <sub>2</sub> O <sub>2</sub> P <sub>2</sub> RuSi
Formula weight	921.99	962.96	827.94
Crystal system	Orthorhombic	Triclinic	Monoclinic
Space group	<i>P</i> 2 <sub>1</sub> 2 <sub>1</sub> 2 <sub>1</sub>	<i>P</i> -1	<i>P</i> 2 <sub>1</sub> / <i>n</i>
a (Å)	12.9317(12)	10.1203(4)	14.8100(8)
b (Å)	17.7125(15)	11.7277(5)	17.6070(10)
c (Å)	20.3557(16)	20.6158(9)	16.9584(9)
α (deg)	90	102.745(2)	90
β (deg)	90	99.465(2)	106.458(3)
γ (deg)	90	92.991(2)	90
Volume (Å <sup>3</sup> )	4662.5(7)	2344.10(17)	4240.9(4)
Z	4	2	4
d (calc) gcm <sup>-3</sup>	1.313	1.364	1.297
R(int.)	0.0342	0.0211	0.0694
Abs coeff, μ, mm <sup>-1</sup>	0.478	0.581	0.510
Data collected	10727	10635	9706
Variables	536	543	455
>2σ(F <sub>o</sub> <sup>2</sup> )	9841	9710	6806
R(>2σ)	0.0250	0.0310	0.0708
R <sub>w</sub> (>2σ)	0.0519	0.0827	0.2303
GOF	1.050	1.050	1.543

## Chapter 2 References

- (1) Noyori, R. *Angew. Chem. Int. Ed.* **2002**, *41*, 2008–2022.
- (2) Glaser, P. B.; Tilley, T. D. *J. Am. Chem. Soc.* **2003**, *125*, 13640–13641.
- (3) Grubbs, R. H. *Angew. Chem. Int. Ed.* **2006**, *45*, 3760–3765.
- (4) Belderrain, R.; Grubbs, R. H. *Organometallics* **1997**, *16*, 4001–4003.
- (5) McKinty, A. M.; Stephan, D. W. *Dalton Trans.* **2014**, *43*, 2710–2712.
- (6) Cabeza, J. A.; Damonte, M.; García-Álvarez, P.; Pérez-Carreño, E. *Organometallics* **2013**, *32*, 4382–4390.
- (7) Cabeza, J. A.; Damonte, M.; García-Álvarez, P.; Pérez-Carreño, E. *Chem. Commun.* **2013**, *49*, 2813–2815.
- (8) Park, B. Y.; Luong, T.; Sato, H.; Krische, M. J. *J. Am. Chem. Soc.* **2015**, *137*, 7652–7655.
- (9) Gilbert-Wilson, R.; Field, L. D.; Colbran, S. B.; Bhadbhade, M. M. *Inorg. Chem.* **2013**, *52*, 3043–3053.
- (10) Trathen, N.; Greenacre, V. K.; Crossley, I. R.; Roe, S. M. *Organometallics* **2013**, *32*, 2501–2504.
- (11) Barrios-Francisco, R.; Balaraman, E.; Diskin-Posner, Y.; Leitun, G.; Shimon, L. J. W.; Milstein, D. *Organometallics* **2013**, *32*, 2973–2982.
- (12) Gaillard, S.; Renaud, J.-L. *Dalton Trans.* **2013**, *42*, 7255–7270.
- (13) Samojłowicz, C.; Bieniek, M.; Grela, K. *Chem. Rev.* **2009**, *109*, 3708–3742.
- (14) Bantreil, X.; Schmid, T. E.; Randall, R. A. M.; Slawin, A. M. Z.; Cazin, C. S. J. *Chem. Commun.* **2010**, *46*, 7115–7117.
- (15) Abdellah, I.; Boggio-Pasqua, M.; Canac, Y.; Lepetit, C.; Duhayon, C.; Chauvin, R. *Chem. Eur. J.* **2011**, *17*, 5110–5115.

- (16) Abdellah, I.; Lepetit, C.; Canac, Y.; Duhayon, C.; Chauvin, R. *Chem. Eur. J.* **2010**, *16*, 13095–13108.
- (17) Ellis, B. D.; Ragogna, P. J.; Macdonald, C. L. B. *Inorg. Chem.* **2004**, *43*, 7857–7867.
- (18) Kelly, R. A.; Clavier, H.; Giudice, S.; Scott, N. M.; Stevens, E. D.; Bordner, J.; Samardjiev, I.; Hoff, C. D.; Cavallo, L.; Nolan, S. P. *Organometallics* **2008**, *27*, 202–210.
- (19) Huang, J.; Stevens, E. D.; Nolan, S. P.; Petersen, J. L. *J. Am. Chem. Soc.* **1999**, *121*, 2674–2678.
- (20) Zoller, U. *Tetrahedron* **1988**, *44*, 7413–7426.
- (21) Azouri, M.; Andrieu, J.; Picquet, M.; Cattey, H. *Inorg. Chem.* **2009**, *48*, 1236–1242.
- (22) Böttcher, T.; Bassil, B. S.; Zhechkov, L.; Heine, T.; Röschenthaler, G.-V. *Chem. Sci.* **2013**, *4*, 77–83.
- (23) Azouri, M.; Andrieu, J.; Picquet, M.; Richard, P.; Hanquet, B.; Tkatchenko, I. *Eur. J. Inorg. Chem.* **2007**, 4877–4883.
- (24) Marchenko, A. P.; Koidan, H. N.; Hurieva, A. N.; Pervak, I. I.; Shishkina, S. V.; Shishkin, O. V.; Kostyuk, A. N. *Eur. J. Org. Chem.* **2012**, 4018–4033.
- (25) Kühnel, E.; Shishkov, I. V.; Rominger, F.; Oeser, T.; Hofmann, P. *Organometallics* **2012**, *31*, 8000–8011.
- (26) Marchenko, A. P.; Koidan, H. N.; Pervak, I. I.; Huryeva, A. N.; Zarudnitskii, E. V.; Tolmachev, A. A.; Kostyuk, A. N. *Tetrahedron Lett.* **2012**, *53*, 494–496.
- (27) Marchenko, A. P.; Koidan, H. N.; Huryeva, A. N.; Zarudnitskii, E. V.; Yurchenko, A. A.; Kostyuk, A. N. *J. Org. Chem.* **2010**, *75*, 7141–7145.
- (28) Mosaferi, E.; Pan, L.; Wang, T.; Sun, Y.; Pranckevicius, C.; Stephan, D. W. *Dalton Trans.* **2016**, *45*, 1354–1358.
- (29) Ai, P.; Danopoulos, A. a; Braunstein, P.; Monakhov, K. Y. *Chem. Commun.* **2014**, *50*,

103–105.

- (30) Marchenko, A. P.; Koidan, H. N.; Hurieva, A. N.; Gutov, O. V.; Kostyuk, A. N.; Tubaro, C.; Lollo, S.; Lanza, A.; Nestola, F.; Biffis, A. *Organometallics* **2013**, *32*, 718–721.
- (31) Nägele, P.; Herrlich, U.; Rominger, F.; Hofmann, P. *Organometallics* **2013**, *32*, 181–191.
- (32) Brown, C. C.; Plessow, P. N.; Rominger, F.; Limbach, M.; Hofmann, P. *Organometallics* **2014**, *33*, 6754–6759.
- (33) Massard, A.; Braunstein, P.; Danopoulos, A. A.; Choua, S.; Rabu, P. *Organometallics* **2015**, *22*, 2429–2438.
- (34) Benhamou, L.; Wolf, J.; César, V.; Labande, A.; Poli, R.; Lugano, N.; Lavigne, G. *Organometallics* **2009**, *28*, 6981–6993.
- (35) Brown, C. C.; Rominger, F.; Limbach, M.; Hofmann, P. *Inorg. Chem.* **2015**, *54*, 10126–10140.
- (36) Cassani, M. C.; Brucka, M. A.; Femoni, C.; Mancinelli, M.; Mazzanti, A.; Mazzoni, R.; Solinas, G. *New J. Chem.* **2014**, *38*, 1768–1779.
- (37) Gusev, D. G. *Organometallics* **2009**, *28*, 763–770.
- (38) Mathew, J.; Koga, N.; Suresh, C. H. *Organometallics* **2008**, *27*, 4666–4670.
- (39) Fogler, E.; Iron, M. A.; Zhang, J.; Ben-David, Y.; Diskin-posner, Y.; Leitus, G.; Shimon, L. J. W.; Milstein, D. *Inorg. Chem.* **2013**, *52*, 11469–11479.
- (40) Davies, C. J. E.; Lowe, J. P.; Mahon, M. F.; Poulten, R. C.; Whittlesey, M. K. *Organometallics* **2013**, *32*, 4927–4937.
- (41) Grumbine, S. K.; Mitchell, G. P.; Straus, D. A.; Tilley, T. D.; Rheingold, A. L. *Organometallics* **1998**, *17*, 5607–5619.
- (42) Derrah, E. J.; Pantazis, D. A.; McDonald, R.; Rosenberg, L. *Organometallics* **2007**, *26*, 1473–1482.

- (43) Hübler, K.; Hübler, U.; Roper, W. R.; Schwerdtfeger, P.; Wright, L. J. *Chem. Eur. J.* **1997**, *3*, 1608–1616.
- (44) Lemke, F. R.; Simons, R. S.; Youngs, W. J. *Organometallics* **1996**, *15*, 216–221.
- (45) *Apex 2 Software Package*; Bruker AXS Inc., 2013.
- (46) Cromer, D. T.; W., J. T. *Int. Tables X-Ray Crystallography*; 1974; Vol. 4.

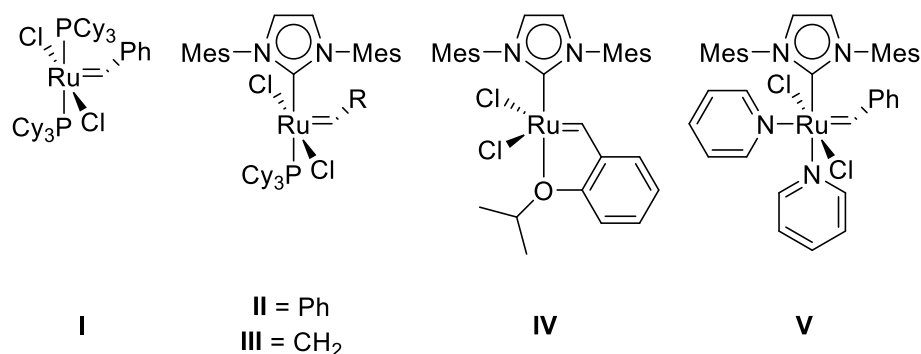
## Chapter 3

### Rearrangement and Decomposition of Ru-NHCP Complexes

#### 3.1 Introduction

##### 3.1.1 Catalyst Decomposition and Deactivation

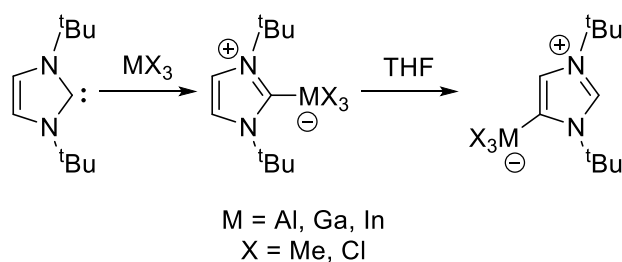
Catalyst decomposition occurs when the active species of a catalytic cycle is irreversibly altered to form a different, inactive species. In many cases this deactivation pathway involves aggregation of the metal centers to form the elemental metal, which is usually deposited out of solution. Other times, it operates through transformation of the catalyst to a discrete species. Thus, to better understand the reactivity and selectivity of any catalytic process, it is crucial to examine the relevant deactivation and decomposition pathways and products. In the case of olefin metathesis, Grubbs *et al.* have carried out significant studies on the decomposition of ruthenium metathesis catalysts (Figure 3.1.1).<sup>1</sup> Furthermore, it has been shown that the decomposition of complexes I and II with primary alcohols leads to complete degradation of the alkylidene complex to  $\text{RuHCl}(\text{CO})(\text{L})(\text{PCy}_3)$  ( $\text{L} = \text{NHC}$  or  $\text{PCy}_3$ ).<sup>2-4</sup> As well, Diver *et al.* have reported on the CO-promoted insertion of the alkylidene fragments of II and III into the mesityl substituent of the NHC ligand.<sup>5</sup> Furthermore, studies on tertiary phosphine ligands have identified P-C bond cleavage reactions as a key process in the aggregation and deactivation of several Fe, Ru, Co, and Ir catalysts that are involved in hydroformylation and hydrogenation reactions.<sup>6</sup>



**Figure 3.1.1: Various olefin metathesis catalysts studied for decomposition and deactivation.**

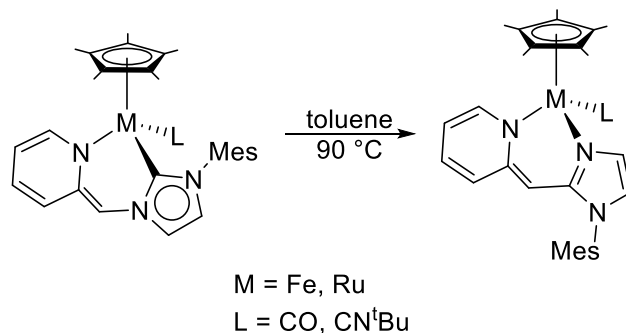
### 3.1.2 Rearrangement Reactivity of NHC complexes

Since their first isolation by Arduengo, N-heterocyclic carbenes have been widely employed in the coordination sphere of transition metals.<sup>7-14</sup> These versatile ligands have generally been shown to act as spectator ligands, aiding in the stabilization of transition metal species. However, examples of non-innocent behaviour have been documented that result in rearrangement to abnormal carbenes *via* C-H activation of the backbone (Scheme 3.1.1).<sup>15-18</sup>



**Scheme 3.1.1: Synthesis of “normal” carbene adducts and their migration to “abnormal” imidazolylidene carbenes.**

In comparison to “normal” NHCs, abnormal carbenes exhibit significantly stronger  $\sigma$ -donating character, owing to the vinylic nature of the backbone carbene. Furthermore, since the metal-binding carbon is situated further away from the N-substituents, abnormal NHCs are often less sterically hindered and this may further promote the rearrangement reaction from a normal carbene to an abnormal one.<sup>19</sup> As well, coordination of nitrogen following the loss of a substituent (Scheme 3.1.2),<sup>20</sup> activation of C-H and C-C substituents,<sup>21</sup> and reductive elimination have also been observed.<sup>22,23</sup>

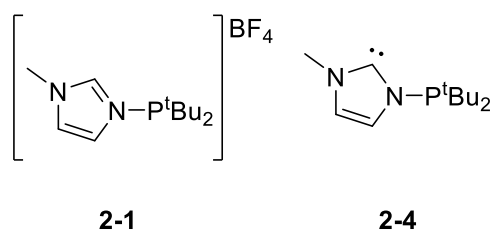


**Scheme 3.1.2: Rearrangement of N-picolyl substituted NHC *via* cleavage of C-N bond.**

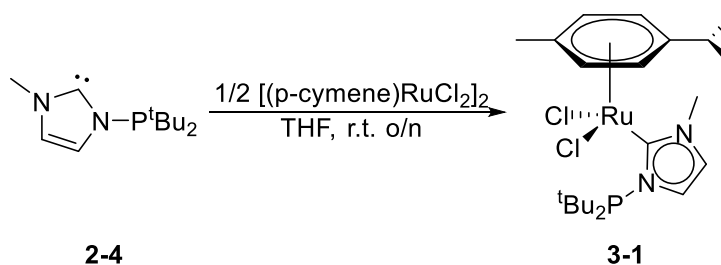
This chapter will describe the synthesis of several ruthenium-NHCP complexes and will focus on their degradation and decomposition pathways. The catalytic utility of the isolated complexes will also be discussed.

## 3.2 Results and Discussion

Compounds **2-1** and **2-4** (Figure 3.2.1) were synthesized according to procedures described in Chapter 2. Reaction of **2-4** in THF with a half-equivalent of  $[\text{RuCl}_2(p\text{-cymene})]_2$  dimer for several hours results in complete conversion to **3-1** (Scheme 3.2.1). Complex **3-1** can be isolated as a yellow-orange solid in 77% yield. NMR spectroscopy studies of **3-1** reveal a  $^{31}\text{P}$  NMR resonance at 121 ppm and it seems to suggest the phosphorus arm is not ligated to the metal center in solution, as such a binding mode in related complexes generally appears further upfield in the  $^{31}\text{P}$  NMR spectrum.<sup>24</sup> However, this cannot be unambiguously assigned due to difficulties in obtaining single crystal X-ray diffraction studies. Furthermore, the  $^1\text{H}$  NMR spectrum shows four inequivalent aromatic proton resonances ranging from 5.37-6.54 ppm. As well, the *tert*-butyl groups on phosphorus display inequivalent methyl resonances in solution, each integrating to nine protons.

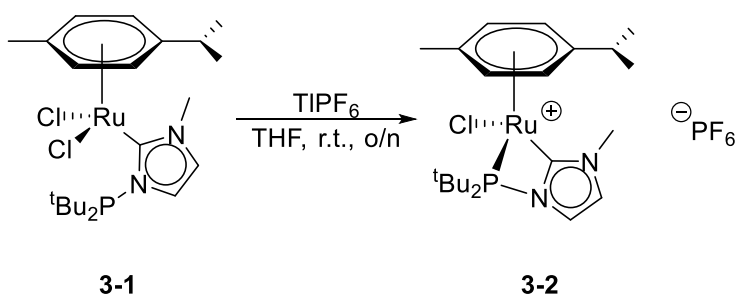


**Figure 3.2.1: Phosphorylated imidazolium (2-1) and imidazolylidene (2-4) compounds.**

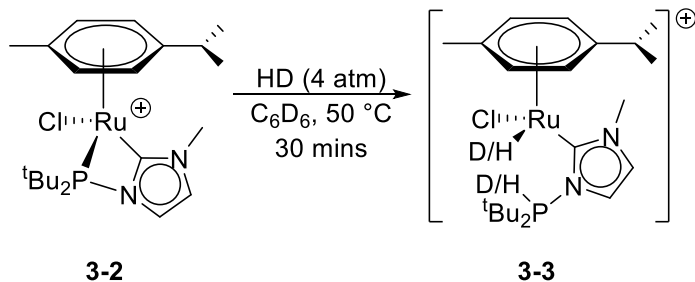


**Scheme 3.2.1: Synthesis of half-sandwich complex 3-1.**

The treatment of complex **3-1** with one equivalent of thallium hexafluorophosphate at room temperature overnight yields the corresponding cation, complex **3-2**, which was isolated as a bright yellow solid in 66% yield (Scheme 3.2.2). The  $^{31}\text{P}$  NMR resonance of **3-2** remains unchanged relative to **3-1**. However, changes in the chemical shifts of the aromatic protons, as well as the backbone of the NHC ligand, in the  $^1\text{H}$  NMR spectrum, coupled with the drastically reduced solubility in THF solvent, indicate **3-2** as the product. Unfortunately, complex **3-2** could not be characterized by X-ray diffraction studies and thus, we are unable to determine the true binding mode of the NHCP ligand. Initially, the  $^{31}\text{P}$  NMR spectrum led us to believe the phosphine arm was not coordinated; however, crystallographic study of related compounds provide evidence for coordination of the phosphine moiety and will be discussed in detail in later parts of this chapter. Heating complex **3-2** with deuterium hydride (4 atm) at  $50\text{ }^\circ\text{C}$  leads to rapid scrambling of HD to form  $\text{H}_2$  and  $\text{D}_2$  in less than one hour *via* formation of **3-3** (Scheme 3.2.3).



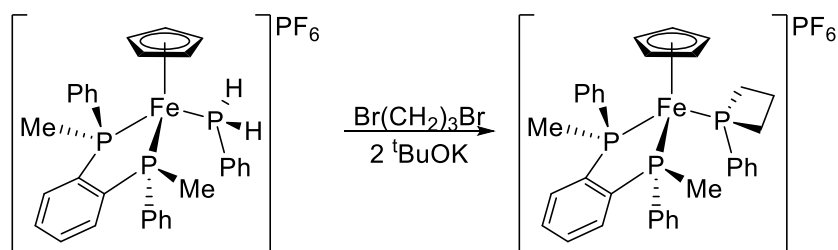
**Scheme 3.2.2: Synthesis of cationic Ru-arene complex 3-2.**



**Scheme 3.2.3: Reversible activation of dihydrogen by 3-2 to form statistical mixtures of  $\text{H}_2$  and  $\text{D}_2$ .**

The above non-innocent reactivity of the cationic complex with  $\text{H}_2$  has literature precedent. Reactions of coordinated phosphines have been reported by Wild whereby primary phosphines are used in electrophilic reactions with dihalo-alkanes to furnish tertiary phosphines (Scheme

3.2.4).<sup>25</sup> As well, template synthesis using coordinated ligands has gained traction in the last two decades as it provides a facile route to synthesize coordination complexes without the need to purify ligands separately.<sup>26–28</sup> In 2013 Morris and coworkers demonstrated the use of an asymmetric Fe(PNNP) catalyst that effects asymmetric transfer hydrogenation of ketones.<sup>29</sup> The ligand was shown to be protonated with an H<sub>2</sub> surrogate such as *iso*-propanol to yield an Fe-H/N-H species that proceeds to reduce ketones to alcohols *via* an outer-sphere mechanism. Similar to Noyori's catalyst,<sup>30–32</sup> the Fe(PNNP) catalyst takes advantage of the ambiphilic nature of the amine ligands to provide catalytic turnover. However, related heterolytic cleavage of dihydrogen using coordinated phosphines, as shown above, is relatively less common. In the present case, activation of dihydrogen is driven by the high basicity of the pendant phosphine arm, likely after coordination of H<sub>2</sub> to the cationic Ru center following dissociation of the coordinated phosphine.



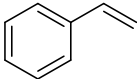

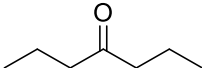
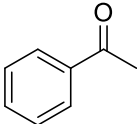
**Scheme 3.2.4: Base-promoted functionalization of coordinated phosphines.**

In order to probe the mechanism of hydrogen activation, a concentrated solution of **3-2** was treated with dihydrogen (4 atm) at 50 °C in THF-d<sub>8</sub> and monitored by <sup>31</sup>P NMR spectroscopy; a small resonance at 62 ppm can be observed with a one-bond P-H coupling constant of 424 Hz, indicating a proton is attached directly to the P(V) center. Attempts at recrystallizing this complex under either N<sub>2</sub> or H<sub>2</sub> atmospheres were not fruitful. Complexes **3-1** and **3-2** were used in hydrogenation studies of olefins and carbonyl compounds (Table 3.2.1). Individual olefin and ketone trials were subject to 4 atm of H<sub>2</sub> at 60 °C in THF-d<sub>8</sub> in J-Young tubes for various lengths of time and monitored by NMR spectroscopy. Nitrile butadiene rubber (NBR) was obtained as 6 wt% in water as well as C<sub>6</sub>H<sub>5</sub>Cl and degassed before use. Trial runs were performed in a Parr reactor with 50 bar H<sub>2</sub> in C<sub>6</sub>H<sub>6</sub> or chlorobenzene, as indicated. Products of NBR hydrogenation were analyzed by IR spectroscopy.

As seen below, complexes **3-1** and **3-2** are not well-suited for catalytic hydrogenation, despite the facile and reversible activation of dihydrogen by complex **3-2**. The primary reason behind the

lack of reactivity is likely due to the basicity of the coordinated phosphine arm and the difficulty in protonating substrates. This is reflected in the slight increase in catalytic activity with respect to polar substrates such as ketones. In the case of NBR emulsion, low catalyst loadings do not yield any catalytic activity; however, increasing the catalytic loading leads to cross-linking of the nitrile groups of the polymer with no significant hydrogenation of olefinic residues observed.

**Table 3.2.1: Catalytic hydrogenation of olefins, carbonyls, and NBR rubber using 3-1 and 3-2.**

Substrate	Catalyst	Loading (% mol)	Time (h)	Conversion (%)
	<b>3-1</b>	0.1	6	N.R.
		0.1	12	N.R.
		1.0	12	trace
	<b>3-2</b>	0.1	6	trace
		0.1	12	trace
		1.0	12	trace
	<b>3-2</b>	0.1	12	N.R.
		1.0	12	N.R.
	<b>3-2</b>	0.1	12	trace
		1.0	12	5
		0.1	12	trace
	<b>3-2</b>	0.1	12	7
		1.0	12	7
		0.1	12	N.R.
nitrile butadiene rubber latex <sup>a,c,d</sup>	<b>3-2</b>	1.0	12	N.R.
		5.0	12	N.R.
		0.1	12	N.R.
nitrile butadiene rubber <sup>b,c,d</sup>	<b>3-2</b>	1.0	12	cross-link
		5.0	12	cross-link
		0.1	12	N.R.

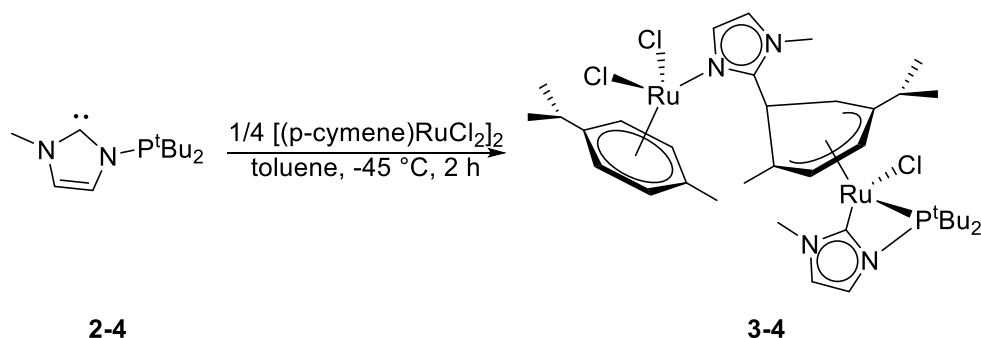
<sup>a</sup> Used as emulsion in degassed water, C<sub>6</sub>H<sub>6</sub> solvent

<sup>b</sup> Used as solution in degassed C<sub>6</sub>H<sub>5</sub>Cl

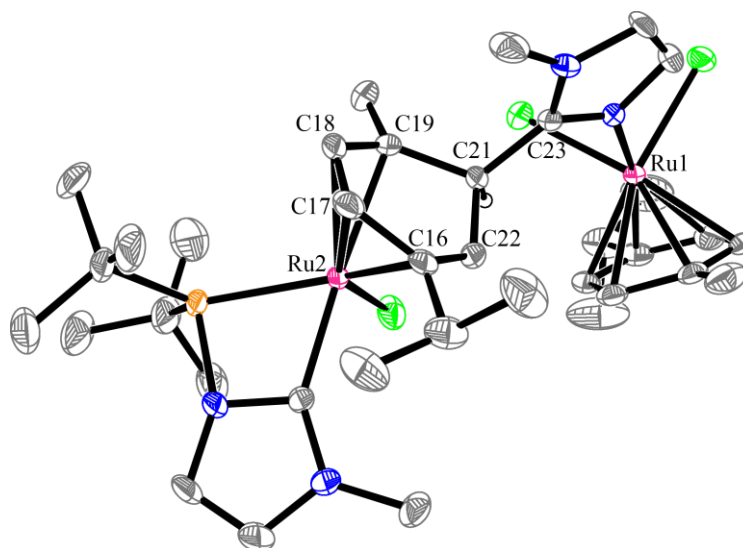
<sup>c</sup> In Parr reactor, 50 bar H<sub>2</sub>, 60 °C

<sup>d</sup> Catalytic loading in wt%

During the formation of complex **3-1**, it was found that excess free carbene leads to a mixture of products. Carrying out the reaction at  $-45\text{ }^{\circ}\text{C}$  in  $\text{C}_6\text{D}_6$  for 2 hours yields complex **3-4** as the major product, along with concomitant release of  ${}^t\text{Bu}_2\text{PCl}$ , as evidenced by  ${}^{31}\text{P}$  NMR spectroscopy (Scheme 3.2.5). Isolation of **3-4** proved challenging as the complex readily decomposes in solution to an intractable mixture of other products. However, X-ray quality crystals were obtained after multiple recrystallization attempts of the product and confirm a very unusual structure for **3-4** (Figure 3.2.2). As shown in the solid-state structure, both ruthenium centers maintain a piano-stool geometry where the loss of  ${}^t\text{Bu}_2\text{PCl}$  is consistent with the coordination sphere of  $\text{Ru}_2$ . While in the solid-state complex **3-4** can be stored for several days in the freezer; however, solutions of the compound rapidly decompose at room temperature within 1-2 hours. The Choudhury group has reported on the tendency of this particular Ru starting material to form homobimetallic species using coordination sites on the NHC ligand.<sup>33</sup>

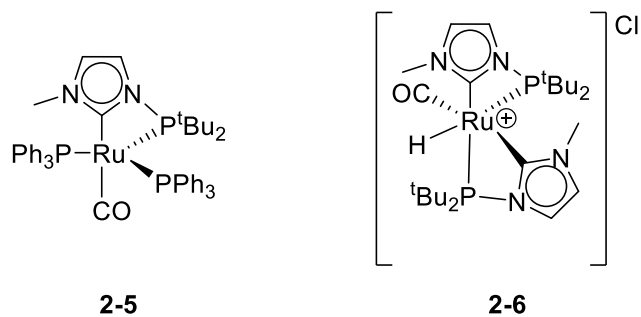


**Scheme 3.2.5: Synthesis of arene-activated product 3-4.**

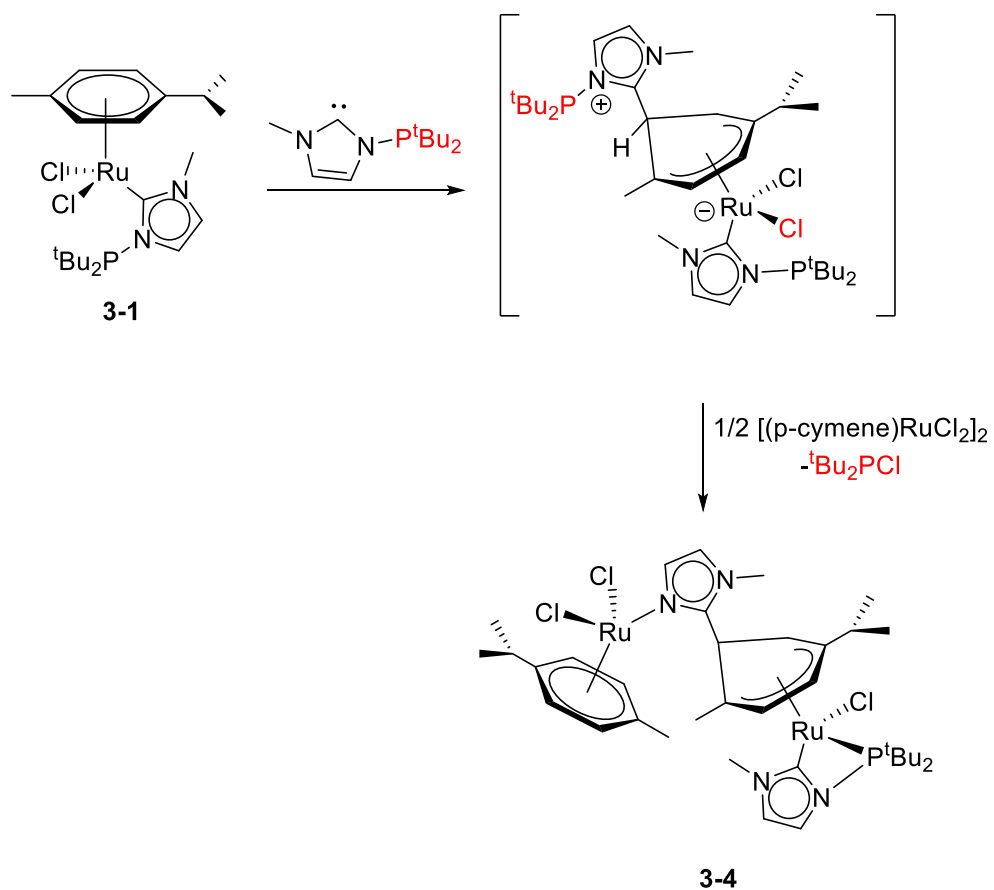


**Figure 3.2.2: Thermal ellipsoid plot of 3-4. Solvent and hydrogen atoms (except C21 proton) omitted for clarity. Grey: Carbon, Blue: Nitrogen, Orange: Phosphorus, Green: Chlorine, Pink: Ruthenium.**

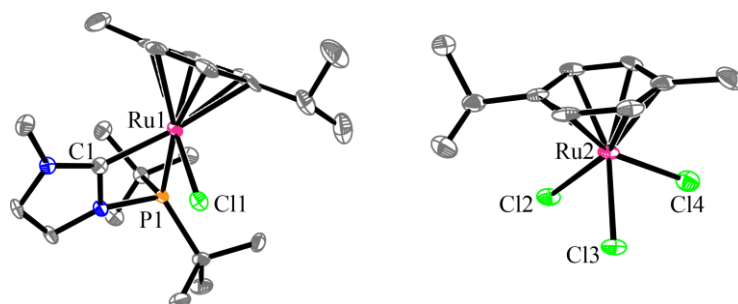
Furthermore, bond parameters confirm the partial dearomatization of one of the arene rings. Indeed, C21-C23, C21-C19, and C21-C22 have bond lengths of 1.500(9) Å, 1.523(10) Å, and 1.514(10) Å, respectively, and are typical of C-C single bonds. Conversely, the carbon-carbon bond lengths for atoms C16, C17, C18, C19, and C22 range from 1.389(12) Å to 1.436(13) Å, indicative of aromatic C-C bond lengths. Additionally, the C<sub>carbene</sub>-Ru2-P bond angle is 65.6(2)°, similar to the analogous 4-membered metallacycles reported for compounds **2-5** and **2-6** in Chapter 2 (Figure 3.2.3). As well, the Ru-P bond length is 2.357(2) Å, which is also similar to **2-5**. Since the formation of **3-4** is only observed with excess free carbene, a mechanism (Scheme 3.2.6) can be envisioned that begins with formation of **3-1** as the first step followed by nucleophilic attack of the free carbene at the *p*-cymene ring. Subsequently, abstraction of chloride from the Ru center furnishes the phosphine by-product and complex **3-4**. While attempting to isolate the proposed intermediate, complex **3-5** was isolated from the crop of crystals and manually separated (Figure 3.2.4). As seen below, complex **3-5** is a zwitterionic species of the form [RuCl(*p*-cymene)(NHCP)][RuCl<sub>3</sub>(*p*-cymene)]. The Ru1-C1 and Ru1-P1 distances are 2.032(5) Å and 2.4057(15) Å, respectively. Both bond lengths are very similar to the analogous bond distances in complex **2-6** described in Chapter 2, which is also cationic. The C1-Ru1-P1 bond angle is 64.49(15)°, which is also comparable with complex **2-6**.



**Figure 3.2.3: Complexes 2-5 and 2-6, as discussed in Chapter 2.**



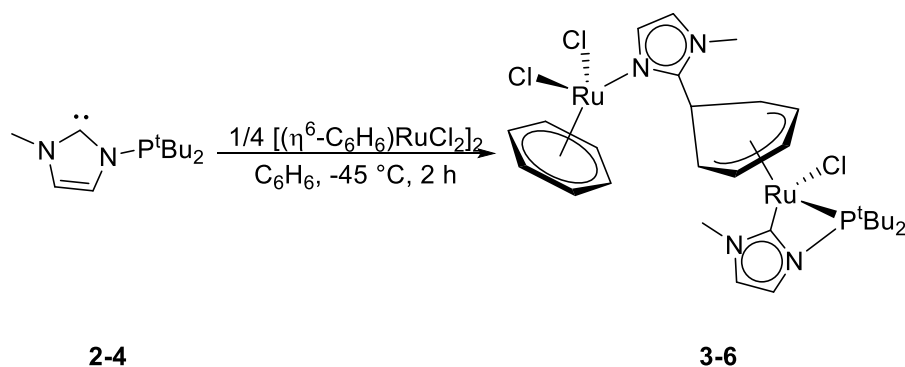
**Scheme 3.2.6: Proposed mechanistic pathway for the formation of 3-4 from half-sandwich complex 3-1.**



**Figure 3.2.4: Thermal ellipsoid plot of 3-5. Hydrogen atoms omitted for clarity. Grey: Carbon, Blue: Nitrogen, Orange: Phosphorus, Green: Chlorine, Pink: Ruthenium.**

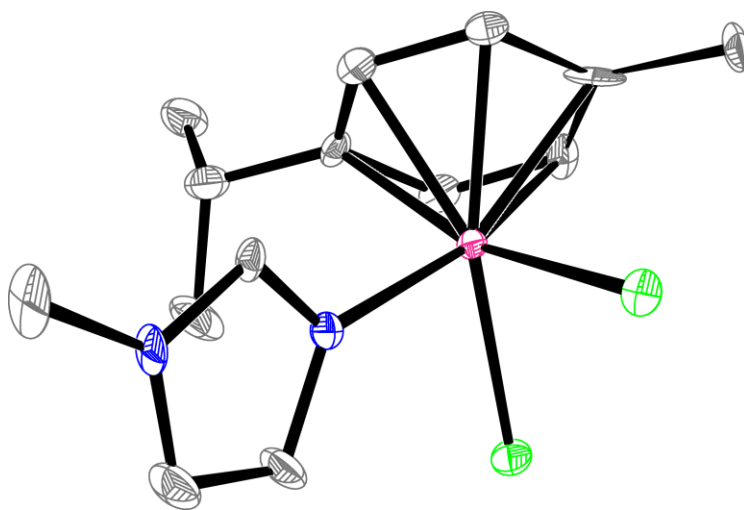
With the structure of this intermediate determined, it is necessary to amend the previous mechanism. Indeed, it is more feasible to envision the excess carbene undergoing nucleophilic attack of the arene moiety in the cationic complex of **3-5**. Thus, the anionic trichloro complex is nucleophilic enough to abstract the phosphine fragment and the resulting neutral imidazole is free to coordinate the second ruthenium center. Furthermore, complex **3-5** is analogous to **3-2**, differing only in the counter-ion.

In order to further demonstrate the electrophilicity of the coordinated arene, compound **2-4** was reacted with  $[\text{RuCl}_2(\eta^6\text{-C}_6\text{H}_6)]_2$  in benzene at room temperature overnight and was monitored by  $^{31}\text{P}$  NMR spectroscopy. The less-electron rich arene was thought to further encourage nucleophilic attack of the carbene to the aromatic structure. Gratifyingly,  $^t\text{Bu}_2\text{PCL}$  was observed in the NMR spectrum and only the arene-activated product (**3-6**) was isolated in 67% yield as a pale-yellow solid (Scheme 3.2.7). As expected, the  $^{31}\text{P}$  NMR spectrum of the product does not change drastically in comparison to **3-4**. However, six individual aromatic proton resonances are observed in the  $^1\text{H}$  NMR spectrum, corresponding to the six inequivalent protons of the activated arene. Ruthenium-arene complexes exchange arene ligands relatively easily,<sup>34–37</sup> thus in aromatic solvents such as  $\text{C}_6\text{D}_6$  or toluene- $d_8$  the aromatic resonance that corresponds to six equivalent protons is lost in the spectrum as a result of rapid exchange with the solvent. However, the  $^1\text{H}$  NMR spectrum in THF- $d_8$  displays this resonance at 5.38 ppm. Complex **3-6** displays significant thermal instability, as mild heating of solution of the complex leads to decomposition to unidentifiable species within 1-2 hours.



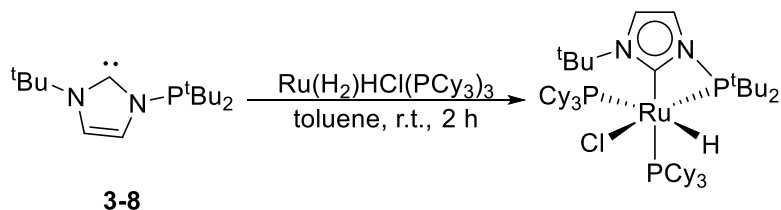
**Scheme 3.2.7: Synthesis of the analogous arene-activated complex 3-6.**

In the course of these studies, other decomposition products have been identified crystallographically, although they could not be isolated in bulk. The weak nature of the P-N bond of the ligand means that the complexes are intolerant of many sources of proton, including adventitious water. During a crystallization attempt of **3-1**, complex **3-7** was isolated and characterized crystallographically (Figure 3.2.5). The carbenic carbon has been protonated and loss of the phosphine arm is observed, presumably as the hydroxy phosphine or its phosphine-oxide tautomer.



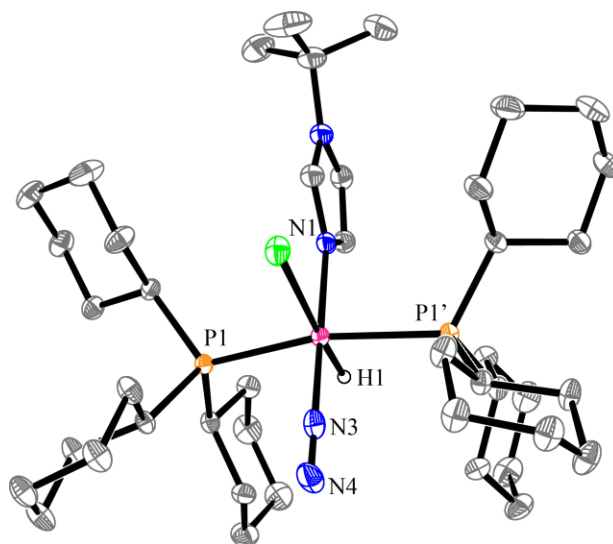
**Figure 3.2.5: Thermal ellipsoid plot of one molecule in the asymmetric unit of 3-7. Hydrogen atoms omitted for clarity. Grey: Carbon, Blue: Nitrogen, Green: Chlorine, Pink: Ruthenium.**

In an attempt to produce a hydrido-ruthenium complex for olefin hydrogenation, compound **3-8** was reacted with  $\text{RuHCl}(\text{H}_2)(\text{PCy}_3)_3$  in toluene at room temperature, and the reaction was monitored by  $^{31}\text{P}$  NMR spectroscopy (Scheme 3.2.8).



**Scheme 3.2.8: Attempted synthesis of a ruthenium-hydride catalyst for olefin hydrogenation.**

While no  $^t\text{Bu}_2\text{P}(\text{Cl})$  was observed in the  $^{31}\text{P}$  NMR spectrum, compound **3-9** was isolated as small crystals and characterized by X-ray crystallography (Figure 3.2.6). The formation of **3-9** can be rationalized by examining the acidity of the dihydrogen complex. Coordination of the free carbene is followed by protonation of the phosphine arm *via* the acidified dihydrogen complex. Subsequently,  $\text{HP}^t\text{Bu}_2$  is lost and is followed by a change in the binding mode of the carbene to the more basic nitrogen. The resulting  $\text{RuH}_2$  intermediate is then acidic enough to protonate the free carbene. Most interestingly, the solid-state structure of the complex reveals a coordinated dinitrogen fragment, likely as a result of the steric bulk of the  $\text{PCy}_3$  ligands precluding the coordination of a stronger ligand. The asymmetric unit of **3-9** shows only half of the molecule, while the other half is symmetry generated by a mirror plane along  $\text{N1-Ru-N3}$ . Thus, the  $\text{Ru-P1}$  and  $\text{Ru-P1}'$  bond distances are identical at  $2.3656(6)$  Å. The  $\text{Ru-N3}$  and  $\text{N3-N4}$  bond lengths are  $1.873(3)$  Å and  $1.116(4)$  Å, respectively. Interestingly, the  $\text{Ru-N3}$  bond length is slightly shorter than the mean analogous bond length of  $1.961(53)$  Å, while the  $\text{N3-N4}$  bond length is slightly longer than the average found in Ru-dinitrogen complexes at  $1.104(30)$  Å (CCDC Conquest, Accessed August 29, 2018). Furthermore, the  $\text{Ru-N1}$  bond distance is  $2.144(3)$  Å and the  $\text{Ru-H1}$  distance refined to  $1.55(4)$  Å. Unfortunately, complex **3-9** could not be synthesized in a rational manner in bulk for further NMR spectroscopy studies.



**Figure 3.2.6: Thermal ellipsoid plot of 3-9. Solvent and hydrogen atoms (except hydride) omitted for clarity. P1' is symmetry generated by a mirror plane along N1-Ru-N3. Grey: Carbon, Blue: Nitrogen, Green: Chlorine, Orange: Phosphorus, Pink: Ruthenium**

### 3.3 Conclusion

A family of piano-stool half-sandwich complexes bearing N-phosphorylated N-heterocyclic carbene ligands were prepared and studied with respect to catalytic activity as well as their role in decomposition reactions. Abstraction of chloride from  $[\text{RuCl}_2(p\text{-cymene})(\text{NHCP})]$  yields the corresponding cationic ruthenium species, which was shown to undergo rapid and reversible activation of dihydrogen under relatively mild conditions. The activation of  $\text{H}_2$  was shown to proceed in an outer-sphere mechanism involving the pendant phosphine ligand from the NHCP carbene. Despite the activation of  $\text{H}_2$ , no significant catalytic reduction of olefins or ketones was observed with this cationic species under various conditions. Attempted hydrogenation of nitrile butadiene rubber at high catalyst loadings led to cross-linking of the polymer. The NHCP ligand was also observed to react differently at various concentrations, wherein an excess of the free carbene leads to formation of an unusual homo-bimetallic species with activation of one of the coordinated arene ligands. Furthermore, other decomposition products involving NHCP ligands were crystallographically characterized but could not be isolated in significant yields.

## 3.4 Experimental Section

### 3.4.1 General Considerations

All manipulations were carried out under and atmosphere of dry, O<sub>2</sub>-free N<sub>2</sub> employing a VAC Atmospheres glove box or a Schlenk vacuum-line. Solvents were purified with a Grubbs-type column system manufactured by Innovative Technology and dispensed into thick-walled Strauss glass flasks equipped with Teflon-valve stopcocks (pentanes, hexanes, toluene, tetrahydrofuran, and dichloromethane). Anhydrous benzene was purchased from Sigma-Aldrich and used without further purification. Deuterated solvents were dried over appropriate agents, vacuum-transferred into storage flasks with Young-type Teflon stopcocks and degassed accordingly (C<sub>6</sub>D<sub>6</sub>, CD<sub>2</sub>Cl<sub>2</sub>, THF-d<sub>8</sub>, and CDCl<sub>3</sub>). <sup>31</sup>P{<sup>1</sup>H} NMR spectra were recorded at 25 °C on a Bruker 400 MHz spectrometer and referenced to 85% H<sub>3</sub>PO<sub>4</sub>. <sup>1</sup>H and <sup>13</sup>C{<sup>1</sup>H} NMR spectra were recorded at 25 °C on a Bruker 500 MHz spectrometer equipped with a cold probe and referenced to the residual solvent signals. Chemical shifts are reported in ppm and coupling constants are scalar values in Hz. Potassium bis(trimethylsilyl)amide (KHMDS), di-*tert*-butylchlorophosphine, 1-methylimidazole, and dichlorobis(*p*-cymene)ruthenium(II) dimer were purchased from Sigma-Aldrich and used without further purification. 1,3-cyclohexadiene was purchased from Alfa Aesar and used without further purification. RuCl<sub>3</sub>•xH<sub>2</sub>O was purchased from Strem and used without further purification. Despite long acquisition times on a 500 MHz cryoprobe NMR spectrometer, some quaternary carbons in the <sup>13</sup>C{<sup>1</sup>H} NMR spectra were not observed. Such instances are specifically mentioned for each occurrence.

### 3.4.2 General Procedure for Hydrogenation

#### 3.4.2.1 Hydrogenation of Discrete Olefin and Carbonyl Substrates

In the glovebox, 1 mmol of the olefin substrate was weighed out in a vial and dissolved in 0.5 mL of C<sub>6</sub>D<sub>6</sub>. The solution was added to a weighed amount of the appropriate catalysts (amounts listed in Table 3.2.1). The solution was syringed into an oven-dried J-Young type NMR tube. The reaction vessel was sealed and degassed three times using successive cycles of freeze-pump-thaw and backfilled with H<sub>2</sub> (4 atm). The reaction vessel was heated as indicated and monitored by NMR spectroscopy.

### 3.4.2.2 Hydrogenation of Nitrile Butadiene Rubber

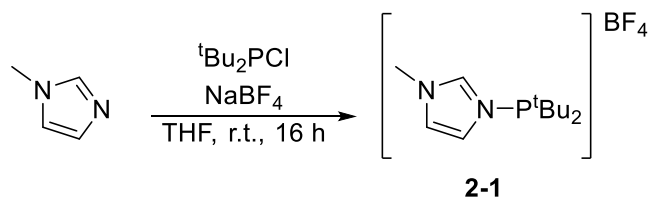
In the glovebox, the appropriate catalyst amount is weighed into a vial and dissolved in C<sub>6</sub>H<sub>5</sub>Cl. The solution was added to a vial containing a solution of 1.00 mL of 5 wt% NBR in chlorobenzene. The reaction vials were charged with stir bars and loaded into a Parr pressure reactor and sealed. The reactor was removed from the glovebox and purged five times with 20 bar H<sub>2</sub> before being pressurized with 45 bar H<sub>2</sub>. The reactor was placed in the oil bath and allowed to equilibrate with the temperature, after which the pressure was increased to 50 bar overall. The reaction was allowed to stir for 6 or 12 hours as indicated. After completion of reaction the reactor was cooled to room temperature and carefully depressurized. The polymer was coagulated with the addition of methanol and vigorously shaken/sonicated. The solvent was decanted and the polymer was dried under vacuum before being dissolved in THF. An aliquot of the solution was placed in between KBr plates and then dried thoroughly in air. IR spectroscopy was used to determine yield of hydrogenated NBR (HNBR).

### 3.4.2.3 Hydrogenation of Nitrile Butadiene Rubber Latex

In the glovebox, the appropriate catalyst amount is weighed into a vial and dissolved C<sub>6</sub>H<sub>6</sub>. The reaction vessels were charged with stir bars and loaded into a Parr reactor pressure and sealed. The reactor was taken into an N<sub>2</sub> glovebag which had previously been purged 25-30 times with inert gas. The reactor was opened and 1 mL of NBR latex (emulsion in water) was added to each vial. The reactor was again sealed and purged five times with 20 bar H<sub>2</sub>. Procedure is then identical to NBR hydrogenation described above.

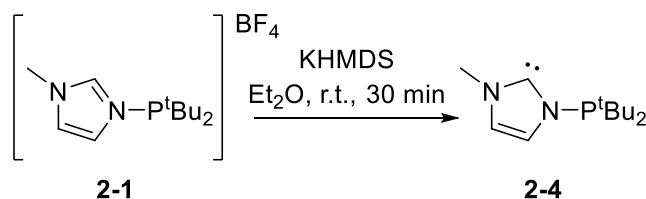
## 3.4.3 Synthetic Procedures

### 3.4.3.1 Synthesis of 1-di(*tert*-butyl)phosphinoyl-3-methyl imidazolium tetrafluoroborate (**2-1**)



Compound **2-1** was synthesized according to literature procedures<sup>24,38,39</sup> and the procedure described in Chapter 2. In a 20 mL scintillation vial, 1-methylimidazole (1.477 g, 17.99 mmol) and sodium tetrafluoroborate (2.195 g, 19.99 mmol) were combined in THF (5 mL) and the suspension was cooled to -45 °C. While stirring, a solution of di-*tert*-butylchlorophosphine (2.290 g, 18.21 mmol) in THF (3 mL) was added drop-wise to the cold suspension. The mixture immediately became cloudy as a white precipitate formed. The reaction was stirred at -45 °C for 30 minutes and then allowed to warm to room temperature and stirred overnight. The suspension was then filtered over a Celite plug and concentrated under vacuum. The white residue was extracted with DCM (5 mL), filtered over Celite, and the residue was washed with DCM (3 x 2 mL). The filtrate was concentrated under vacuum to less than 1 mL and pentanes (10 mL) were added to the stirring solution to afford a cloudy biphasic mixture. The suspension was triturated for several hours until white precipitate formed. The supernatant was decanted, and the white solid was successively triturated with pentanes and decanted. The residue was dried under vacuum to afford the desired product as a white powder (3.856 g, 68%). Characterization of the product is consistent with literature values.<sup>24,38,39</sup>

### 3.4.3.2 Synthesis of 1-di(*tert*-butyl)phosphanyl-3-methyl imidazolyliidene (**2-4**)



A 20 mL vial was charged with **3-1** (0.303 g, 0.965 mmol), suspended in diethyl ether (4 mL) and cooled to -45 °C. KHMDS (0.234 g, 1.172 mmol) in diethyl ether (4 mL) was added drop-wise to the stirring suspension to immediately afford a cloudy pale-yellow solution. The mixture was warmed to room temperature and stirred for a further 30 minutes. Concentration of the mixture afforded an off-white residue which was extracted with pentanes (3 x 3 mL) and filtered over a Celite plug. The residue was washed with pentanes (3 x 1 mL) and the combined filtrates were concentrated under vacuum until off-white crystals began to form. The suspension was placed in the freezer overnight to complete crystallization. The supernatant was then decanted, and the residue washed with cold pentanes (1 mL) and dried under vacuum to afford the product

as flaky, off-white crystals (0.204 g, 93%). Characterization of the product is consistent with literature values.<sup>24</sup>

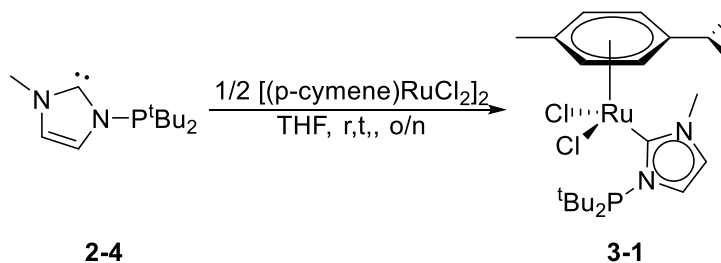
### 3.4.3.3 Synthesis of $[\text{RuCl}_2(\eta^6\text{-C}_6\text{H}_6)]_2$

A 250-mL round bottom flask equipped with a water condenser was charged with  $\text{RuCl}_3 \cdot x\text{H}_2\text{O}$  (2.035 g, 7.783 mmol) and EtOH (100 mL) and stirred at room temperature. 1,3-cyclohexadiene (5.743 g, 71.67 mmol) was added to the black solution, which immediately turned greenish-black, and the flask was heated to 60 °C with vigorous stirring. After 2 hours the mixture turned to red/brown suspension. After heating for a further 2 hours, the flask was removed from the oil bath and cooled to room temperature. The suspension was filtered over a glass frit and washed with EtOH (4 x 25 mL) and Et<sub>2</sub>O (4 x 50 mL). The solid was then collected and dried under vacuum to afford the product as a brown, microcrystalline solid (2.214 g, 57%). Characterization consistent with literature values.<sup>40</sup>

<sup>1</sup>H NMR (DMSO-*d*<sub>6</sub>): δ 5.94 (s, C<sub>6</sub>H<sub>6</sub>).

<sup>13</sup>C{<sup>1</sup>H} NMR (DMSO-*d*<sub>6</sub>): δ 87.7 (s, C<sub>6</sub>H<sub>6</sub>).

### 3.4.3.4 Synthesis of **3-1**



A solution of **2-4** (0.075 g, 0.329 mmol) in THF (2 mL) was added drop-wise to a suspension of  $[\text{RuCl}_2(p\text{-cymene})]_2$  (0.188 g, 0.308 mmol) in THF (1 mL). The red suspension very quickly became bright orange before darkening in colour to a crimson red suspension. The mixture was stirred at room temperature overnight and then collected on a glass frit and washed with diethyl ether (3 x 2 mL). The light orange solid was collected and dried under vacuum. The product was recrystallized by dissolving the orange solid in minimal DCM and layering with pentanes (10 mL) overnight. The supernatant was discarded, and mixture of bright yellow product and dark red starting material were once again dried under vacuum before a second recrystallization

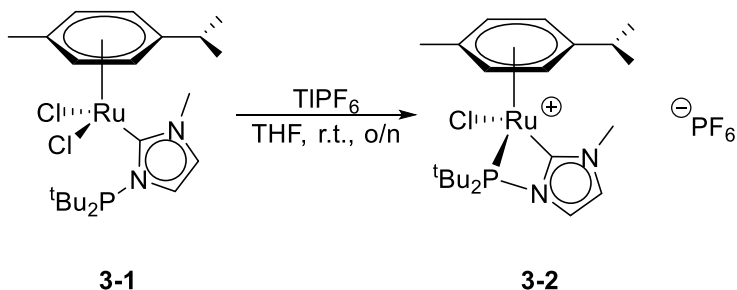
attempt (DCM/pentanes) was carried out in the freezer over 3 days. The orange supernatant was discarded, and the bright yellow solid was washed with pentanes (3 x 5 mL) and dried under vacuum to afford the product (0.126 g, 77%).

**$^1\text{H}$  NMR ( $\text{CDCl}_3$ ):**  $\delta$  1.29 (d,  $^3J_{\text{H-H}} = 7$  Hz, 3H, isopropyl  $\text{CH}_3$ ), 1.31 (d,  $^3J_{\text{H-H}} = 7$  Hz, 3H, isopropyl  $\text{CH}_3$ ), 1.36 (d,  $^3J_{\text{P-H}} = 16$  Hz, 9H,  $^t\text{Bu}$   $\text{CH}_3$ ), 1.53 (d,  $^3J_{\text{P-H}} = 16$  Hz, 9H,  $^t\text{Bu}$   $\text{CH}_3$ ), 2.32 (s, 3H, aryl  $\text{CH}_3$ ), 2.85 (sept,  $^3J_{\text{H-H}} = 7$  Hz, 1H, isopropyl  $\text{CH}$ ), 4.10 (s, 3H, N- $\text{CH}_3$ ), 5.37 (d,  $^3J_{\text{H-H}} = 6$  Hz, 1H, aryl  $\text{CH}$ ), 5.60 (d,  $^3J_{\text{H-H}} = 6$  Hz, 1H, aryl  $\text{CH}$ ), 6.30 (d,  $^3J_{\text{H-H}} = 6$  Hz, 1H, aryl  $\text{CH}$ ), 6.54 (d,  $^3J_{\text{H-H}} = 6$  Hz, 1H, aryl  $\text{CH}$ ), 7.29 (d,  $^3J_{\text{H-H}} = 2$  Hz, 1H, NHC backbone), 7.48 (d,  $^3J_{\text{H-H}} = 2$  Hz, 1H, NHC backbone).

**$^{13}\text{C}\{^1\text{H}\}$  NMR ( $\text{CDCl}_3$ ):**  $\delta$  19.6 (s, aryl  $\text{CH}_3$ ), 21.2 (s, isopropyl  $\text{CH}_3$ ), 23.9 (s, isopropyl  $\text{CH}_3$ ), 28.0 (s, br,  $\text{C}(\text{CH}_3)_3$ ), 30.78 (s, isopropyl  $\text{CH}$ ), 31.8 (d,  $^2J_{\text{P-C}} = 6$  Hz,  $^t\text{Bu}$   $\text{CH}_3$ ), 37.4 (s, N- $\text{CH}_3$ ), 38.9 (d,  $^1J_{\text{P-C}} = 9$  Hz,  $\text{C}(\text{CH}_3)_3$ ), 41.3 (d,  $^2J_{\text{P-C}} = 5$  Hz,  $^t\text{Bu}$   $\text{CH}_3$ ), 86.1 (s, aryl  $\text{CH}$ ), 86.7 (d,  $^3J_{\text{P-C}} = 3$  Hz, NHC backbone), 88.3 (d,  $^3J_{\text{P-C}} = 7$  Hz, NHC backbone), 96.6 (d,  $D_{\text{P-C}} = 5$  Hz, aryl  $\text{CH}$ ), 101.8 (s, *ipso* C), 114.2 (s, *ipso* C), 122.6 (d,  $D_{\text{P-C}} = 7$  Hz, aryl  $\text{CH}$ ), 127.5 (s, aryl  $\text{CH}$ ), 166.6 (d,  $^2J_{\text{P-C}} = 31$  Hz, NHC carbene).

**$^{31}\text{P}\{^1\text{H}\}$  NMR ( $\text{CDCl}_3$ ):**  $\delta$  120.6 (s,  $\text{P}^t\text{Bu}_2$ ).

### 3.4.3.5 Synthesis of **3-2**



Complex **3-1** (0.062 g, 0.116 mmol) was suspended in THF (1 mL) and, while stirring,  $\text{TIPF}_6$  (0.037 g, 0.107 mmol) in THF (2 mL) was added to the yellow suspension. No colour change was observed and the suspension was stirred at room temperature overnight, after which a greyish-white precipitate was observed. The suspension was filtered over a Celite plug and washed with THF (2 x 1 mL). The resulting yellow-orange filtrate was concentrated under vacuum and the residue was taken up in THF (1 mL). The solution was added drop-wise to

stirring pentanes (10 mL) to form an immediate yellow suspension. The mixture was placed in the freezer overnight. The supernatant was then discarded and the solid was washed with pentanes (3 x 1 mL) and dried under vacuum to afford the desired product as a yellow-orange powder (0.045 g, 66%).

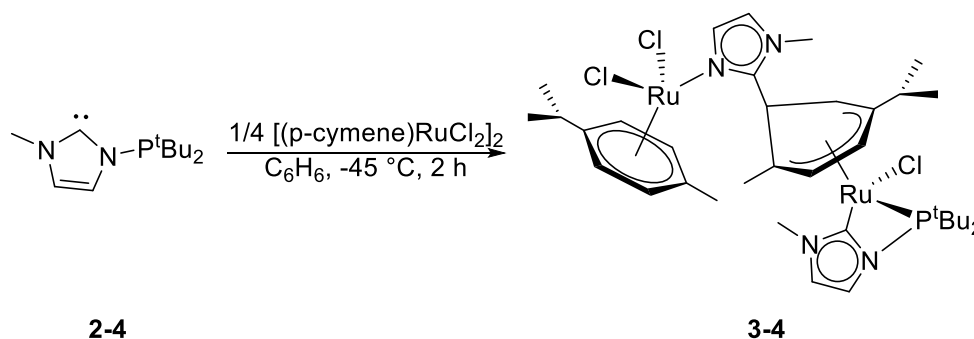
**$^1\text{H}$  NMR ( $\text{CDCl}_3$ ):**  $\delta$  1.29 (d,  $^3J_{\text{H-H}} = 7$  Hz, 3H, isopropyl  $\text{CH}_3$ ), 1.32 (d,  $^3J_{\text{H-H}} = 7$  Hz, 3H, isopropyl  $\text{CH}_3$ ), 1.34 (d,  $^3J_{\text{P-H}} = 16$  Hz, 9H,  $^t\text{Bu}$   $\text{CH}_3$ ), 1.54 (d,  $^3J_{\text{P-H}} = 16$  Hz, 9H,  $^t\text{Bu}$   $\text{CH}_3$ ), 2.29 (s, 3H, aryl  $\text{CH}_3$ ), 2.86 (sept,  $^3J_{\text{H-H}} = 7$  Hz, 1H, isopropyl  $\text{CH}$ ), 4.02 (s, 3H, N- $\text{CH}_3$ ), 5.24 (d,  $^3J_{\text{H-H}} = 6$  Hz, 1H, aryl  $\text{CH}$ ), 5.58 (dd,  $^3J_{\text{H-H}} = 7$  Hz,  $D_{\text{P-H}} = 1.46$  Hz, 1H, aryl  $\text{CH}$ ), 6.23 (d,  $^3J_{\text{H-H}} = 6$  Hz, 1H, aryl  $\text{CH}$ ), 6.37 (dd,  $^3J_{\text{H-H}} = 6$  Hz,  $D_{\text{P-H}} = 1.35$  Hz, 1H, aryl  $\text{CH}$ ), 7.05 (dd,  $^3J_{\text{H-H}} = 2$  Hz, P-H coupling hidden in overlap, 1H, NHC backbone), 7.12 (dd,  $^3J_{\text{H-H}} = 2$  Hz,  $^3J_{\text{P-H}} = 1$  Hz, 1H, NHC backbone).

**$^{13}\text{C}\{^1\text{H}\}$  NMR ( $\text{CDCl}_3$ ):**  $\delta$  19.3 (s, aryl  $\text{CH}_3$ ), 21.3 (s, isopropyl  $\text{CH}_3$ ), 23.8 (s, isopropyl  $\text{CH}_3$ ), 27.7 (s, br,  $^t\text{Bu}$   $\text{CH}_3$ ), 30.9 (s, isopropyl  $\text{CH}$ ), 31.7 (d,  $^2J_{\text{P-C}} = 6$  Hz,  $^t\text{Bu}$   $\text{CH}_3$ ), 37.0 (s, N- $\text{CH}_3$ ), 39.0 (d,  $^1J_{\text{P-C}} = 9$  Hz,  $\text{C}(\text{CH}_3)_3$ ), 41.3 (d,  $^2J_{\text{P-C}} = 5$  Hz,  $^t\text{Bu}$   $\text{CH}_3$ ), 85.9 (s, aryl  $\text{CH}$ ), 86.7 (d,  $^3J_{\text{P-C}} = 3$  Hz, NHC backbone), 87.9 (d,  $^2J_{\text{P-C}} = 7$  Hz, NHC backbone), 96.5 (d,  $D_{\text{P-C}} = 5$  Hz, aryl  $\text{CH}$ ), 102.4 (s, *ipso* C), 114.4 (s, *ipso* C), 122.2 (d,  $D_{\text{P-C}} = 7$  Hz, aryl  $\text{CH}$ ), 126.9 (s, aryl  $\text{CH}$ ), 166.8 (d,  $^2J_{\text{P-C}} = 31$  Hz, NCN).

**$^{31}\text{P}\{^1\text{H}\}$  NMR ( $\text{CDCl}_3$ ):**  $\delta$  120.9 (s,  $\text{P}^t\text{Bu}_2$ ), -144.3 (quint,  $^1J_{\text{P-F}} = 712$  Hz,  $\text{PF}_6$ ).

**Elemental Analysis:** Calculated C: 41.16, H: 5.81, N: 4.36. Found C: 41.15, H: 5.63, N: 4.62.

### 3.4.3.6 Synthesis of **3-4**



A red suspension of  $[\text{RuCl}_2(p\text{-cymene})]_2$  (0.112 g, 0.184 mmol) in toluene (2 mL) was cooled to  $-45$  °C for 15 minutes. Compound **2-4** (0.092 g, 0.408 mmol) was dissolved in toluene (1 mL)

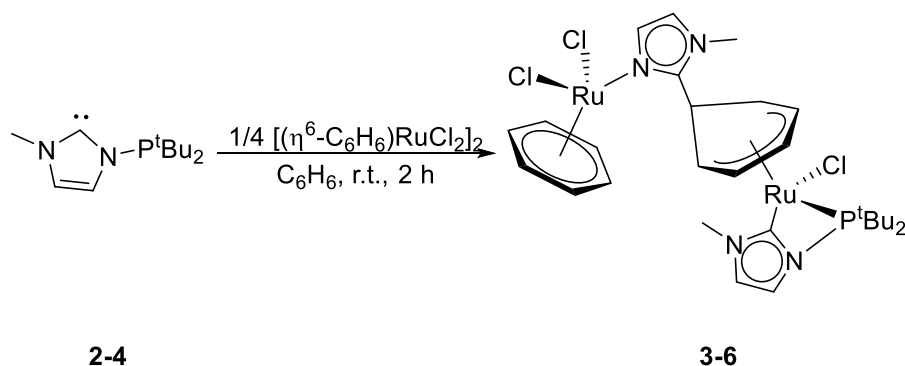
and cooled to  $-45\text{ }^{\circ}\text{C}$ . The carbene solution was added very slowly to the stirring suspension. The mixture became slightly orange and the reaction was stirred at  $-45\text{ }^{\circ}\text{C}$  for two hours while being monitored periodically by  $^{31}\text{P}$  NMR spectroscopy. After two hours, the suspension was poured over pentanes (10 mL), collected on a glass frit, and washed with benzene (3 x 1 mL), THF (1 mL), and pentanes (5 x 1 mL). The yellow solid was dried under vacuum and recrystallized from DCM/pentanes to afford product as an orange solid (0.068 g, 42%). X-ray quality crystals were grown from layering a concentrated DCM solution with pentanes in the freezer over 3 days. Due to the instability of the complex in solution,  $^{13}\text{C}$  NMR data could not be obtained, despite several attempts. Elemental analysis indicates formation of metal-carbides, despite high oxygen concentrations.

**$^1\text{H}$  NMR ( $\text{CDCl}_3$ ):**  $\delta$  0.80 (d,  $^3J_{\text{H-H}} = 7\text{ Hz}$ , 3H, isopropyl  $\text{CH}_3$ ), 1.15 (d,  $^3J_{\text{H-H}} = 7\text{ Hz}$ , 3H, isopropyl  $\text{CH}_3$ ), 1.19 (d,  $^3J_{\text{H-H}} = 9\text{ Hz}$ , 3H, isopropyl  $\text{CH}_3$ ), 1.28 (d,  $^3J_{\text{H-H}} = 7\text{ Hz}$ , 3H, isopropyl  $\text{CH}_3$ ), 1.33 (d,  $^3J_{\text{P-H}} = 14\text{ Hz}$ , 9H,  $^t\text{Bu}$   $\text{CH}_3$ ), 1.42 (d,  $^3J_{\text{P-H}} = 14\text{ Hz}$ , 9H,  $^t\text{Bu}$   $\text{CH}_3$ ), 2.30 (s, 3H, aryl  $\text{CH}_3$ ), 2.77 (m, 1H, isopropyl  $\text{CH}$ ), 3.60 (s, 3H, aryl  $\text{CH}_3$ ), 3.61 (s, 3H, N- $\text{CH}_3$ ), 3.65 (s, 3H, N- $\text{CH}_3$ ), 3.96 (m, 1H, isopropyl  $\text{CH}$ ), 4.82 (m, 1H, aryl  $\text{CH}$ ), 4.87 (m, 1H, aryl  $\text{CH}$ ), 5.36 (s, 1H, aryl  $\text{CH}$ ), 5.51 (d,  $D_{\text{P-H}} = 6\text{ Hz}$ , 1H, aryl  $\text{CH}$ ), 5.56 (d,  $D_{\text{P-H}} = 6\text{ Hz}$ , 1H, aryl  $\text{CH}$ ), 5.94 (d,  $D_{\text{P-H}} = 6\text{ Hz}$ , 1H, aryl  $\text{CH}$ ), 6.37 (d,  $D_{\text{P-H}} = 6\text{ Hz}$ , 1H, aryl  $\text{CH}$ ), 6.41 (s, 1H, NHC backbone), 6.62 (s, 1H, aryl  $\text{CH}$ ), 6.67 (s, 1H, NHC backbone), 6.71 (s, 1H, NHC backbone), 7.51 (s, 1H, NHC backbone).

**$^{31}\text{P}\{^1\text{H}\}$  NMR ( $\text{CDCl}_3$ ):**  $\delta$  119.2 (s,  $\text{P}^t\text{Bu}_2$ ).

**Elemental Analysis:** Calculated C: 48.89, H: 6.38, N: 6.34. Found C: 48.19, H: 6.13, N: 6.06.

### 3.4.3.7 Synthesis of **3-6**



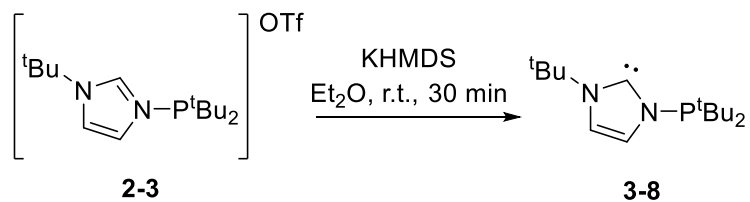
Compound **2-4** (0.127 g, 0.561 mmol) was dissolved in Et<sub>2</sub>O (4 mL) and added slowly to a suspension of [RuCl<sub>2</sub>(η<sup>6</sup>-C<sub>6</sub>H<sub>6</sub>)<sub>2</sub>] (0.074 g, 0.148 mmol) in benzene (2 mL). The brown suspension was stirred at room temperature overnight and monitored by <sup>31</sup>P NMR spectroscopy. The red/brown suspension was filtered over a Celite plug and washed with benzene (3 x 1 mL) and pentanes (3 x 1 mL). The filtrate was concentrated under vacuum to 1 mL and added dropwise to pentanes (10 mL) to afford a yellow solid. The supernatant was then decanted and the solid washed with pentanes (5 x 5 mL) and the residue was dried under vacuum to afford the product as a pale-yellow solid (0.057 g, 50%). Due to the instability of the complex in solution, <sup>13</sup>C NMR data could not be obtained, despite several attempts. Elemental analysis indicates formation of metal-carbides, despite high oxygen concentrations.

**<sup>1</sup>H NMR (CDCl<sub>3</sub>):** δ 1.16 (d, <sup>3</sup>J<sub>P-H</sub> = 13 Hz, 9H, <sup>t</sup>Bu CH<sub>3</sub>), 1.49 (d, <sup>3</sup>J<sub>P-H</sub> = 14 Hz, 9H, <sup>t</sup>Bu CH<sub>3</sub>), 3.21 (m, 1H, aryl CH), 3.48 (m, 2H, aryl CH), 3.55 (s, 3H, N-CH<sub>3</sub>), 3.57 (s, 3H, N-CH<sub>3</sub>), 4.49 (m, 6H, aryl CH), 4.95 (m, 1H, aryl CH), 5.01 (m, 1H, aryl CH), 5.09 (m, 1H, aryl CH), 6.64 (m, 2H, NHC backbone), 6.76 (s, 1H, NHC backbone), 6.84 (s, 1H, NHC backbone).

**<sup>31</sup>P{<sup>1</sup>H} NMR (CDCl<sub>3</sub>):** δ 118.9 (s, P<sup>t</sup>Bu<sub>2</sub>).

**Elemental Analysis:** Calculated C: 43.56, H: 5.22, N: 7.26. Found C: 42.97, H: 5.16, N: 7.22.

### 3.4.3.8 Synthesis of 1-di(*tert*-butyl)phosphanyl-3-*tert*-butyl imidazolyliidene (**3-8**)



Compound **3-8** was synthesized according to literature procedure; data were consistent with literature values.<sup>41</sup>

## 3.4.4 X-ray Crystallography

### 3.4.4.1 X-ray Data Collection and Reduction

Each crystal was coated in Paratone-N oil in the glove-box, mounted on a MiTeGen Micromount and placed under an N<sub>2</sub> stream, thus maintaining a dry, O<sub>2</sub>-free environment. The data were

collected on a Bruker Apex II diffractometer employing Mo K $\alpha$  radiation ( $\lambda = 0.71073 \text{ \AA}$ ). Data collection strategies were determined using Bruker Apex software and optimized to provide >99.5% data completion to a  $2\theta$  value of at least  $55^\circ$ . The data were collected at  $150(\pm 2) \text{ K}$  for all crystals. The frames were integrated with the Bruker SAINT software package using a narrow-frame algorithm. Data were corrected for absorption effects using the empirical multi-scan method (SADABS).<sup>42</sup>

#### 3.4.4.2 X-ray Data Solution and Refinement

Non-hydrogen atomic scattering factors were taken from the literature tabulations.<sup>43</sup> The heavy atom positions were determined using direct methods employing the SHELXTL direct methods routine. The remaining non-hydrogen atoms were located from successive difference Fourier map calculations. The refinements were carried out by using full-matrix least squares techniques on  $F^2$ . In the final steps of each refinement, all non-hydrogen atoms were assigned anisotropic temperature factors in the absence of disorder or insufficient data. In the latter cases atoms were treated isotropically. C-H atom positions were calculated and allowed to ride on the carbon to which they are bonded. H-atom temperature factors were fixed at 1.20 times the isotropic temperature factor of the C-atom to which they are bonded. The H-atom contributions were calculated, but not refined. The locations of the largest peaks in the final difference Fourier map calculation as well as the magnitude of the residual electron densities in each case were of no chemical significance.

**Table 3.4.1: Select crystallographic data for complexes 3-4 and 3-5.**

	(3-4)	(3-5)
Formula	$C_{37}H_{58}Cl_5N_4PRu_2$	$C_{36}H_{61}Cl_4N_2OPRu_2$
Formula weight	969.23	912.77
Crystal system	Tetragonal	Monoclinic
Space group	$P4_12_12_1$	$P2_1/c$
a (Å)	15.3019(11)	15.4919(8)
b (Å)	15.3019(11)	14.0381(7)
c (Å)	44.288(5)	18.9973(11)
$\alpha$ (deg)	90	90
$\beta$ (deg)	90	103.312(3)
$\gamma$ (deg)	90	90
Volume (Å <sup>3</sup> )	10370(2)	4020.5(4)
Z	8	4
d (calc) gcm <sup>-3</sup>	1.242	1.508
R(int.)	0.0488	0.0922
Abs coeff, $\mu$ , mm <sup>-1</sup>	0.896	1.087
Data collected	11955	9211
Variables	443	416
$>2\sigma(F_o^2)$	10855	5871
R( $>2\sigma$ )	0.0482	0.0477
$R_w(>2\sigma)$	0.1530	0.1039
GOF	1.165	1.002

**Table 3.4.2: Select crystallographic data for complexes 3-7 and 3-9.**

	(3-7)	(3-9)
Formula	C <sub>28</sub> H <sub>40</sub> Cl <sub>4</sub> N <sub>4</sub> Ru <sub>2</sub>	C <sub>50</sub> H <sub>87</sub> ClN <sub>4</sub> P <sub>2</sub> Ru
Formula weight	776.58	942.69
Crystal system	Orthorhombic	Monoclinic
Space group	<i>Pna</i> 2 <sub>1</sub>	<i>P</i> 2 <sub>1</sub> / <i>c</i>
a (Å)	12.0392(8)	9.3655(9)
b (Å)	8.7685(6)	20.8434(19)
c (Å)	29.260(2)	13.0161(10)
α (deg)	90	90
β (deg)	90	104.104(4)
γ (deg)	90	90
Volume (Å <sup>3</sup> )	3088.8(4)	2464.3(4)
Z	4	2
d (calc) gcm <sup>-3</sup>	1.670	1.270
R(int.)	0.0278	0.0262
Abs coeff, μ, mm <sup>-1</sup>	1.349	0.474
Data collected	7101	5881
Variables	344	307
>2σ(F <sub>o</sub> <sup>2</sup> )	6792	5144
R(>2σ)	0.0391	0.0299
R <sub>w</sub> (>2σ)	0.0988	0.0922
GOF	1.168	1.167

## Chapter 3 References

- (1) Hong, S. H.; Wenzel, A. G.; Salguero, T. T.; Day, M. W.; Grubbs, R. H. *J. Am. Chem. Soc.* **2007**, *129*, 7961–7968.
- (2) Dinger, M. B.; Mol, J. C. *Eur. J. Inorg. Chem.* **2003**, 2827–2833.
- (3) Dinger, M. B.; Mol, J. C. *Organometallics* **2003**, *22*, 1089–1095.
- (4) Banti, D.; Mol, J. C. *J. Organomet. Chem.* **2004**, *689*, 3113–3116.
- (5) Galan, B. R.; Gembicky, M.; Dominiak, P. M.; Keister, J. B.; Diver, S. T. *J. Am. Chem. Soc.* **2005**, *127*, 15702–15703.
- (6) Garrou, P. E. *Chem. Rev.* **1985**, *85*, 171–185.
- (7) Schuster, O.; Yang, L.; Raubenheimer, H. G.; Albrecht, M. *Chem. Rev.* **2009**, *109*, 3445–3478.
- (8) Hahn, F. E.; Jahnke, M. C. *Angew. Chem. Int. Ed.* **2008**, *47*, 3122–3172.
- (9) Poyatos, M.; Mata, J. A.; Peris, E. *Chem. Rev.* **2008**, *109*, 3677–3707.
- (10) Díez-González, S.; Marion, N.; Nolan, S. P. *Chem. Rev.* **2009**, *109*, 3612–3676.
- (11) Arnold, P. L.; Casely, I. J. *Chem. Rev.* **2009**, *109*, 3599–3611.
- (12) Nelson, D. J.; Nolan, S. P. *Chem. Soc. Rev.* **2013**, *42*, 6723–6753.
- (13) Hopkinson, M. N.; Richter, C.; Schedler, M.; Glorius, F. *Nature* **2014**, *510*, 485–496.
- (14) Johnson, C.; Albrecht, M. *Coord. Chem. Rev.* **2017**, *352*, 1–14.
- (15) Schnee, G.; NietoFaza, O.; Specklin, D.; Jacques, B.; Karmazin, L.; Welter, R.; Silvalópez, C.; Dagonne, S. *Chem. Eur. J.* **2015**, *21*, 17959–17972.
- (16) Ellul, C. E.; Mahon, M. F.; Saker, O.; Whittlesey, M. K. *Angew. Chem. Int. Ed.* **2007**, *46*, 6343–6345.

- (17) Ghadwal, R. S.; Rottschäfer, D.; Andrada, D. M.; Frenking, G.; Schürmann, C. J.; Stammler, H.-G. *Dalton Trans.* **2017**, *46*, 7791–7799.
- (18) Schneider, H.; Krahfuß, M. J.; Radius, U. *Z. Anorg. Allg. Chem.* **2016**, *642*, 1282–1286.
- (19) Crabtree, R. H. *Coord. Chem. Rev.* **2013**, *257*, 755–766.
- (20) Liang, Q.; Salmon, A.; Kim, P. J.; Yan, L.; Song, D. *J. Am. Chem. Soc.* **2018**, *140*, 1263–1266.
- (21) Danopoulos, A. A.; Pugh, D.; Wright, J. A. *Angew. Chem. Int. Ed.* **2008**, *47*, 9765–9767.
- (22) Würtemberger-Pietsch, S.; Radius, U.; Marder, T. B. *Dalton Trans.* **2016**, *45*, 5880–5895.
- (23) Lake, B. R. M.; Chapman, M. R.; Willans, C. E. *Organomet. Chem.* **2016**, *40*, 107–139.
- (24) Mosaféri, E.; Pan, L.; Wang, T.; Sun, Y.; Pranckevicius, C.; Stephan, D. W. *Dalton Trans.* **2016**, *45*, 1354–1358.
- (25) Bader, A.; Kang, Y. B.; Pabel, M.; Pathak, D. D.; Willis, A. C.; Wild, S. B. *Organometallics* **1995**, *14*, 1434–1441.
- (26) Edwards, P. G.; Haigh, R.; Li, D.; Newman, P. D. *J. Am. Chem. Soc.* **2006**, *128*, 3818–3830.
- (27) Thompson, M. C.; Busch, D. H. *J. Am. Chem. Soc.* **1964**, *86*, 213–217.
- (28) Lebbe, T.; Machnitzki, P.; Stelzer, O.; Sheldrick, W. S. *Tetrahedron* **2000**, *56*, 157–164.
- (29) Zuo, W.; Lough, A. J.; Li, Y. F.; Morris, R. H. *Science* **2013**, *342*, 1080–1083.
- (30) Noyori, R.; Ohkuma, T.; Kitamura, M.; Takaya, H.; Sayo, N.; Kumobayashi, H.; Akutagawa, S. *J. Am. Chem. Soc.* **1987**, *109*, 5856.
- (31) Noyori, R. *Angew. Chem. Int. Ed.* **2002**, *41*, 2008–2022.
- (32) Ohkuma, T.; Ooka, H.; Ikariya, T.; Noyori, R. *J. Am. Chem. Soc.* **1995**, *117*, 10417–10418.

- (33) Semwal, S.; Ghorai, D.; Choudhury, J. *Organometallics* **2014**, *33*, 7118–7124.
- (34) Perekalin, D. S.; Karslyan, E. E.; Petrovskii, P. V.; Borissova, A. O.; Lyssenko, K. A.; Kudinov, A. R. *Eur. J. Inorg. Chem.* **2012**, 1485–1492.
- (35) Soni, R.; Jolley, K. E.; Clarkson, G. J.; Wills, M. *Org. Lett.* **2013**, *15*, 5110–5113.
- (36) Konovalov, A. I.; Karslyan, E. E.; Perekalin, D. S.; Nelyubina, Y. V.; Petrovskii, P. V.; Kudinov, A. R. *Mendeleev Commun.* **2011**, *21*, 163–164.
- (37) Tobita, H.; Hasegawa, K.; Minglana, J. J. G.; Luh, L.-S.; Okazaki, M.; Ogino, H. *Organometallics* **1999**, *18*, 2058–2060.
- (38) Marchenko, A. P.; Koidan, H. N.; Huryeva, A. N.; Zarudnitskii, E. V.; Yurchenko, A. A.; Kostyuk, A. N. *J. Org. Chem.* **2010**, *75*, 7141–7145.
- (39) Nägele, P.; Herrlich, U.; Rominger, F.; Hofmann, P. *Organometallics* **2013**, *32*, 181–191.
- (40) Zelonka, R. A.; Baird, M. C. *Can. J. Chem.* **1972**, *50*, 3063–3072.
- (41) Brown, C. C.; Rominger, F.; Limbach, M.; Hofmann, P. *Inorg. Chem.* **2015**, *54*, 10126–10140.
- (42) *Apex 2 Software Package*; Bruker AXS Inc., 2013.
- (43) Cromer, D. T.; W., J. T. *Int. Tables X-Ray Crystallography*; 1974; Vol. 4.

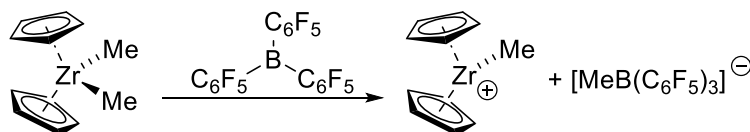
## Chapter 4

### Frustrated Lewis Pair and Lewis Acid Chemistry of Carbon-Based Lewis Acids

#### 4.1 Introduction

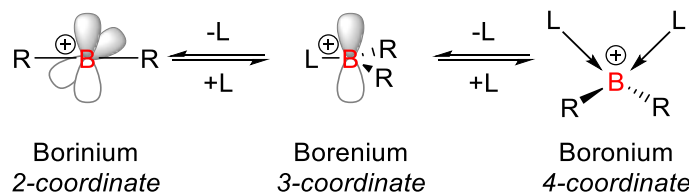
##### 4.1.1 Group 13 Lewis Acids

Before Gilbert N. Lewis lent his name to the class of acids and bases so familiar today in chemistry, Charles Friedel and James Crafts pioneered the field of electrophilic aromatic substitution, aided by what will later be called a Lewis acid.<sup>1-5</sup> Today, boron Lewis acids are ubiquitous due to the range of acidity offered by changing the substituents at the boron center. Tris(pentafluorophenyl)borane, commonly referred to as BCF, is a particularly common Lewis acid that sees use as an activator in Ziegler-Natta olefin polymerization reactions (Scheme 4.1.1).<sup>6,7</sup>



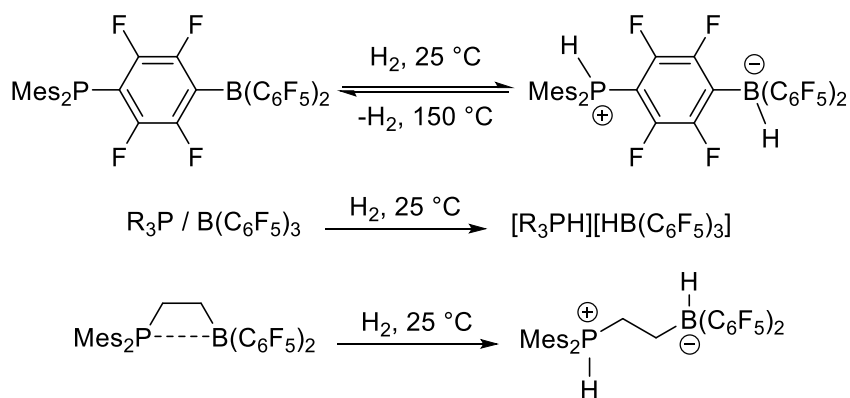
**Scheme 4.1.1: Activation of  $\text{Cp}_2\text{ZrMe}_2$  by tris(pentafluorophenyl)borane via methyl abstraction.**

Furthermore, BCF is frequently used as a catalyst for a variety of organic transformations.<sup>8-11</sup> A rich library of neutral boranes exist with combinations of alkyl, aryl, and halogen substituents that are used extensively in borylation reactions, producing new B-E bonds.<sup>12,13</sup> As well, exploration of other boron-containing motifs has led to the isolation and use of cationic species that are broadly categorized into three groups: boronium, borenium, and borinium cations (Scheme 4.1.2). These species are reviewed by Nöth, Piers, and others.<sup>14-17</sup>

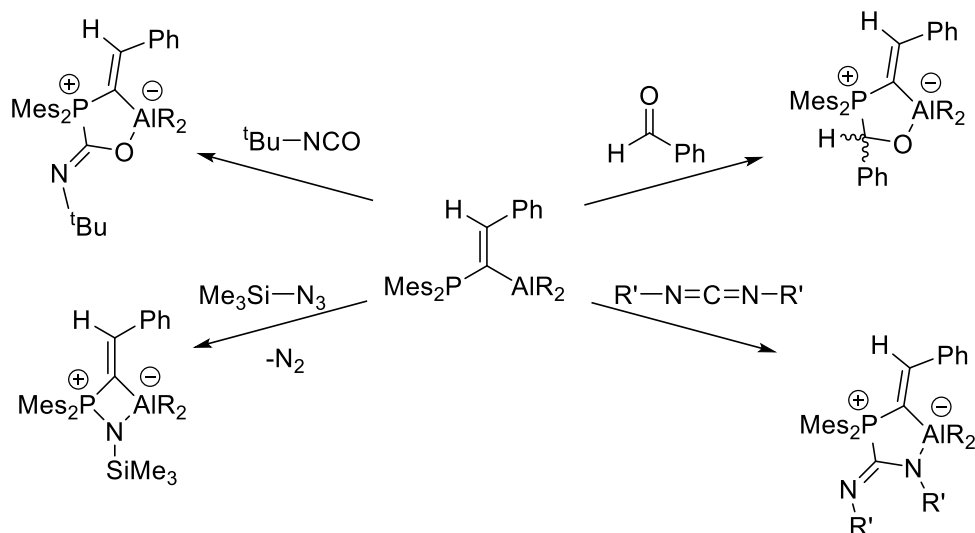


**Scheme 4.1.2: Borocation structure motifs with vacant p-orbitals explicitly shown.**

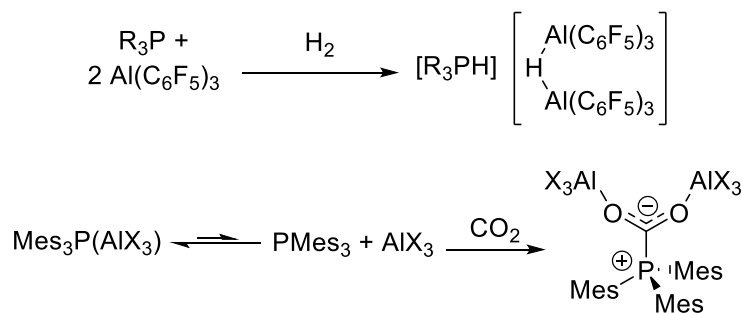
Furthermore, boron-based Lewis acids have been extensively employed in the field of Frustrated Lewis Pairs (FLP). In conjunction with Lewis bases, the combination of the two species has been used to activate carbon dioxide and dihydrogen (Scheme 4.1.3), and the latter has been used to hydrogenate a variety of unsaturated substrates.<sup>10,18–24</sup> While boron constitutes the bulk of Group 13 Lewis acids, it is by no means the only choice amongst such a group. Aluminum-based Lewis acids have been used extensively in FLP chemistry, ranging from carbon dioxide fixation and reduction to small molecule activation, including dihydrogen, carbodiimides, isocyanates, azides, and carbonyl compounds (Scheme 4.1.4 and Scheme 4.1.5).<sup>25–34</sup> Additionally, in recent reports, gallium and indium have been employed as Lewis acids by themselves as well as partners in FLP chemistry.<sup>35–42</sup>



**Scheme 4.1.3: First FLP activation of dihydrogen.**



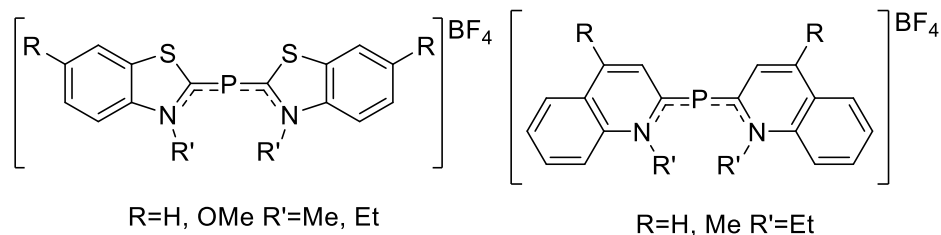
**Scheme 4.1.4: Small molecule activation by a geminal Al/P Frustrated Lewis Pair (R=CH<sub>2</sub><sup>t</sup>Bu, R'=p-tolyl).**



**Scheme 4.1.5: Dihydrogen activation by an intermolecular Al/P frustrated Lewis pair (R=<sup>t</sup>Bu, Mes) (top). Carbon dioxide fixation by an intermolecular Al/P frustrated Lewis pair (X=Cl, Br) (bottom).**

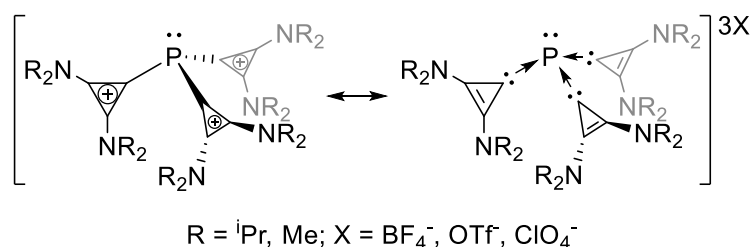
## 4.1.2 Lewis Acids Beyond Group 13

Recently, efforts have been focused on the derivation of Lewis acids outside of the Group 13 elements. Trivalent phosphorus compounds are generally considered Lewis bases and indeed, a large portion of their chemistry revolves around their use as ligands and stabilizing agents in transition metal and coordination chemistry. However, in recent years attention has been devoted towards creating Lewis acidic phosphorus (III) and (V) compounds and exploiting their unusual reactivity in catalysis. Following the first report of a phosphonium ion in 1964 (Figure 4.1.1), Cowley and Kempe reviewed several other phosphonium cations.<sup>43,44</sup>



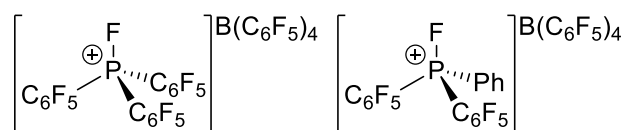
**Figure 4.1.1: The first isolated phosphonium cations.**

Highlighted uses of these compounds included insertion into C-H bonds and additions to various dienes in Diels-Alder type reactions to afford cyclopentene-phosponium derivatives. In 2011, Alcarazo reported the first instance of a tricationic carbene-stabilized phosphonium compound that, despite the high positive charge, still has a non-bonding pair of electrons that allows it to be coordinated onto metals as well as a low-lying LUMO that confers high  $\pi$ -accepting ability to the phosphorus center (Figure 4.1.2).<sup>45</sup>



**Figure 4.1.2: Mesomeric forms of the first tricationic carbene-stabilized phosphonium species.**

While phosphorus(V) Lewis acids are comparatively less studied,<sup>46</sup> it is important to note that P(V) Lewis acids are at the heart of the phosphorus ylides that make up the Wittig reactions of converting carbonyl compounds to olefins.<sup>47</sup> In 2013, Stephan and coworkers developed the highly Lewis acidic P(V) species [(C<sub>6</sub>F<sub>5</sub>)<sub>3</sub>PF][B(C<sub>6</sub>F<sub>5</sub>)<sub>4</sub>] and [(C<sub>6</sub>F<sub>5</sub>)Ph<sub>2</sub>PF][B(C<sub>6</sub>F<sub>5</sub>)<sub>4</sub>] (Figure 4.1.3).<sup>48</sup> These species have been shown to be effective Lewis acid catalysts on their own and as part of an FLP in the activation and delivery of dihydrogen to olefins.<sup>49-52</sup>

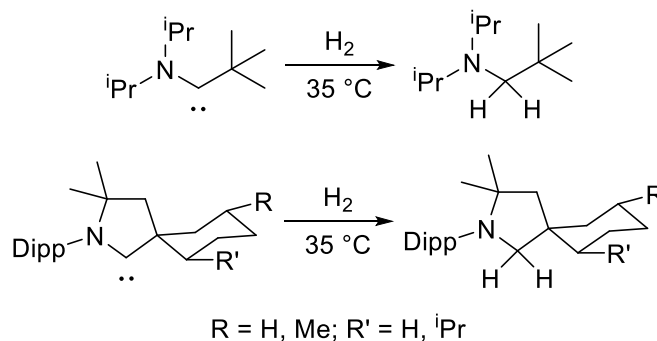


**Figure 4.1.3: Highly Lewis acidic fluorophosponium cations.**

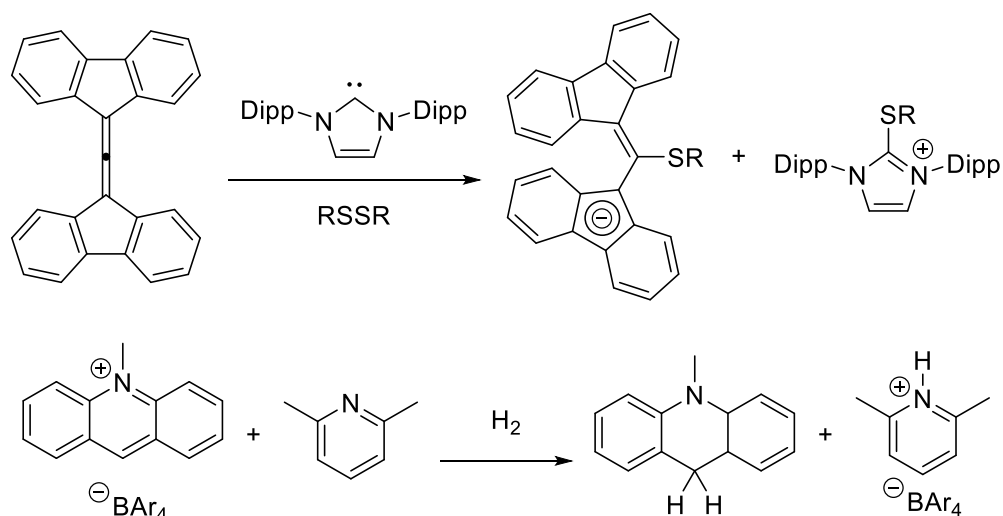
Sandwiched in between Group 13 and 15 are the Lewis acids derived from Group 14. The most common of these incorporate silicon cations and have been widely used to catalyze a variety of reactions.<sup>53</sup> In 2010 Manners *et al.* used  $\text{Me}_3\text{SiOTf}$  to effect the dehydrogenation of the ammonia-borane adduct  $\text{Me}_2\text{NH-BH}_3$ .<sup>54</sup> More recently, silicon Lewis acids comprised of trivalent silylium cations, which have been known for some time, have shown to be excellent participants in FLP chemistry, owing to their isoelectronic relationship to boranes and their potent Lewis acidity.<sup>55-57</sup> In a seminal work by the Müller group, the authors showed that the bulky silylium cation  $[(\text{C}_6\text{Me}_5)_3\text{Si}][\text{B}(\text{C}_6\text{F}_5)_4]$  was able to activate dihydrogen when paired with  $\text{PMes}_3$ , yielding the corresponding neutral silane and phosphonium salt.<sup>58</sup> This work was then expanded to include other sterically demanding phosphines and silylenes as the Lewis basic partners in the FLP cleavage of  $\text{H}_2$ .<sup>59</sup>

While the carbon analogue of  $\text{B}(\text{C}_6\text{F}_5)_3$  is the hydridophilic trityl cation  $[\text{CPh}_3]^+$ , the use of such a Lewis acid in FLP chemistry has been limited due to the tendency to form strong adducts with many Lewis bases. Indeed, while less common than their boron-based counterparts, carbon Lewis acids have been employed in both Lewis acid catalysis as well as in FLP chemistry. Indeed, an interesting take on the FLP chemistry of carbon-based Lewis acids was presented by Bertrand and coworkers in 2007, whereby (alkyl)(amino)carbenes (AACs) were shown to irreversibly activate dihydrogen at the same carbon center (Scheme 4.1.6).<sup>60</sup> Compared to N-heterocyclic carbenes, these singlet carbenes possess a HOMO that is slightly higher in energy while at the same time have a singlet-triplet gap that is much smaller. Thus, AACs are slightly more nucleophilic than NHCs but significantly more electrophilic. This increase in reactivity of both the Lewis basic and acidic properties of AACs means that nucleophilic attack of the carbene to dihydrogen is followed by abstraction of a hydride-like hydrogen atom from the complex by the empty p-orbital present on the same carbenic center. Furthermore, in 2014, the Ingleson group demonstrated the use of N-methylacridinium salts as effective carbon-based Lewis acids for use in the FLP activation of dihydrogen (Scheme 4.1.7).<sup>61</sup> This work was expanded through the use of N-methylbenzothiazolium salts as the Lewis acid as well as N-heterocycle-ligated borocations, which demonstrated enhanced Lewis acidity at the carbon atom.<sup>62,63</sup> As well, Alcarazo *et al.* have shown a unique use of carbon Lewis acids by exploiting the ability of trityl cations to delocalize the positive charge into the aryl substituents. Such an approach was used to design an allene Lewis acid that could delocalize negative charge into the bound fluorene

ligands, thus producing an electrophilic carbon atom. In combination with NHCs, this unique all-carbon FLP was shown to undergo heterolytic cleavage of disulfide bonds (Scheme 4.1.7).<sup>64,65</sup> Finally, the Stephan group has pursued a novel approach to the generation of carbon-based Lewis acids. A Ru- $\eta^6$ -arene complex, when paired with PCy<sub>3</sub>, was shown to undergo nucleophilic attack at the *ortho* and *para* positions of the aromatic ring bound to the ruthenium center.<sup>66</sup> However, when the phosphine base is changed to Mes<sub>3</sub>P or <sup>t</sup>Bu<sub>3</sub>P, nucleophilic attack at the aryl ring was not observed. Instead, the phosphine and Ru complex form a frustrated Lewis pair that is able to heterolytically cleave dihydrogen between the phosphine base and carbon Lewis acid; this unusual FLP combination was shown to catalyze the hydrogenation of imines. Herein, the synthesis and use of air- and moisture-stable trityl cations will be discussed. Furthermore, their utility as FLP Lewis acid partners and catalytic activity will be explored.



**Scheme 4.1.6: Dihydrogen activation at the same carbon center using (alkyl)(amino)carbenes.**

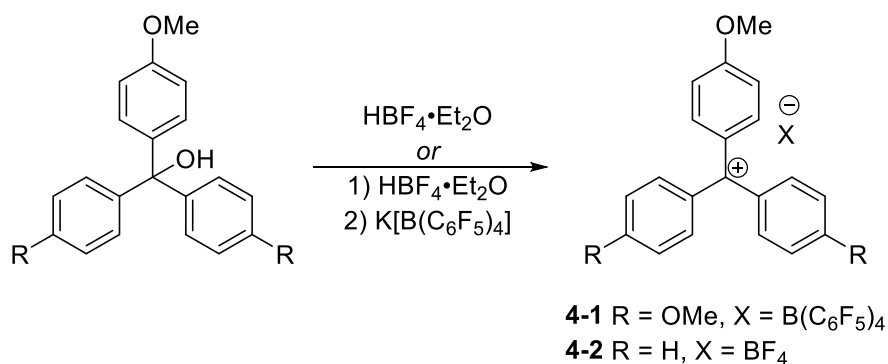


**Scheme 4.1.7: All-carbon FLP using allenes (top) and acridinium Lewis acid in cleavage of H<sub>2</sub> (bottom).**

## 4.2 Results and Discussion

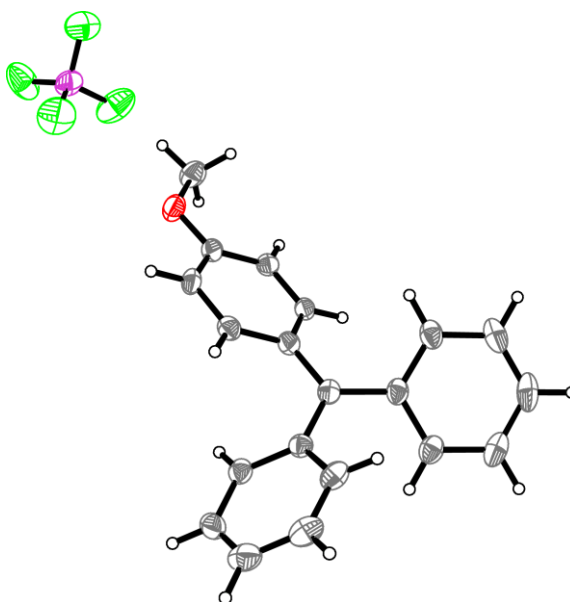
### 4.2.1 Synthesis of Air-Stable Trityl Cations

The methoxy-derived trityl cation salts [(*p*-MeO-C<sub>6</sub>H<sub>4</sub>)<sub>3</sub>C][B(C<sub>6</sub>F<sub>5</sub>)<sub>4</sub>] (**4-1**) and [(*p*-MeO-C<sub>6</sub>H<sub>4</sub>)CPh<sub>2</sub>][BF<sub>4</sub>] (**4-2**) were prepared following a modified literature procedure<sup>67</sup> involving treatment of the corresponding triarylalcohol with ethereal tetrafluoroboric acid (Scheme 4.2.1). For **4-1**, the use of tetrafluoroborate anion produced difficulties in isolation as the product was often waxy and difficult to purify. Thus, anion exchange with a bulkier non-coordinating anion such as tetrakis(pentafluorophenyl)borate was employed to effectively furnish the desired product cleanly.

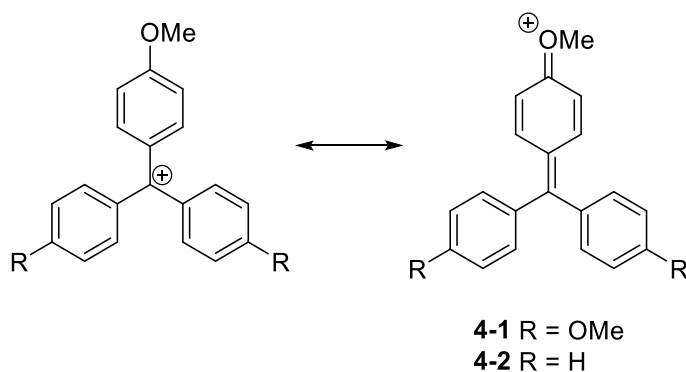


**Scheme 4.2.1: Synthesis of air-stable trityl cations.**

The solid-state structure of **4-2** (Figure 4.2.1) confirmed the expected trigonal planar geometry of the central carbon atom. The  $C_{\text{central}}\text{-C}$  bond lengths were found to be 1.418(7) Å, 1.455(7) Å, and 1.454(7) Å, with the shortest bond value corresponding to the ring bearing the methoxy substituent. These data are consistent with the resonance stabilization of compounds **4-1** and **4-2**, which presumably accounts for the air-stability observed for compounds **4-1** and **4-2** (Scheme 4.2.2). Indeed, these compounds can be stored for extended periods of time and handled openly in the air without degradation.



**Figure 4.2.1: Thermal ellipsoid plot of solid-state structure of 4-2. Grey: Carbon, Red: Oxygen, Green: Fluorine, Purple: Boron, White: Hydrogen.**

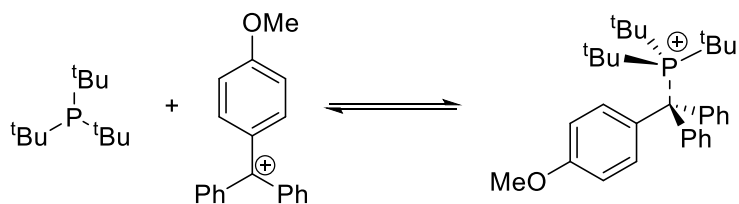


**Scheme 4.2.2: Mesomeric stabilization of trityl cations.**

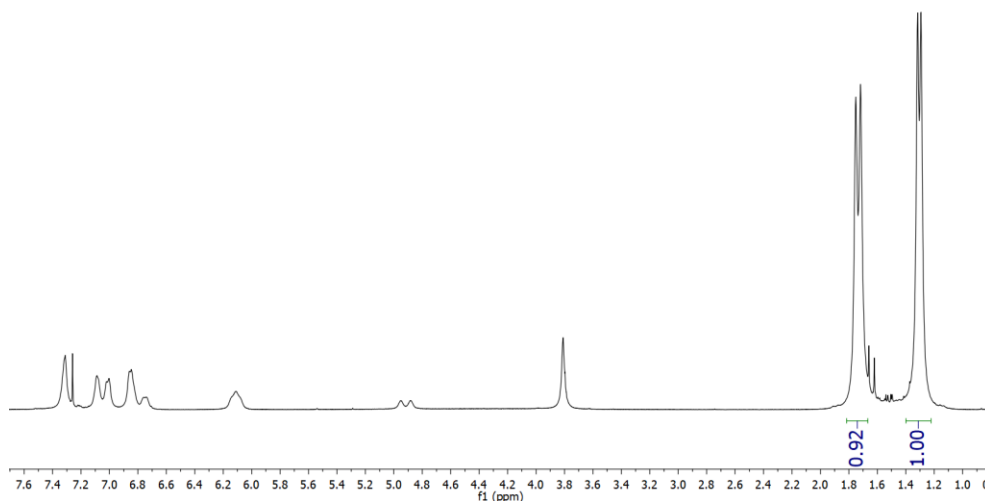
## 4.2.2 Catalysis and Reactivity of Trityl Cations

### 4.2.2.1 Frustrated Lewis Pair Chemistry of Trityl Cations

With the air-stable Lewis acids in hand, the FLP chemistry of the cations were explored. Initially, the reaction between **4-1** and tris(*tert*-butyl)phosphine ( $t\text{Bu}_3\text{P}$ ) was probed. While reversible adducts were formed in solution at room temperature, when the solution was pressurized with  $\text{H}_2$  (4 atm) no activation of dihydrogen was observed, likely due to the weak Lewis acidity of the trityl cation. Analogously, an equimolar solution of **4-2** and  $t\text{Bu}_3\text{P}$  was examined by  $^1\text{H}$  and  $^{31}\text{P}$  NMR spectroscopy. At room temperature a reversible adduct was observed, as evidenced by the  $^{31}\text{P}\{^1\text{H}\}$  resonances at 62.4 ppm and 49.6 ppm, attributed to free  $t\text{Bu}_3\text{P}$  and the adduct, respectively (Scheme 4.2.3). Similarly, the adduct is also readily observed in the  $^1\text{H}$  NMR spectrum and integration of the *tert*-butyl resonances yields an approximate 1:1 ratio of free phosphine and adduct (Figure 4.2.2).



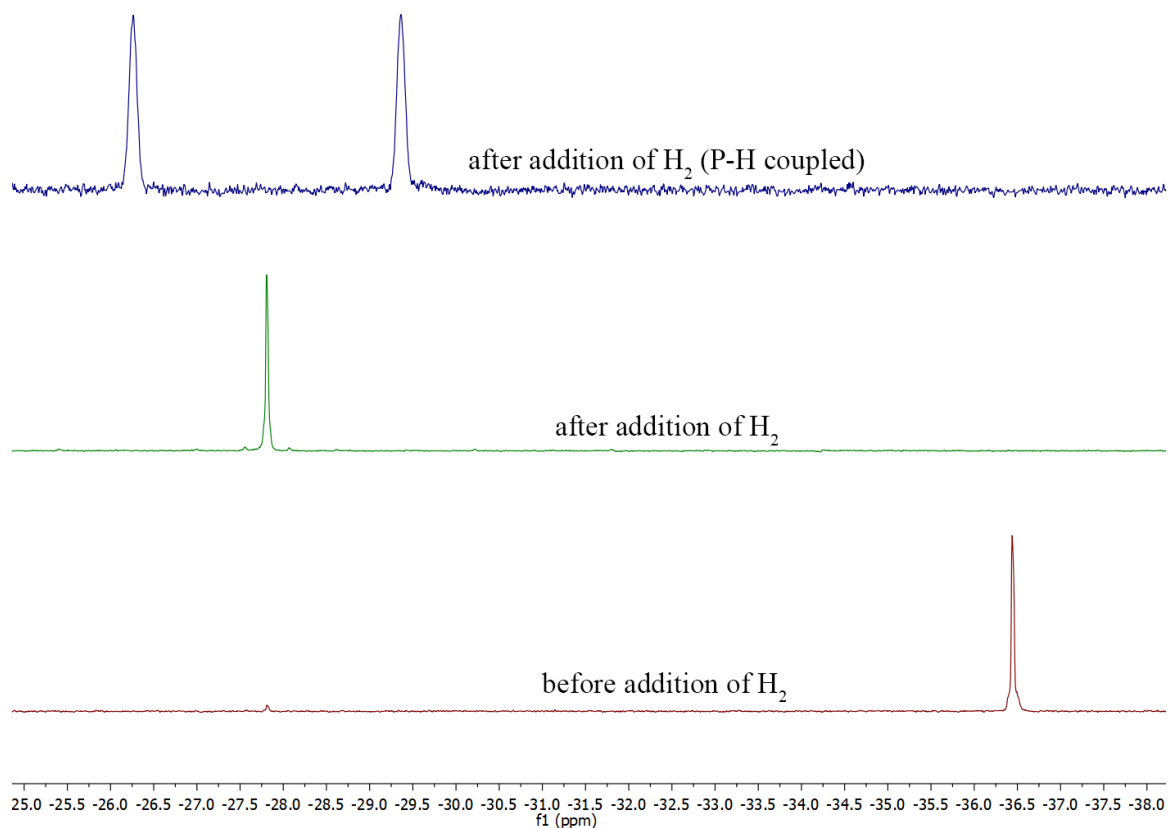
**Scheme 4.2.3: Reversible adduct formation between 4-2 and  $t\text{Bu}_3\text{P}$ .**



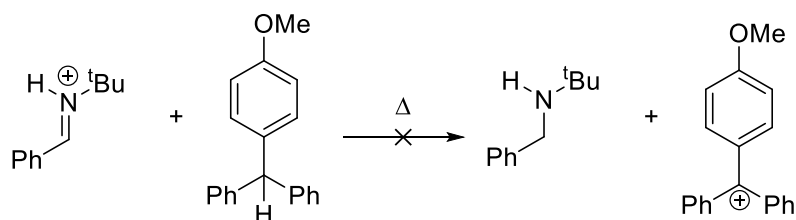
**Figure 4.2.2:  $^1\text{H}$  NMR spectrum of 4-2 and  $t\text{Bu}_3\text{P}$  showing approximate ratio of adduct and free phosphine.**

Subsequently, this solution was subject to dihydrogen (4 atm) and the  $^{31}\text{P}\{^1\text{H}\}$ NMR spectrum showed complete conversion to  $[\text{HP}^t\text{Bu}_3][\text{BF}_4]$  at 51.4 ppm and, upon proton-coupling, the resonance was expanded into a doublet with a coupling constant of  $^1J_{\text{P-H}} = 466$  Hz, characteristic of P(V) P-H coupling constants.<sup>68</sup> Although the Lewis acids presented herein are robust in the presence of air and moisture, the addition of Lewis bases such as phosphines can lead to rapid activation of water and thus the reactions must be carried out with strict exclusion of moisture.

To test the viability of this system for catalysis, a second equimolar solution of  $^t\text{Bu}_3\text{P}$  and **4-2** was subject to deuterium hydride (HD). Here, scrambling of HD to form statistical mixtures of HD,  $\text{H}_2$ , and  $\text{D}_2$  would indicate reversible activation of dihydrogen. However, no HD scrambling was observed, and this is attributed to the high basicity of the phosphine. Thus, a less basic phosphine was employed. In a similar manner, **4-2** and tris(2,4,6-trimethylphenyl)phosphine ( $\text{Mes}_3\text{P}$ ) were combined and monitored by  $^1\text{H}$  and  $^{31}\text{P}$  NMR spectroscopy. In contrast to the previous experiments, no adduct was observed and the only  $^{31}\text{P}\{^1\text{H}\}$  NMR resonance was attributed to free  $\text{Mes}_3\text{P}$  at -36.5 ppm (Figure 4.2.3). This solution was then degassed and backfilled with  $\text{H}_2$  and the reaction was monitored. Within 30 minutes quantitative conversion to the hydrogen-split product was observed, as evidenced by a  $^{31}\text{P}$  NMR resonance at -27.8 ppm with a one-bond P-H coupling constant of  $^1J_{\text{P-H}} = 502$  Hz. Similarly, the  $^1\text{H}$  NMR spectrum displays the characteristic P-H doublet centered at 8.64 ppm while the methine proton of the neutral triarylmethane product is observed as a broadened singlet at 5.70 ppm. It is worth noting that no trace of triaryl alcohol was observed in the reaction mixture, indicating there is no competitive activation of water in the reaction. Unfortunately, when subject to deuterium hydride no scrambling was observed, likely due to the poor hydricity of the triarylmethane. While phosphine bases proved ineffective at reversibly activating  $\text{H}_2$ , reactions were attempted with nitrogen bases instead. Reaction of **4-2** and N-benzylidene-*tert*-butylamine did not produce a shift in the methoxy protons of the trityl cations, and the addition of  $\text{H}_2$  did not result in the corresponding amine, even upon heating to 100 °C for several days. Additionally, the reaction of an iminium salt with the neutral triarylmethane did not result in abstraction of the hydride to produce an amine product, indicative of the poor hydricity of the  $\text{C}_{\text{central}}\text{-H}$  hydrogen atom of triarylmethane (Scheme 4.2.4).



**Figure 4.2.3: Activation of H<sub>2</sub> by 4-2/Mes<sub>3</sub>P FLP. Free Mes<sub>3</sub>P before addition of dihydrogen (bottom), phosphonium product (middle), and depiction of P-H coupling in phosphonium (top).**

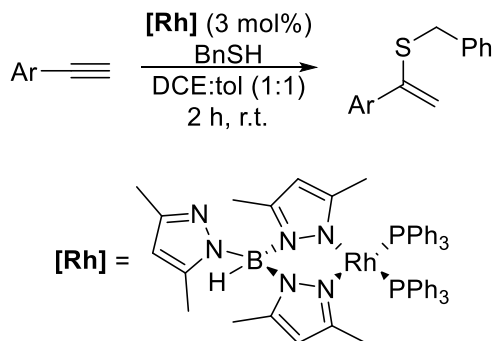


**Scheme 4.2.4: Attempted step-wise reduction of an iminium salt using triarylmethane.**

#### 4.2.2.2 Hydrothiolation of Olefins

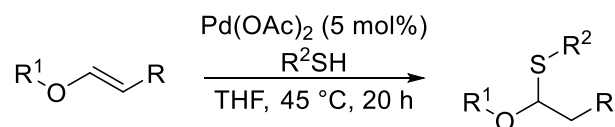
The introduction of sulfur in organic compounds and materials has important applications, including the generation of synthetic intermediates, reagents, pharmaceuticals, or functional materials.<sup>69,70</sup> Indeed, the utility of sulfur in organic materials was realized by Charles Goodyear when he discovered the process of rubber vulcanization.<sup>71</sup> Since then, the field has expanded rapidly to include sulfur substituents and additives in many processes and chemical products.

One method of obtaining these products involves the addition of thiols to unsaturated substrates. Such “hydrothiolations” have been known for over a century,<sup>72</sup> however, they are generally carried out by free radicals,<sup>73–75</sup> acids,<sup>76–79</sup> or bases,<sup>80–84</sup> and often result in mixtures of products. Recently, transition metal catalysts have offered significant improvements in selective hydrothiolations.<sup>85–87</sup> The Love group has demonstrated the use of Rh-pyrazoleborate catalysts to effect the hydrothiolation of alkynes to form 1,1-disubstituted alkenes (Scheme 4.2.5).<sup>88</sup>



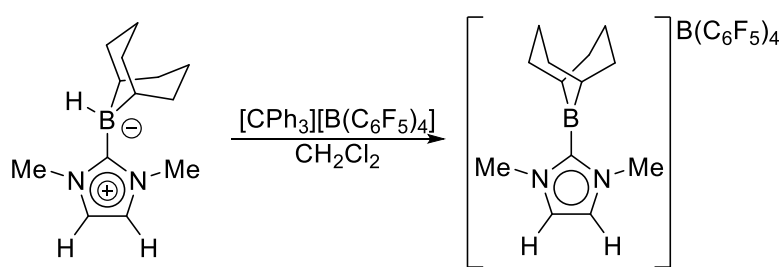
**Scheme 4.2.5: Rh-catalyzed hydrothiolation of alkynes to 1,1-disubstituted olefins.**

While the hydrothiolation of alkynes has been extensively studied, the analogous reactions involving alkenes have drawn less attention.<sup>89</sup> For instance, Ogawa and coworkers have also used Pd(OAc)<sub>2</sub> to hydrothiolate heteroatom-activated alkenes to yield the Markovnikov product (Scheme 4.2.6).<sup>90,91</sup> Furthermore, stoichiometric additions of Lewis acids such as SnCl<sub>4</sub>, AlCl<sub>3</sub>, and TiCl<sub>4</sub> were shown to generate similar moieties,<sup>92,93</sup> while a recent study has also shown that Sc(OTf)<sub>3</sub>-catalyzed hydrothiolation proceeds in an anti-Markovnikov fashion.<sup>94</sup> Metal-free approaches to this transformation are underdeveloped and thus it is noteworthy that Duñach and coworkers reported the use of the Lewis acid InBr<sub>3</sub> as an effective catalyst for the Markovnikov hydrothiolation of olefins,<sup>95</sup> while the group of Sinha<sup>96</sup> have demonstrated the utility of ionic liquid-mediated hydrothiolations.

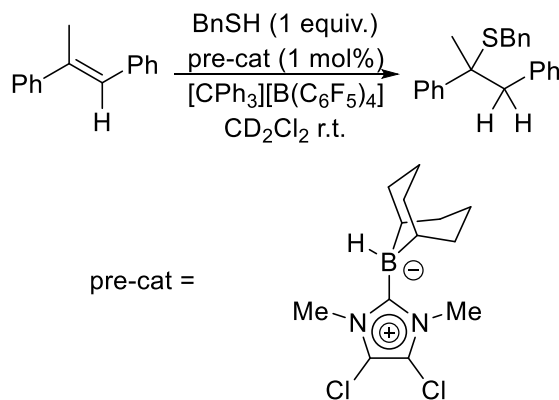


**Scheme 4.2.6: Hydrothiolation of heteroatom-activated alkenes using Pd(OAc)<sub>2</sub>.**

Hydrothiolation of olefins were initially explored using previously synthesized Lewis acids (Table 4.2.1). One of the initial goals of the hydrothiolation chemistry was to use borenium cations such as those described by Stephan and coworkers.<sup>97,98</sup> The overall goal was to later use chiral borenium cations synthesized in the group<sup>99</sup> to facilitate chiral addition of S-H bonds to unsaturated substrates. These borenium catalysts are initially produced *in-situ* by the addition of a hydride-abstrating agent such as  $[\text{CPh}_3]^+$  (Scheme 4.2.7). Thus, the first hydrothiolation reaction was carried out in the presence of the borane pre-catalyst and the reaction was initiated using the trityl reagent (Scheme 4.2.8).



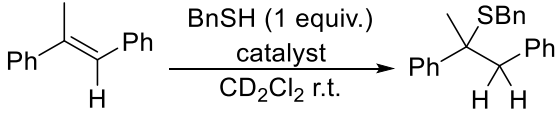
**Scheme 4.2.7: Generation of borenium cation *via* abstraction of hydride from borane.**



**Scheme 4.2.8: Initial proposed catalytic hydrothiolation of methylstilbene using an *in-situ* generated borenium catalyst.**

It was found that the reaction proceeded to completion in minutes, as observed by  $^1\text{H}$  NMR spectroscopy. However, during the course of control studies it was found that the trityl cation alone could catalyze this reaction. Thus, we proceeded to explore the reactivity of these cations. Trityl tetrakis(pentafluorophenyl)borate was used as a reference catalyst for the hydrothiolation of several unsaturated substrates (Table 4.2.2).

**Table 4.2.1: Hydrothiolation of methyl stilbene using various known Lewis acid catalysts.**

			
Catalyst	Loading (mol%)	Time	Conversion (%)
$[\text{CPh}_3][\text{B}(\text{C}_6\text{F}_6)_4]$	1	15 min	99
$[(\text{C}_6\text{F}_5)_3\text{PF}][\text{B}(\text{C}_6\text{F}_5)_4]$	1	15 min	99
$\text{B}(\text{C}_6\text{F}_5)_3$	10	2 h	95
Trifluoroacetic acid	10	3 d	0

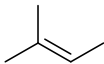
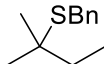
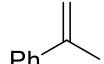
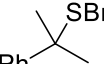
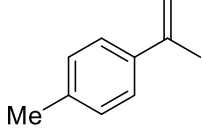
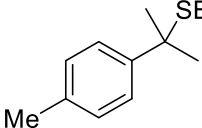
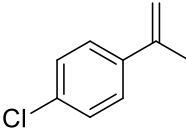
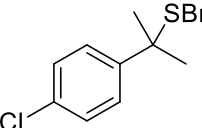
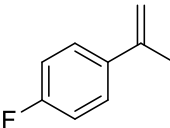
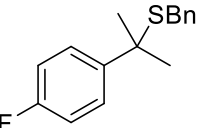
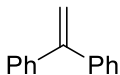
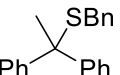
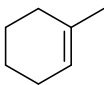
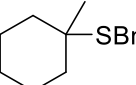
**Table 4.2.2: Catalytic olefin hydrothiolation using trityl tetrakis(pentafluorophenyl)borate.**

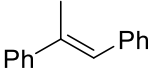
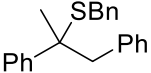
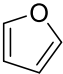
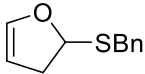
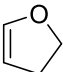
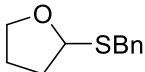
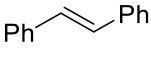
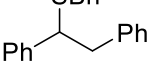
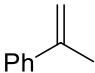
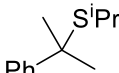
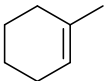
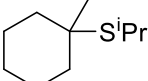
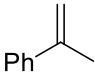
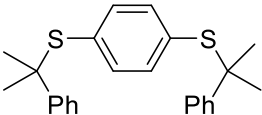
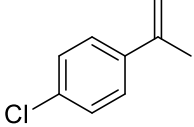
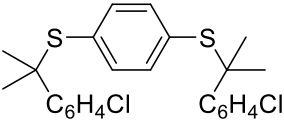
Entry	Substrate	Product	Time (h)	Conversion (%)
1			6	99
2			0.25	99
3			0.25	96
4			0.25	99
5			0.25	99
6			0.25	4
7			24	3
8			72	75

Compound **4-2** proved to be an ineffective catalyst for the hydrothiolation of olefins upon heating to 50 °C (Table 4.2.3). A series of olefins were shown to undergo hydrothiolation with benzylthiol to give the corresponding Markovnikov addition products with conversions of 70-99% in 1-2 hours, with isolated yields ranging from 18-99% after work-up. Efforts to effect addition to furan, dihydrofuran, or *trans*-stilbene were unsuccessful, even on heating for 24 hours. This may reflect the lower Lewis acidity of **4-2** compared to [CPh<sub>3</sub>][B(C<sub>6</sub>F<sub>5</sub>)<sub>4</sub>]. Double hydrothiolation was also possible, using 1,4-dithiobenzene and two equivalents of the corresponding alkene. While the use of **4-2** as a catalyst requires elevated temperatures in

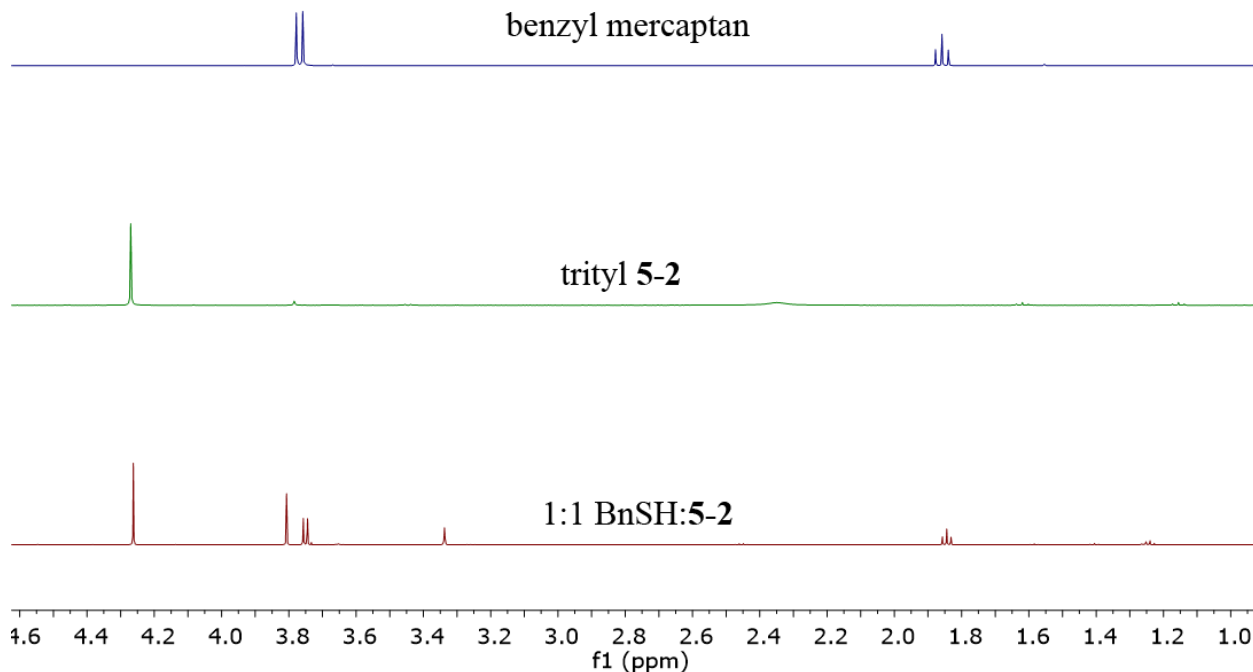
contrast to  $[\text{CPh}_3][\text{B}(\text{C}_6\text{F}_5)_4]$ , compound **4-2** is far more robust. Thus, the hydrothiolations presented in Table 4.2.3 were carried out on the benchtop using commercial grade chloroform solvent, without the need for further purification of solvents or reagents. Following reactions *via*  $^1\text{H}$  NMR spectroscopy showed only traces of the triarylmethanol, likely because of some small degree of hydrolysis of the cation. In addition, the products were readily separated from the catalyst and the traces of triarylmethanol *via* elution of hexanes solution of the crude mixture through a short silica plug.

**Table 4.2.3: Catalytic hydrothiolation of unsaturated species using catalyst 4-2.**

Entry	Substrate	Product	Time (h)	Conversion (%)
<b>Benzyl thiol</b>				
	$\begin{array}{c} \text{R}' \\   \\ \text{R}-\text{C}=\text{C}-\text{R}'' \\   \\ \text{H} \end{array} \xrightarrow[\text{CHCl}_3, 50^\circ\text{C}]{\begin{array}{c} \text{BnSH (1 equiv.)} \\ \mathbf{4-2} \\ (1 \text{ mol}\%) \end{array}} \begin{array}{c} \text{R}' \quad \text{SBn} \\   \quad   \\ \text{R}-\text{C}-\text{C}-\text{R}'' \\   \quad   \\ \text{H} \quad \text{H} \end{array}$			
1			2	99(95)
2			1	99(99)
3			1	96(92)
4			1	99(64)
5			1	95(34)
6			2	70
7			2	99(99)

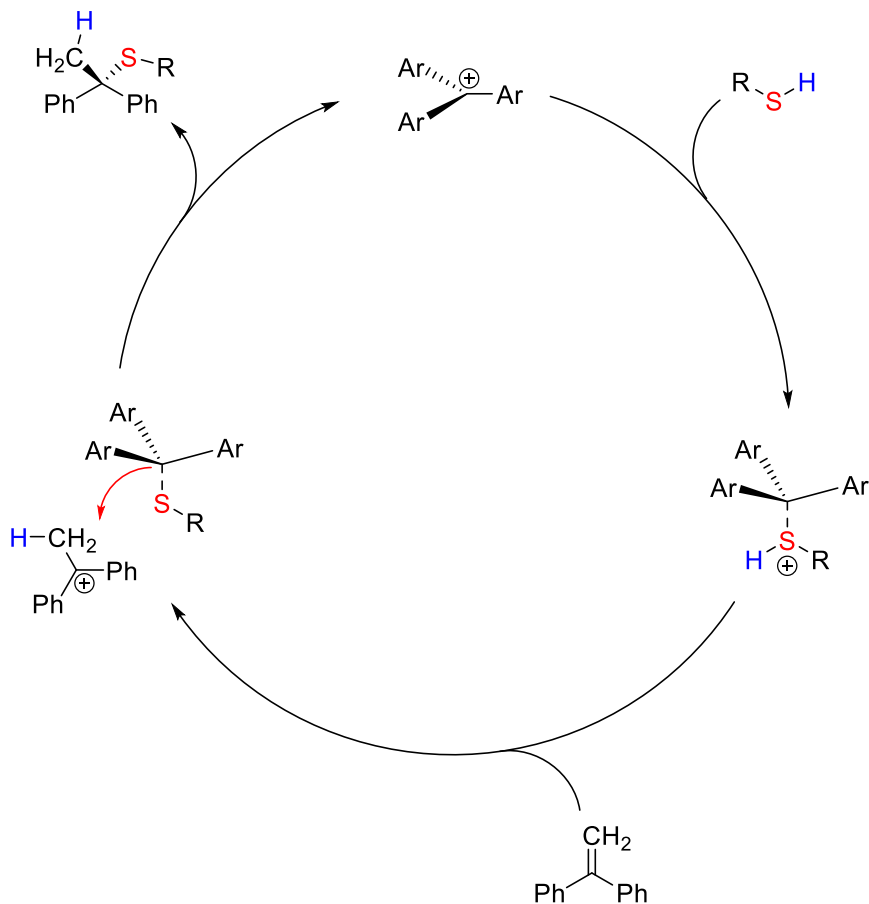
8			6	99(39)
9			24	0
10			24	0
11			24	0
<b>iso-propyl thiol</b>				
12			2	92(86)
13			2	99(13)
<b>1,4-dithiobenzene</b>				
14			2	80(61)
15			1	95(18)

The mechanism of hydrothiolation of diphenylethylene using **4-2**,  $[\text{CPh}_3][\text{B}(\text{C}_6\text{F}_5)_4]$ , or  $\text{B}(\text{C}_6\text{F}_5)_3$  as the catalyst is thought to be analogous to that previously proposed for fluorophosphonium cations.<sup>100</sup> In the present case, the catalysis is thought to be initiated by interaction of the thiol with the carbocation. The resulting enhancement in acidity of the thiol proton prompts protonation of the disubstituted olefin, affording a transient carbocation. This view is supported by the observation of a weak interaction between benzyl thiol and **4-2** by NMR spectroscopy (Figure 4.2.4). Herein, the  $^1\text{H}$  NMR resonance corresponding to the methylene protons is shown as a doublet at approximately 3.7 ppm, which is shifted upfield to roughly 3.3 ppm and is seen as a broad singlet. The thiol proton signal as well as the methoxy protons of the trityl cation are similarly shifted upfield. Furthermore, resonances pertaining to unquenched Lewis acid and base indicate that the interaction is reversible at room temperature.



**Figure 4.2.4:** <sup>1</sup>H NMR spectrum of equimolar solution of trityl 4-2 and benzyl mercaptan, depicting upfield shift in proton resonances.

In the context of the catalytic cycle, the transiently formed carbocation is both more sterically accessible as well as less electronically stable, prompting thiolate transfer and thus affording the Markovnikov hydrothiolation product and regeneration of the carbocation catalyst (Scheme 4.2.9). This mechanism is consistent with the lack of reactivity of primary and 1,2-disubstituted alkenes, where the generation of primary or secondary carbocations presents a significant thermodynamic barrier. The proposed mechanism is distinct from known routes involving thiol activation where the reactions are triggered by formation of free radicals, deprotonation by a base, or by oxidative addition of S-H bonds to a metal center.<sup>87</sup>



**Scheme 4.2.9: Proposed catalytic cycle for hydrothiolation of olefins using trityl catalysts.**

### 4.3 Conclusion

A series of air-stable trityl cations were synthesized and their reactivity as frustrated Lewis pair partners and Lewis acid catalysts was explored. The Lewis acid variants differ in the electron-donating ability of the substituents. Reaction of **4-1** and **4-2** with tris(*tert*-butyl)phosphine yields a reversible adduct while the bulkier base trimesitylphosphine does not display any interaction at room temperature. When subjected to four atmospheres of dihydrogen in the presence of either base, only **4-2** is Lewis acidic enough to activate  $\text{H}_2$  and thus yield the corresponding phosphonium salts and neutral triarylmethane. However, this activation is not reversible and cannot be used to effect addition of  $\text{H}_2$  across unsaturated substrates. In addition to their FLP chemistry, trityl cations can be used to effect addition of S-H bonds across olefins. The use of trityl **4-2** presents an air-stable catalyst system that can be employed without the need for rigorously anhydrous and/or oxygen-free environments.

## 4.4 Experimental Section

### 4.4.1 General Considerations

Where necessary, all manipulations were carried out under an atmosphere of dry, O<sub>2</sub>-free N<sub>2</sub>, employing a VAC Atmospheres glove box or a Schlenk vacuum-line. Unless stated otherwise, all proteo- and deuterio-solvents (pentanes, hexanes, toluene, tetrahydrofuran, dichloromethane, and chloroform) and reagents (tetrafluoroboric acid, mercaptans, and alkenes) were purchased from commercial sources and used without further purification. In specific cases requiring air- and moisture-free conditions, solvents were purified with a Grubbs-type column system manufactured by Innovative Technology and dispensed into thick-walled Schlenk glass flasks equipped with Teflon-valve stopcocks. Deuterated solvents were dried over the appropriate agents, vacuum-transferred or distilled into storage flasks with Young-type Teflon stopcocks, and degassed accordingly (CD<sub>2</sub>Cl<sub>2</sub>, CDCl<sub>3</sub>, C<sub>6</sub>D<sub>6</sub>, THF-*d*<sub>8</sub>). Where required, reagents were dispensed into thick-walled Schlenk glass flasks equipped with Teflon-valve stopcocks and degassed *via* repeated cycles of freeze-pump-thaw. <sup>1</sup>H and <sup>13</sup>C{<sup>1</sup>H} NMR spectra were recorded at 25 °C on a Bruker 500 MHz spectrometer equipped with a cold probe. Chemical shifts are given relative to SiMe<sub>4</sub> and referenced to the residual solvent signal (<sup>1</sup>H and <sup>13</sup>C). Chemical shifts are reported in ppm and coupling constants as scalar values in Hz. <sup>11</sup>B{<sup>1</sup>H} and <sup>19</sup>F{<sup>1</sup>H} NMR spectra were recorded at 25 °C on a Bruker 400 MHz spectrometer and chemical shifts are given relative to 15% BF<sub>3</sub>•Et<sub>2</sub>O and CFCl<sub>3</sub>, respectively. <sup>31</sup>P{<sup>1</sup>H} NMR spectra were recorded at 25 °C on a Bruker 400 MHz spectrometer and referenced to 85% H<sub>3</sub>PO<sub>4</sub>.

### 4.4.2 Synthetic Procedures

#### 4.4.2.1 General Procedure for Hydrothiolation

To a mixture of thiol (1 mmol) and alkene (1 mmol) was added the corresponding trityl catalyst in chloroform or dichloromethane (5 mL). Reactions were either carried out at room temperature or at 50 °C for a period of time, as indicated in Table 4.2.3. The reaction was monitored by <sup>1</sup>H NMR spectroscopy and upon completion was evacuated to dryness and the residue re-dissolved in hexanes. The suspension was then passed through a short silica plug to remove the catalyst as well as hydrolysis by-products. The filtrate was then concentrated to dryness to afford the product. In most cases no further purification was required. In some instances, the isolated yields

of the products were significantly lower than their conversion yields due to the volatility and/or solubility in hydrocarbon solvents.

#### 4.4.2.2 Synthesis of [(*p*-MeO-C<sub>6</sub>H<sub>4</sub>)<sub>3</sub>C][B(C<sub>6</sub>F<sub>5</sub>)<sub>4</sub>] (**4-1**)

4,4',4''-trimethoxytrityl alcohol (0.312 g, 0.866 mmol) was dissolved in Et<sub>2</sub>O (50 mL) and cooled to 0 °C. Tetrafluoroboric acid (50-55 w/w% in diethyl ether, 3.2 mL, 22 mmol) was added dropwise to the cold solution over a period of 15 minutes. The clear, colourless solution immediately turned into a dark crimson red oil with clear supernatant. The mixture was stirred at 0 °C for 1 hour and then all volatiles were removed under vacuum. The residue was washed with pentanes (5 x 10 mL) and diethyl ether (5 x 10 mL), then taken up in toluene. The dark red solution was combined with K[B(C<sub>6</sub>F<sub>5</sub>)<sub>4</sub>] (0.565 g, 0.787 mmol) and the solution was stirred at room temperature overnight, which was then filtered over a Celite plug and concentrated in volume to 1 mL. Concentrated solution was added to stirring pentanes (10 mL) and the dark red oil was triturated for several hours until orange precipitate was observed. The supernatant was decanted and solid washed with pentanes (5 x 5 mL) to afford product as an orange powder (0.587 g, 67%). Some carbon resonances pertaining to the borate anion could not be resolved due to broadened signals.

<sup>1</sup>H NMR (CDCl<sub>3</sub>): δ 4.05 (s, 9H, OCH<sub>3</sub>), 7.18 (d, <sup>3</sup>J<sub>H-H</sub> = 9 Hz, 6H, Ar-H), 7.48 (d, <sup>3</sup>J<sub>H-H</sub> = 9 Hz, 6H, Ar-H).

<sup>13</sup>C{<sup>1</sup>H} NMR (CDCl<sub>3</sub>): δ 56.9 (s, OCH<sub>3</sub>), 116.5 (s, *o*-C<sub>6</sub>H<sub>4</sub>), 132.0 (*p*-C<sub>6</sub>H<sub>4</sub>), 136.3 (d, <sup>1</sup>J<sub>C-F</sub> = 249 Hz, B(C<sub>6</sub>F<sub>5</sub>)<sub>4</sub>), 142.7 (s, *m*-C<sub>6</sub>H<sub>4</sub>), 148.2 (d, <sup>1</sup>J<sub>C-F</sub> = 241 Hz, B(C<sub>6</sub>F<sub>5</sub>)<sub>4</sub>), 170.6 (s, *ipso*-C<sub>6</sub>H<sub>4</sub>), 192.5 (s, CPh<sub>3</sub>).

<sup>19</sup>F{<sup>1</sup>H} NMR (CDCl<sub>3</sub>): δ -132.6 (s, br, *o*-C<sub>6</sub>F<sub>5</sub>), -163.1 (m, *p*-C<sub>6</sub>F<sub>5</sub>), -166.9 (m, *m*-C<sub>6</sub>F<sub>5</sub>).

<sup>11</sup>B{<sup>1</sup>H} NMR (CDCl<sub>3</sub>): δ -16.7 (s).

#### 4.4.2.3 Synthesis of [(*p*-MeO-C<sub>6</sub>H<sub>4</sub>)CPh<sub>2</sub>][BF<sub>4</sub>] (**4-2**)

In a 100 mL round-bottom flask open to air, (4-methoxyphenyl)diphenylmethanol (0.995 g, 3.43 mmol) was dissolved in diethyl ether (20 mL). The flask was stoppered with a rubber septum and stirred at 0 °C for 15 minutes. Tetrafluoroboric acid (50-55% w/w in diethyl ether, 2.5 mL, 17 mmol) was added dropwise to the cold solution over a period of 15 minutes. The clear,

colourless solution immediately turned into a bright orange suspension. Upon addition of the tetrafluoroboric acid solution, the reaction was allowed to continue at 0 °C for 1 hour. The mixture was then evacuated to dryness to afford an orange-red oil and was dissolved in dichloromethane (10 mL). Diethyl ether (100 mL) was added to precipitate the product as a bright orange solid. Product was filtered over a fine-pore glass frit and washed with diethyl ether until filtrate was clear and colourless. Solid was dried under vacuum overnight to afford desired product as a bright orange powder (1.185 g, 96%).

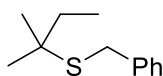
**<sup>1</sup>H NMR (CDCl<sub>3</sub>):** δ 4.3 (s, 3H, OCH<sub>3</sub>), 7.51-7.54 (m, 6H, Ar-H), 7.73-7.76 (m, 4H, Ar-H), 7.84-7.86 (m, 2H, Ar-H), 7.98-8.00 (m, 2H, Ar-H).

**<sup>13</sup>C{<sup>1</sup>H} NMR (CDCl<sub>3</sub>):** δ 58.9 (s, OCH<sub>3</sub>), 119.2 (s, *m*-C<sub>6</sub>H<sub>4</sub>), 129.7 (s, *m*-C<sub>6</sub>H<sub>5</sub>), 133.4 (s, *ipso*-C<sub>6</sub>H<sub>4</sub>), 138.6 (s, *ipso*-C<sub>6</sub>H<sub>5</sub>), 138.9 (s, *o*-C<sub>6</sub>H<sub>5</sub>), 139.2 (s, *o*-C<sub>6</sub>H<sub>4</sub>), 147.9 (s, *p*-C<sub>6</sub>H<sub>5</sub>), 177.0 (s, C(OMe)), 203.9 (s, (*p*-MeO-C<sub>6</sub>H<sub>4</sub>)CPh<sub>2</sub>).

**<sup>19</sup>F{<sup>1</sup>H} NMR (CDCl<sub>3</sub>):** δ -153.2 (s, BF<sub>4</sub>).

**<sup>11</sup>B{<sup>1</sup>H} NMR (CDCl<sub>3</sub>):** δ -1.0 (BF<sub>4</sub>).

#### 4.4.2.4 Characterization of Hydrothiolation Products

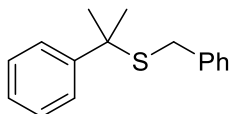


Pale yellow liquid, 0.1846 g, 95 %.

**<sup>1</sup>H NMR (CDCl<sub>3</sub>):** δ 1.00 (t, <sup>3</sup>J<sub>H-H</sub> = 7 Hz, 3H, CH<sub>3</sub>), 1.32 (s, 6H, CH<sub>3</sub>), 1.61 (q, <sup>3</sup>J<sub>H-H</sub> = 7 Hz, 2H, CH<sub>2</sub>), 3.72 (s, 2H, CH<sub>2</sub>), 7.22-7.38 (m, 5H, Ph).

**<sup>13</sup>C{<sup>1</sup>H} NMR (CDCl<sub>3</sub>):** δ 9.2 (s, CH<sub>3</sub>), 28.4 (s, CH<sub>3</sub>), 32.9 (s, CH<sub>2</sub>), 34.9 (s, CH<sub>2</sub>), 46.7 (s, C(CH<sub>3</sub>)<sub>2</sub>), 126.8 (s, *p*-C<sub>6</sub>H<sub>5</sub>), 128.5 (s, *m*-C<sub>6</sub>H<sub>5</sub>), 129.1 (s, *o*-C<sub>6</sub>H<sub>5</sub>), 138.7 (s, *ipso*-C<sub>6</sub>H<sub>5</sub>).

**DART-MS** exact mass calculated for (C<sub>12</sub>H<sub>19</sub>S)<sup>+</sup> require m/z 195.12, found m/z 195.12.

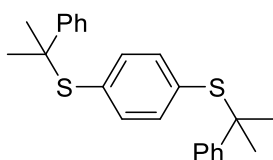


Colourless liquid, 0.240 g, 99 %.

**$^1\text{H}$  NMR ( $\text{CDCl}_3$ ):**  $\delta$  1.73 (s, 6H,  $\text{CH}_3$ ), 3.41 (s, 2H,  $\text{CH}_2$ ), 7.13-7.26 (m, 6H, Ar-H), 7.34-7.38 (m, 2H, Ar-H), 7.58-7.60 (m, 2H, Ar-H).

**$^{13}\text{C}\{^1\text{H}\}$  NMR ( $\text{CDCl}_3$ ):**  $\delta$  30.2 (s,  $\text{CH}_3$ ), 34.5 (s,  $\text{CH}_2$ ), 48.5 (s,  $\text{C}(\text{CH}_3)_2$ ), 126.5 (s, *p*- $\text{C}_6\text{H}_5$ ,  $\text{C}(\text{CH}_2)\text{Ph}$ ), 126.6 (s, *o*- $\text{C}_6\text{H}_5$ ,  $\text{C}(\text{CH}_2)\text{Ph}$ ), 126.7 (s, *p*- $\text{C}_6\text{H}_5$ ,  $\text{SCH}_2\text{Ph}$ ), 128.1 (s, *m*- $\text{C}_6\text{H}_5$ ,  $\text{C}(\text{CH}_2)\text{Ph}$ ), 128.3 (s, *m*- $\text{C}_6\text{H}_5$ ,  $\text{SCH}_2\text{Ph}$ ), 128.9 (s, *o*- $\text{C}_6\text{H}_5$ ,  $\text{SCH}_2\text{Ph}$ ), 138.1 (s, *ipso*- $\text{C}_6\text{H}_5$ ,  $\text{SCH}_2\text{Ph}$ ), 146.3 (s, *ipso*- $\text{C}_6\text{H}_5$ ,  $\text{C}(\text{CH}_2)\text{Ph}$ ).

DART-MS exact mass calculated for  $(\text{C}_{16}\text{H}_{19}\text{S})^+$  require  $m/z$  243.12, found  $m/z$  243.12.

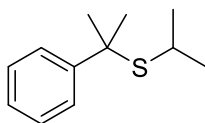


Off-white solid, 0.232 g, 61 %.

**$^1\text{H}$  NMR ( $\text{CDCl}_3$ ):**  $\delta$  1.66 (s, 12H,  $\text{CH}_3$ ), 6.90 (s, 4H, phenylene  $\text{CH}$ ), 7.18-7.21 (m, 2H, Ar-H), 7.24-7.26 (m, 4H, Ar-H), 7.35-7.37 (m, 4H, Ar-H).

**$^{13}\text{C}\{^1\text{H}\}$  NMR ( $\text{CDCl}_3$ ):**  $\delta$  29.7 (s,  $\text{CH}_3$ ), 51.2 (s,  $\text{C}(\text{CH}_3)_2$ ), 126.5 (s, *o*- $\text{C}_6\text{H}_5$ ), 126.6 (s, *p*- $\text{C}_6\text{H}_5$ ), 127.9 (s, *m*- $\text{C}_6\text{H}_5$ ), 133.6 (s, *ipso*-phenylene), 135.9 (s, phenylene  $\text{CH}$ ), 146.1 (s, *ipso*- $\text{C}_6\text{H}_5$ ).

DART-MS exact mass calculated for  $(\text{C}_{24}\text{H}_{27}\text{S}_2)^+$  require  $m/z$  379.15, found  $m/z$  379.15.

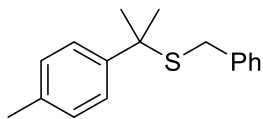


Colourless liquid, 0.167 g, 86 %.

**$^1\text{H}$  NMR ( $\text{CDCl}_3$ ):**  $\delta$  1.04 (d,  $^3J_{\text{H-H}} = 7$  Hz, 6H,  $\text{CH}_3$ ), 1.72 (s, 6H,  $\text{CH}_3$ ), 2.56 (sept,  $^3J_{\text{H-H}} = 7$  Hz, 1H,  $\text{CH}$ ), 7.20 (m, 1H, Ar-H), 7.31 (m, 2H, Ar-H), 7.56 (m, 2H, Ar-H).

**$^{13}\text{C}\{^1\text{H}\}$  NMR ( $\text{CDCl}_3$ ):**  $\delta$  25.2 (s,  $\text{CH}(\text{CH}_3)_2$ ), 30.9 (s,  $\text{SC}(\text{CH}_3)_2$ ), 34.2 (s,  $\text{CH}(\text{CH}_3)_2$ ), 48.2 (s,  $\text{SC}(\text{CH}_3)_2$ ), 126.3 (s, *p*- $\text{C}_6\text{H}_5$ ), 126.6 (s, *o*- $\text{C}_6\text{H}_5$ ), 127.9 (s, *m*- $\text{C}_6\text{H}_5$ ), 147.1 (s, *ipso*- $\text{C}_6\text{H}_5$ ).

DART-MS exact mass calculated for  $(C_{12}H_{19}S)^+$  require  $m/z$  195.12, found  $m/z$  195.12.

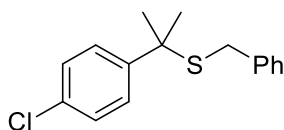


Pale-yellow liquid, 0.236 g, 92%.

$^1H$  NMR ( $CDCl_3$ ):  $\delta$  1.71 (s, 6H,  $CH_3$ ), 2.36 (s, 3H,  $p-CH_3$ ), 3.41 (s, 2H,  $CH_2$ ), 7.14-7.18 (m, 5H, Ar-H), 7.21-4.24 (m, 2H, Ar-H), 7.46-7.49 (m, 2H, Ar-H).

$^{13}C\{^1H\}$  NMR ( $CDCl_3$ ):  $\delta$  20.9 (s,  $p-CH_3$ ), 30.3 (s,  $CH_3$ ), 34.5 (s,  $CH_2$ ), 48.4 (s,  $C(CH_3)_2$ ), 126.5 (s,  $o-C_6H_4$ ), 126.6 (s,  $p-C_6H_5$ ), 128.3 (s,  $m-C_6H_5$ ), 128.8 ( $o-C_6H_5$ ), 128.9 ( $m-C_6H_4$ ), 136.1 (s,  $C(CH_3)_2$ ), 138.2 (s,  $ipso-C_6H_5$ ), 143.3 (s,  $ipso-C_6H_4$ ).

DART-MS exact mass calculated for  $(C_{17}H_{21}S)^+$  require  $m/z$  257.14, found  $m/z$  257.14.

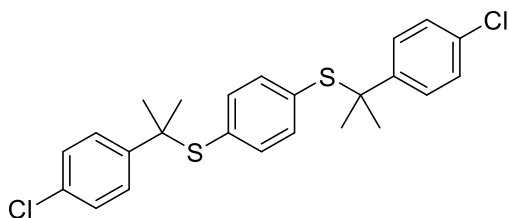


Colourless liquid, 0.182 g, 64 %.

$^1H$  NMR ( $CDCl_3$ ):  $\delta$  1.69 (s, 6H,  $CH_3$ ), 3.40 (s, 2H,  $CH_2$ ), 7.11-7.16 (m, 2H, Ar-H), 7.16-7.20 (m, 1H, Ar-H), 7.21-7.25 (m, 2H, Ar-H), 7.28-7.32 (m, 2H, Ar-H), 7.48-7.52 (m, 2H, Ar-H).

$^{13}C\{^1H\}$  NMR ( $CDCl_3$ ):  $\delta$  30.2 (s,  $CH_3$ ), 34.5 (s,  $CH_2$ ), 48.1 (s,  $SC(CH_3)_2$ ), 126.8 (s,  $p-C_6H_5$ ), 128.1 (s,  $o-C_6H_5Cl$ ), 128.2 (s,  $m-C_6H_5Cl$ ), 128.4 (s,  $m-C_6H_5$ ), 128.9 (s,  $o-C_6H_5$ ), 132.2 (s,  $C-Cl$ ), 137.8 (s,  $ipso-C_6H_5$ ), 145.0 (s,  $ipso-C_6H_4Cl$ ).

DART-MS exact mass calculated for  $(C_{18}H_{18}SCl)^+$  require  $m/z$  277.08, found  $m/z$  277.08.

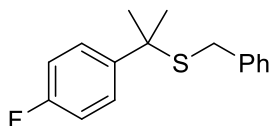


Colourless solid, 18%.

**$^1\text{H NMR}$  ( $\text{CDCl}_3$ ):**  $\delta$  1.63 (s, 12H,  $\text{CH}_3$ ), 6.91 (s, 4H, Ar-H), 7.21-7.22 (m, 2H, Ar-H), 7.23-7.24 (m, 2H, Ar-H), 7.26-7.27 (m, 2H, Ar-H), 7.28-7.29 (m, 2H, Ar-H).

**$^{13}\text{C}\{^1\text{H}\}$  NMR ( $\text{CDCl}_3$ ):**  $\delta$  29.7 (s,  $\text{CH}_3$ ), 50.8 (s,  $\text{C}(\text{CH}_3)_2$ ), 127.9 (s, *o*- $\text{C}_6\text{H}_4\text{Cl}$ ), 128.0 (s,  $\text{C}_6\text{H}_4$ ), 132.3 (s,  $\text{C}-\text{Cl}$ ), 133.5 (s, *ipso*- $\text{C}_6\text{H}_4$ ), 136.0 (s, *m*- $\text{C}_6\text{H}_4\text{Cl}$ ), 144.8 (s, *ipso*- $\text{C}_6\text{H}_4\text{Cl}$ ).

DART-MS exact mass calculated for  $(\text{C}_{24}\text{H}_{25}\text{S}_2\text{Cl}_2)^+$  require  $m/z$  447.08, found  $m/z$  447.08.

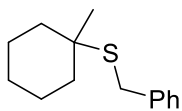


Colourless solid, 0.090 g, 34%.

**$^1\text{H NMR}$  ( $\text{CDCl}_3$ ):**  $\delta$  1.70 (s, 6H,  $\text{CH}_3$ ), 3.41 (s, 2H,  $\text{CH}_2$ ), 7.00-7.03 (m, 2H, Ar-H), 7.11-7.15 (m, 2H, Ar-H), 7.15-7.20 (m, 1H, Ar-H), 7.20-7.25 (m, 2H, Ar-H), 7.51-7.56 (m, 2H, Ar-H).

**$^{13}\text{C}\{^1\text{H}\}$  NMR ( $\text{CDCl}_3$ ):**  $\delta$  30.5 (s,  $\text{CH}_3$ ), 34.7 (s,  $\text{CH}_2$ ), 48.2 (s,  $\text{C}(\text{CH}_3)_2$ ), 114.9 (d,  $^2J_{\text{C-F}} = 21$  Hz, *m*- $\text{C}_6\text{H}_4\text{F}$ ), 126.9 (s, *ipso*- $\text{C}_6\text{H}_5$ ), 128.4 (d,  $^2J_{\text{C-F}} = 8$  Hz, *o*- $\text{C}_6\text{H}_4\text{F}$ ), 128.5 (s, *m*- $\text{C}_6\text{H}_5$ ), 129.0 (s, *ipso*- $\text{C}_6\text{H}_4\text{F}$ ), 138.1 (s, *o*- $\text{C}_6\text{H}_5$ ), 142.3 (s, *p*- $\text{C}_6\text{H}_5$ ), 161.5 (d,  $^1J_{\text{C-F}} = 245$  Hz,  $\text{C}-\text{F}$ ).

DART-MS exact mass calculated for  $(\text{C}_{16}\text{H}_{18}\text{SF})^+$  require  $m/z$  261.11, found  $m/z$  261.11.

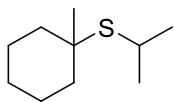


Colourless liquid, 0.223 g, 99 %.

**$^1\text{H NMR}$  ( $\text{CDCl}_3$ ):**  $\delta$  1.37 (s, 3H  $\text{CH}_3$ ), 1.42-1.54 (m, 5H,  $\text{CH}_2$ ), 1.66-1.77 (m, 5H,  $\text{CH}_2$ ), 3.68 (s, 2H,  $\text{CH}_2$ ), 7.19-7.23 (m, 1H, Ar-H), 7.27-7.31 (m, 2H, Ar-H), 7.33-7.68 (m, 2H, Ar-H).

**$^{13}\text{C}\{^1\text{H}\}$  NMR ( $\text{CDCl}_3$ ):**  $\delta$  22.3 (s,  $\text{CH}_2$ , cyclohexyl), 25.9 (s,  $\text{CH}_3$ ), 28.9 (br, s, quaternary carbon), 32.0 (s,  $\text{SCH}_2$ ), 38.3 (s,  $\text{CH}_2$ , cyclohexyl), 47.1 (s,  $\text{CH}_2$ , cyclohexyl), 126.7 (s, *p*- $\text{C}_6\text{H}_5$ ), 128.4 (s, *m*- $\text{C}_6\text{H}_5$ ), 129.0 (*o*- $\text{C}_6\text{H}_5$ ), 138.7 (*ipso*- $\text{C}_6\text{H}_5$ ).

DART-MS exact mass calculated for  $(C_{14}H_{21}S)^+$  require  $m/z$  221.14, found  $m/z$  221.14.

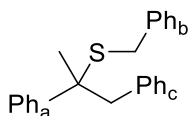


Volatile, colourless liquid, 0.023 g, 12 %.

$^1H$  NMR ( $CDCl_3$ ):  $\delta$  1.29 (d,  $^3J_{H-H} = 7$  Hz, 6H,  $CH_3$ ), 1.34 (s, 3H,  $CH_3$ ), 1.39-1.52 (m, 6H,  $CH_2$ ), 1.62-1.73 (m, 4H,  $CH_2$ ), 2.90 (hept,  $^3J_{H-H} = 7$  Hz, 1H,  $CH$ ).

$^{13}C\{^1H\}$  NMR ( $CDCl_3$ ):  $\delta$  22.5 (s,  $CH_2$ , cyclohexyl), 25.9 (s,  $CH(CH_3)_2$ ), 26.3 (s,  $CH_3$ ), 29.3 (br, s, quaternary carbon), 31.8 (s,  $CH(CH_3)_2$ ), 39.0 (s,  $CH_2$ , cyclohexyl), 47.3 (s,  $CH_2$ , cyclohexyl).

DART-MS exact mass calculated for  $(C_{10}H_{21}S)^+$  require  $m/z$  173.14, found  $m/z$  173.14.



White crystalline solid, 0.124 g, 39%.

$^1H$  NMR ( $CD_2Cl_2$ ):  $\delta$  1.68 (s, 3H,  $CH_3$ ), 3.20 (m, 2H,  $CH_2$ , diastereotopic), 3.38 (m, 2H,  $SCH_2$ , diastereotopic), 6.85-6.87 (m, 3H, Ar-H), 7.10-7.27 (m, 8H, Ar-H), 7.33-7.36 (m, 2H, Ar-H), 7.53-7.56 (m, 2H, Ar-H).

$^{13}C\{^1H\}$  NMR ( $CD_2Cl_2$ ):  $\delta$  25.3 (s,  $CH_3$ ), 33.9 (s,  $SCH_2$ ), 49.4 (s,  $C(CH_3)_2$ ), 53.1 (s,  $CH_2$ ), 126.3 ( $p$ - $Ph_a$ ), 126.6 ( $p$ - $Ph_c$ ), 126.7 ( $p$ - $Ph_b$ ), 127.5 ( $o$ - $Ph_a$ ), 127.7 ( $o$ - $Ph_c$ ), 128.0 ( $m$ - $Ph_a$ ), 128.3 ( $m$ - $Ph_c$ ), 128.9 ( $o$ - $Ph_b$ ), 130.6 ( $m$ - $Ph_c$ ), 136.9 ( $ipso$ - $Ph_c$ ), 138.1 ( $ipso$ - $Ph_b$ ), 144.4 ( $ipso$ - $Ph_a$ ).

DART-MS exact mass calculated for  $(C_{22}H_{23}S)^+$  require  $m/z$  319.15, found  $m/z$  319.15.

#### 4.4.3 X-ray Crystallography

##### 4.4.3.1 X-ray Data Collection and Reduction

Crystals were coated in Paratone-N oil in the glove-box, mounted on a MiTeGen Micromount and placed under a cold  $N_2$  stream, thus maintaining a dry,  $O_2$ -free environment for each crystal. The data were collected on a Bruker Apex II diffractometer employing  $Mo\ K\alpha$  radiation ( $\lambda =$

0.71073 Å). Data collection strategies were determined using Bruker Apex software and optimized to provide >99.5% data completion to a  $2\theta$  value of at least  $55^\circ$ . The data were collected at 150( $\pm$ 2) K for all crystals. The frames were integrated with the Bruker SAINT software package using a narrow-frame algorithm. Data were corrected for absorption effects using the empirical multi-scan method (SADABS).<sup>101</sup>

#### 4.4.3.2 X-ray Data Solution and Refinement

Non-hydrogen atomic scattering factors were taken from the literature tabulations.<sup>102</sup> The heavy atom positions were determined using direct methods employing the SHELXTL direct methods routine. The remaining non-hydrogen atoms were located from successive difference Fourier map calculations. The refinements were carried out by using full-matrix least squares techniques on  $F$ , minimizing the function  $\omega(F_o - F_c)^2$  where the weight  $\omega$  is defined as  $4F_o^2/2\sigma(F_o^2)$  and  $F_o$  and  $F_c$  are the observed and calculated structure factor amplitudes, respectively. In the final cycles of each refinement, all non-hydrogen atoms were assigned anisotropic temperature factors in the absence of disorder or insufficient data. In the latter cases atoms were treated isotropically. C-H atom positions were calculated and allowed to ride on the carbon to which they are bonded. H-atom temperature factors were fixed at 1.20 times the isotropic temperature factor of the C-atom to which they are bonded. The H-atom contributions were calculated, but not refined. The locations of the largest peaks in the final difference Fourier map calculation as well as the magnitude of the residual electron densities in each case were of no chemical significance.

**Table 4.4.1. Select Crystallographic Data for 4-2.**

<b>(4-2)</b>	
Formula	C <sub>20</sub> H <sub>17</sub> BF <sub>4</sub> O
Formula weight	360.14
Crystal system	Monoclinic
Space group	<i>P</i> 2 <sub>1</sub> / <i>n</i>
a (Å)	7.7761(16)
b (Å)	15.354(3)
c (Å)	14.480(3)
α (deg)	90
β (deg)	95.766(8)
γ (deg)	90
Volume (Å <sup>3</sup> )	1720.2(7)
Z	4
d (calc) gcm <sup>-3</sup>	1.391
R(int.)	0.0327
Abs coeff, μ, mm <sup>-1</sup>	0.113
Data collected	3970
Variables	236
>2σ(F <sub>o</sub> <sup>2</sup> )	3093
R(>2σ)	0.1119
R <sub>w</sub> (>2σ)	0.3289
GOF	1.108

## Chapter 4 References

- (1) Friedel, C.; Crafts, J. M. *Compte. Rend.* **1877**, *84*, 1392,1450.
- (2) Bandini, M.; Melloni, A.; Umani-Ronchi, A. *Angew. Chem. Int. Ed.* **2004**, *43*, 550–556.
- (3) You, S.-L.; Cai, Q.; Zeng, M. *Chem. Soc. Rev.* **2009**, *38*, 2190–2201.
- (4) Poulsen, T. B.; Jørgensen, K. A. *Chem. Rev.* **2008**, *108*, 2903–2915.
- (5) Rueping, M.; Nachtsheim, B. J. *Beilstein J. Org. Chem.* **2010**, *6*.
- (6) Marks, T. J. *Acc. Chem. Res.* **1992**, *25*, 57–65.
- (7) Yang, X.; Stern, C. L.; Marks, T. J. *J. Am. Chem. Soc.* **1994**, *116*, 10015–10031.
- (8) Melen, R. L. *Chem. Commun.* **2014**, *50*, 1161–1174.
- (9) Piers, W. E.; Marwitz, A. J. V.; Mercier, L. G. *Inorg. Chem.* **2011**, *50*, 12252–12262.
- (10) Stephan, D. W.; Erker, G. *Angew. Chem. Int. Ed.* **2010**, *49*, 46–76.
- (11) Piers, W. E.; Chivers, T. *Chem. Soc. Rev.* **1997**, *26*, 345–354.
- (12) Mkhaliid, I. A. I.; Barnard, J. H.; Marder, T. B.; Murphy, J. M.; Hartwig, J. F. *Chem. Rev.* **2010**, *110*, 890–931.
- (13) Lawson, J. R.; Melen, R. L. *Inorg. Chem.* **2017**, *56*, 8627–8643.
- (14) Kölle, P.; Nöth, H. *Chem. Rev.* **1985**, *85*, 399–418.
- (15) Piers, W. E.; Bourke, S. C.; Conroy, K. D. *Angew. Chem. Int. Ed.* **2005**, *44*, 5016–5036.
- (16) De Vries, T. S.; Prokofjevs, A.; Vedejs, E. *Chem. Rev.* **2012**, *112*, 4246–4282.
- (17) Eisenberger, P.; Crudden, C. M. *Dalton Trans.* **2017**, *46*, 4874–4887.
- (18) Stephan, D. W. *Org. Biomol. Chem.* **2008**, *6*, 1535–1539.
- (19) Stephan, D. W. *Org. Biomol. Chem.* **2012**, *10*, 5740–5746.

- (20) Stephan, D. W. *J. Am. Chem. Soc.* **2015**, *137*, 10018–10032.
- (21) Stephan, D. W. *Acc. Chem. Res.* **2015**, *48*, 306–316.
- (22) Chase, P. A.; Welch, G. C.; Jurca, T.; Stephan, D. W. *Angew. Chem. Int. Ed.* **2007**, *46*, 8050–8053.
- (23) Spies, P.; Erker, G.; Kehr, G.; Bergander, K.; Fröhlich, R.; Grimme, S.; Stephan, D. W. *Chem. Commun.* **2007**, *2*, 5072–5074.
- (24) Welch, G. C.; Stephan, D. W. *J. Am. Chem. Soc.* **2007**, *129*, 1880–1881.
- (25) Ménard, G.; Stephan, D. W. *Angew. Chem. Int. Ed.* **2012**, *51*, 8272–8275.
- (26) Dureen, M. A.; Brown, C. C.; Stephan, D. W. *Organometallics* **2010**, *29*, 6594–6607.
- (27) Dureen, M. A.; Stephan, D. W. *J. Am. Chem. Soc.* **2009**, *131*, 8396–8397.
- (28) Ménard, G.; Stephan, D. W. *J. Am. Chem. Soc.* **2010**, *132*, 1796–1797.
- (29) Courtemanche, M.-A.; Larouche, J.; Légaré, M.-A.; Bi, W.; Maron, L.; Fontaine, F.-G. *Organometallics* **2013**, *32*, 6804–6811.
- (30) Boudreau, J.; Courtemanche, M.-A.; Fontaine, F.-G. *Chem. Commun.* **2011**, *47*, 11131–11133.
- (31) Stennett, T. E.; Pahl, J.; Zijlstra, H. S.; Seidel, F. W.; Harder, S. *Organometallics* **2016**, *35*, 207–217.
- (32) Appelt, C.; Westenberg, H.; Bertini, F.; Ehlers, A. W.; Slootweg, J. C.; Lammertsma, K.; Uhl, W. *Angew. Chem. Int. Ed.* **2011**, *50*, 3925–3928.
- (33) Pleschka, D.; Layh, M.; Rogel, F.; Uhl, W. *Phil. Trans. R. Soc. A* **2017**, *375*, 20170011.
- (34) Roters, S.; Appelt, C.; Westenberg, H.; Hepp, A.; Slootweg, J. C.; Lammertsma, K.; Uhl, W. *Dalton Trans.* **2012**, *41*, 9033–9045.
- (35) Gabbai, F. P. In *Group 13 Chemistry*; Shapiro, P. J., Atwood, D. A., Eds.; Oxford

University Press: Washington, DC, 2002; pp 118–130.

- (36) Osten, K. M.; Mehrkhodavandi, P. *Acc. Chem. Res.* **2017**, *50*, 2861–2869.
- (37) Uzelac, M.; Armstrong, D. R.; Kennedy, A. R.; Hevia, E. *Chem. Eur. J.* **2016**, *22*, 15826–15833.
- (38) Backs, J.; Lange, M.; Possart, J.; Wollschläger, A.; Mück-Lichtenfeld, C.; Uhl, W. *Angew. Chem. Int. Ed.* **2017**, *56*, 3094–3097.
- (39) Possart, J.; Uhl, W. *Organometallics* **2018**, *37*, 1314–1323.
- (40) Uzelac, M.; Kennedy, A. R.; Hevia, E. *Inorg. Chem.* **2017**, *56*, 8615–8626.
- (41) Uhl, W.; Willeke, M.; Hengesbach, F.; Hepp, A.; Layh, M. *Organometallics* **2016**, *35*, 3701–3712.
- (42) Surya Prakash, G. K.; Mathew, T.; Olah, G. A. *Acc. Chem. Res.* **2012**, *45*, 565–577.
- (43) Dimroth, K.; Hofmann, P. *Angew. Chem. Int. Ed.* **1964**, *3*, 384–384.
- (44) Cowley, A. H.; Kemp, R. A. *Chem. Rev.* **1985**, *85*, 367–382.
- (45) Petušková, J.; Patil, M.; Holle, S.; Lehmann, C. W.; Thiel, W.; Alcarazo, M. *J. Am. Chem. Soc.* **2011**, *133*, 20758–20760.
- (46) Werner, T. *Adv. Synth. Catal.* **2009**, *351*, 1469–1481.
- (47) Wittig, G.; Schollkopf, U. *Chem. Ber.* **1954**, *97*, 1318–1330.
- (48) Caputo, C. B.; Hounjet, L. J.; Dobrovetsky, R.; Stephan, D. W. *Science* **2013**, *341*, 5535–5539.
- (49) Bayne, J. M.; Stephan, D. W. *Chem. Soc. Rev.* **2015**, *45*, 765–774.
- (50) Mehta, M.; Holthausen, M. H.; Mallov, I.; Pérez, M.; Qu, Z. W.; Grimme, S.; Stephan, D. W. *Angew. Chem. Int. Ed.* **2015**, *54*, 8250–8254.
- (51) Holthausen, M. H.; Mehta, M.; Stephan, D. W. *Angew. Chem. Int. Ed.* **2014**, *53*, 6538–

6541.

- (52) Vom Stein, T.; Pérez, M.; Dobrovetsky, R.; Winkelhaus, D.; Caputo, C. B.; Stephan, D. *W. Angew. Chem. Int. Ed.* **2015**, *54*, 10178–10182.
- (53) Weicker, S. A.; Stephan, D. W. *Bull. Chem. Soc. Jpn.* **2015**, *88*, 1003–1016.
- (54) Whittell, G. R.; Balmond, E. I.; Robertson, A. P. M.; Patra, S. K.; Haddow, M. F.; Manners, I. *Eur. J. Inorg. Chem.* **2010**, 3967–3975.
- (55) Lambert, J. B.; Zhang, S.; Stern, C. L.; Huffman, J. C. *Science* **1993**, *260*, 1917–1918.
- (56) Schäfer, A.; Reißmann, M.; Schäfer, A.; Saak, W.; Haase, D.; Müller, T. *Angew. Chem. Int. Ed.* **2011**, *50*, 12636–12638.
- (57) Kim, K.-C.; Reed, C. A.; Elliott, D. W.; Mueller, L. J.; Tham, F.; Lin, L.; Lambert, J. B. *Science* **2002**, *297*, 825–827.
- (58) Reißmann, M.; Schäfer, A.; Jung, S.; Müller, T. *Organometallics* **2013**, *32*, 6736–6744.
- (59) Schäfer, A.; Reißmann, M.; Schäfer, A.; Schmidtman, M.; Müller, T. *Chem. Eur. J.* **2014**, *20*, 9381–9386.
- (60) Frey, G. D.; Lavallo, V.; Donnadiu, B.; Schoeller, W. W.; Bertrand, G. *Science* **2007**, *316*, 439–441.
- (61) Clark, E. R.; Ingleson, M. J. *Angew. Chem. Int. Ed.* **2014**, *53*, 11306–11309.
- (62) Radcliffe, J. E.; Dunsford, J. J.; Cid, J.; Fasano, V.; Ingleson, M. J. *Organometallics* **2017**, *36*, 4952–4960.
- (63) Fasano, V.; Radcliffe, J. E.; Curless, L. D.; Ingleson, M. J. *Chem. Eur. J.* **2017**, *23*, 187–193.
- (64) Palomas, D.; Holle, S.; Inés, B.; Bruns, H.; Goddard, R.; Alcarazo, M. *Dalton Trans.* **2012**, *41*, 9073–9082.
- (65) Inés, B.; Holle, S.; Goddard, R.; Alcarazo, M. *Angew. Chem.* **2010**, *49*, 8389–8391.

- (66) Boone, M. P.; Stephan, D. W. *J. Am. Chem. Soc.* **2013**, *135*, 8508–8511.
- (67) Horn, M.; Mayr, H. *Chem. Eur. J.* **2010**, *16*, 7469–7477.
- (68) Himmel, D.; Krossing, I.; Schnepf, A. *Angew. Chem. Int. Ed.* **2014**, *53*, 6040–6046.
- (69) *Organosulfur Chemistry I*; Page, P. C. B., Ed.; Springer: Berlin, 1991.
- (70) *Organosulfur Chemistry II*; Page, P. C. B., Ed.; Springer: Berlin, 1991.
- (71) Akiba, M.; Hashim, A. S. *Prog. Polym. Sci.* **1997**, *22*, 475–521.
- (72) Posner, T. *Ber. Dtsch. Chem. Ges. B.* **1905**, *38*, 646.
- (73) Griesbaum, K. *Angew. Chem. Int. Ed.* **1970**, *9*, 273–287.
- (74) Benati, L.; Capella, L.; Montecvecchi, P. C.; Spagnolo, P. *J. Chem. Soc., Perkin Trans. 1* **1995**, 1035–1038.
- (75) Conte, M. Lo; Pacifico, S.; Chambery, A.; Marra, A.; Dondoni, A. *J. Org. Chem.* **2010**, *75*, 4644–4647.
- (76) Ipatieff, V. N.; Pines, H.; Friedman, B. S. *J. Am. Chem. Soc.* **1938**, *60*, 2731–2734.
- (77) Kipnis, F.; Ornfelt, J. *J. Am. Chem. Soc.* **1951**, *73*, 822–822.
- (78) Screttas, C. G.; Micha-Screttas, M. *J. Am. Chem. Soc.* **1979**, *44*, 713–719.
- (79) Kanagasabapathy, S.; Sudalai, A.; Benicewicz, B. C. *Tetrahedron Lett.* **2001**, *42*, 3791.
- (80) Truce, W. E.; Simms, J. A.; Boudakian, M. M. *J. Am. Chem. Soc.* **1956**, *78*, 695–696.
- (81) Wadsworth, D. H.; Detty, M. R. *J. Org. Chem.* **1980**, *45*, 4611–4615.
- (82) Waters, M. S.; Cowen, J. A.; McWilliams, J. C.; Maligres, P. E.; Askin, D. *Tetrahedron* **2000**, *41*, 141–144.
- (83) Kondoh, A.; Takami, K.; Yorimitsu, H.; Oshima, K. *J. Org. Chem.* **2005**, *70*, 6468–6473.
- (84) Yu, A. H.; Qiu, R. H.; Tan, N. Y.; Peng, L. F.; Xu, X. H. *Chin. Chem. Lett.* **2011**, *22*, 687–

690.

- (85) Wathier, M.; Love, J. A. *Eur. J. Inorg. Chem.* **2016**, 2391–2402.
- (86) Ritleng, V.; Henrion, M. L.; Chetcuti, M. J. *ACS Catal.* **2016**, 6, 890–906.
- (87) Castarlenas, R.; Giuseppe, A. Di; Pérez-Torrente, J. J.; Oro, L. A. *Angew. Chem. Int. Ed.* **2013**, 52, 211–222.
- (88) Yang, J.; Sabarre, A.; Fraser, L. R.; Patrick, B. O.; Love, J. A. *J. Org. Chem.* **2009**, 74, 182–187.
- (89) *Transition-Metal-Catalyzed S-H and Se-H Bonds Addition to Unsaturated Molecules*; Ananikov, V. P., Tanaka, M., Eds.; Springer: New York, 2011.
- (90) Ogawa, A. In *Top Organomet Chem*; Beller, M., Dixneuf, P. H., Dupont, J., Furstner, A., Glorius, A., GooBen, L. J., Ikariya, T., Nolan, S. P., Okuda, J., Oro, L. A., Willis, M., Zhou, Q.-L., Eds.; Springer: Berlin, 2013; Vol. 43, pp 325–360.
- (91) Tamai, T.; Ogawa, A. *J. Org. Chem.* **2014**, 79, 5028–5035.
- (92) Mukaiyama, T.; Izawa, T.; Saigo, K.; Takei, H. *Chem. Lett.* **1973**, 355–356.
- (93) Belley, M.; Zamboni, R. *J. Org. Chem.* **1989**, 54, 1230–1232.
- (94) Kuciński, K.; Pawluc, P.; Hreczycho, G. *Adv. Synth. Catal.* **2015**, 357, 3936–3942.
- (95) Weïwer, M.; Coulombel, L.; Duñach, E. *Chem. Commun.* **2005**, 0, 332–334.
- (96) Kumar, R.; Saima; Shard, A.; Andhare, N. H.; Richa; Sinha, A. K. *Angew. Chem. Int. Ed.* **2015**, 54, 828–832.
- (97) Farrell, J. M.; Posaratnanathan, R. T.; Stephan, D. W. *Chem. Sci.* **2015**, 6, 2010–2015.
- (98) Farrell, J. M.; Hatnean, J. A.; Stephan, D. W. *J. Am. Chem. Soc.* **2012**, 134, 15728–15731.
- (99) Lam, J.; Günther, B. A. R.; Farrell, J. M.; Eisenberger, P.; Bestvater, B. P.; Newman, P. D.; Melen, R. L.; Crudden, C. M.; Stephan, D. W. *Dalton Trans.* **2016**, 45, 15303–15316.

- (100) Pérez, M.; Mahdi, T.; Hounjet, L. J.; Stephan, D. W. *Chem. Commun.* **2015**, *51*, 11301–11304.
- (101) *Apex 2 Software Package*; Bruker AXS Inc., 2013.
- (102) Cromer, D. T.; W., J. T. *Int. Tables X-Ray Crystallography*; 1974; Vol. 4.

## Chapter 5 Conclusion and Future Work

### 5.1 Thesis Summary

The work presented herein was inspired by the desire to study the reactivity and coordination chemistry of N-phosphorylated N-heterocyclic carbene ligands. Furthermore, motivated by an industrial collaboration, the catalytic hydrogenation activity of the newly-synthesized complexes were studied. As well, while transition metal catalysts tend to be more prevalent as competent catalysts, their increased costs, rarity, and environmental impacts led us to pursue metal-free hydrogenation catalysts in the form of frustrated Lewis pairs.

Chapter 2 explored the coordination chemistry of N-phosphorylated N-heterocyclic carbene ligands with ruthenium precursors. It was found that a novel zero-valent complex could be readily isolated. This complex undergoes rapid oxidative addition of silanes and dihydrogen to afford the corresponding Ru(II) species. Interestingly, the dihydride product was shown to undergo reversible activation of dihydrogen and as a result was used in the hydrogenation of simple olefins. However, the large catalytic loadings and long reaction times preclude this complex as a viable and efficient hydrogenation catalyst.

Attempting to synthesize a similar Ru(0) species as above using a bulkier NHCP ligand was not successful, and instead resulted in a cyclometalated product derived from the N-substituent of the carbene. This species was also shown to undergo reversible and facile activation of molecular hydrogen. When treated with deuterium, scrambling was observed, indicating the N-substituent is involved in the reversible oxidative addition/reductive elimination process. This species was also studied for its catalytic activity and it showed improvement over the previous species, but still suffered from long reaction times and elevated temperatures. Additionally, it does not hydrogenate olefinic residues of nitrile butadiene rubber.

In Chapter 3, further reactivity of the NHCP ligands was probed. A piano-stool half-sandwich ruthenium complex was synthesized and further modified to a cationic species *via* abstraction of halide. The cationic ruthenium complex readily activates dihydrogen between the Lewis acidic metal center and Lewis basic pendant phosphorus ligand and readily scrambles deuterium hydride, indicating reversible activation of dihydrogen. Unfortunately, the complex is not a

competent hydrogenation catalyst for olefins, ketones, or nitrile butadiene rubber. In the case of nitrile butadiene rubber, the catalyst was observed to promote cross-linking of the rubber polymer through the nitrile functional groups. The inactivity of the catalyst towards hydrogenation is attributed to the high basicity of the phosphine ligand and the inability to protonate substrates.

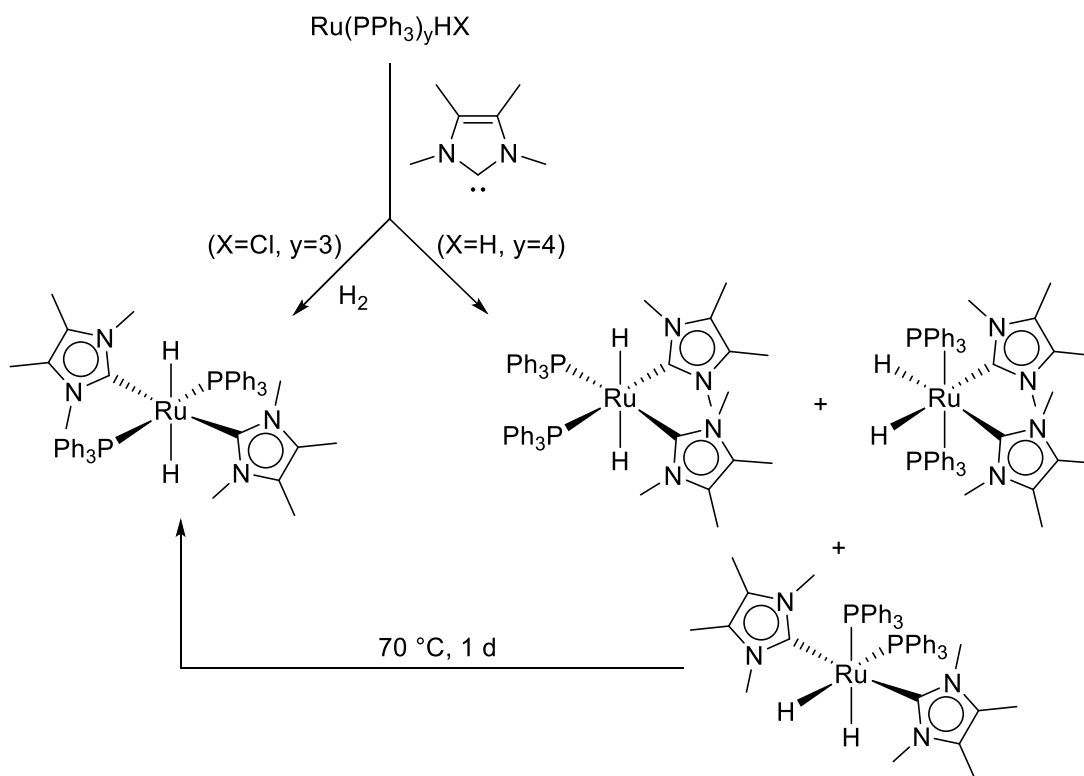
As mentioned above, the need to move away from the financial and environmental costs of transition metal catalysts directed our efforts towards development of metal-free main group catalysts in the context of frustrated Lewis pairs. Recognizing the gap in carbon-based Lewis acids, a series of *p*-methoxytrityl cations were synthesized. The cations were found to be very air- and moisture-stable and thus easily stored under ambient conditions. When combined with sterically congested tertiary phosphines, the pair were found to irreversibly activate dihydrogen. Due to the irreversibility, the FLP were not able to hydrogenate unsaturated substrates. Serendipitously, however, the Lewis acidic trityl cations were found to readily catalyze the addition of S-H bonds across olefins under mild conditions, without the need for an anhydrous or oxygen-free environment. A simple, high-yielding, and bench top-stable methodology was developed for carbon-sulfur bond formations using the air-stable trityl catalyst.

The development of Ru-NHCP complexes, as well as the synthesis of air- and moisture-stable carbon-based Lewis acids presented herein has afforded a large volume of new ruthenium and transition metal-free chemistry. The knowledge gained from this work can be used in the further development of new, more active hydrogenation catalysts.

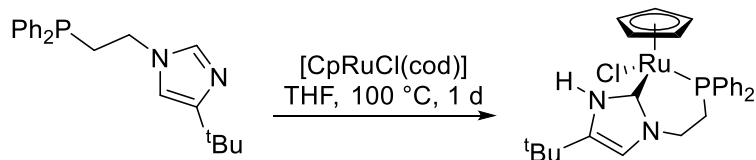
## 5.2 Future Work

The synthesis of all the N-phosphorylated N-heterocyclic carbenes presented in this work were conducted with *tert*-butyl-substituted phosphines. Thus, an obvious area for further development would be to investigate the effects of other substituents. Perhaps the use of different groups on the phosphorus center would impart better stability with respect to the P-N bond. Additionally, complex **2-7** was shown to undergo C-H metalation of the *tert*-butyl substituent on N and thus, changing the substituent to a different group, such as adamantyl, may inhibit this side-reaction. The complexes discussed in Chapter 2 were shown to be less than ideal for hydrogenation of olefins, likely as a result of the electron-withdrawing nature of the carbonyl group. Thus, new synthetic approaches to utilizing ruthenium precursors lacking carbonyl groups would greatly aid

the development of active catalytic species. The Whittlesey group has reported the synthesis of ruthenium-dihydride species bearing NHCs and phosphines (Scheme 5.2.1).<sup>1</sup> Furthermore, the Hahn and Grotjahn groups has demonstrated the utility of post-synthetic modification techniques in the synthesis of metal-NHC complexes (Scheme 5.2.2).<sup>2,3</sup> With regard to piano-stool half-sandwich complexes presented in Chapter 3, changing of the phosphorus substituents to phenyl would theoretically decrease the basicity of the phosphorus center and perhaps allow the complex to act as a better bifunctional hydrogenation catalyst. However, based on preliminary studies the reduced basicity of the phosphine is appears to be correlated with decreased stability of the P-N bond and would subject the complex to further degradation. Indeed, according to Marchenko and coworkers, diphenylphosphino substituents exhibit greater cleavage of the P-N bond relative to more basic phosphine substituents such as <sup>t</sup>Bu<sub>2</sub>P or (<sup>i</sup>Pr<sub>2</sub>N)<sub>2</sub>P.<sup>4</sup>

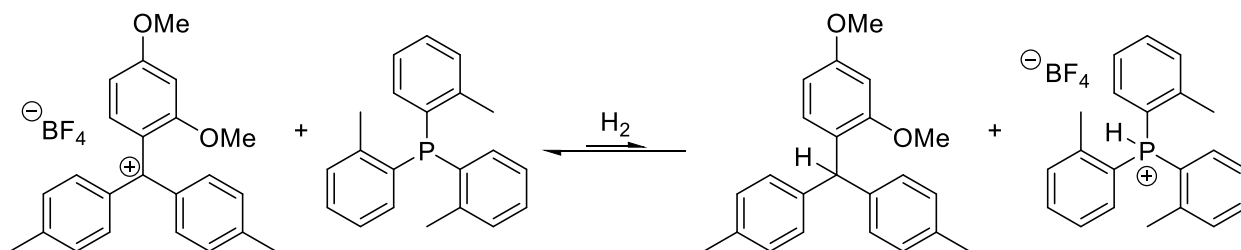


**Scheme 5.2.1: Synthesis of various isomers of ruthenium-dihydride species bearing NHC ligands.**



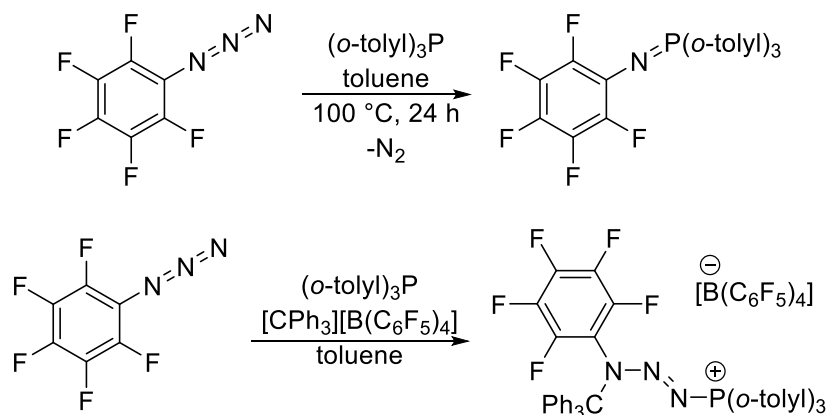
**Scheme 5.2.2: Ruthenium transfer hydrogenation catalyst bearing phosphino-NHC ligand. NHC can be modified to bear N-substituents post-synthesis.**

In the case of methoxy-substituted trityl cations, the lack of reversibility of hydrogen activation is a result of the low hydricity of the corresponding triarylmethane. Thus, further substitution of the Lewis acid with more electron donating groups would greatly enhance the hydricity and favour the release of H<sub>2</sub> from the FLP activated product. Early evidence from the group suggests the introduction of methoxy substituents at the *ortho* position of the aryl rings leads to a small degree of reversible H<sub>2</sub> activation at elevated temperatures when combined with bulky phosphine bases (Scheme 5.2.3).



**Scheme 5.2.3: Reversible activation of dihydrogen using a highly-substituted trityl cation.**

Of course, increasing the number of electron-rich substituents on the cation would also serve to reduce the Lewis acidity of the species and thus act to prevent hydrogen activation. As a result, care must be taken to strike a balance between Lewis acidity and hydricity of the two compounds. The Stephan group has shown other examples of carbon FLPs involving trityl cations, where the trityl cation interrupts the normal Staudinger reaction between an azide and tertiary phosphine, yielding an intermediate product (Scheme 5.2.4).<sup>5</sup>



**Scheme 5.2.4: Staudinger formation of phosphinimine (top), and arrested intermediate in Staudinger reaction trapped by trityl cation (bottom).**

Finally, the scope of the Lewis acidic cations should be broadened. The reactivity of the cations should be explored as catalysts or initiators in hydrosilylation or hydroboration reactions of olefins, provided the counterion does not cause interference. In this reaction, the decreased Lewis acidity is beneficial as it would prevent side reactions that degrade the silane or borane reagents.

## Chapter 5 References

- (1) Davies, C. J. E.; Lowe, J. P.; Mahon, M. F.; Poulten, R. C.; Whittlesey, M. K. *Organometallics* **2013**, *32*, 4927–4937.
- (2) Aznarez, F.; Gao, W.-X.; Lin, Y.-J.; Hahn, F. E.; Jin, G.-X. *Dalton Trans.* **2018**, *47*, 9442–9452.
- (3) Miranda-Soto, V.; Grotjahn, D. B.; Cooksy, A. L.; Golen, J. A.; Moore, C. E.; Rheingold, A. L. *Angew. Chem. Int. Ed.* **2011**, *50*, 631–635.
- (4) Marchenko, A. P.; Koidan, H. N.; Huryeva, A. N.; Zarudnitskii, E. V.; Yurchenko, A. A.; Kostyuk, A. N. *J. Org. Chem.* **2010**, *75*, 7141–7145.
- (5) Zhou, J.; Cao, L. L.; Liu, L.; Stephan, D. W. *Dalton Trans.* **2017**, *46*, 9334–9338.